PHONONS IN COPPER
AT ELEVATED TEMPERATURES

by

ANDRÉ LAROSE, M.Sc.

A Thesis

Submitted to the Faculty of Graduate Studies

in Partial Fulfilment of the Requirements

for the Degree

Doctor of Philosophy

McMaster University

October, 1975

PHONONS IN COPPER AT ELEVATED TEMPERATURES

DOCTOR OF PHILOSOPHY
(Physics)

McMASTER UNIVERSITY
Hamilton, Ontario, CANADA.

TITLE: Phonons in Copper at Elevated Temperatures

AUTHOR: André Larose, B.Sc. (1968) Université de Montréal
M.Sc. (1970) McMaster University

SUPERVISOR: Professor B. N. Brockhouse

NUMBER OF PAGES: xiii, 253

ABSTRACT: The technique of inelastic scattering of thermal neutrons offers a versatile, yet powerful, method of observing the spectra of elementary excitations in condensed matter. In this thesis, this technique was used in the determination of the phonon spectra of three metals, using monocrystalline specimens.

The first study concerns the temperature dependence of the phonon spectrum of Cu in the range 20°C to 1063°C, i.e. up to 20°C below the melting point, and in the various directions of high symmetry accessible in a (001) scattering plane. Resolution effects were taken into account in the determination of intrinsic phonon frequencies and linewidths. The results indicate a general softening of the lattice as a function of temperature, the vibrations of transverse polarization being significantly more affected (on a relative basis) than those of longitudinal polarization. Most of the signals have remained observable up to the vicinity of the melting point. A high resolution study of the small wavevector domain was also performed in order to determine the temperature dependence of the (adiabatic) elastic constants in a temperature range inaccessible to the usual ultrasonic methods. Of particular interest is the fact that the T_1 branch was found to manifest a peculiarity at the approximate reduced wavevector $\zeta \approx 0.2$; a careful examination did not reveal any corresponding distinctive behaviour in the linewidth (lifetime). A search for possible manifestations of the Kohn effect at high temperature was also performed at other positions in reciprocal space.

A similar study (extending up to 1050°C) was also carried on the small wavevector phonons in Pd. It is known, from other workers, that this substance shows a peculiar temperature dependence in the T_1 branch, this dependence being opposite to that observed in Cu.

Finally, the third study deals with an unsuccessful attempt to observe a predicted weak Kohn effect in the room temperature phonon spectrum of W.

Technical details concerning the apparatus built for the high temperature measurements are to be found in chapter III following a review chapter on the crystal dynamics of metals and the technique of triple-axis spectroscopy, with particular emphasis on the optimization of experimental variables and the correction of resolution induced effects.

In appendix, various projects not having an immediate relevance to this research are discussed, i.e. triple-axis spectrometer automation by paper tape, compilation of a bibliography covering most of the literature concerning thermal neutron scattering, various computer programmes.

ACKNOWLEDGMENTS

The research reported in this thesis was done under the supervision of Dr. B. N. Brockhouse. He has provided me with the opportunity of discovering the ecstasy derivable from the measurement of those evanescent entities known as phonons.

The experiments were performed on the McMaster triple-axis spectrometers, both at Chalk River and on campus. These two instruments were kept in perfect condition and continuously improved thanks to the electronics expertise of Mr. J. Couper.

The technical problems encountered during the construction of the neutron scattering oven were often times discussed with Dr. A. Becker and Messrs. D. Hodgson and H. Newmayer. They provided an immense store of technical knowledge which they were always happy to share.

The required machine shop work was done by the Senior Sciences Complex machinists, Gino, Jeff, Michael and Wilhem under the wise guidance of Mr. S. Kocsis who could make sense of rather vague drawings and specifications. It is also a pleasure to acknowledge the patient instructions of Mr. L. Hensher in the art of being a machinist and a musician.

Mr. Jake Vanderwal has shown a truly remarkable sense of duty in his work on "THE" bibliography (see appendix III). Without his contribution, this compilation would never have reached a status suitable for publication and a cumulated time of approxi-

mately one and a half years of my life would have been lost on a dead-end project. Jake, you came as a blessing.

During the various trips to Chalk River, I have enjoyed instructive and diversified discussions with Drs. W.J.L. Buyers (re: music and physics), G. Dolling (re: skiing and physics), T. M. Holden (re: literature and physics), P. Martel (re: politics and physics), L. Piseri (re: international affairs and physics), B.T.M. Powell (re: humour and physics), E.C. Svensson (re: animal kingdom and physics) and A.D.B. Woods (re: Newfoundland, France and physics). Technical assistance when needed was always provided efficiently and courteously by their technical associates, Messrs. R. Campbell, H. Nieman and M. Potter.

Much gratitude is due to AECL for making available the extraordinary facility located at the NRU reactor.

My colleagues within the neutron physics group have provided a congenial atmosphere. Of these, Messrs. J.R.D. Copley, W.A. Kamitakahara and R.R. Dymond should be mentioned: the first one for sharing his vast knowledge of computers, the second one for telling me all that I ever wanted to know about triple-axis spectrometry but was afraid to ask and the third one for helping to maintain some form of sanity within the group.

Those familiar with the Physics department of this university will recognize, from the quality of the typescript, the touch of Mrs. H. Kennelly who has metamorphosed a difficult manuscript. For this, I am grateful, as well as for her secretarial assistance in

the initial stages of the compilation of "THE" bibliography discussed in appendix III.

The financial assistance coming from a McMaster University Graduate Fellowship has insured my subsistence while providing me with very few temptations to deviate from my ascetic philosophy.

Finally, I would like to thank the makers of "Snopake" correction fluid and "Scotch" magic transparent tape for making available such truly useful products. Yes, some American influence can be good.

This thesis is dedicated to my parents.

TABLE OF CONTENTS

LIST OF TABLES

LIST OF FIGURES

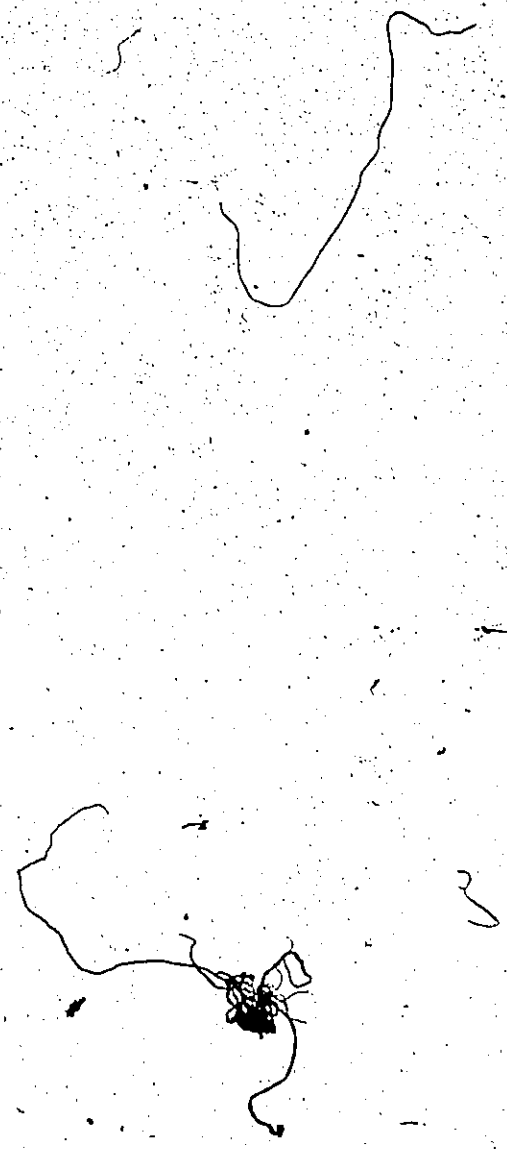

The wisest person amongst you is the one who, like Socrates, has recognized the fact that, in truth, his knowledge is worth nothing.

Plato: Apology of Socrates.

CHAPTER I

INTRODUCTION

The modern theory of solids has convincingly established the concept of phonons. Although such a concept is really quantum mechanical in nature, its acceptability by the solid state physicists community is now in no way less wide-spread than that of other more classical ideas. It has provided a key to a successful interpretation of thermodynamic data, as well as of some of the manifestations of the interactions between condensed matter and external radiation, mainly X-rays, infrared light and neutrons. However, it must be remembered that, whilst the early study of thermodynamic properties provided the initial support in favor of the bold application of the quantum theory to the fundamental understanding of condensed matter [EI07], it was not until the advent of technologies making possible neutron fluxes of sufficient intensity that actual measurements could be carried out on individual phonons. Hence, instead of determining a quantity which is a statistical average over all phonon states, as in the case of calorimetric measurements, the technique of thermal neutron scattering made possible the mapping of phonon spectra throughout the whole of the Brillouin zone, thus providing a much greater insight at the microscopic level [BA53; LO54].

In what follows, we will discuss from the point of view of an experimentalist, the results obtained about the behaviour of phonons in a metal at elevated temperatures, and particularly near the melting point. One may ask: what happens to the phonon spectrum as the melting temperature is approached from below? We know, for example, that at the melting point, the long range order (characteristic of crystalline solids) disappears, leaving only short range order (characteristic of the liquid phase). Obviously, such a drastic transformation in the structure is bound to have profound consequences on the phonon spectrum. Not so evident is the effect of temperature on the eigenfrequencies within the solid phase and particularly in the vicinity of the melting point. If a strictly harmonic theory of solids were a true representation of the physical reality, i.e. if the interatomic potential were well approximated by a quadratic function of the displacements from equilibrium, the answer to the above question would be simple: the eigenfrequencies of the normal modes would be temperature independent and the phonon lifetimes, infinite. This is a consequence of the total absence of phonon-phonon interaction in the harmonic formalism.

On the other hand, we know that the harmonic theory is an idealization of reality: it cannot possibly account for the phenomena of thermal expansion, nor the behaviour of the specific heat at high temperatures, nor the fact that the adiabatic and isothermal elastic constants are numerically different as well

as temperature and pressure dependent [KI67, p.180]. These phenomena, which are all indirect manifestations of phonon-phonon interactions, were well documented before the advent of thermal neutron spectroscopy. However, as we said before, only by probing a solid with thermal neutrons can we observe directly and unambiguously the normal modes eigenvalues and lifetimes. And this is the subject of this research.

Already some neutron scattering work in the anharmonic regime has been performed in the case of metals having a relatively low melting temperature. However, this field of research has been receiving much less attention than the study of phonons in systems at room temperature or below [LA74, section 10A]. This probably reflects the larger degree of complexity, both from the technical as well as the theoretical point of view. Some of the "high" temperature work on the elements so far, has included the following substances: Al at $T \approx 625°C$ [LA60], Bi at $T \approx 270°C$ [TU68], Fe at $T < 874°C$ [GO73], Ge at $T \leq 607°C$ [NE74], Nb at $T < 775°C$ [PO72], Pb at $T \leq 152°C$ [BR60A] and Zr at $T \leq 800°C$ [MO73]. One notable exception to this list is graphite which has been investigated up to 1920°C [PA67; PA68; BR72; RO73].

The temperature dependence studies reported in this thesis are concerned with copper and, to a lesser extent, palladium and were performed using triple-axis neutron spectrometry. The temperature was varied between room temperature and 1076°C in the case of Cu and 1050°C in the case of Pd; the respective melting temperatures are 1083°C and 1552°C [E5]. The

point of view will be that of an experimentalist. The reader should not expect to discover in this text theoretical concepts which are either original or of a high level of abstraction. Rather, the goal was to obtain an extensive set of high quality data and every effort was made to achieve this. At the risk of sounding presumptous, one could make an analogy between these results and those patiently and carefully accumulated by Tycho Brahé; it is now up to some modern Kepler to supply a satisfactory theoretical interpretation. Consequently, the content of this thesis will reflect a rather pragmatic approach. The theory will be kept at a minimum by avoiding derivations which are judged superfluous and which can readily be found elsewhere. It seems reasonable also to assume that the reader is familiar with the physics of the solid state and the technique of triple-axis neutron spectroscopy; this will allow us to go early to the heart of the subject. Hence, we will avoid discussing basic solid state concepts, historical notes, descriptions of standard equipment and procedures as well as the relative merits of neutron beams as probes of condensed matter.

This thesis is divided along the following lines. The theory is to be found in the next chapter (chapter II) where we will consider in turn generalities about metals, and various aspects of crystal dynamics in the harmonic and anharmonic theory. Then we will briefly discuss the theory of the Kohn effect and the difference between first and zero sound. Finally, we will

terminate this chapter by reviewing the theory of the neutron-phonon interaction, the considerations behind the optimization of experimental variables and the adopted procedure for the correction of resolution effects. Chapter III is strictly technical and contains a description of the high temperature apparatus. Chapters IV, V and VI discuss the results in copper, palladium and tungsten respectively; in this latter instance measurements were only made at room temperature in order to search for a predicted Kohn effect [RI70] and to verify the published data [CH64]. In the appendices, projects which do not have an immediate relationship with the physics of this thesis are described.

* * * * * * * * * *

Before terminating this brief introduction, a few words should be said about the adopted notation. The references listed in the bibliography at the end of the thesis are indicated by a code within rectangular brackets [ ]. There are four types of such references, dealing with techniques, handbooks, general and specific references, and they are grouped accordingly in the final bibliography. This bibliography lists each specific reference in a condensed manner and includes, if possible, key words from each title and, in the case of neutron papers, the address in the volume "Scattering of Thermal Neutrons: A Bibliography (1932-1974)" [LA74] where more information may be obtained.

The notation adopted is this thesis is the conventional one. In the case where custom symbols were required, the reader will be referred to the table below where these symbols are defined once and for all.

Table I-1. List of important symbols.

- a: lattice parameter
- $A(\lambda)$: phonon coordinate
- BZ: Brillouin zone
- c: phonon group velocity
- C_ν (C_ζ): correction to experimentally observed ν (ζ)
- $C_{2\Gamma_\nu}$ ($C_{2\Gamma_\zeta}$): correction to experimentally observed linewidth in ν (ζ)
- $e(\lambda)$: polarization vector of mode λ
- E_o (E'): incident (scattered) energy
- E_F: Fermi energy
- k: wavevector
- k_B: Boltzman constant
- k_F: Fermi wavevector
- k_o (k'): incident (scattered) wavevector
- m: neutron mass
- M: atom mass
- m_e: electron mass
- $n(\lambda)$: population factor of mode λ
- q: wavevector in BZ
- $\hbar Q$: momentum transfer
- $Q(\lambda)$: normal coordinate
- S: entropy
- T: temperature
- T_m: melting temperature
- u_i^m: i^{th} component of the displacement vector from the equilibrium position at site m
- Ze: ionic charge
- ζ: reduced wavevector
- χ: generalized susceptibility
- ω_D: Debye circular frequency
- θ_D: Debye temperature
- $h\nu=\hbar\omega$: harmonic phonon energy
- $\hbar\Omega$: energy transfer
- $\Delta(\lambda,\Omega)$: frequency shift w.r.t. the harmonic frequency
- $2\Gamma(\lambda,\Omega)$: phonon energy width
- λ: wavelength
- (λ): mode (q,j); j:branch number
- λ_o (λ'): incident (scattered) λ
- ν_o (ν'): incident (scattered) neutron frequency
- $\omega(q)$: dispersion relation
- ϑ (ζ): fixed value of ν (ζ) during a scan
- ν_x (ζ_x): experimentally observed value of ν (ζ)
- $2\Gamma_{\nu x}$ ($2\Gamma_{\zeta x}$): experimentally observed value of the linewidth in ν (ζ)
- $\Delta\nu$ ($\Delta\zeta$): uncertainty on ν (ζ)
- ν (ζ): intrinsic value of ν (ζ)
- $2\Gamma_\nu$ ($2\Gamma_\zeta$): intrinsic value of the linewidth in ν (ζ)
- α_1 (α_2): horizontal collimation in the incident (analysed) beam
- β_1 (β_2): vertical collimation in the incident (analysed) beam
- $2\theta_m$ ($2\theta_a$): monochromator (analyser) scattering angle

Note: Contrary to common practice, absolute temperature units were abreviated as [K], not [°K]; this follows the convention adopted in the S.I. system of units. It should be noted, however, that the symbol [°C] holds for Celsius degrees, in order to avoid confusion with the one for the unit of charge, the Coulomb [C].

CHAPTER II

THEORETICAL BACKGROUND MATERIAL CONCERNING PHONONS IN METALS AND THEIR MEASUREMENT BY NEUTRON INELASTIC SCATTERING

A - GENERAL CHARACTERISTICS OF METALS

Solids are, by definition, a phase of condensed matter with a resistance to shear strains and, depending on their macroscopic electrical properties, they can be classified into four main classes, i.e. metals, semimetals, semiconductors and insulators. A metal is characterized by a large electrical conductivity which decreases at high temperatures and a semimetal has similar properties except for a much smaller population of conduction electrons, perhaps by as much as 10^{-4}. On the other hand, an insulator carries a negligible current under the influence of a typical macroscopic electric field as a result of having a completely filled valence band which is separated from an empty "conduction" band by a gap much larger than $k_B T \cong 30$ meV (at $T \cong 300$ K). The fourth and last class, i.e. semiconductors, has qualitative similarities with insulators except that, in this case, electrical conductivity increases with temperature as a result of a much smaller band gap. With such a wide range of values, it is not surprising then that, of all physical properties, it is effectively the electrical conductivity which spans the largest range, i.e. 24 orders of magnitude, between that of a good conductor, i.e. silver, and

that of a good insulator, i.e. fused quartz [MO58].

Solids can also be classified according to the nature of the binding at the atomic (microscopic) level, and here again there are also four classes, i.e. the ionic, Van der Waals, covalent and metallic types. In the first two types, the solid may be regarded as being made up of saturated units whereas the "building blocks" of the other two types are non-saturated units. In this context, a unit is said to be saturated if it is made up either of atoms having a rare gas configuration or of chemically saturated molecules. Born and Huang [BO54] explain that "speaking physically, one can picture that the electronic wave functions of unsaturated units, when brought together, are liable to be drastically altered" whereas, for the saturated units, comparatively little alteration takes place. One can relate these properties to the macroscopic property (i.e. conductivity) already discussed by noting that ionic solids are typical insulators* while metallic binding implies the presence of a (partially filled) conduction band, resulting in a correspondingly high electrical conductivity.

There is one attribute which fortunately is common to the vast majority of solids and which is of fundamental importance in any attempt to gain some theoretical insight at the microscopic levels. This attribute is the presence of long range order. This, however, does not mean that all solids are perfect crystals! Rather, they are most commonly

*) This statement for ionic solids is true as far as the electronic contribution to the electrical conductivity is concerned; it does not apply to the ionic contribution, which increases with temperature.

encountered under a polycrystalline form. But, the structure which is thermodynamically the most stable, is the one which has the lowest Gibbs free energy (U + PV - TS). [BO54,p.154]; it is indeed fortunate, then, that such a stable configuration in solids is generally one having also some form of periodicity. This property has provided astounding simplifications in the mathematics of the many-body problems peculiar to solid state physics and, without this good will gesture on the part of nature, our understanding of the solid phase would probably be as sketchy as the one that we now have of the liquid phase, where no such long range order is present.

What are the implications of long range order? It means that, by definition, the solid is invariant under a group of translation operations. Such a translation operation can be explicitly represented by an integer vector sum of three (non-coplanar) primitive translation vectors $\underset{\sim}{\tau}_1, \underset{\sim}{\tau}_2$ and $\underset{\sim}{\tau}_3$, i.e.

$$\underset{\sim}{T}(n_1,n_2,n_3) = \sum_{i=1}^{3} n_i \underset{\sim}{\tau}_i \quad (n_i:\text{integers}) \quad (A1)$$

It also means that, associated with each type of real space lattices, there exists a reciprocal (or wavenumber) lattice. Such a lattice forms an indispensable element for the mathematical representation of the translation group of the real lattice as we will see below. The three primitive wavenumber vectors are of the form

$$\underset{\sim}{k}_i = \frac{2\pi}{v} (\underset{\sim}{\tau}_j \wedge \underset{\sim}{\tau}_k) \quad (A2)$$

where $v = \underset{\sim}{\tau}_1 (\underset{\sim}{\tau}_2 \wedge \underset{\sim}{\tau}_3) \neq 0$ is the volume of the unit cell in real space and (i,j,k) form a cyclic permutation of the indices (1,2,3).

Any function of the position coordinates (e.g. electron wavefunctions, phonon wavefunctions, etc.....) within the crystal must reflect the periodicity of the lattice. Since the translation group (not necessarily the space group, however) is an abelian group, i.e. its elements all commute with each other, we know, from group theory [KO57, p.212], that its irreducible representation is one-dimensional and is of the form

$$D^{(\underset{\sim}{k})}(\underset{\sim}{T}_n) = e^{-i\underset{\sim}{k}\cdot\underset{\sim}{T}_n} \qquad \text{(A3)}$$

Each wavevector "$\underset{\sim}{k}$" is said to belong to a different irreducible representation of the group.

A general theorem, having its origin in pure mathematics (Floquet's theorem) and extended by Bloch [BL28] to physical applications, concerns the general functional form of a lattice function which is shown to be of the form

$$\psi_{\underset{\sim}{k}}(\underset{\sim}{r}) = e^{i\underset{\sim}{k}\cdot\underset{\sim}{r}}\, u_{\underset{\sim}{k}}(\underset{\sim}{r}) \qquad \text{(A4)}$$

where $u_{\underset{\sim}{k}}$ has the full periodicity of the lattice.

So far, no mention was made of the finite dimensions of any macroscopic crystal and hence, of the finite number of lattice points and degrees of freedom. A convenient quantization procedure, taking this into account, is based on the cyclic boundary conditions of Born [BO54, p.45], whereby the specimen is considered as a parallelipiped of dimensions

$(N_1\tau_1)x(N_2\tau_2)x(N_3\tau_3)$. Hence, in equation (A1), we have

$$0 \leq n_i \leq N_i \qquad \text{(A5)}$$

and the total number of lattice sites in the specimen (i.e. the total number of possible translation operations) is $N_1N_2N_3$. Born's cyclic (or periodic) boundary conditions restrict any wavevector dependent function of the crystal to wavevectors of the form

$$\underset{\sim}{k} = \sum_{i=1}^{3} \frac{n_i}{N_i} \underset{\sim}{k}_i \qquad (n_i: \text{integers} \leq N_i) \qquad \text{(A6)}$$

Because of the fact that $N_1N_2N_3$ is of the order of Avogadro's number, the geometrical aspects of the volume chosen for the application of such boundary conditions are unimportant. This can be proven formally and the result is known as Ledermann's theorem which states that only a fraction of order $1/\sqrt[3]{N_1N_2N_3}$ of the frequencies will enter or leave any frequency interval when we change from one boundary condition to another and this is negligible for any macroscopic specimen [MA63, p 21; MA71, p 43].

From equations (A3), (A5) and (A6), we see that there are as many irreducible representations as there are symmetry operations in the translation group. Thus, the Brillouin zone contains the same number of allowed wavevectors as there are primitive cells within the crystal and this is a fact of great significance when considering the occupation of band states by electrons.

The subject of this thesis will be exclusively concerned with metals and, from here on, the theoretical considerations of this chapter will be restricted accordingly. A brief review of metallic properties seems to be appropriate at this point in order to set the stage for the discussion of lattice dynamical aspects which will follow.

All metals are crystalline in nature and most of them tend to have a close-packed structure [HA70, p.2]. The most common metallic structures are FCC, HCP and BCC*. In this thesis, two of the metals studied (Cu and Pd) are FCC and the third one (W) is BCC. Certainly, a few metals like Mn and Hg do occur in more complicated structures but these are the exceptions rather than the rule. However, like those with a simpler structure, they are characterized by a dense packing. Harrison [HA70, p.5] points out that "the essential feature of the metallic structure is its close packing rather than the details of its structure. If a metal is melted, it loses all of its crystalline order but remains in a rather close-packed configuration. Even with this total loss of crystalline structure, however, the electrical properties remain very much the same."

Within a metal, the electronic distribution reflects this dense packing and valence (i.e. conduction) electrons tend to be uniformly distributed throughout, except in the immediate vicinity of the nuclei where the density resulting from the core electrons is large. This nearly uniform distribution leads to energy bands which are not drastically different from

*) Although BCC is a commonly occurring metallic structure, it is not a close-packed structure.

those predicted by the nearly free electron gas model (NFE) even though the potential at the sites of the nuclei is far from negligible [MO58, p.59]. Conduction electron wavefunctions reflect this strong interaction by showing large oscillations in the vicinity of the nuclear sites and this requires that they be represented as a sum of a large number of components, possibly 10^6 [HE70, p.14;CO70, p.42] if a plane wave expansion is used. Such an approach leads to a slow convergence and is utterly impractical. Heine [HE70,p.6] also mentions the fact that a band structure calculation will yield for the lowest energy eigenvalues, not the NFE conduction bands, but the absolute lowest eigenvalue in the given potential, i.e. the tight-binding band of 1s atomic orbitals at $E \approx -1000$ eV. In such an approach, the lowest NFE band is obtained after all levels corresponding to the core states have been calculated.

Fortunately, it is possible to transform Schrödinger's equation in such a way that the conduction electron eigenfunctions are greatly simplified while their eigenvalues are largely unaffected. Such a wavefunction is called a pseudo-wavefunction and it has the property that it is identically equal to the real wavefunction outside the atomic cores while extending smoothly (i.e. without strong wiggles) inside the core. If a pseudopotential is well chosen ("by interpolating, extrapolating, cajoling and cudgeling, one should be able to produce a useful pseudopotential for many elements in many situations" [CO70,p.40]), a well-behaved wavefunction will result which

will require in general much less than 100 terms in the summation for a suitable convergence. The great advantage of this formalism, however, lies in the fact that such a pseudopotential is often times sufficiently weak for perturbation theory to yield a rapid convergence.

Strictly speaking, the pseudopotential formalism is not applicable to transition metals where the "d" or "f" bands are neither free-atom-like (and hence cannot be considered as core states), nor free-electron-like (hence indicating that the required pseudopotential is not a small perturbation like in the case of the alkali). However, by using a slightly different approach, it has been possible to generalize the pseudopotential method for simple metals to transition metals [HA69] in such a way as to make possible the use of perturbation theory.

The method is based on the fact that, for a pseudopotential treatment of a transition metal like copper, we cannot include atomic "d" states with the cores since the atomic states are not solutions in the metal, yet the "d"-like states are sufficiently strongly localized that their expansion in plane waves would be slowly convergent [HA70, p.201]. However, when the problem is formulated in terms of an expansion in an "over-complete" set of wavefunctions including atomic "d" states, one can obtain a rapidly converging expansion of the "d"-like wavefunctions [DE67]. The details of this type of calculations are outside the scope of this thesis.

B - SOME ASPECTS OF THE CRYSTAL DYNAMICS OF METALS

The thermal vibrations of the nuclei in the vicinity of their respective equilibrium lattice sites largely determine the thermodynamic properties of solids and their spectrum depends on the internal (i.e. interatomic) potential. This interatomic potential, being a function of all nuclear and electronic space coordinates (i.e. "$\underset{\sim}{R}$" and "$\underset{\sim}{r}$" respectively) may be written as:

$$H(\underset{\sim}{R},\underset{\sim}{r}) = H_i(\underset{\sim}{R}) + H_e(\underset{\sim}{r}) + H_{i-e}(\underset{\sim}{R},\underset{\sim}{r}). \qquad (B1)$$

A Schrödinger equation may be written for such a many-body system and solved formally [BO54, p.166].

After separation of variables, the problem can be simplified if one assumes that the electrons, because of their small mass relative to that of the nuclei, will respond quasi-instantaneously to the local distortions created by the lattice waves. Hence, the set of nuclear coordinates acts only as a group of parameters in the electronic wavefunctions. Physically, this means that no modulation of the lattice is rapid enough to cause electronic transitions.

This is the basis for the adiabatic approximation first introduced by Born and Oppenheimer [BO27] and, as such, this is really an extension of a well known result from the theory of molecules [SL51, appendix 18]. In such cases, the assumption of an absence of transitions between electronic eigenstates is justified when

$$V\hbar/\ell \ll \Delta E \qquad (B2)$$

where "V" is a characteristic velocity of the nuclei, "ℓ" is the distance by which the nuclei have to move to produce an appreciable change in the ground state wavefunction and "ΔE" is the energy difference between the first excited electronic level and the ground state, at fixed values of the nuclear coordinates [PE55, p.5].

This criterion alone would tend to exclude metals from the domain of applicability of the adiabatic approximation as a result of the infinitely small energy separation of electron states in the conduction band. For this reason, Peierls [PE55, p.6] has concluded that the adiabatic approximation is not applicable to metals. However, this view is not shared universally and many other authors have invoked other considerations to prove otherwise [e.g. BO54;CO64]. In particular, Migdal [MI58] has shown that the adiabatic parameter is the ratio $\hbar\omega_D/E_F$, where ω_D is the Debye frequency and E_F is the Fermi energy. When this parameter is small, the adiabatic approximation is valid for metals; in what follows, the validity of this approximation will be taken for granted since $\hbar\omega_D/E_F \approx 0.005$ for most metals.

Consider an ideal crystal, with one atom per unit cell, where each lattice site is occupied by the same type of atoms. As a consequence of the adiabatic approximation, there exists a potential for the nuclei, and this potential is only a func-

tion of the set of nuclear coordinates.

Such a potential can be expanded in a Taylor series in terms of the displacement "$\underset{\sim}{u}^{(m)}$" around each equilibrium position ($\underset{\sim}{R}^{(m)}$) of the nuclear coordinates:

$$\Phi(\{\underset{\sim}{R}^{(m)}+\underset{\sim}{u}^{(m)}\}) = \phi_0 + \phi_1 + \phi_2 + \phi_3 + \phi_4 + \ldots \qquad \text{(B3)}$$

where

$$\phi_0 = \Phi(\{\underset{\sim}{R}^{(m)}\}) \qquad \text{(B4-0)}$$

$$\phi_1 = \sum_{\substack{m \\ i}} \phi_i^m u_i^m \qquad \text{(B4-1)}$$

$$\phi_2 = \frac{1}{2} \sum_{\substack{mn \\ ij}} \phi_{ij}^{mn} u_i^m u_j^n \qquad \text{(B4-2)}$$

$$\phi_3 = \frac{1}{3!} \sum_{\substack{mnp \\ ijk}} \phi_{ijk}^{mnp} u_i^m u_j^n u_k^p \qquad \text{(B4-3)}$$

$$\phi_4 = \frac{1}{4!} \sum_{\substack{mnpq \\ ijk\ell}} \phi_{ijk\ell}^{mnpq} u_i^m u_j^n u_k^p u_\ell^q \qquad \text{(B4-4)}$$

and u_i^m is the i^{th} component of the nuclear displacement from the equilibrium position "$\underset{\sim}{R}^{(m)}$" at site "m".

This is a general formulation, free of any assumptions concerning the nature of the interatomic potential and forms the basis for the Born-von Kármán theory [BO12]. The coefficients of the n^{th} order terms are tensors of rank "n" which represent the n^{th} order derivatives of the potential, evaluated at the equilibrium positions; these are known as atomic force constants (AFC's) or coupling parameters (CP's).

Various general considerations can be used to reduce the number of independent AFC's; this has been discussed at length by numerous authors [LE61; MA63; MA71; BR67]. Invariance under infinitesimal translations or rotations of the crystal as a whole must be satisfied by the AFC's since the potential Φ is a function of relative, not absolute, positions. In particular, translational invariance yields relationships of the form

$$\sum_m \phi_i^m = 0 \qquad \text{(B5-1)}$$

$$\sum_m \phi_{ij}^{mn} = 0 \qquad \text{(B5-2)}$$

$$\sum_m \phi_{ijk}^{mnp} = 0 \; . \qquad \text{(B5-3)}$$

Rotational invariance, on the other hand, interconnects AFC's of n^{th} and $(n+1)^{th}$ order.

Furthermore, from the various symmetry operations which transform the lattice into itself, it follows that the AFC's are not specifically functions of the absolute site indices but of their differences. For example

$$\phi_i^m = \phi_i^0 \qquad \text{(B6-1)}$$

$$\phi_{ij}^{mn} = \phi_{ij}^{(m-n),0} \qquad \text{(B6-2)}$$

Finally, consideration of all possible point group operations further reduces the number of independent coefficients in the tensor corresponding to the n^{th} neighbour force constants; for example,

there are only 3 first neighbour and 2 second neighbour AFC's in a FCC crystal.

Within a lattice, nuclear displacements are known to be restricted to a small range, even in the vicinity of the melting point where

$$\sqrt{\langle u^2 \rangle} / a \gtrsim 0.1 \qquad \text{(B7)}$$

for most solids; this is the basis for Lindeman's criterion[LI10] which assumes that melting occurs when the RMS amplitude of vibrations reaches a certain common fraction of the interparticle spacing*, typically 0.071 (0.113) for FCC (BCC) lattices [SH70]. The HARMONIC THEORY makes use of this fact and neglects all terms in (B3) of higher order than the quadratic terms. This results in an enormous simplification which provides a starting point to compare theory with experiment, at least in the low temperature regime. We will avoid tedious repetitions of well known derivations [MA63] and list only the most important equations of the Born-von Kármán theory in the harmonic regime, (for a perfect lattice with one atom of mass M per primitive cell).

- Equilibrium requirement $\quad \phi_i^m = 0 \qquad \text{(B8-1)}$
- Kinetic energy of the system $\quad T = \frac{M}{2} \sum_{m,i} (\dot{u}_i^m)^2 \qquad \text{(B8-2)}$
- Hamiltonian of the system $\quad H_o = T + \phi_0 + \phi_2 \qquad \text{(B8-3)}$
- Dynamical Equation $\quad -M\ddot{u}_j^n = \frac{\partial H}{\partial u_j^n} = \sum_{i,m} \phi_{ij}^{mn} u_i^m \qquad \text{(B8-4)}$
- Particular solution $\quad \underset{\sim}{u}^m = \frac{\underset{\sim}{e}(\lambda)}{\sqrt{M}} \exp\{i(\underset{\sim}{q}\cdot\underset{\sim}{r}_m - \omega(\lambda)t)\} \qquad \text{(B8-5)}$

*) An example of a related quantity which is also correlated with the melting temperature is the self-diffusion activation energy [AS70].

- Eigenvalue equation $\omega^2 e_i(\lambda) = \sum_j D_{ij}(q) e_j(\lambda)$ (B8-6)

- Dynamical matrix $D_{ij}(\underset{\sim}{q}) = \frac{1}{M} \sum_\ell \phi_{ij}^{0\ell} \{\exp(-i\underset{\sim}{q}\cdot\underset{\sim}{r}_\ell)\}$ (B8-7)

- Eigenvalues $\omega \equiv \omega(\lambda)$ (B8-8)

N.B.: $-\lambda \equiv (\underset{\sim}{q}, j)$; $j = 1, 2, 3$

-The dispersion surface is defined as the set of points in the 4-dimensional $(\underset{\sim}{q},\omega)$ space where the dispersion relation (B8-8) is satisfied.

The same considerations as in section II-A concerning the finite number of degrees of freedom of periodic excitations are valid in the case of the phonon gas; the cyclic boundary conditions yield 3N possible allowed wavevectors distributed uniformly within the first Brillouin zone.

Strictly speaking, the Born-von Kármán theory of crystal dynamics is not a first-principle theory, since the various AFC's are determined by fitting to experimental data. Just the same, it is a powerful approach because of the fact that it makes possible the calculation of phonon eigenfrequencies and eigenvectors throughout the whole of the Brillouin zone and,hence,of various phonon related properties, e.g.superconducting transition temperature [CA69].

The expression for the Hamiltonian in the harmonic theory being a quadratic function of the displacement coordinates and momenta, such an expression can be diagonalized by transforming to normal coordinates [GO51] which are usually defined by the following relation:

$$u_i^m = \frac{1}{\sqrt{NM}} \sum_\lambda e_i(\lambda) Q(\lambda) \exp\{i\underset{\sim}{q}\cdot\underset{\sim}{r}\}. \qquad \text{(B9)}$$

In terms of these normal coordinates, the Hamiltonian (B8-3) now can be written as

$$H = \frac{1}{2} \sum_\lambda \{\dot{Q}^*(\lambda)\dot{Q}(\lambda) + \omega^2(\lambda) Q^*(\lambda) Q(\lambda)\}. \qquad \text{(B10)}$$

This is the familiar expression for the Hamiltonian of a set of harmonic oscillators. As equation (B9) illustrates, the general motion within the crystal is given as a superposition of normal coordinates, each weighted by the coefficient $e(\lambda)\exp\{i\underset{\sim}{q}\cdot\underset{\sim}{r}\}$. The total number of normal modes is the same as the total number of degrees of freedom of the lattice.

Once the eigenfrequencies are known for an ensemble of harmonic oscillators, the various thermal properties can be calculated. This requires a summation over all the normal modes and this is conveniently performed by defining a quasi-continuous frequency distribution

$$g(\omega) = \sum_{j=1,2,3} \int_{BZ} \delta(\omega - \omega(\underset{\sim}{q},j))\, d\underset{\sim}{q}\,. \qquad \text{(B11)}$$

This leads to the following expression for the Helmholtz free energy

$$F = 3Nk_BT \int_0^{\omega_{max}} \ln\{2 \sinh(\frac{\hbar\omega}{2k_BT})\} g(\omega)\, d\omega \qquad \text{(B12)}$$

from which other functions may be calculated in a straight-

forward manner.

- internal energy: $U = F - T \left(\frac{\partial F}{\partial T}\right)_V$ (B13-1)

- specific heat at constant volume: $C_V = \left(\frac{\partial U}{\partial T}\right)_V$ (B13-2)

- entropy: $S = -\left(\frac{\partial F}{\partial T}\right)_V$ (B13-3)

The elegance of the harmonic theory is largely due to the uncoupled nature of the normal modes; this however is also an indication of its limitations. Indeed, it is "a priori" conceivable that, at low temperatures, where very few phonon states are populated, the phonon-phonon interaction may be a phenomenon altogether negligible. Surely, this is not so near the melting point and we must consider a strictly harmonic theory to be a first, albeit possibly very good, approximation to a real physical system.

Obviously then, the neglect of high order terms in (B3) becomes less and less justifiable as a solid approaches its melting point. In chapter I, the severe limitations of the harmonic theory were briefly mentioned; the inadequacies of the harmonic theory usually start to manifest themselves at temperatures above θ_D. Moreover, as we said before, rotational invariance forbids a strictly harmonic theory ($\phi_3 = \phi_4 = \ldots 0$) on the grounds that, since the AFC's of n^{th} and $(n+1)^{th}$ order are interconnected, it leads to an isotropically elastic model with a negative compressibility [LE61, pp.285,297].

Some progress can be achieved if one considers high order terms in equation (B3). Since ϕ_3 and ϕ_4 introduce effects of comparable magnitudes, they must be considered together in a perturbation calculation ; similarly for ϕ_5 and ϕ_6 [LE61,p.283]. In practice, inclusion of terms up to ϕ_4 is found to be sufficient in most calculations.

The complexity of the mathematics in the anharmonic theory is rather formidable and will not be dealt with here. However, we will remark that a "simplified" formulation is possible within the framework of the quantum field theory [CO63]. In this context, a natural variable turns out to be a linear combination of phonon creation and annihilation operators ($a(q,j)$ and $a^*(-q,j)$), i.e.

$$A(q,j) = a(q,j) + a^*(-q,j) = A(\lambda) \quad . \qquad \text{(B14)}$$

The operator "A" is known as the phonon coordinate.

The Hamiltonian can now be written as a sum of an harmonic component H_o and an anharmonic component H_a where

$$H_o = \frac{1}{2}\hbar \sum_{\lambda} \omega(\lambda)\{a(\lambda)a^*(\lambda)+a^*(\lambda)a(\lambda)\} \qquad \text{(B15-1)}$$

and

$$H_a = \sum_{\lambda_1\lambda_2\lambda_3} V(\lambda_1\lambda_2\lambda_3)A(\lambda_1)A(\lambda_2)A(\lambda_3)$$

$$+ \sum_{\lambda_1\lambda_2\lambda_3\lambda_4} V(\lambda_1\lambda_2\lambda_3\lambda_4)A(\lambda_1)A(\lambda_2)A(\lambda_3)A(\lambda_4)$$

$$+ \ldots \qquad \text{(B15-2)}$$

The anharmonic coefficients can be expressed in terms of those of Born and Huang [BO54, p.304]:

$$V(\lambda_1\lambda_2\lambda_3) = \frac{1}{6}\,\Delta(\underset{\sim}{q}_1+\underset{\sim}{q}_2+\underset{\sim}{q}_3)\left[\frac{\hbar^3}{8N\omega(\lambda_1)\omega(\lambda_2)\omega(\lambda_3)}\right]^{1/2}\Phi(\lambda_1\lambda_2\lambda_3) \qquad \text{(B16-1)}$$

and

$$V(\lambda_1\lambda_2\lambda_3\lambda_4) = \frac{1}{24}\,\Delta(\underset{\sim}{q}_1+\underset{\sim}{q}_2+\underset{\sim}{q}_3+\underset{\sim}{q}_4)\left[\frac{\hbar^4}{16N^2\omega(\lambda_1)\omega(\lambda_2)\omega(\lambda_3)\omega(\lambda_4)}\right]^{1/2}\Phi(\lambda_1\lambda_2\lambda_3\lambda_4) \qquad \text{(B16-2)}$$

where

$$\Phi(\lambda_1\lambda_2\lambda_3) = \frac{1}{M^{3/2}}\sum_{\alpha}\sum_{\ell'\beta}\sum_{\ell''\gamma}\Phi^{0\ell'\ell''}_{\alpha\beta\gamma}\,e_\alpha(\lambda_2)e_\beta(\lambda_1)e_\gamma(\lambda_3)$$

$$\times\ \exp\{i[\underset{\sim}{q}_2\cdot\underset{\sim}{R}(\ell') + \underset{\sim}{q}_3\cdot\underset{\sim}{R}(\ell'')]\} \qquad \text{(B16-3)}$$

and

$$\Phi(\lambda_1\lambda_2\lambda_3\lambda_4) = \frac{1}{M^2}\sum_{\alpha}\sum_{\ell'\beta}\sum_{\ell''\gamma}\sum_{\ell'''\delta}\Phi^{0\ell'\ell''\ell'''}_{\alpha\beta\gamma\delta}\,e_\alpha(\lambda_1)e_\beta(\lambda_2)e_\gamma(\lambda_3)e_\delta(\lambda_4)$$

$$\times\ \exp\{i[\underset{\sim}{q}\cdot\underset{\sim}{R}(\ell') + \underset{\sim}{q}_2\cdot\underset{\sim}{R}(\ell'') + \underset{\sim}{q}_3\cdot\underset{\sim}{R}(\ell''')]\} \qquad \text{(B16-4)}$$

These expressions do not convey much intuitive meaning, even though they have been written in a "simplified" form appropriate to a perfect lattice with only one type of atom (of mass M) per unit cell.

We finally write down the expressions for the frequency shift $\Delta(\lambda,\Omega)$, relative to the harmonic frequencies, and half-width $\Gamma(\lambda,\Omega)$ of a mode $\lambda \equiv (\underset{\sim}{q},j)$ driven by a probe of circular frequency Ω:

$$\Delta(\lambda,\Omega) = -\frac{18}{\hbar^2}\sum_{\lambda_1\lambda_2}\left|V(\lambda,\lambda_1,\lambda_2)\right|^2$$
$$\times\left\{\frac{n_1+n_2+1}{\omega_1+\omega_2+\Omega}+\frac{n_1+n_2+1}{\omega_1+\omega_2-\Omega}+\frac{n_2-n_1}{\omega_1-\omega_2+\Omega}+\frac{n_2-n_1}{\omega_1-\omega_2-\Omega}\right\}$$
$$+\frac{12}{\hbar}\sum_{\lambda_1}V(\lambda,-\lambda,\lambda_1,-\lambda_1)(2n_1+1) \qquad \text{(B17-1)}$$

$$\Gamma(\lambda,\Omega) = \frac{18\pi}{\hbar^2}\sum_{\lambda_1\lambda_2}\left|V(\lambda,\lambda_1,\lambda_2)\right|^2$$
$$\times\left[(n_1+n_2+1)\{\delta(\omega_1+\omega_2-\Omega)-\delta(\omega_1+\omega_2+\Omega)\}\right.$$
$$\left.+(n_2-n_1)\{\delta(\omega_1-\omega_2-\Omega)-\delta(\omega_1-\omega_2+\Omega)\}\right] \qquad \text{(B17-2)}$$

Here we have used $n_1 \equiv n(\lambda_1)$ and $\omega_1 \equiv \omega(\lambda_1)$.

As has been pointed out by Cowley [CO68], "the width is proportional to the two-phonon density of states, so that a mode will appear to be strongly attenuated if there is a peak in the joint density of states at Ω. Likewise the shift will show a resonant behaviour in this region". We will later return to a discussion of these last two equations when considering the expression for the neutron-phonon cross-section.

C - SCREENING AND THE KOHN EFFECT

Any attempt to calculate the interatomic potential from first principles must take into account the presence of the conduction electrons. However, before tackling the general case, we can pause to make some classical considerations which will illustrate the importance of the electron gas on the phonon spectrum of metals.

Consider a long wavelength longitudinal phonon; thus the local displacement ($\delta\underset{\sim}{r}$) at site $\underset{\sim}{r}$ is parallel to the propagation wavevector $\underset{\sim}{q}$ and may be written as

$$\delta\underset{\sim}{r} = \underset{\sim}{u}(\underset{\sim}{q})e^{i\underset{\sim}{q}\cdot\underset{\sim}{r}} . \qquad (C1)$$

This corresponds to local density fluctuations which, in turn, will result in a long wavelength periodic potential (Poisson's equation). In this long wavelength limit, the ions (of mass M) will respond to this potential with a wavevector independent frequency given by

$$\omega^2 = 4\pi Z^2 e^2/M\Omega_o \qquad \Omega_o: \text{ atomic volume} \qquad (C2)$$

This is identical with the well known expression in plasma theory.

However, we know from ultrasonic or neutron measurements, that the frequency of longitudinal acoustic modes is linearly related to wavevector in the long wavelength limit, i.e.

$$\omega(\underset{\sim}{q}) \underset{q\to 0}{\to} c|\underset{\sim}{q}|$$

We can take into account the screening of the long range Coulomb potential by the conduction electrons by using an expression for the static dielectric constant valid in the limit $|\underset{\sim}{q}| \to 0$ and which will be discussed further below, e.g.

$$\varepsilon(q\to 0) = \frac{4\pi e^2}{q^2} n(E_F). \qquad (C3)$$

Thus the phonon frequencies are no longer wavevector independent and are given by

$$\omega = \left(\frac{2ZE_F}{3M}\right)^{1/2} |\underset{\sim}{q}| \quad . \qquad \text{(C4)}$$

Now the acoustical phonon frequencies show the right behaviour in the long wavelength limit. The frequency q-gradient, i.e. the term in brackets in equation (C4) gives the sound velocity for longitudinal phonons. This expression for the speed of sound is known as the Bohm-Staver value [BO51]. One will note that this value is simply $\left(\frac{Zm_e}{3M}\right)^{1/2}$ times the Fermi velocity for the electrons, where m_e is the electronic mass.

A general description of screening effects in the presence of a probe of wave vector $\underset{\sim}{Q}$ can be achieved by assuming that the electron gas is free-electron-like; thus, the dielectric constant can now be written as [BA37]:

$$\varepsilon(Q) = 1 - \frac{4\pi e^2}{Q^2} \chi(Q) \qquad \text{(C5-1)}$$

where

$$\chi(Q) = -\frac{n(E_F)}{2}\left\{1 + \frac{1-\eta^2}{2\eta} \ln\left|\frac{1+\eta}{1-\eta}\right|\right\} \qquad \text{(C5-2)}$$

$$\eta = Q/2k_F \qquad \text{(C5-3)}$$

$n(E_F) = \frac{3}{2}\frac{ZN}{E_F}$ is the electronic density of states at the Fermi energy . (C5-4)

In the long wavelength limit, $\chi(Q)$ converges to $-n(E_F)$ and the dielectric constant becomes the expression which we have used in equation (C3). The fact that it diverges at Q=0 shows that an electric field is totally screened over large distances in a conducting medium.

On the other hand, in the short wavelength limit, equation (C5-2) goes to zero as $1/Q^2$ and hence, $\varepsilon(Q) \to 1$. Physically, this means that electrons do not respond to perturbations with a wavelength much smaller than those of the electron having energies comparable to E_F; this is strictly a quantum effect.

In the intermediate range, we note that equation (C5-2) has a logarithmic singularity when $\eta=1$, i.e. $Q = 2k_F$. Although the free-electron approximation used in the derivation of this equation is questionable for most metals except possibly for the alkali, it remains that its analytic form shows features similar to those obtained using a more rigorous formalism where correlation effects are taken into account [SH63; SH65].

The singularity in the dielectric constant at $Q = 2k_F$ is reflected in the phonon spectrum, as has been shown by Kohn [KO59]. Indeed, during the scattering from a phonon of wavevector $\underset{\sim}{q}$ of an electron from state $\underset{\sim}{k}$ to state $\underset{\sim}{k}'$, the total momentum must be conserved:

$$\underset{\sim}{Q} = \underset{\sim}{k}'-\underset{\sim}{k} = \underset{\sim}{G}+\underset{\sim}{q} \qquad (\underset{\sim}{G}\text{: a reciprocal space vector}) \quad \text{(C6)}$$

Because of the fact that typical phonon energies, e.g. 25 meV, are so much smaller than typical values of the Fermi energy, e.g. 5 eV, only electronic transitions on the Fermi surface need to be considered. Thus, depending on whether $|\underset{\sim}{Q}|$ is smaller or larger than $2k_F$, the screening ability of the electron gas will be different. Phonon frequencies will undergo a discontinuity in slope when their wavevector cross the so-called

"Kohn surface", which is defined as the locus of $\underset{\sim}{q}$ vector where

$$2k_F = |\underset{\sim}{G}+\underset{\sim}{q}| \qquad (C7)$$

The phonon frequencies vary across the "Kohn surface" according to the following simple rule: "if, with increasing value of $\underset{\sim}{q}$, the vector $\underset{\sim}{q}+\underset{\sim}{G}$ (for some $\underset{\sim}{G}$) passes through the Fermi surface from the inside to the outside, the frequency rises abruptly; if from the outside to the inside, the frequency drops" [WO62]. This rule has always been confirmed ever since the early measurements on Pb [BR61].

Calculations taking into account the electronic band structure have been published [TA63; RO66]. Qualitatively speaking, these have shown that electron correlations tend to attenuate the strength of Kohn anomalies. Also, the band structure leads to the possibility of a "cusp"-type structure in the dispersion curves instead of the logarithmic singularity predicted using the free electron model; this is the feature predicted for tungsten [RI70] and which forms the justification for the measurements reported in chapter VI.

D - LONG WAVES AND ELASTIC CONSTANTS

When the wavelength of a phonon propagating in a solid becomes much larger than the interatomic separation, one expects "a priori" that the details of the microscopic structure do not matter greatly and hence, that the solid may be viewed as a continuum. In practice, such large wavelengths correspond to "sound" waves with frequencies typically less than 1 GHz (for $\frac{\lambda}{a} >> 1000$). One notes that, although this is a high frequency by "audio" standards, it is still far below the frequencies

accessible by thermal neutron spectroscopy and such a regime is usually referred to as "first-sound".

In this long wavelength limit, the "wave equations" for the system can be solved by a straight extension of Hooke's law. Elastic constants, i.e. coefficients relating the constraint (stress) to the deformation (strain) in a given volume element of the crystal, are defined and, in general, they form a fourth rank tensor with 21 independent constants. Particular symmetry requirements usually reduce this number; for example, in the case of crystals with cubic symmetry, there are only 3 such independent constants and this will be the case of interest for this thesis.

A set of dynamical equations of sound can be written for waves with arbitrary directions of propagation [DE56, p.263]; their solution happens to be simply three plane waves with appropriately chosen wavevectors. In the case of waves propagating in arbitrary directions, the polarizations are, in general, neither purely longitudinal nor purely transverse, unless the material is elastically isotropic, i.e. unless $c_{11}-c_{12}=2c_{44}$. On the other hand, in directions of high symmetry, the elastic constants are related to the wave (phase) velocities ($U = \omega/|\underline{q}|$) and to the initial slopes of the dispersion relation with respect to the reduced wavevector "ζ" ($V = \lim_{\zeta \to 0} |\frac{\nu}{\zeta}|$), as indicated by the following equations, where "ρ" is the macroscopic crystal density and "a", the lattice parameter:

1) $\underline{q}$ in (100) direction

a) T waves $c_{44}/\rho = U_T^2(100) = a^2 V_T^2(100)$ (D1-1)

b) L waves $c_{11}/\rho = U_L^2(100) = a^2 V_L^2(100)$ (D1-2)

2) $\underline{q}$ in (110) direction

a) T_1 waves $(c_{11}-c_{12})/2\rho = U_{T1}^2(110) = \frac{a}{2}^2 V_{T1}^2(110)$ (D2-1)

b) T_2 waves $c_{44}/\rho = U_{T2}^2(110) = \frac{a}{2}^2 V_{T2}^2(110)$ (D2-2)

c) L waves $(c_{11}+c_{12}+2c_{44})/2\rho = U_L^2(110) = \frac{a}{2}^2 V_L^2(110)$ (D2-3)

3) $\underline{q}$ in (111) direction

a) T waves $(c_{11}-c_{12}+c_{44})/3\rho = U_T^2(111) = \frac{a^2}{3_2} V_T^2(111)$ (D3-1)

b) L waves $(c_{11}+2c_{12}+4c_{44})/3\rho = U_L^2(111) = \frac{a}{3} V_L^2(111)$ (D3-2)

Measurements of these elastic constants, in the first-sound regime, are usually done by measuring the transit time of a 10 MHZ (typically) pulse propagating in the (110) direction. This allows a determination of the three elastic constants without modifying the alignment of the crystal; only the polarization of the ultrasonic generator needs to be varied. The results of such measurements are usually quoted with an accuracy ranging from 0.5% to 2%.*

The thermal neutron probe does not allow the measurements of phonon frequencies below 0.1 THz (10^5 MHz); this value is typical of the energy resolution in triple-axis spectrometry and any measurement attempted below this value is spoiled by the proximity of the Bragg peak. However, by systematically measuring the initial slopes of the various branches and extra-

*) It should be noted that, because of limitations on the transducers, ultrasonic measurements are possible only up to approximately 600°C.

polating to $\underset{\sim}{q} \to 0$, it is possible to obtain by thermal neutron scattering the elastic constants of waves propagating in the so-called "zero-sound" mode and this, at <u>all</u> temperatures.

In order that the results be at all meaningful, it is important to correct for the aberration caused by resolution effects on measurements performed in the vicinity of the Bragg peak, i.e., where over a $(\underset{\sim}{Q},\omega)$ space volume element comparable to that of the resolution function of a triple-axis spectrometer (see section II-G), the relative change in frequency is large and the dispersion surface shows a pronounced curvature. The procedure for doing so will be described below in section II-H.

Once the initial slopes are determined for at least three branches, equations (D1-1) to (D3-2) can be solved for the elastic constants. If the measurements and correction procedures are performed consistently, it should really not matter which set of three branches is chosen for this determination and, similarly, a least-squares fit to more than three branches would yield similar results. In practice, for the results described in chapters IV and V, only the initial slopes along the $[00\zeta]$T&L and $[0\zeta\zeta]T_1$&L were available because of the fact that all measurements were made with the specimen mounted with a (001) plane in the scattering plane; this provided four orthogonal values to determine three elastic constants and no consistency problems were encountered.

One will note from equations (D1-1) to (D3-2) that, in such a determination of the elastic constants, one needs to

calculate the product "ρa^2". Under these assumptions that there are no vacancies present in the bulk of the crystal ...

$$\rho a^2 = \frac{nM}{a} = n \times 1.66 \times 10^{-24} \times \frac{A[\text{a.m.u.}]}{a[\text{cm}]} \qquad \text{(D4)}$$

where n: number of atoms in the unit cell,

M: mass of one atom in the unit cell,

a: lattice parameter (in cm)

A: average atomic mass at each lattice site (in a.m.u.)

If the presence of vacancies were taken into account, the term "ρa^2" and hence, the calculated elastic constants, would be slightly reduced. However, in practice, it is not possible to measure the macroscopic density at elevated temperatures ($T \approx 1000°C$) and equation (D4) was used in the determination of the elastic constants. This produces an error which increases at elevated temperatures but this contribution to the total uncertainty is much smaller than the one caused by the uncertainty on the initial slopes. Quoting Kittel [KI67, p.561]: "In metals with close-packed structures, the proportion of lattice sites vacant at temperatures just below the melting point is of the order of 10^{-3} to 10^{-4}". Hence, the actual density differs proportionately from the value calculated using the temperature dependence of the lattice parameter and, in the case of Cu and Pd (chapters IV and V) of interest here, we will consider the formation of vacancies an effect altogether negligible.

The temperature dependence of the elastic constants reflects the anharmonic nature of the interatomic potential and

is characterized by two general features: (1) an approach with zero slope to the limit T→0, and (2) a negative slope at temperatures usually higher than θ_D [HU58, p. 237]. This is a direct consequence of the behaviour of the Helmholtz free energy function from which the elastic constants can be calculated by a suitable combination of derivatives with respect to temperature and strains [LE61, p. 312.].

The experimental procedure for the determination of the temperature dependence of the zero-sound elastic constants was as follows. The spectrometer was calibrated for high resolution work, i.e. using low values for the incident neutron energy (e.g. 4.2 THz) as well as for both the horizontal (e.g. 43') and vertical (e.g. 86') collimations*. Because of the small value of the incident energy, momentum transfers were restricted to the vicinity of the few reciprocal lattice points nearest to the origin. The best type of scan for each branch was determined empirically at the start of the measurements. After this, measurements were performed along a given branch, starting with the lowest energy phonon that could be measured without interference from the Bragg peak. Scans were usually taken about one full resolution width apart; (the resolution function was always measured, at the beginning of a run, using the procedure of Møller [MO68]). In general, a minimum of three phonons (and more often than not, five phonons) were observed on each branch, each one being measured both by neutron energy gain and loss. Such measurements are usually done at equivalent but opposite positions with respect to reciprocal lattice points in order to optimize

*) The quoted values for the collimations are FWHM.

focussing since, generally, a focussing configuration for energy gain measurements is a defocussing configuration for energy loss and vice versa. The fact that the initial slopes were measured at mirror positions with respect to a reciprocal lattice point also means that the interpolation of the slopes (i.e. phonon phase velocity) at $q \to 0$ could be achieved without being critically dependent on an exact knowledge of the lattice parameter and on an exact alignment of the crystal. All these high resolution measurements were corrected for resolution effects as discussed below in section II-H.

E - FIRST-SOUND AND ZERO-SOUND REGIMES

In the previous section, we have introduced the concepts of first-sound and zero-sound as the regimes corresponding to phonon frequencies typically of the order of 10^9 Hz and 10^{12} Hz respectively. Here, we will attempt a brief description of the physics of these two regimes.

Were it not for the presence of anharmonicity, there would not be two such different modes of propagation. However, because of the finite lifetimes of phonons resulting from their interaction with other excitations in the crystal, e.g. phonons, electrons, magnons, one can define, for the phonon gas, a quantity known as a typical lifetime (τ) [ZI60, p.157]; the inverse of this lifetime is a measure of the uncertainty in the energy of the individual phonons.

A phonon will propagate differently whether its frequency is smaller or larger than the typical inverse lifetime. If $\nu << \frac{1}{\tau}$, there will be sufficient phonon-phonon collisions during

each period of the propagating phonon so as to set up local thermodynamic equilibrium in the population of thermal phonons. This is a "collision-dominated" mode of propagation also known as the hydrodynamic or first-sound regime. On the other hand, if $\nu >> \frac{1}{\tau}$, there are not sufficient collisions during each period of the propagating phonon to significantly alter the population of the phonon gas. Hence, the local temperature of the crystal is unaffected and such a "collision-free" mode of propagation is referred to as zero-sound regime.

Cowley has discussed at length the cause of the differences between zero-sound and first-sound using the formalism of quantum field theory [CO67A]. This is basically a manifestation of anharmonic interactions which result in different velocity of phonon propagation (and hence, elastic constants) in the two regimes. The anharmonic contribution to the elastic constants is proportional to the generalized susceptibility [CO68].

$$\chi(\lambda,\underset{\sim}{Q}\Omega) = \frac{n(\lambda)(n(\lambda)+1)(\nabla_{\underset{\sim}{Q}}\omega(\lambda)\cdot\underset{\sim}{Q})}{k_B T(\nabla_{\underset{\sim}{Q}}\omega(\lambda)\cdot\underset{\sim}{Q}-\Omega)} \qquad \text{(E1)}$$

where $n(\lambda)$ is the population of the phonon of mode $\lambda \equiv (\underset{\sim}{q},j)$ and $\omega(\lambda)$ is its circular frequency.

Here $\underset{\sim}{Q}$ and Ω are the wavevector and circular frequency of the excitation probe, i.e. the propagating phonon. One sees that the susceptibility can make a positive or negative contribution to the harmonic elastic constants depending on whether the velocity of the probe $\Omega/|\underset{\sim}{Q}|$ is less or greater than the group velocity $\nabla\omega(\lambda)$ of the excitations. However, in the case of phonons, the elastic wave usually has a greater velocity than

the other phonons and hence, equation (E1) is small and negative, giving a small positive contribution to the elastic constant c_{11}" [CO68A].

F - NEUTRON-PHONON INTERACTION

The interaction of thermal neutrons with matter is rather diversified [SH67]. Let us restrict our considerations to nuclear scattering and how it can be used to probe the spectrum of phonons in solids. Amongst the attributes which favor the neutron for this type of work are the following:

- Thermal neutron wavelengths and energies are comparable to those of the phonons, thus allowing simultaneous measurements of both momentum and energy transfers.
- For most substances, the coherent scattering cross-section is large enough to make phonon measurements possible.
- As a result of the electrical neutrality of the neutron, the attenuation of neutron beams in bulk matter is minimal, except for a few substances where nuclear resonances occur [BR36, BR53].
- The neutron-nucleon interaction does not lead to preferential scattering by high Z nuclei, like X-rays do.

A formal theory of neutron scattering by nuclei is still not possible at present because of our incomplete knowledge of nuclear interactions. However, a phenomenological argument can be brought into the picture whereby, following Fermi [FE36], the neutron-nucleus interaction is assumed to be represented by a pseudopotential of the form

$$V(\underset{\sim}{r}) = \frac{2\pi\hbar^2}{m} b\, \delta(\underset{\sim}{r}) \qquad \text{(F1)}$$

where m is the neutron mass and

b is an adjustable parameter called the scattering length [BA62].

The assumed form of this pseudopotential is intuitively acceptable since the range of nuclear potentials (i.e. 10^{-13} cm) is much smaller than the wavelengths of thermal neutrons (i.e. 10^{-8} cm); hence, the neutrons can rightly be considered to interact with a "point" source, i.e. much smaller than the extent of the neutron wave packet.

For similar reasons, our considerations on thermal neutron scattering need not be concerned with any but S-wave scattering. Indeed, at thermal velocities, any neutron, whose angular momentum is different from zero, is too remote from a nucleus to be scattered. This leads to a form factor which is independent of the scattering angle, i.e. the scattering by a single nucleus is isotropic.

Van Hove [VA54] has shown that the differential cross-section for a system of N particles is of the form

$$\frac{d^2\sigma}{d\Omega d\varepsilon} = A\, S(\underset{\sim}{Q},\omega) \qquad \text{(F2-1)}$$

where

$$A = \frac{m^2}{4\pi^2\hbar^5} \frac{k'}{k_o} \left\{ \int \exp(i\underset{\sim}{Q}\cdot\underset{\sim}{r}) V(\underset{\sim}{r})\, d\underset{\sim}{r} \right\}^2 \qquad \text{(F2-2)}$$

$$= \left(\frac{b}{\hbar}\right)^2 \frac{k'}{k_o} \quad \text{(if } V(\underset{\sim}{r}) \text{ is given by equation (F1))} \qquad \text{(F2-3)}$$

$$S(\underset{\sim}{Q},\omega) = \sum_n g(n) \sum_m \left| \langle m | \sum_{\ell=1}^{N} \exp(i\underset{\sim}{Q}\cdot\underset{\sim}{r}_\ell(t)) | n \rangle \right|^2 \delta(\hbar\omega + E_n - E_m) \qquad \text{(F2-4)}$$

$$\underset{\sim}{Q} = \underset{\sim}{k}_o - \underset{\sim}{k}' \quad \text{(wavevector transfer)} \qquad \text{(F2-5)}$$

$$\varepsilon = E_o - E' = \hbar\omega = \hbar^2(k_o^2 - k'^2)/2m \qquad \text{(F2-6)}$$

(energy transfer)

$$g(n) = \exp(-E_n/k_B T)/\Sigma_i \exp(-E_i/k_B T) \qquad \text{(F2-7)}$$

(statistical weight of state n)

Here $\underset{\sim}{k}_o(E_o)$ and $\underset{\sim}{k}'(E')$ refer to the initial and final wavevectors (energies) of a neutron (of mass m) which has interacted with the system.

The structure and the dynamics of the scattering system are contained entirely in $S(\underset{\sim}{Q},\omega)$. This function, for which the only variables depending on the scattering process are the momentum and energy transfers, is effectively the Fourier transform of the generalized pair distribution function $G(\underset{\sim}{r},t)$. In an actual physical system, where the scattering length can vary from particle to particle as a result of isotopic composition and/or of spin-spin interaction between the neutron and the target, the total scattering may be divided into coherent and incoherent contributions. Coherent scattering occurs as a result of interference between waves scattered by identical nuclei (i.e. same isotopes, same spins). Incoherent scattering, on the other hand, occurs in the absence of interference, i.e. one-nucleus scattering. The scattering cross-section must now be written in terms of the self- and distinct- correlation functions $G_s(\underset{\sim}{r},t)$ and $G_d(\underset{\sim}{r},t)$:

$$\frac{d^2\sigma}{d\Omega d\varepsilon} = \frac{d^2\sigma_{coh}}{d\Omega d\varepsilon} + \frac{d^2\sigma_{inc}}{d\Omega d\varepsilon} \qquad \text{(F3-1)}$$

where*

$$\frac{d^2\sigma_{coh}}{d\Omega d\varepsilon} = \frac{\langle b\rangle^2 N}{2\pi\hbar}\frac{k'}{k_o}\int \exp(i(\underset{\sim}{Q}\cdot\underset{\sim}{r}-\omega t))(G_s(\underset{\sim}{r},t)+G_d(\underset{\sim}{r},t))d\underset{\sim}{r}dt \quad \text{(F3-2)}$$

$$\frac{d^2\sigma_{inc}}{d\Omega d\varepsilon} = \frac{(\langle b^2\rangle-\langle b\rangle^2)}{2\pi\hbar} N \frac{k'}{k_o}\int \exp(i(\underset{\sim}{Q}\cdot\underset{\sim}{r}-\omega t)G_s(\underset{\sim}{r},t)d\underset{\sim}{r}dt \; . \quad \text{(F3-3)}$$

As such, these expressions are most useful in the case of fluids where the possibility to analyse the system in terms of its inter-particle correlations provides a clear physical understanding. However, in solids, where atoms are not bound like in a fluid but are confined to execute small displacements $\underset{\sim}{u}_\ell$ around each lattice site $\underset{\sim}{R}_\ell$, we can write

$$\underset{\sim}{r}_\ell = \underset{\sim}{R}_\ell + \underset{\sim}{u}_\ell \qquad \text{(F4)}$$

and substitute this into equation (F2-4). In addition, if a time variable is introduced to eliminate the delta function [WI54], the result is now (for the coherent scattering contribution):

$$S(\underset{\sim}{Q},\omega) = \frac{1}{2\pi}\sum_{\ell\ell'}\exp(i\underset{\sim}{Q}\cdot\underset{\sim}{R}_{\ell\ell'})\int_{-\infty}^{\infty} dt\, e^{i\omega t}$$

$$\langle\langle \exp(-i\underset{\sim}{Q}\cdot\underset{\sim}{u}_\ell(t))\exp(i\underset{\sim}{Q}\cdot\underset{\sim}{u}_{\ell'}(0))\rangle\rangle \qquad \text{(F5)}$$

The thermal average of the function of the displacements $u_\ell(t)$, denoted by the double brackets, can be simplified using the operator identity [WI54]

$$e^A e^B = e^{A+B} e^{\frac{1}{2}[A,B]} \; .$$

In the harmonic theory, the displacements are written as a linear

*) For an explicit definition of the functions $G_s(\underset{\sim}{r},t)$ and $G_d(\underset{\sim}{r},t)$, the reader should refer to [VA54].

combination of normal modes (equation B8-5) and the result is, after some manipulations, an expression which contains explicit contributions from all n-phonons processes (n=0,1,2,...).

We are particularly interested in the one-phonon processes, since these are the ones which contain the "signature" of the phonon spectrum in solids. Higher order processes, i.e. multi-phonon processes, contribute a uniform background level in the scattering while the zeroth order processes correspond to the familiar Bragg-scattering. The one-phonon scattering law for the case of a monoatomic lattice (in the harmonic theory) can now be written as

$$S_1(\underset{\sim}{Q},\omega) = (2\pi)^3 \frac{N}{V} \frac{\hbar}{2m} \exp(-2W(\underset{\sim}{Q})) \sum_{\lambda} \left[\frac{\langle |\underset{\sim}{Q}\cdot\underset{\sim}{e}(\lambda)|^2 \rangle}{\omega(\lambda)} \right. \qquad \text{(F6-1)}$$

$$\left. (n(\lambda) + \frac{1}{2} \pm \frac{1}{2}) \, \delta(\omega \mp \omega(\lambda)) \Delta(\underset{\sim}{Q}-\underset{\sim}{q})^{\lambda} \right]$$

$$\text{where} \qquad W(\underset{\sim}{Q}) = \langle \underset{\sim}{Q}\cdot\underset{\sim}{u} \rangle = \frac{\hbar Q^2}{2Nm} \sum_{\lambda} \frac{2n(\lambda)+1}{\omega(\lambda)} \qquad \text{(F6-2)}$$

In the first equation, the upper (lower) sign refers to neutron energy loss (gain) processes, i.e. scattering by phonon creation (annihilation). The second equation is the Debye-Waller factor which represents the decrease in the one-phonon scattering at high temperature (i.e. large $n(\lambda)$) and/or large momentum transfer.

In the anharmonic theory, the derivation of the one-phonon cross-section is a much more complex affair than in the harmonic theory [MA62]. Strangely enough, however, the result

differs from that of the harmonic theory in that the delta function of energy is now replaced by a pseudo-lorentzian; (in a strictly lorentzian function, Δ and Γ would be independent of λ and ω).

$$\frac{\Gamma(\lambda,\omega(\lambda))}{[\omega \mp \omega(\lambda) \mp \Delta(\lambda,\omega(\lambda))]^2 + \Gamma^2(\lambda,\omega(\lambda))} \qquad \text{(F7)}$$

As usual, the upper (lower) sign refers to neutron energy loss (gain) processes. The expressions for the frequency shifts Δ (relative to the harmonic frequencies) as well as the intrinsic linewidth 2Γ have already been given in equations (B17-1) and (B17-2).

Thus, from equation (F6-1), we see that the natural variables in neutron scattering by one phonon processes are also the momentum $\hbar Q$ and the energy $\hbar\omega$ transfers. The triple-axis spectrometer uses this property in an ingenious way and its superiority for the measurement of phonons in solids is generally recognized [WO69]. McMaster University has two such instruments, respectively located on campus at the McMaster reactor and in Chalk River at the NRU reactor; both were used for this research.

We will avoid repeating a description of their features, since this has already been well done elsewhere [BR68]; the original contribution of the author with respect to these instruments is described in appendix I.

G - OPTIMIZATION OF EXPERIMENTAL VARIABLES IN TRIPLE-AXIS SPECTROMETRY

1) General considerations

In order to apply the formalism of the previous section to the actual measurement of phonons, certain practical considerations must be taken into account. Those which depend on the intrinsic nature of triple-axis spectrometry will be the subject of this sub-section while those resulting from optimizations of intensities will be considered under resolution effects.

A triple-axis spectrometer can be operated while scanning either in energy, momentum or both. A particular choice depends on the gradient of the dispersion surface at the $(\underset{\sim}{Q},\omega)$ space point where the measurements are performed. The first and second modes of operation correspond to the well-known constant-$\underset{\sim}{Q}$ and constant-E procedures [BR60]. The third one requires extremely fine angular positioning (e.g. to the nearest 0.01°) in order to obtain a linear scan in $(\underset{\sim}{Q},\omega)$ space and is not generally used.

The fact that a triple-axis spectrometer "looks" at only one point in $(\underset{\sim}{Q},\omega)$ space at a time (as opposed to a time-of-flight instrument) means that the experimenter is free to choose a position in reciprocal space where the scattering is contributed mainly, if not exclusively, by a preselected mode. This is so because of the term $|\underset{\sim}{Q}\cdot\underset{\sim}{e}(\lambda)|^2$ in the equation (F6-1) for the cross-section; hence, scattering is caused predominantly by modes whose eigenvectors are near-parallel to the momentum transfer. This results in an enormous simplification since the eigenvectors

in directions of high symmetry are always known "a priori".

The population factor in equation (F6-1), or more precisely the ratio $(n(\lambda) + \frac{1}{2} \pm \frac{1}{2})/\omega(\lambda)$ determines the relative merit of neutron energy loss and energy gain experiment. This ratio is plotted as a function of the "reduced frequency" $x = h\nu/k_B T$ in fig. II-1 which clearly shows that both neutron energy gain and energy loss experiments are possible if $x < 1$ while only those of neutron energy loss are practical if $x > 1$. The possibility to obtain experimental data both by phonon creation and by phonon annihilation has been applied to the determination of the zero-sound elastic constants in order to minimize some systematic errors (see section II-D) and to the measurement of high energy phonons in Cu near the melting point where definite improvements in the quality of the one-phonon signal resulted from the phonon annihilation experiments compared with those by phonon creation (see chapter III).

In experiments where either the incident or analysed neutron energy is varied, an undesirable effect is introduced resulting from the variation of crystal reflectivities as a function of the scattering angle. Hence, if the scan is of the fixed-E_o type, the effective sensitivity of the analyser is now energy dependent and, unless corrected for, can introduce distortions in the experimental results, especially in the case of wide energy scans. On the other hand, a fixed-E' mode of operation is more attractive for the following reasons:

- The analyser crystal being maintained in a fixed scattering angle configuration, the need to correct for variations of the analyser reflectivity is eliminated.
- The "$\frac{1}{v}$" sensitivity of the fission counter, which monitors the monochromatized incident beam, compensates for the "$\frac{1}{k_o}$" term in the expression for the cross-section (equation F3-1). Thus, the Fourier transform of the correlation functions is measured directly; this is of interest for experiments on fluids.
- The fact that $|\underset{\sim}{k}'|$ is fixed makes possible the use of a filter, e.g. Be with cut-off at 1.2 THz, in the analyzed beam [BR59]. Such a small $|k'|$, however, severely restricts the accessible range in reciprocal space. Also, because of the correspondingly small value of the ratio $|k'|/|k_o|$ (see equation F2-2), the cross-section for a given phonon is drastically reduced. All this, as well as the low effective luminosity resulting from the improved resolution at such large analyser scattering angles, makes the use of filters generally unattractive, unless there is a high energy contaminant which cannot be eliminated otherwise.
- As a result of the maxwellian nature of the thermal neutron gas in the pile as well as of the worsening of the monochromator resolution at small $2\theta_m$, the intensity of the monochromatized beam typically increases monotonically (neglecting small dips caused by simultaneous reflections) up to an energy of $\approx$ 8 THz where it levels off up to $\approx$ 12 THz. This feature is advantageous if used in conjunction with neutron energy loss experiments since the effective incident flux increases at large energy

transfers and thereby compensates for the smaller values of the cross-section corresponding to these excitations. However, it should be noted that, in the case of neutron energy gain measurements (generally practical if $h\nu/k_BT<1$), the argument works in the opposite way, thus making a fixed-E_o procedure recommended.

- Finally, there is another advantage which is common to both neutron energy loss by constant-E' as well as neutron energy gain by constant-E_o measurements. This advantage results from the fact that the accessible range in momentum transfer increases with the energy transfer instead of inversely proportional to it. This is a definite asset in high resolution measurements (i.e. at large scattering angle) of longitudinal acoustic phonons since these are usually measured radially away from the origin in reciprocal space; hence, the spectrometer can simultaneously reach large momentum and energy transfers.

2) Resolution effects

We have seen that the important term for the cross-section of a one phonon process in neutron scattering is given by equation (F6-1). However, the observed intensity is actually a convolution of the cross-section with the instrumental resolution, integrated over the 4-dimensional $(\underset{\sim}{Q},\omega)$ space. If the resolution function were a delta function of the four variables, the observed intensities would simply be proportional to the value of the cross-section at this nominal $(\underset{\sim}{Q},\omega)$ point.

In practical triple-axis spectrometry, the experimental configuration yields a resolution function having the topology of an ellipsoid in $(\underset{\sim}{Q},\omega)$ space; this is a perfectly general feature [CO67]. The dimensions of the ellipsoid are a measure of instrumental resolution and, because of the contingencies set by the low neutron fluxes generally available, high resolution is usually sacrificed in return for practical counting rates. This is achieved by relaxing the various collimations (typically set at 43' FWHM) and selecting a monochromator and an analyser crystals which have a certain degree crystalline imperfection (typical mosaicity of 30' FWHM) [DY70].

The actual resolution function of a triple-axis spectrometer (set for elastic scattering) can be measured "in situ" [MO68] as well as calculated from the known values of the individual components [CO67]. In the course of an experiment, the resolution function varies as a function of the region in $(\underset{\sim}{Q},\omega)$ space "seen" by the spectrometer and at points other than reciprocal lattice points, its actual value can only be calculated. The validity of such a calculation, however, can be checked by comparing the calculated and observed lineshapes at "low" temperatures, i.e. where resolution line broadening is much larger than the anharmonic contribution.

Mathematically, the resolution function of a triple-axis spectrometer can be written as

$$R(\hat{\underset{\sim}{Q}}+\Delta\underset{\sim}{Q},\hat{\omega}+\Delta\omega) = R_o \exp(-\underset{\sim}{X}^T \underset{\approx}{M} \underset{\sim}{X}/2) \qquad (G1)$$

where $\hat{\underset{\sim}{Q}}$ and $\hat{\omega}$ are the nominal setting of the spectrometer, R_o is an empirical factor which depends on the transmission and reflectivity of the various spectrometer components, $\underset{\approx}{M}$ is a 4×4 symmetric matrix whose elements depend on a complicated manner on the various collimations and reflectivities [CO67;LA70] and $\underset{\sim}{X}$ is a 4-dimensional vector in $(\underset{\sim}{Q},\omega)$ space which depends on $\Delta\underset{\sim}{Q}$ and $\Delta\omega$ and hence, is a measure of the deviation in $\underset{\sim}{Q}$ and ω from the nominal setting of maximum sensitivity, i.e. $\hat{\underset{\sim}{Q}}$ and $\hat{\omega}$. For mathematical convenience, this vector $\underset{\sim}{X}$ is usually expressed as follows: three of its orthogonal components are those of $\Delta\underset{\sim}{Q}$: $\underset{\sim}{X}_1$ parallel to the momentum transfer $\underset{\sim}{Q}$, $\underset{\sim}{X}_2$ perpendicular to $\underset{\sim}{Q}$ but in the scattering plane, $\underset{\sim}{X}_3$ perpendicular to both $\underset{\sim}{Q}$ and to the scattering plane. The fourth component is perpendicular to the other three and is equal in magnitude to $\Delta\omega$.

For any positive value "p", the equation

$$\underset{\sim}{X}^T\underset{\approx}{M}\underset{\sim}{X} = p \qquad \text{(G2)}$$

defines an isosensitivity ellipsoidal contour in $(\underset{\sim}{Q},\omega)$ space. The method of experimentally measuring the resolution function [MO68] consists in scanning systematically the $(\underset{\sim}{Q},\omega)$ space region in the immediate vicinity of a Bragg peak, and joining together the $(\underset{\sim}{Q},\omega)$ space point of equal intensity. These scans are chosen along the $\underset{\sim}{Q}$-space directions where actual phonon measurements are performed, thus yielding immediately a projection of the resolution ellipse for the experimental situation of interest. These directions of interest in the scattering plane generally

do not coincide with the direction of the components X_1 and X_2; however, the transformation is equivalent to a trivial change of coordinates in $(\underset{\sim}{Q},\omega)$ space [LA70].

The expression for the observed intensity (per unit solid angle) when the spectrometer is set for a nominal $(\hat{\underset{\sim}{Q}},\hat{\omega})$ point is given as a convolution of equations (G1) and (F6-1):

$$I(\hat{\underset{\sim}{Q}},\hat{\omega}) = \int R(\hat{\underset{\sim}{Q}}+\Delta\underset{\sim}{Q},\hat{\omega}+\Delta\omega)\,\frac{d^2\sigma}{d\Omega d\omega}\,(\hat{\underset{\sim}{Q}}+\Delta\underset{\sim}{Q},\hat{\omega}+\Delta\omega)\,d(\Delta\underset{\sim}{Q})\,d(\Delta\omega). \quad (G3)$$

In general, such an expression can only be calculated numerically as a result of the complexity of equation (F6-1); this is the procedure adopted here (see section II-H). An analytic solution is possible, however, under the assumption of a planar dispersion surface [CO67], whereby $\Delta\omega$ is linearly related to $\Delta\underset{\sim}{Q}$ and the $\underset{\sim}{Q}$ dependence of the eigenvectors is neglected. Obviously, such an approximation breaks down where a meaningful resolution calculation is most important, i.e. near the singularities in the dispersion surface resulting from the reciprocal lattice point positions. The planar approximation was not used in any of the calculations for this thesis.

Focussing results when the resolution ellipsoid is properly correlated with the dispersion surface (see note below equation B8-8). The resolution ellipsoid, being an object in a 4-dimensional space, has 4 principal axes. Two of them are parallel to the normal to the scattering plane (i.e. $\underset{\sim}{X}_3$) and to the momentum transfer (i.e. $\underset{\sim}{X}_1$) respectively; the other two are at an inter-

mediate position with respect to the "energy" (i.e. $\underset{\sim}{X}_4$) axis and the perpendicular to the momentum transfer in the scattering plane (i.e. $\underset{\sim}{X}_2$) [CO67].

It is this last feature which results in strong focussing possibilities in the measurement of transverse phonons. Indeed, in this case, the momentum transfer $\underset{\sim}{Q}$ is closely perpendicular to the phonon wavevector, since the momentum transfer must be near parallel to the phonon eigenvector (see equation F6-1), and the dispersion surface can be strongly correlated with the resolution ellipsoid. In the case of longitudinal phonons, which are measured mainly radially away from the origin in $\underset{\sim}{Q}$-space, no such strong focussing possibilities exist. However, under suitable conditions, it is possible to deviate slightly from a strictly radial position with corresponding improvements in the linewidth; this is discussed in chapter VI where this method was used.

3) Spurions

One of the most severe limitations of a crystal spectrometer is that of order contamination, whereby neutrons Bragg-scattered from the monochromator or the analyser are not only those of (first order) wavelength λ, but also those with λ/m ($m = 2,3,4,\ldots$). Although the λ^3-dependence of the crystal reflectivity in Bragg scattering [BA62] considerably decreases the importance of such processes, especially in a spectrometer with a double crystal monochromator (e.g. E2 spectrometer at the NRU reactor), order contamination can often lead to spurious peaks. In what follows, we will consider two types of such spurions, other types having been considered in details elsewhere [CO70A].

One of the most commonly occurring and easily predictable type involves what could be called an elastic CIC process, i.e. a Coherent/Incoherent/Coherent process from the monochromator target and analyser respectively. This troublesome scattering from the specimen (or from any material in the beam, e.g. radiation shields) being partly diffuse and incoherent, it is independent of scattering angle. Such a spurion will be observed if the same spurious wavelength (λ_s) can be reflected by both the monochromator and the analyser at a given setting, i.e.

$$\lambda_s = \frac{\lambda_o}{m} = \frac{\lambda'}{n} \qquad (m,n:\text{integer} > 1) \qquad (G4)$$

where $\lambda_o(\lambda')$ is the first-order incident (analysed) wavelength and m, n are the corresponding indices of these orders. Since $\nu \propto 1/\lambda^2$ for thermal neutrons, the above condition is identical with

$$m^2\nu_o = n^2\nu' \qquad (G5)$$

where $\nu_o(\nu')$ is the frequency (i.e. energy) of the incident (analysed) beam. A CIC spurion will likely appear at an energy transfer $h\nu$ when ν is a certain ratio of the fixed incident (or analysed) frequency as given in table II-1.

In general, one needs only to worry about the indices (m,n) less than 4 because of the decreasing reflectivity of higher order reflections. However, in the case of a monochromator fixed at a very low incident energy, the order contamination may extend slightly higher than normally because these high order contaminants may be close to the peak of the (near maxwellian) distribution of the polychromatic beam impinging on the monochromator.

Table II-1. $\alpha(i,j)$ and $\beta(i,j)$. Ratio of spurion energy to the fixed energy (incident or analysed) for CIC spurions in triple-axis spectrometry.

j=i \ i=	1	2	3	4	5	$\beta(i,j) = i^2/j^2-1$
		3	8	15	24	$1 \le j \le i$
2	3/4		5/4	3	21/4	
3	8/9	5/9		7/9	16/9	
4	15/16	3/4	7/16		9/16	
5	24/25	21/25	16/25	9/25		

$\alpha(i,j) = 1-i^2/j^2; \quad 1 < i \le j$

The following may help to clarify how the above table was obtained.

Neutron Energy Loss: $\nu_o \ge \nu'$

$1 < m \le n$ for spurion

a) Fixed ν_o: $\nu' = \nu_o - \nu$

$$\frac{m^2}{n^2} = \frac{\nu'}{\nu_o} = 1 - \frac{\nu}{\nu_o}$$

$$\therefore \frac{\nu}{\nu_o} = 1 - \frac{m^2}{n^2} \quad (1<m\le n)$$

$$= \alpha(m,n) \qquad (G6\text{-}1)$$

b) Fixed ν': $\nu_o = \nu' + \nu$

$$\frac{n^2}{m^2} = \frac{\nu_o}{\nu'} = 1 + \frac{\nu}{\nu'}$$

$$\therefore \frac{\nu}{\nu'} = \frac{n^2}{m^2} - 1 \quad (1<m\le n)$$

$$= \beta(n,m) \qquad (G6\text{-}2)$$

Neutron Energy Gain: $\nu_o \le \nu'$

$1 < n \le m$ for spurion

a) Fixed ν_o: $\nu' = \nu_o + \nu$

$$\frac{m^2}{n^2} = \frac{\nu'}{\nu_o} = 1 + \frac{\nu}{\nu_o}$$

$$\therefore \frac{\nu}{\nu_o} = \frac{m^2}{n^2} - 1 \quad (1<n\le m)$$

$$= \beta(m,n) \qquad (G7\text{-}1)$$

b) Fixed ν': $\nu_o = \nu' - \nu$

$$\frac{n^2}{m^2} = \frac{\nu_o}{\nu'} = 1 - \frac{\nu}{\nu'}$$

$$\therefore \frac{\nu}{\nu'} = 1 - \frac{n^2}{m^2} \quad (1<n\le m)$$

$$= \alpha(n,m) \qquad (G7\text{-}2)$$

Another type of spurions which can be particularly troublesome during measurements at high temperatures results from a combination of scattering by multi-phonon (as well as multi-event) processes in the specimen and from high order processes in the monochromator and/or analyser. In multi-phonon processes, conservation of wavevector and energy can be written as:

$$\underset{\sim}{Q} = \underset{\sim}{k}_o - \underset{\sim}{k}' = \underset{\sim}{G} + \sum_i \underset{\sim}{q}_i \qquad \text{(G8-1)}$$

$$\varepsilon = E_o - E' = \sum_i \hbar\nu_i \qquad \text{(G8-2)}$$

$$\nu_i = \nu(\underset{\sim}{q}_i) \begin{cases} > 0 \text{ for neutron energy loss} \\ < 0 \text{ for neutron energy gain.} \end{cases} \qquad \text{(G8-3)}$$

This should be compared with equations (B8-8), (F2-5) and (F2-6) corresponding to the one-phonon situation.

It is well known that such a system of equations only has a discrete set of solutions (in $\underset{\sim}{q}$ and ν) in the case of single-phonon processes and a continuum-type solution in the case of multi-phonon processes [BR65]. Consequently, any multi-phonon scattering in the specimen contributes a nearly uniform background above which the one-phonon signal is superimposed. At low temperatures, multi-phonon processes are generally unimportant (at any practical values of the momentum transfer $\hbar Q$) because of the low population of the phonon states. However, at high temperatures, the multi-phonon contribution in the detected signal increases both via the first-order processes in the monochromator and/or analyser as well as via the higher order processes. In the first

instance, the resulting contribution is, strictly speaking, a "bona fide" signal although it does not contain much useful information. In the second instance, however, the result is a worsening of the signal-to-noise ratio which can be avoided by a proper choice of instrumental parameters.

We will explicitly consider below how this can be achieved by examining the various possibilities. Let ν_{max} be the highest frequency in the phonon spectrum of the specimen. Hence, the spectrometer scans will be in the range

$$0 \leq \nu \leq \nu_{max}$$

If the scans are limited to the low part of the spectrum, e.g. for lack of sufficient neutron fluxes to cover the ehtire frequency range, we can instead define $\alpha \leq 1$ such that

$$0 \leq \nu \leq \alpha\nu_{max} \qquad \text{(G9)}$$

Unfortunately, there is no such thing as a triple-axis spectrometer setting which will result in a total elimination of the multi-phonon (or multi-event) contributions detected via high order processes in the monochromator and/or analyser. However, in both of these cases, the situation will be greatly improved if, for all values of ν during a scan, two inequalities, labeled below as equations (G11-0) and (G12-0), are satisfied. In these inequalities, it is assumed that the most likely multi-phonon processes are those where the total energy transfer is less than $h\nu_{max}$ as a result of the much higher population of the low energy states. These two inequalities lead to explicit restrictions on the choice of the fixed incident or analysed frequency. These restrictions can be

grouped in pairs corresponding respectively to the monochromator and the analyser contributions; they will be simultaneously satisfied if the following relations hold:

a) Fixed ν_o and neutron energy loss: $\frac{(4\alpha+1)}{3}\nu_{max} \leq \nu_o$ (G10-1)

b) Fixed ν_o and neutron energy gain: $\frac{(\alpha+1)}{3}\nu_{max} \leq \nu_o$ (G10-2)

c) Fixed ν' and neutron energy loss: $\frac{(\alpha+1)}{3}\nu_{max} \leq \nu'$ (G10-3)

d) Fixed ν' and neutron energy gain: $\frac{(4\alpha+1)}{3}\nu_{max} \leq \nu'$ (G10-4)

Thus, in the case of measurements at "small" energy transfers (i.e. $\alpha << 1$), these inequalities can be satisfied easily, since all of them lead to practical choices (i.e. $\approx \frac{\nu_{max}}{3}$) for the calibration of the spectrometer, assuming physically realistic values for ν_{max}. However, this is not so in the case of measurements at "large" energy transfers (i.e. $\alpha \approx 1$); in this case, equations (G10-1) and (G10-4) lead to large values for a suitable fixed ν_o or ν' (i.e. $\approx \frac{5}{3}\nu_{max}$) which cannot but lead to measurements of poor resolution, especially at small energy transfers. Thus, the superiority of the "fixed ν_o and neutron energy gain" and "fixed ν' and neutron energy loss" combinations, which had previously been discussed in sub-section II-G-1, is once again made evident, since the restrictions defined by equations (G10-2) and (G10-3) can generally be easily satisfied without undue sacrifice in resolution; this is so because of the low values required for suitable fixed ν_o or ν' (i.e. $\approx \frac{2}{3}\nu_{max}$).

Explicit derivations of the conditions minimizing the multi-phonon contribution via second order (and higher order) scattering in:

A) The Monochromator	B) The Analyser
if $\nu'+\nu_{max} \leq 4\nu_o$ (G11-0)	if $\nu_o+\nu_{max} \leq 4\nu'$ (G12-0)
a) Fixed ν_o and neutron energy loss: $\nu' = \nu_o - \nu$	
$\nu_o-\nu+\nu_{max} \leq 4\nu_o$	$\nu_o+\nu_{max} \leq 4\nu_o-4\nu$
$\nu_{max}-3\nu_o \leq \nu$	$\nu \leq (3\nu_o-\nu_{max})/4$
These inequalities, as well as (G9), will be satisfied if...	
$\nu_{max}-3\nu_o \leq 0$	$\alpha\nu_{max} \leq (3\nu_o-\nu_{max})/4$
$\frac{\nu_{max}}{3} \leq \nu_o$ (G11-1)	$(4\alpha+1)\frac{\nu_{max}}{3} \leq \nu_o$ (G12-1)
b) Fixed ν_o and neutron energy gain: $\nu' = \nu_o + \nu$	
$\nu_o+\nu+\nu_{max} \leq 4\nu_o$	$\nu_o+\nu_{max} \leq 4\nu_o+4\nu$
$\nu \leq 3\nu_o-\nu_{max}$	$(\nu_{max}-3\nu_o)/4 \leq \nu$
These inequalities, as well as (G9), will be satisfied if...	
$\alpha\nu_{max} \leq 3\nu_o-\nu_{max}$	$(\nu_{max}-3\nu_o)/4 \leq 0$
$(\alpha+1)\frac{\nu_{max}}{3} \leq \nu_o$ (G11-2)	$\frac{\nu_{max}}{3} \leq \nu_o$ (G12-2)
c) Fixed ν' and neutron energy loss: $\nu_o = \nu' + \nu$	
$\nu'+\nu_{max} \leq 4\nu'+4\nu$	$\nu'+\nu+\nu_{max} \leq 4\nu'$
$(\nu_{max}-3\nu')/4 \leq \nu$	$\nu \leq 3\nu'-\nu_{max}$
These inequalities, as well as (G9), will be satisfied if...	
$(\nu_{max}-3\nu')/4 \leq 0$	$\alpha\nu_{max} \leq 3\nu'-\nu_{max}$
$\frac{\nu_{max}}{3} \leq \nu'$ (G11-3)	$(\alpha+1)\frac{\nu_{max}}{3} \leq \nu'$ (G12-3)
d) Fixed ν' and neutron energy gain: $\nu_o = \nu' - \nu$	
$\nu'+\nu_{max} \leq 4\nu'-4\nu$	$\nu'-\nu+\nu_{max} \leq 4\nu'$
$\nu \leq (3\nu'-\nu_{max})/4$	$\nu_{max}-3\nu' \leq \nu$
These inequalities, as well as (G9), will be satisfied if...	
$\alpha\nu_{max} \leq (3\nu'-\nu_{max})/4$	$\nu_{max}-3\nu' \leq 0$
$(4\alpha+1)\frac{\nu_{max}}{3} \leq \nu'$ (G11-4)	$\frac{\nu_{max}}{3} \leq \nu'$ (G12-4)

H - PRACTICAL DETERMINATION OF EXPERIMENTAL AND INTRINSIC PEAK POSITIONS

The peak position of an experimentally obtained neutron group is usually determined in a straightforward manner using the mid-position of the full width at half height (above background). It is generally assumed that one tenth of this linewidth is a very conservative estimate of the uncertainty on the peak position [SV67] and, as a result of the near symmetry of most neutron groups, the uncertainty on the position of the half maximum usually has little effect on the determination of the peak position.

However, the observed lineshape is a convolution of the lorentzian intrinsic lineshape with the gaussian instrumental resolution; see equations (F6-1), (F7), (G1) and (G3). There are various methods which can be used in order to extract the intrinsic peak position from the experimental lineshape. The most meaningful of these seem to be the ones which (numerically) integrate the actual dispersion surface over the resolution function of the spectrometer according to equation (G3). Such an approach, if it is to be self-consistent, will take into account the curvature of the dispersion surface as well as the wavevector dependence of the phonon eigenvectors. Both of these factors are especially important in the case of small wavevector phonons where the simplifying assumption of a planar dispersion surface [CO67;LA70] is far from valid. Also, the neglect of the variation of the eigenvectors within the resolution ellipsoid can sometimes yield a lineshape which is qualitatively different

from the observed one [CO71].

The procedure for the numerical integration* of equation (G3) consists in dividing into a fine mesh of points the $\underset{\sim}{Q}$-space region around the nominal $\hat{\underset{\sim}{Q}}$ value corresponding to the spectrometer setting. At each of these points, the phonon eigenfrequencies and eigenvectors are computed using an appropriate set of AFC's and the individual contributions to the integral are summed up. The result is a calculated lineshape which is a function of ν or $\underset{\sim}{Q}$ depending on whether the calculation is for a constant-$\underset{\sim}{Q}$ or a constant-E scan. By comparing with the frequency (or wavevector) value derived from the AFC's alone and which corresponds to the nominal fixed values of $\underset{\sim}{Q}$ (for constant-$\underset{\sim}{Q}$) or ν (for constant-E), a resolution correction which gives a measure of the apparent peak shift as a result of resolution induced effects can be calculated for various points along a branch.

In principle, these calculated corrections depend on the topology of the dispersion surface and hence on the AFC's. However, in practice, the dispersion surface changes relatively little as a function of temperature and hence, one set of correction values obtained using the AFC's corresponding to one temperature is applicable over the whole temperature range of the crystal phase. A possible difficulty may arise with Kohn "anomalies" which tend to be smeared out at high temperatures; in this case it is preferable to choose a set of AFC's appropriate to the mid-temperature range in order to even out the possible effects on the calculated corrections.

*) The computer programme used for the lineshape calculation was originally written by S.A.Werner and R.Pynn. It was later modified by J.Skalyo-Jr who kindly sent us his improved version [WE71].

In such a formalism, which is really based on the harmonic theory, the linewidth of the calculated lineshape is only caused by resolution effects. In practice, anharmonicity will make the experimentally observed linewidth broader (see equation F7). We will now describe the procedure used to extract the intrinsic linewidth from the experimental linewidth.

I - PRACTICAL DETERMINATION OF EXPERIMENTAL AND INTRINSIC LINEWIDTHS

Because of the relatively poor statistics characteristic of the data obtained by triple-axis spectrometry, linewidth measurements are much less accurately determined than those of the peak positions. Even with a well defined neutron group, there are two major points to take into account:

1) The determination of the background level is affected with a large degree of arbitrariness and, since it is usually a significant fraction of the peak level (especially at high temperatures), this arbitrariness results in a corresponding uncertainty on the value of the experimental linewidth. In order to obtain meaningful data, we have adopted a procedure, which could be called a "planimeter procedure" and which consists in normalizing the integrated intensities of experimental lineshapes along a given branch with respect to a "standard" phonon so selected because of its high quality and its unambiguous background level.

   The integrated intensity of this standard phonon is obtained by measuring with a planimeter the area under the one-phonon

peak; this area is then converted trivially to an integrated intensity. A similar procedure is used on the other phonons along this branch and their background levels are individually adjusted until their integrated intensities are consistent with that of the standard phonon. Such a comparison can only be made rigourously on the basis of equations (F2-1) and (F6-1). However, under the assumption that these phonons are all measured in the same general region of $(\underset{\sim}{Q},\omega)$ space, we can neglect variations of the most slowly varying terms in these equations, i.e. $|\underset{\sim}{Q}\cdot\underset{\sim}{e}(\lambda)|^2$, $|\underset{\sim}{k}'|/|\underset{\sim}{k}_o|$ and $e^{-W(\underset{\sim}{Q})}$ as well as neglect possible variations in the resolution function and in analyser reflectivity (in the case of fixed-E_o scans). Thus, one is left with the following expression for the ratio of the integrated intensities:

$$\frac{A_2}{A_1} = \left\{\frac{n(x_2)+1}{x_2} \Big/ \frac{x_1}{n(x_1)+1}\right\} \frac{M_2}{M_1} \qquad \text{(I1-1)}$$

where

$$x_i = h\nu_i/k_BT \cong 48\ \nu_i[\text{THz}]/T[\text{K}] \qquad \text{(I1-2)}$$

$$n(x) = 1/(e^x-1)$$

A_1: Measured integrated intensity of the standard phonon of frequency ν_1

A_2: Calculated integrated intensity of a phonon of frequency ν_2

M_1 (M_2): Value of the incident beam monitor for the standard (calculated) phonon.

These expressions are valid for both neutron energy gain and energy loss measurements if the usual convention is followed

whereby energy loss (gain) values are represented by positive (negative) values of the frequency. This is a natural consequence of the identity:

$$\frac{n(-x)+1}{-x} = \frac{n(x)}{x} \qquad (I2)$$

A simple calculation based on equation (I1-1) can easily be handled using a small electronic calculator. If a "hand calculation" has to be done, figure II-1 will help to simplify the task.

2) Once the background level has been satisfactorily estimated, the experimental linewidth is determined from the total linewidth at the half intensity level above the background. Since the observed lineshape results from a convolution of the intrinsic lineshape (pseudo-lorentzian) with the resolution function (gaussian) of the spectrometer (see sub-section II-G-2), the intrinsic linewidth cannot be simply extracted from the experimental data. However, in a situation where the intrinsic linewidth is comparable to or larger than the resolution width, it has been verified numerically by Buyers and Cowley [BU69] that such a deconvolution procedure can be simplified by assuming that the intrinsic lineshape is also gaussian; thus, the intrinsic linewidth can be extracted trivially. None of the measurements reported in this thesis were done at temperatures below room temperature; consequently, in all but the very lowest energy phonons that could be observed, the intrinsic linewidth was always non-negligible relative to the resolution width and permitted the use of this simplified calculation.

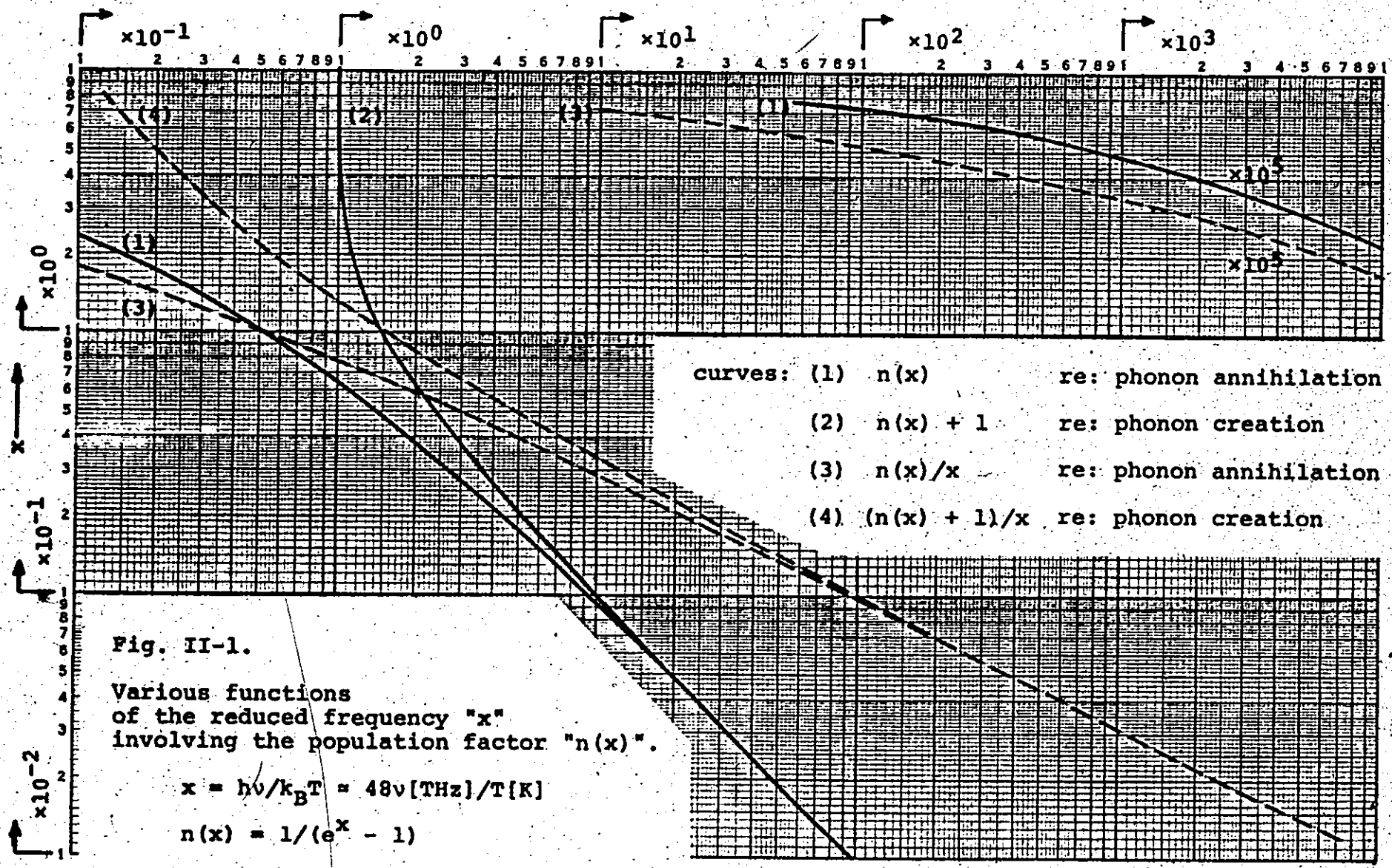

Fig. II-1.

Various functions
of the reduced frequency "x"
involving the population factor "n(x)".

$$x = h\nu/k_B T \approx 48\nu[\mathrm{THz}]/T[\mathrm{K}]$$

$$n(x) = 1/(e^x - 1)$$

CHAPTER III

THE FURNACE: DESIGN, CONSTRUCTION AND OPERATION

A - INTRODUCTION

The high temperature measurements described elsewhere in this thesis were performed using a furnace whose technical characteristics will now be reviewed; consequently, this chapter will be quite technical. Before proceeding further in this vein, it would be appropriate to acknowledge many helpful discussions with Messrs. D. Hodgson, H. Newmayer and Dr. A. Becker during the various stages of the design; a large fraction of the machining was done professionally by the employees of the University Machine Shop under the expert guidance of Mr. S. Kocsis.

This furnace has operated for months at 1063°C. The safe upper limit of the present design is estimated to be 1250°C, this value being dictated by the maximum operating temperature of the heater. It is believed that this upper temperature limit could safely be extended to 1600°C by adding two inner molybdenum radiation shields and replacing the present Kanthal heater either with a platinum one or a platinum-10% rhodium element, or better still, by installing one of the high temperature low voltage heaters supplied by Sylvania [T1] in a variety of configurations. In order to reach still higher temperatures

it is felt that the distance between beam centre and the top of the specimen table, presently set at 15 cm, should be increased to allow for proper insulation and reasonable gradients in temperatures. This suggestion will be dealt with in more detail in the sub-section on the vacuum chamber.

B - GENERALITIES

Ideally, in a high temperature neutron scattering experiment, one would like a system capable of maintaining a specimen at any desired elevated temperature with utmost stability and uniformity and with a minimum of interference with the neutron beam. Needless to say, the conditions should be such that the specimen is not deteriorated by chemical (e.g. oxidation) or physical (e.g. phase transitions) processes. In practice, the heart of the furnace will have a vertical cylindrical geometry because of the fact that neutron spectrometers are restricted to analysing neutrons scattered in the horizontal plane only.

C - THE COMPONENTS

Let us consider in turn

1) the furnace itself
2) the associated components

1) The Furnace

Basically the furnace is a vacuum chamber with a heat source arranged to give an homogeneous temperature distribution in a region called the scattering volume; this region refers to the volume in real space "seen" by the spectrometer. Since

the neutron beam has a cross-section of 5.2×5.2 cm and since we are only interested in the scattering in the horizontal plane, the scattering volume has the dimensions of a vertical cylinder of height and diameter equal to 5.2 cm. In practice it is desirable to design the hot zone larger than the scattering volume so as to minimize the end effects which would tend to create temperature inhomogeneities. Also it is important to avoid the presence of furnace material, e.g. heater, radiation shield, etc..., in the scattering volume so as to minimize the diffuse, coherent and/or the incoherent scattering in the analyser by this polycrystalline material.

The heat source was chosen to be a resistive element and will be described later; the possibility of induction heating was rejected for reasons of economy. The choice of a vacuum environment was selected because it eliminated one possible form of heat loss and provided an environment incapable of reacting with or diffusing in the specimen. Since at high temperature (T>700°C), thermal equilibrium is attained mostly by radiation, the vacuum atmosphere has no significant effect on the thermal time constant of the system and the homogeneity of the temperature distribution; this is not so at lower temperature (T<400°C), and, in such a situation, it is possible to inject an exchange gas in the system. In principle this gas should be helium because of its high thermal conductivity and chemical inertness, but air can also be used in the

case where the specimen is relatively non-reactive at the given temperature.

For the sake of reliability, a very conservative design was adopted, since the furnace was expected to operate for months without major technical problems in order to sustain the prolonged high temperature regime for the normal duration of a neutron scattering experiment. Particular attention was given to the pumping capacity, the heat dissipation, the optimization of the radiation shield design and the conservative loading of the heater. That this concern was worthwhile was later demonstrated by the good ultimate vacuum that was obtained, even at the highest temperatures, and the speed at which outgassing could be handled when the temperature is increased. The efficient cooling obviously meant that the external surface ($T<40°C$) was safe both for the operator and the rubber seals and insulations. Finally, the design of the heater has provided a satisfactory performance, and was adopted by S. Boronkay in a similar project, after encountering difficulty with one of another type [BO73]. In order to illustrate the characteristics of the furnace, table III-1 is given.

We will now briefly consider the various components of the furnace proper, i.e.

a) the vacuum chamber
b) the pumping system
c) the radiation shields
d) the heater
e) the specimen holder
f) the temperature sensors
g) the heat dissipation.

Table III-1

Technical Characteristics of the Furnace

Dimension of the heart of the furnace: vertical cylinder of height = 12 cm and diameter = 8 cm

Heater type and geometry: Kanthal-A wound as a vertical concentric double loop; [T4].

Number of radiation shields: 1 to 7 (adjustable)

Primary pump: Alcatel #2012, double stage, 300 lit/min. operating at 1-10 μm Hg; [T10].

Secondary pump: Edwards #E02, oil diffusion type, 150 lit/sec ultimate vacuum: 10^{-7} mm Hg; water cooled; [T11].

Typical vacuum at 1000°C : 1×10^{-6} mm Hg

Power requirement: 20 W at 400°C
130 W at 700°C
475 W at 1063°C

Power Supply: 117 VAC 1 phase (stabilized)
3.2 KVA Variac
120 V/48 V, 2KVA step-down transformer

Cooling requirement: 1 litre H_2O/min.

Thermocouples: 4 ceramocouples type 5K-1110A, 1.6 mm O.D.
Supplier: Thermoelectric, Brampton, Ontario; [T5].

Reference junction temperature: 0°C (ice bath).

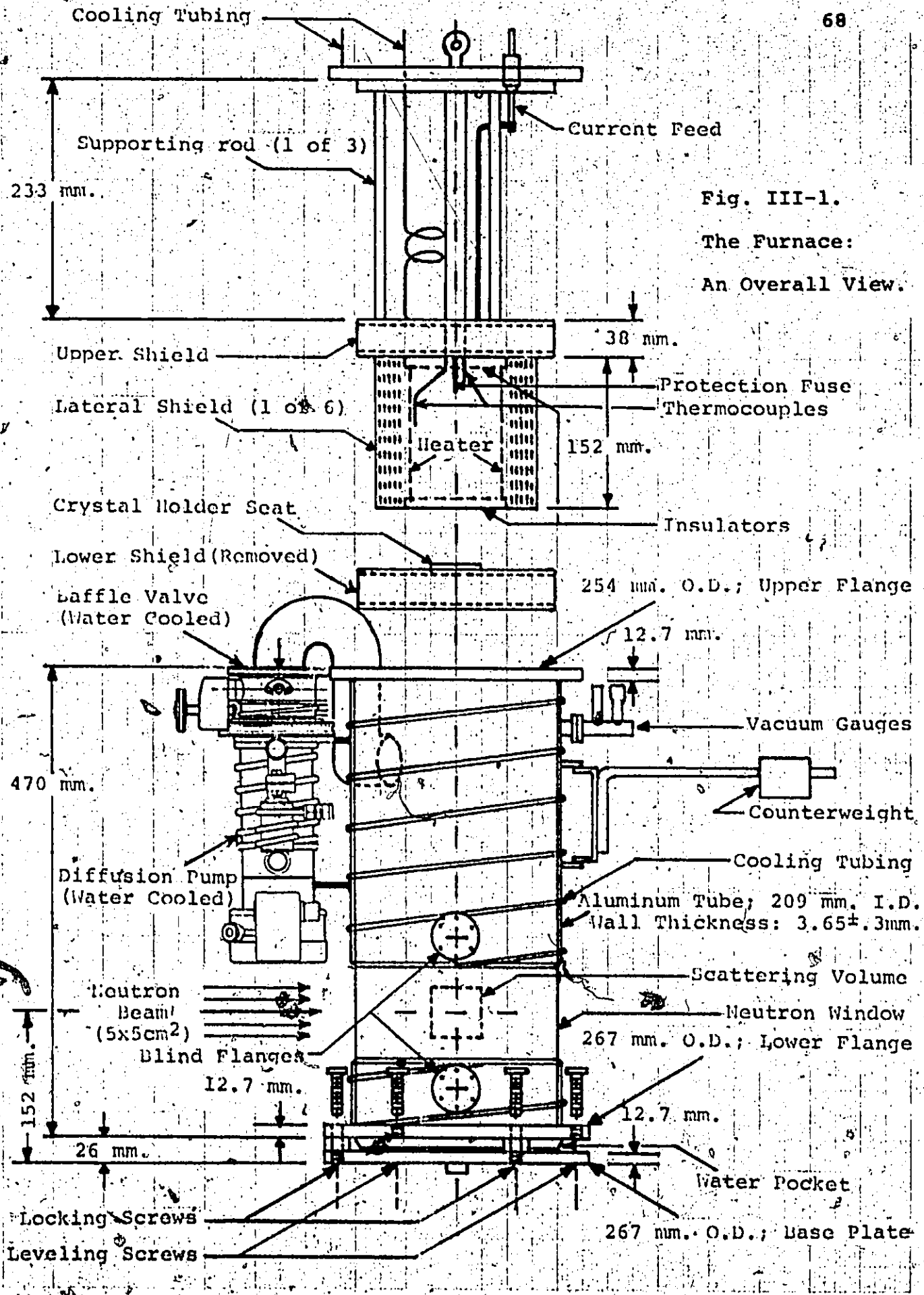

Fig. III-1.

The Furnace:

An Overall View.

a) The Vacuum Chamber

As figure III-1 illustrates, this is basically a vertical cylinder with the top end open to give access to the inside and to receive the top plate which holds the heater, the radiation shields and the feed-throughs. In the region where the neutron beam penetrates in the chamber, both the outer and inner faces of the cylinder were machined to produce a neutron window of constant thickness all around the chamber. This chamber sits on the spectrometer through a base plate which holds it by a three-point support which is used for fine alignment of the specimen; the coarse alignment (within 1°) is achieved in a similar way by tilting the high temperature crystal holder itself when the top of the furnace is removed. There is a gap of approximately 15 mm between the base plate and the bottom of the chamber so as to accommodate a water pocket through which a continuous flow of water is maintained in order to dissipate the heat coming from the heart of the furnace which is just some 50 mm above the bottom plate. Cooling of the lateral wall is achieved by a water flow circulating in a spiralled coil in contact with the chamber wall.

The tube is made of aluminum because it offers the best compromise between mechanical strength, machinability and transparency to neutrons. Unfortunately, this is a difficult material to weld and the intimate contact between the cooling coil and the aluminum chamber could not be achieved by welding. Instead,

the coil was wound as tightly as possible on the chamber, both above and below the neutron window, and a sufficient thermal contact was achieved by coating the region where the pipe was wound by a special high conductivity resin [T2].

A total of four ports were machined on the side of the chamber as an aid during assembly and also to give access to the thermocouple feed-throughs. In normal operation, these were capped with a brass blind flange. The diffusion pump was mounted above the neutron window on the side of the chamber and was connected to the chamber via an 8 cm diameter short copper pipe in order to minimize the effect of pipe impedance on the pumping speed. Since the particular diffusion pump and baffle used weigh some 10 Kg, it was necessary to have a counterweight installed to stabilize the system.

It is hoped that the McMaster spectrometer will eventually be modified in order to have a 1.000 metre clearance between the neutron beam axis and the top of the specimen table. For usual room temperature measurements, a removable adapter would bring the effective clearance to the standard value of 15 cm. On the other hand, such a modified spectrometer would accomodate a furnace with a long hot zone, thus minimizing the edge effect on the temperature distribution and providing a reasonable temperature gradient for work at extremely elevated temperatures (T>1600°C). Also it would be possible, with such a design, to mount the high vacuum pump below the heart of the furnace,

thus minimizing pipe impedances and resulting in an equilibrated mass distribution not requiring a counterweight.

b) The Pumping System

The diffusion pump chosen was an Edwards make, model EO2 [T11], with a rated capacity of 150 litres/sec and which requires a loading of 75 cm^3 of oil; type #704 oil [T12] was selected because of its low vapour pressure and because of its inertness in presence of oxygen. This meant that an accidental admission of air in the chamber while it is being evacuated by the diffusion pump will only result in minor damages. This protection proved worthwhile since a strained weld once developed a major leak which did not affect the pump oil.

During operation, the temperature is always raised slowly (< 10°/min) in order to give the primary pump the possibility to maintain the diffusion pump fore pressure at values less than 200 µm Hg, and also to avoid stresses on the ceramic components caused by thermal expansion. In a stabilized situation, the pressure in the furnace was of the order of 1×10^{-6} mm Hg at 1000°C and was monitored by an ionization gauge unit [T13] which fed both a chart recorder [T6] and an excess pressure monitoring circuit (BNC5 of safety monitor; see below). The pump itself was water cooled, so was its baffle to minimize backstreaming. Its temperature and the water flow were checked by a thermal switch and a differential pressure switch connected respectively to BNC3 and BNC4 of the safety monitor.

c) The Radiation Shields

Two types of shields were used:

i) the vertical cylindrical shields
ii) the horizontal inferior and superior shields.

i) The Vertical Shields

These must be such as to produce a minimum of attenuation on the neutron beam and the adopted design consisted of concentric cylinders of stainless steel foils. The height of the cylindrical shield is equal to the width of standard shim stock material, i.e. 15 cm. Since the beam height is 5 cm, this leaves 5 cm for each of the two regions above and below the beam.

The purpose of the radiation shields being to reflect back in the heart of the furnace the escaping radiation, thus reducing the power input requirements and hence the loading on the heater, their arrangement must be optimized to accomplish this with the minimum of attenuation of the neutron beam. The number of shields was calculated in a simple-minded fashion assuming that radiation is the sole mode of heat loss, yielding the following relation between the temperatures of the various shields:

$$T_{n+1} = (2)^{1/4} T_n$$

the high index corresponding to the inner shield. If we assume that the above relation holds for all shields we get

$$n+1 = \frac{4}{\log 2} \log\left(\frac{T_{n+1}}{T_o}\right)$$

where T_o is the temperature of the external wall and

T_{n+1} is the temperature of the specimen.

In the case of an experiment performed at 1336 K (1063°C) with the external wall maintained at 313 K (40°C) for obvious safety reasons, we obtain n ≈ 7. Using the above relation, the temperature of the various shields can be calculated and we obtain the following approximate values: 372, 442, 526, 626, 744, 885, and 1053 K. All shields were as thin as possible (25 μm) except for the three inner ones which were respectively 75, 125 and 250 μm thick in order not to deform at high temperature*.

ii) The Horizontal Shields

These do not need to be transparent to neutrons; hence, they consisted of fiberized alumina compacted between two metal plates separated by 3 cm. The plate on the low temperature side was kept cooled either by direct contact with a cooling coil in the case of the upper shield or by contact with the water pocket in the case of the lower shield (see fig. III-1). The trade name of the fiberized alumina is Fiberfrax [T3]. This provided lightweight and efficient insulation which could be compacted wherever required.

d) The Heater

The region where a uniform high temperature is desired has a cylindrical symmetry with the height and the diameter both equal to 5.2 cm. In order to obtain a uniform hot zone, an element design consisting of a vertical concentric double loop was adopted. From considerations of the beam size and the restricted distance between the beam centre and the top of the specimen table, the

*) The nuts, bolts and spacers required for the assembly of the vertical radiation shields were made of tungsten and were obtained from "Sylvania Emissive Products" [T1].

ratio of height to diameter of this element was set approximately equal to 2. Had it been possible to use a larger ratio, the end effects with the corresponding temperatures inhomogeneities, would have been minimized; but in the case of the measurements reported here, we have actually measured "in situ" the temperature distribution in the scattering volume and found it to be homogeneous within ±6°C; the presence of a metallic specimen would further homogenize any temperature differentials along the length of the specimen.

The heater material itself was Kanthal A [T4] which allows a maximum filament temperature of 1375°C and a surface loading of approximately 2 watts/cm^2 at this temperature. Kanthal A is an alloy of the following composition: 62% Fe, 22% Cr, 5.5% Al, and 0.5% Co. The manufacturer does not recommend it for applications in vacuum because the aluminum fraction will evaporate instead of forming a protective oxide as in air. However, it was found that by properly oxidizing the element in air during assembly (i.e. 24 hrs at 1100°C as measured with a pyrometer), a sufficiently thick oxide coating was obtained to provide sufficient protection for operation in vacuum. At a high temperature (T>1000°C), there was a noticeable manifestation of evaporation of the filament material as indicated by the fact that the temperature was slowly decreasing ($\lesssim$ 1/2°C/day) thus reflecting a change in resistance of the filament. This was compensated by a small manual adjustment of the input voltage.

The vertical arrangement adopted for the heater meant that a minimum amount of heater material should be used, to minimize interference with the neutron beam. The strip type of Kanthal-A was chosen because of the fact that for a given length of a given resistance (i.e. a given volume of heater material), it has a larger radiating surface than the cylindrical wire type. The strip dimensions are 3×0.3 mm^2; this is the smallest size available. The resistive material was formed into two parallel connected heaters which were wound between an upper and a lower ceramic ring machined from pyrophilitte. The lower ring was entirely supported by the upper one through the filament and it was allowed a vertical clearance in order to compensate for the thermal expansion of the heater. The maximum safe voltage that can be applied at its terminal is 55 V.A.C. supplied by a step-down transformer which also effectively eliminates possibilities of short-circuits should a grounded metallic object (e.g. radiation shield) come in contact with the heater during operation at high temperature.

e) The Specimen Holder

Experiments to be carried out near the melting point of substances having a reasonably high melting temperature must provide a means of mounting the specimen crystal in such a way as to satisfy the following requirements.

i) Containment of the liquid metal in case of accidental melting.

ii) Minimum of attenuation of the neutron beam by the foreign material in the neutron path.

iii) The material of the crystal holder should not contaminate the crystal by molecular diffusion during the prolonged operation at high temperature.

iv) The design should be such as to provide firm mechanical support over a wide range of temperature where differential thermal expansion may produce large effects.

v) Finally, in the case of substances like copper having a low value of the bulk modulus near the melting point, the crystal should be held in position in such a way as to create a minimum of stress within its volume.

For these reasons, the usual method of clamping the crystal or that of enclosing it in a tight fitting cylinder (if its geometry so allows) were not used in our experiments.

In the case of copper, which becomes soft near the melting point, the crystal holder was such as to provide a close contact of the crystal external surface with the crucible material in the vicinity of the melting point. This was possible because the Cu crystal had been grown with a near perfect cylindrical geometry. Close contact at high temperature meant that the crucible material had to have a linear expansion coefficient less or equal to that of the crystal. Graphite was chosen for the crucible material because it satisfied requirements "ii" and "iii". It also has a small coefficient of thermal expansion and it can be easily machined.

As fig. III-2 shows, the crystal holder consists of a thin walled graphite cylinder which can be mounted on the 3 points support in the heart of the furnace. There is provision for mounting small crucibles containing various temperature standards both at the top and bottom of this main crucible. When the crystal is aligned in a (001) plane, the axis of the crystal holder is nearly vertical. Two small notches of conical shape were made at the top and bottom of the crystal, on the axis, and to a depth of $\sim$ 2 mm. These are meant to sit on little pointers machined in the top and lower part of the crucible. At low temperature, the crystal is kept oriented by these two contact points on the axis since there is a gap between the crystal and the vertical surface of the crucible. As the temperature is increased, this gap is decreased because of the different thermal expansion and the top of the crystal pushes on the graphite piston which is driven up.

At the highest temperature, the copper crystal should be of the same O.D. as the value of the I.D. of the crucible, thus providing uniform support.

We have verified that this method maintained perfect crystal alignment (within 0.05°) as the temperature is increased. However, upon cooling, the graphite piston does not slide down by itself but has to be pushed down by hand after opening up the furnace. For this reason, the measurements were performed at progressively higher temperatures.

Fig. III-2. Holders for the Palladium and Copper Crystals.

Material: Graphite; all dimensions in mm. ±0.5 mm.

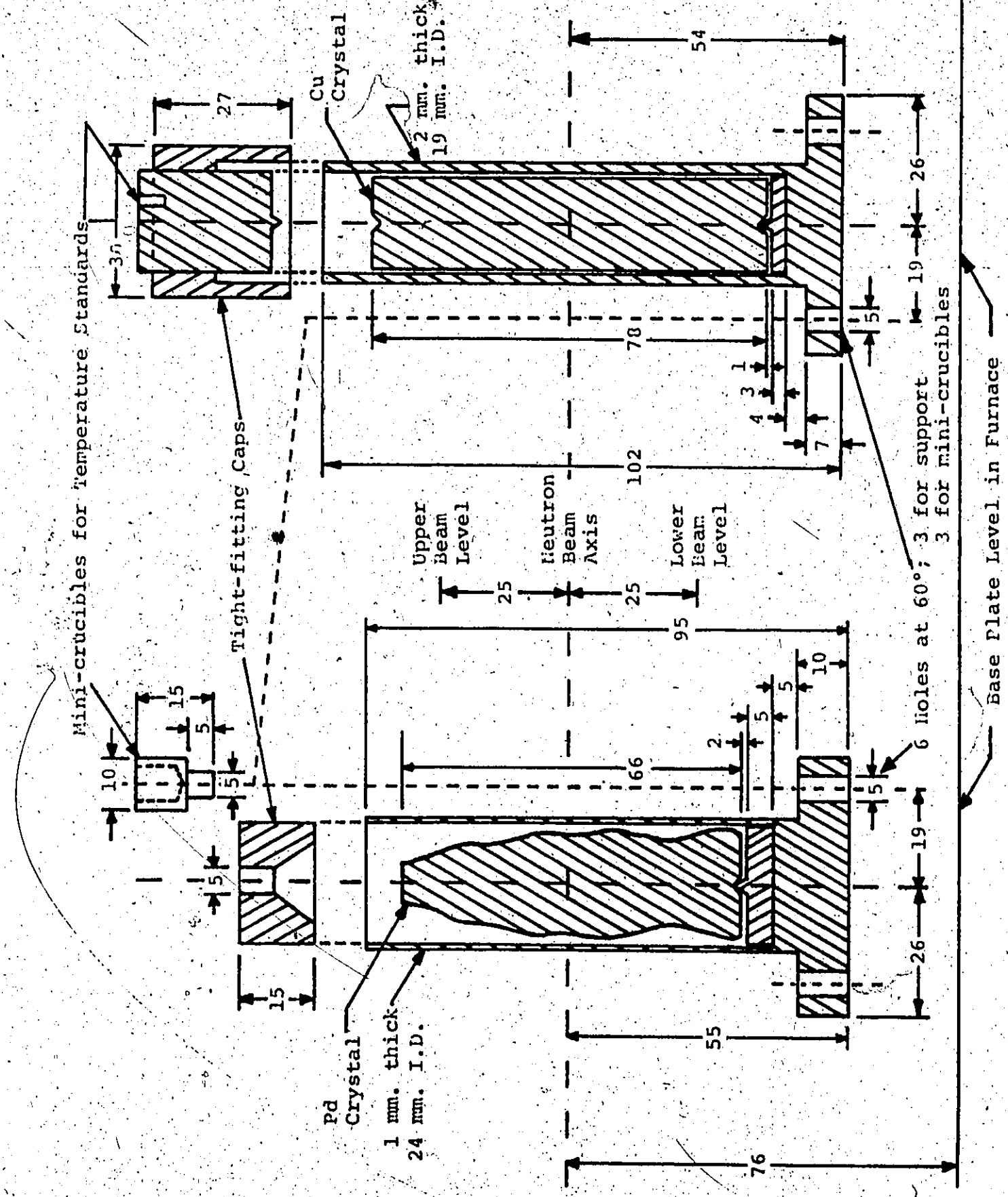

Using the following average values of $3.6\times10^{-6}\cdot C^{-1}$ and $20\times10^{-6}\cdot C^{-1}$ for the respective linear expansion coefficients of polycrystalline graphite and monocrystalline copper [H1], we calculated that the room temperature difference between the crystal O.D. and the crucible I.D. should be 0.317 mm in order for the two to make intimate contact near the melting point.

In the case of the crystal holder for the palladium experiment, the requirements were slightly different in the sense that measurements were not to be performed in the immediate vicinity of the melting point (T_m = 1552°C, [H2]), but at the relatively low temperature of 1050°C where the crystal is still rigid enough to be self-supporting. However, in order to maintain a good crystal alignment at all temperatures, we have used a modified version of the "movable piston" type of mount. In this case, it was not necessary to have intimate contact between the crystal surface and the inside of the crucible. Consequently the crystal was left in its rough shape resulting from it being grown by pulling from the melt. Fig. III-2 also illustrates the palladium crystal in its mount.

f) The Temperature Sensors

The temperature was continuously monitored by four chromel-alumel thermocouples with the reference junction maintained at 0°C using a water-ice mixture. These were of the commercial type, Ceramocouple type 5K1110A [T5], with an operating range between -200°C and 1370°C and a typical sensitivity of ∿ 40 μV/°C.

From the mechanical point of view, these are encapsulated in a stainless steel sleeve 1.6 mm in diameter and 450 mm in length. As with any thermocouples, it is important to minimize the perturbation caused by the thermal flow through the thermocouple wires and sleeve. This was achieved by choosing the diameter of the sleeve as small as possible while of sufficient thickness to withstand prolonged operation without pitting. Also, all thermocouples were mounted such that a significant fraction of their length was in the hot zone, so again as to avoid falsification of the temperature readings by thermal conductivity. The sensing junction of each was mounted as follows: three were monitoring the temperature at the mid-beam and lower beam levels and the upper furnace level while the fourth one was immersed in one of the lower lateral mini-crucibles (cf fig. III-2). These were filled with a convenient temperature standard (e.g. Ag; T_m = 960.8°C; [H2]) in order to allow "in situ" calibration of the thermocouples. The mini-crucibles were made of graphite since the standards were always noble metals and these are known not to "wet" graphite.

From the electrical point of view, the thermocouples were electrically grounded to the sleeve in order to provide fast thermal response. Three of them were connected to a voltage divider and then to a 12-channel chart recorder [T6]. The fourth one, that is the one closest to the mid-level of the specimen, was connected to a high-impedance differential voltmeter [T7], whose output, i.e. the amplified deviation of the thermocouple voltage from a pre-set value, was used to feed, among other things, the 12-channel recorder. More details will be found in the section on the associated components.

In order to minimize the noise level in the necessarily long wires connected to the thermocouple, we have done as follows:

- The required extension wire carrying the thermocouple signal was of the same nature as the thermocouple itself (i.e. chromel-alumel).

- The only junctions with a dissimilar metal in the circuit (i.e. copper) was maintained at 0°C both in the case of the chromel-copper and alumel-copper junctions. This prevented the generation of spurious thermal E.M.F. while providing a fixed temperature standard.

- All wires (2 conductors) were twisted and shielded to minimize interference pick-up, and the shield was grounded at one end only to avoid "ground-loops".

As a further precaution meant to increase our confidence in the temperature readings given by the thermocouples, we inserted flattened gold pellets and copper chips (T_m respectively

1063°C and 1083°C; [H2]) in two of the upper and two of the lower mini-crucibles. After a series of measurements at the gold point (and possibly 5°C above) were completed, we verified that this temperature had really been attained by inspecting the content of the mini-crucibles. In all cases, the gold pellet had become spherical while the copper chips were unaffected except for a discoloration probably caused by a "getter effect".

It is felt that an upper limit on the accuracy of the temperature measurement is ±7°C. This is a consequence of the above considerations and also of the fact that some measurements were performed on the Cu crystal at 1076°C (i.e. T_m - 7°C) without destroying the crystal. However, when later dismantling the furnace, it was realized that the lower 9 mm of the crystal had melted and recrystallized. Temperature stability however was much better, being of the order of ±0.5°C, thanks to the fact that we used a regulated power supply [T9] to feed the furnace. With such an arrangement, negative feedback is not required to provide the desired temperature stability.

g) Heat Dissipation

As we said before, water cooling was chosen to cool the furnace chamber itself and for this reason it was also used to cool the diffusion pump. This method offered the following advantages:

- possibility to cool the baffle valve, thus minimizing the backstreaming from the diffusion pump.
- In case of power failure, cooling would still be maintained as opposed to the case where forced air cooling is used.

- A small water flow (∿1 litre/min.) was sufficient to cool all components with a temperature rise between inlet and outlet of the order of 5°C.

- The water flow could easily be automatically monitored on the return line thus detecting possible problems with the cooling and interrupting the power before serious damage was done.

The various elements requiring cooling were connected in series with Tygon pressure tubing in the following order, the first few of these being those requiring water at the lowest possible temperature:

Water supply (∿1 litre/min.)
Baffle valve
Diffusion pump
Main O-ring
Upper wall of the chamber
Lower wall of the chamber
Water pocket
Upper shield
Water pressure monitor
Water return line.

During operation above 1000°C, the hottest external element was the neutron window; its temperature was of the order of 40°C because it is not in direct contact with the cooling coils.

The water pressure monitor consisted of a pressure-sensing switch, commercially known as a "Mercoid Pressure Control" [T8]. The water flow was checked by measuring the pressure differential across a valve immediately downstream from the "Mercoid", this valve being adjusted to create a pressure differential of ∿ ½ Kg/cm^2 under conditions of normal flow. The internal switch of the "Mercoid", electrically closed when the cooling water circulates normally, was connected to BNC4 of the Safety Monitor (see below).

2) The Associated Components

The previous sections dealt with the furnace proper, that is the part of the system that is directly mounted on the neutron spectrometer. We will now briefly consider other components and fig. III-3 illustrates their arrangement.

The furnace is fed from a controller which, in turn, is fed from a voltage regulator [T9]. The controller supplies both the diffusion pump and the heater, but on different circuits, the reason being that there may be anomalies which require the interruption of power in only one of these. The controller is a slave unit to the safety monitor which, as its name indicates, monitors the status of five variables related to the safe operation of the furnace. A twelve-channel chart recorder [T6] keeps track of the behaviour of the vacuum and temperature at various points in the furnace as well as the incident neutron flux in order to detect possible deviation of the reactor from a steady state condition which could affect the signal/noise ratio. One of the temperature recording channels was actually reading the difference from a preset value, after amplification by the differential voltmeter [T7] circuitry. This allowed us to graphically resolve temperature fluctuations of the order of 0.1°C.

a) The Furnace Controller (fig. III-4)

This unit provides direct control of the power reaching the diffusion pump and the heater. The former requires only 117 VAC/3A which can be supplied to it only if there is a 24 VDC level on BNC2, that is, only if the diffusion pump temperature, the water flow and the vacuum are normal.

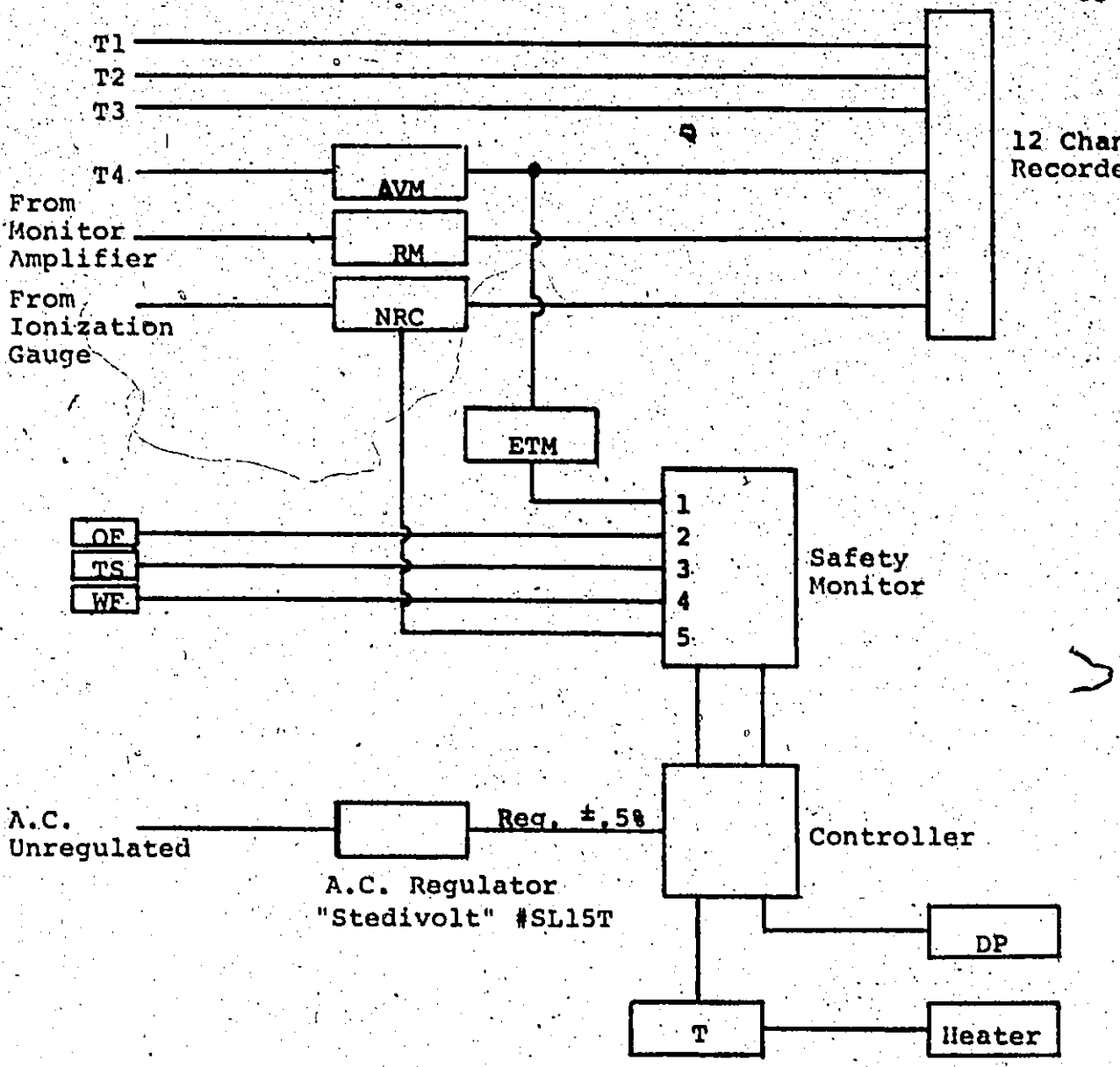

Fig. III-3.
Schematic Of The Furnace Related Components.

DP: Edwards type EO2 Oil Diffusion Pump.
ETM: Excess Temperature Monitor.
NRC: NRC Type 710B Ionization Gauge Control.
OF: Oven Fuse Made Of Material Melting At Suitable Temperature (e.g. Au).
RM: Rate Meter.
T : Step-down transformer, 2KVA, 140v/55v.
TS: Thermal Switch Mounted On Diffusion Pump.
T1-T4: Chromel-Alumel Thermocouples, Thermo-Electric Type 5K 1110A.
AVM: DC Differential Votmeter, Hewlett-Packard #3420A.
WF: Water Flow Monitor, Mercoid Type DA-31-3-3A.

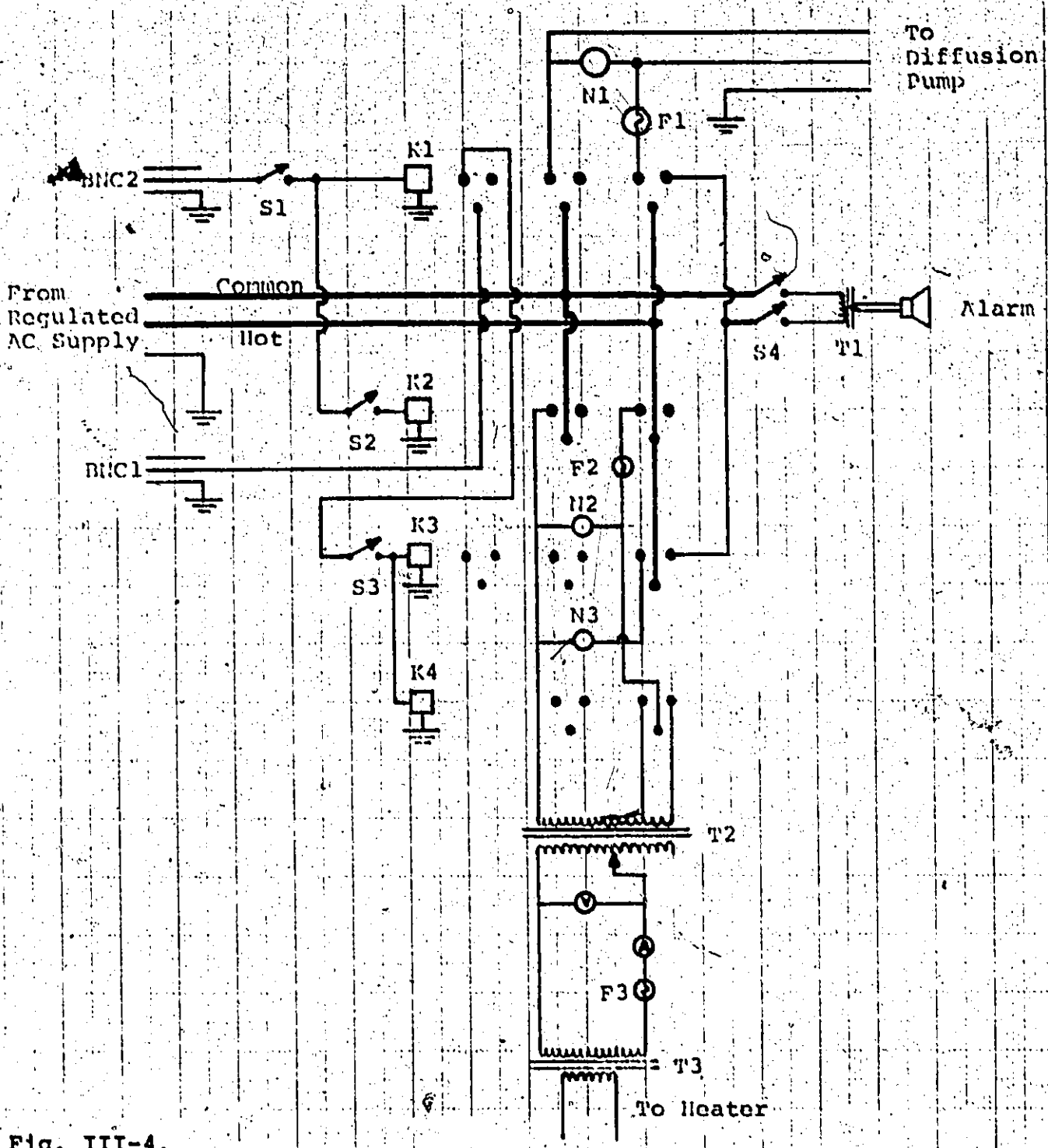

Fig. III-4.
Furnace Controller Circuit Diagram.

F1: 4A. Slow-Blow Fuse
F2: 20A. Slow-Blow Fuse
F3: 20A. Slow-Blow Fuse
S1, S2, S3, S4: DPDT Switches
N1, N2, N3: Neon Lamps (117VAC), DIALCO Type 507-4537
T1: Step-down Transformer 117v/9v.
T2: Variac, 3.2KVA, 1Phase, 117v/117v or 140v depending on connection
T3: Step-down Transformer 140v/55v, 2KVA; actually 2x1KVA Transformers
BNC1: +24VDC from BNC 12 of Safety Monitor.
BNC2: +24VDC " " 345 " " "
K1, K3: Potter&Brumfield #KUP14D55, 24VDC Relays, Rating:10A, 3PDT.
K2, K4: " " #R11DY , 24VDC Relays, Rating:25A, DPDT.

On the other hand, the heater circuit contains a Variac and a step-down transformer to provide 0-55 VAC required by the heater. The Variac's input has two windings; in normal operation (i.e. with a 24 VDC level on BNC 1), a step-up value of 1:1.2 is used while a 1:1 ratio is used if a preset temperature limit has been exceeded (i.e. no voltage level on BNC1). This arrangement allows the furnace to cool sufficiently (i.e. ~ 150°C) in case of excessive temperature without undergoing the sudden cooling that would take place if the power was completely interrupted. Thus, the temperature can be reset more rapidly and the crystal is less likely to loose its alignment than if the temperature drops by a few hundred degrees. Only if there is an anomaly affecting the diffusion pump temperature, the water flow and/or the vacuum will the heater circuit be completely de-energized, as well as that of the diffusion pump.

b) The Safety Monitor (fig. III-5)

This is simply a bank of five relays monitoring five different variables; these are the vacuum, the diffusion pump temperature, the water flow and the temperature measured by two different sensors. Each of these is a switch which has its contacts closed under normal conditions, thus allowing the relays 1 to 5 to be maintained energized. When an anomaly occurs, the corresponding relay is de-energized and stays so until manually reset, thus allowing to identify the variable that has triggered the alarm, from the corresponding neon-lamp that lights up.

The various sensors are as follows:

- Vacuum: internal relay in ionization control unit (See fig. III-6 for modifications).

- Diffusion pump temperature: Bi-metal switch mounted on the diffusion pump.

- Water flow: Mercoid Pressure Control [T8], in series with a "pinching" valve.

- Temperature sensor #1: this is basically an oven "fuse", made of a fine wire having a suitable melting point. A copper wire was used most often.

- Temperature sensor #2: The voltage from one of the thermocouples is fed to the differential voltmeter; its output is fed to one channel of the recorder and a digital voltmeter [T14] calibrated to read the temperature deviation in °C as well as an operational amplifier biased so as to break the circuit to BNC #1, if the differential voltmeter exceeds its full scale value.

When the temperature in the furnace is increased, two of these monitoring relays are effectively inhibited by the bypass switch (S6 on fig. III-5) in the case of the vacuum monitor and by decreasing the sensitivity of the differential voltmeter in the case of the temperature sensor #2.

An abnormal condition on either of the temperature sensors will remove the bias at BNC12 thus switching to the smaller transformer ratio in the Variac. Similarly an abnormal condition on either the vacuum sensor, the diffusion pump sensor and/or the flow sensor will remove the bias at BNC345, thus shutting off the diffusion pump and the heater.

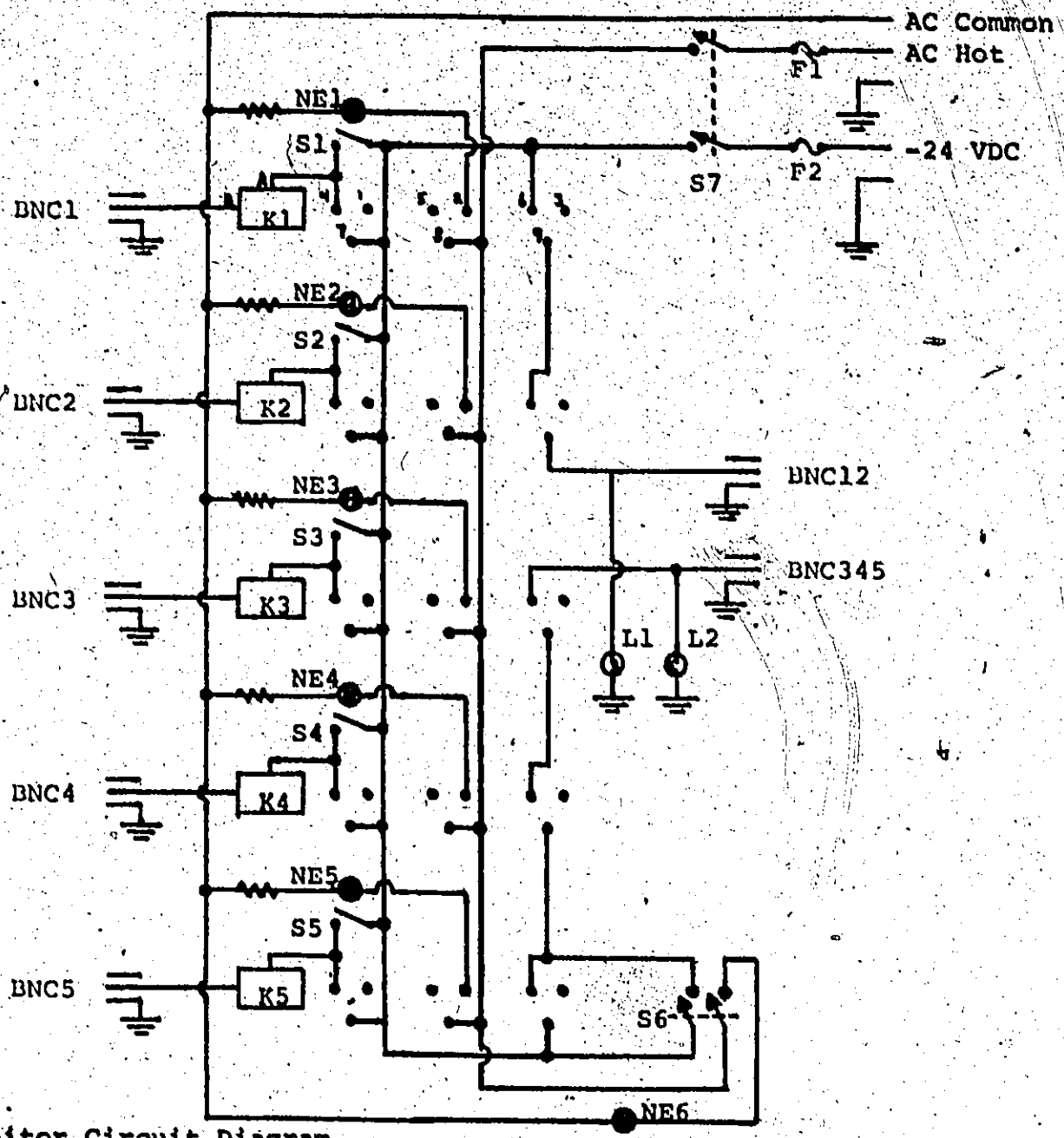

Fig. III-5.
Safety Monitor Circuit Diagram.

K1-K5: Potter & Brumfield #KUP14D55, 24VDC Relays, 3PDT.
BNC1: From Preset Excess Temperature Monitor.
BNC2: From Oven Fuse.
BNC3: From Cooling Water Flow Monitor.
BNC4: From Thermal Switch On Diffusion Pump.
BNC5: From Vacuum Monitor.
BNC12: To BNC1 Of Furnace Controller.
BNC345: To BNC2 " " "
S1-S5: N.O. Switches Energizing Corresponponding Monitoring Relay.
S6: DPDT Switch Inhibiting Vacuum Monitor (Used On Initial Pumping).
S7: DPDT Power Switch.
NE1-NE5: Neon Lamps Indicating Anomalies.
N.B. S1 and NE1 up to S5 and NE5 are single units "Gray-Hill"#40-1
NE6: Neon Lamp Indicating When The Vacuum Monitor Is Inhibited (S6 Closed)
L1, L2: Type T-1 3/4 Lamps (28Volts).
F1: Fuse On AC Line, 1/16A Fast-Blow.
F2: Fuse On DC Line, 3/4 A Slow-Blow.

c) The Primary Pump

This was connected to the diffusion pump via a short length (∿ 2m) of Tygon pressure tubing. The particular model chosen, Alcatel #2012 [T10], was a double stage unit which can provide, according to the specifications, an ultimate vacuum ∿ 0.05 μm and a pumping speed of ∿ 300 lit/min. Here, it is important to have a reasonable pumping speed in the primary stage in order to cope rapidly with the outgassing whenever the temperature is increased. Under stable conditions, this unit maintained a pressure of ∿ 5 μm Hg at the outlet of the diffusion pump; this pressure was never allowed to exceed 200 μm Hg when the temperature is increased in order to operate the diffusion pump in the recommended regime. This was sufficient if the temperature rise is less than 10°C per minute.

* * * * * * * * * *

Fig. III-6, Modification to the Ionization Gauge Control Unit to allow Interfacing with Safety Monitor.

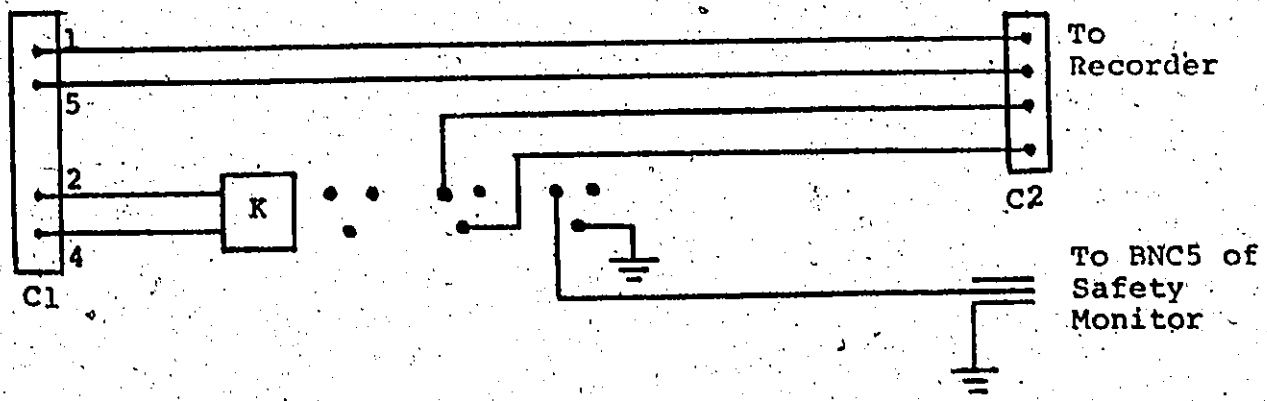

C1: Rear Socket Connector on NRC type 710B Ionization Gauge; [T13].
C2: Externally Mounted Connector
K : Potter & Brumfield AC Relay, type KUP14A55.

Fig. III-7. Two views of the specimen holders.
-Upper picture: from left to right, we see a minicrucible, the specimen holder for the experiment on Cu, the Cu crystal with the graphite piston sitting on top of it, the stainless steel weight that fits inside the piston and the compression ring. This photo was taken after the termination of the experiment and the near-melting that took place during the high temperature measurements is readily apparent from the recrystallisation at the base of the crystal. The shiny color on the external surfaces of the graphite component is caused by Ag deposition during temperature calibration.
-Lower picture: the assembled specimen holders for the Cu crystal (on the left) and for the Pd crystal (on the right). In the latter case, the holder is mounted on the lower radiation shield which has been removed from the furnace.

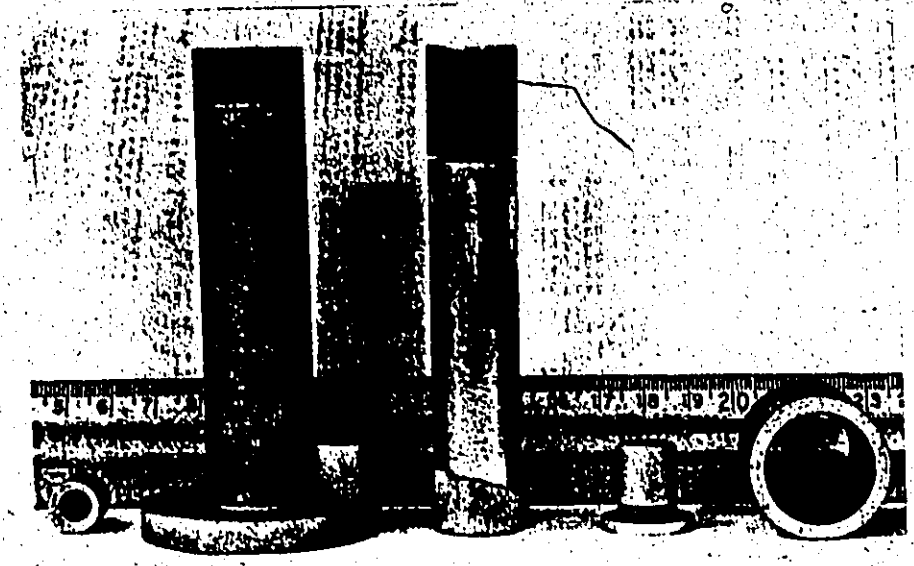

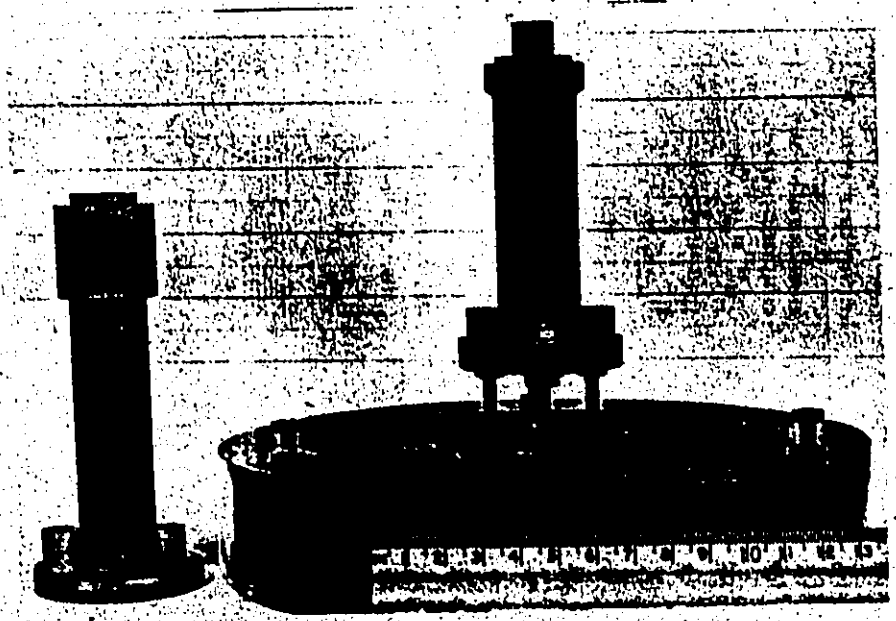

Fig. III-8. The furnace on the triple-axis spectrometer at the McMaster University reactor during the course of the experiment on Pd (summer 1974). The control unit for the furnace is in the foreground.

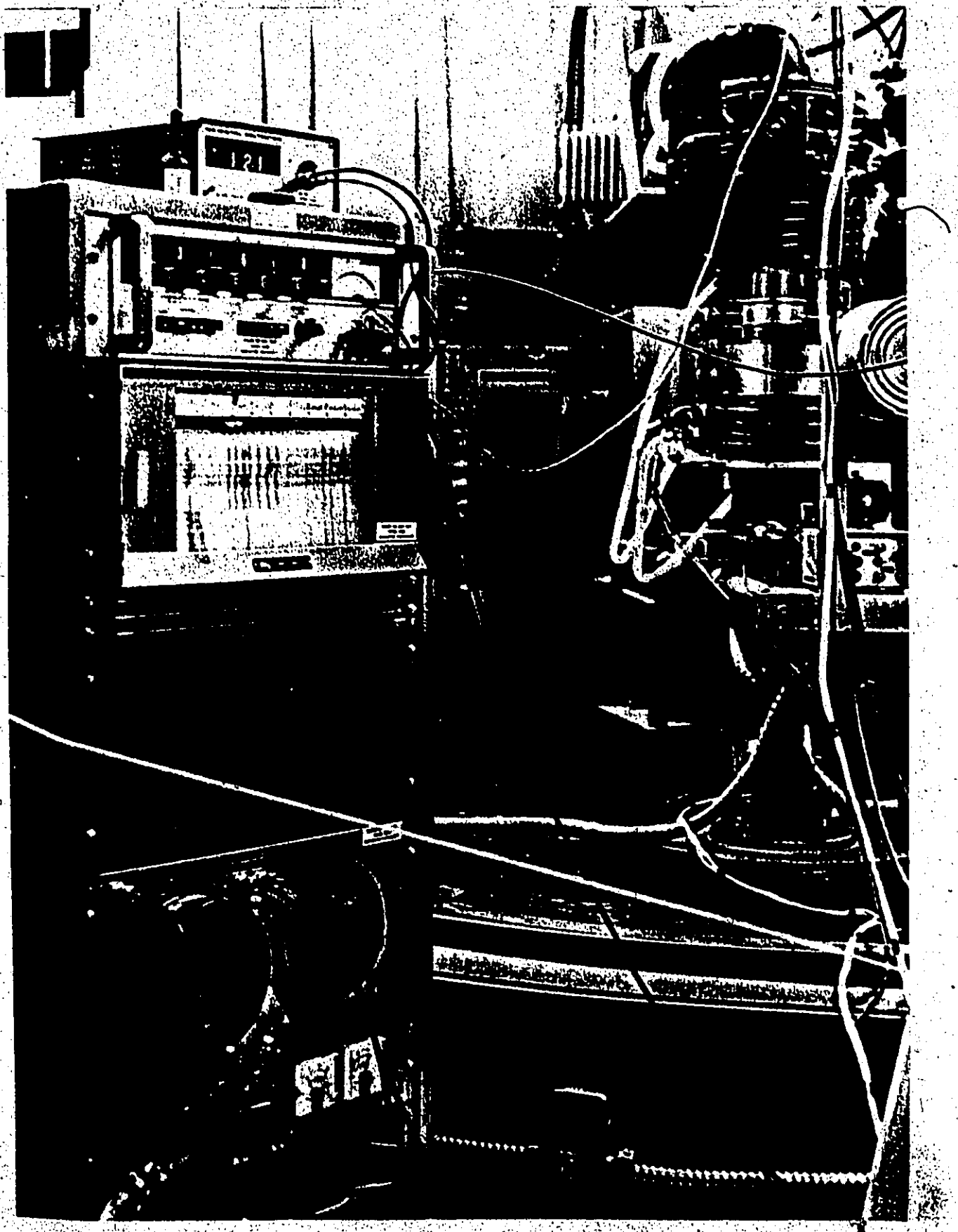

Fig. III-9. A view of the furnace on the two different McMaster triple-axis spectrometers used for this research.
-Upper picture: at the McMaster University reactor.
-Lower picture: at the NRU reactor, Chalk River.

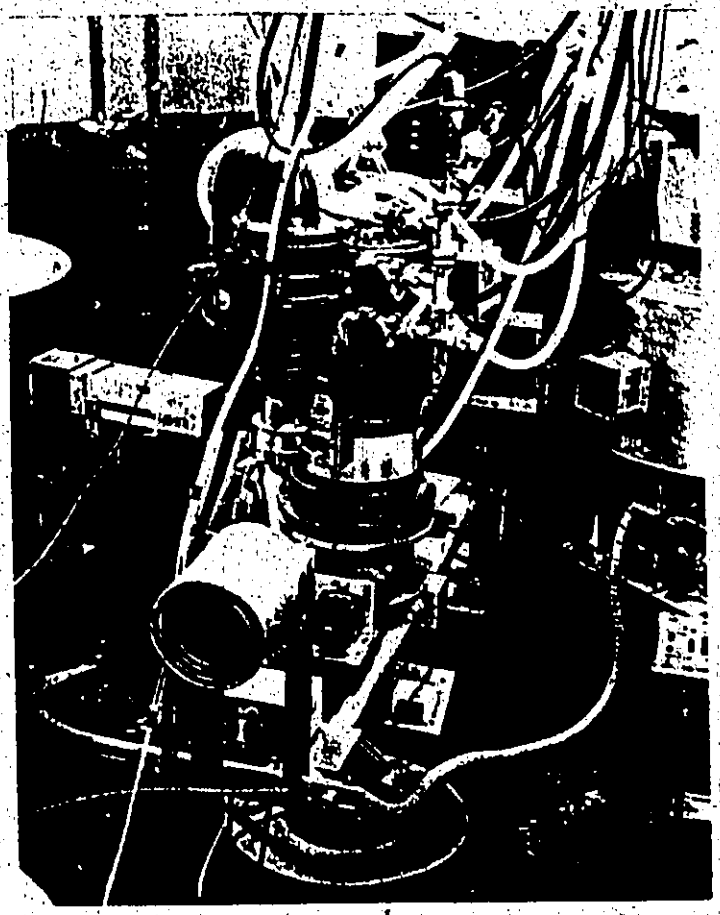

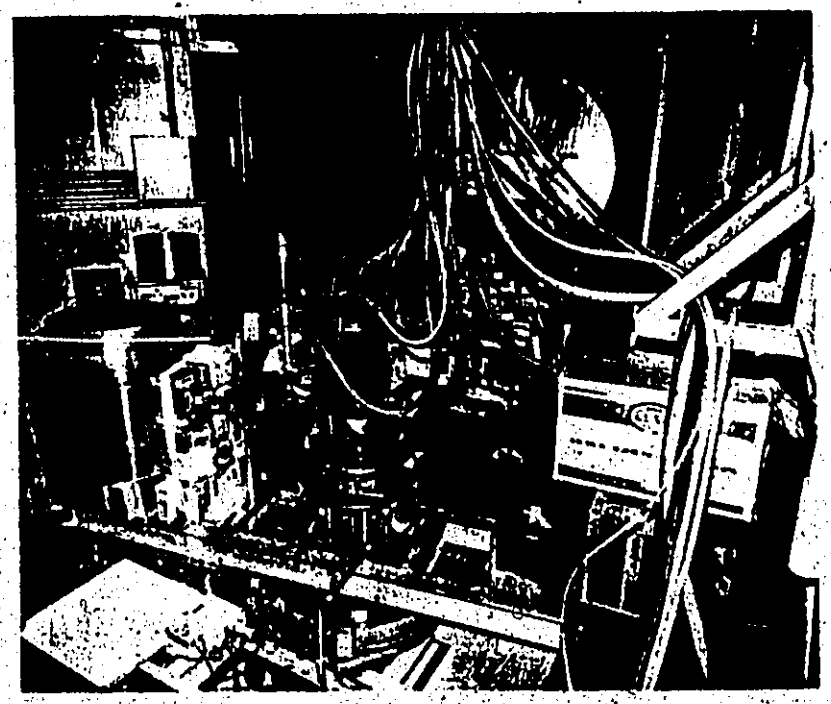

Report on research

(By André Larose)

McMaster's nuclear reactor is an important tool in the research effort taking place on campus. It provides irradiation facilities and beams of nuclear radiation used in the study of biological and physical systems. The recent improvement in available fluxes of neutrons resulting from the upgrading of the heat exchanger's capacity of 5000 Kilowatts operation has increased the usefulness of this research instrument.

Neutrons are one of the by-products of a nuclear reaction and can be profitably put to use in the investigation of condensed matter (solids and liquids). This arises from the fact that thermal neutrons have a "de Broglie wavelength" comparable to interatomic spacings in condensed matter and an energy similar to that of elementary excitations, e.g. phonons, magnons. Thus changes in momentum and energy after the interaction of a neutron with an elementary excitation can be precisely measured.

The technique of thermal neutron spectroscopy consists in using this property to obtain information concerning elementary excitations whose energy spectrum depends on the internal potentials of condensed matter.

An instrument which has gained universal acceptance for this type of measurement is called a triple axis spectrometer and was developed by Dr. B.N. Brockhouse, of the Physics Department. Basically, it selects neutrons of a given energy from the reactor spectrum by Bragg reflection using a monocrystal. This monochromatic beam is then allowed to interact with a target specimen and the scattered neutrons are energy analyzed by Bragg reflection as well. Scanning is done in a predetermined way and the spectrometer is controlled indirectly by a computer.

Current programs of research using the triple-axis spectrometer are the study of the temperature dependence of the phonon spectrum of copper up to the melting point (1083°C) and a determination of the spectrum of mercury, a substance having a very high capture cross-section and consequently a very difficult material for this type of work.

These studies are being carried out by Messrs. André Larose and R. Dymond, respectively.

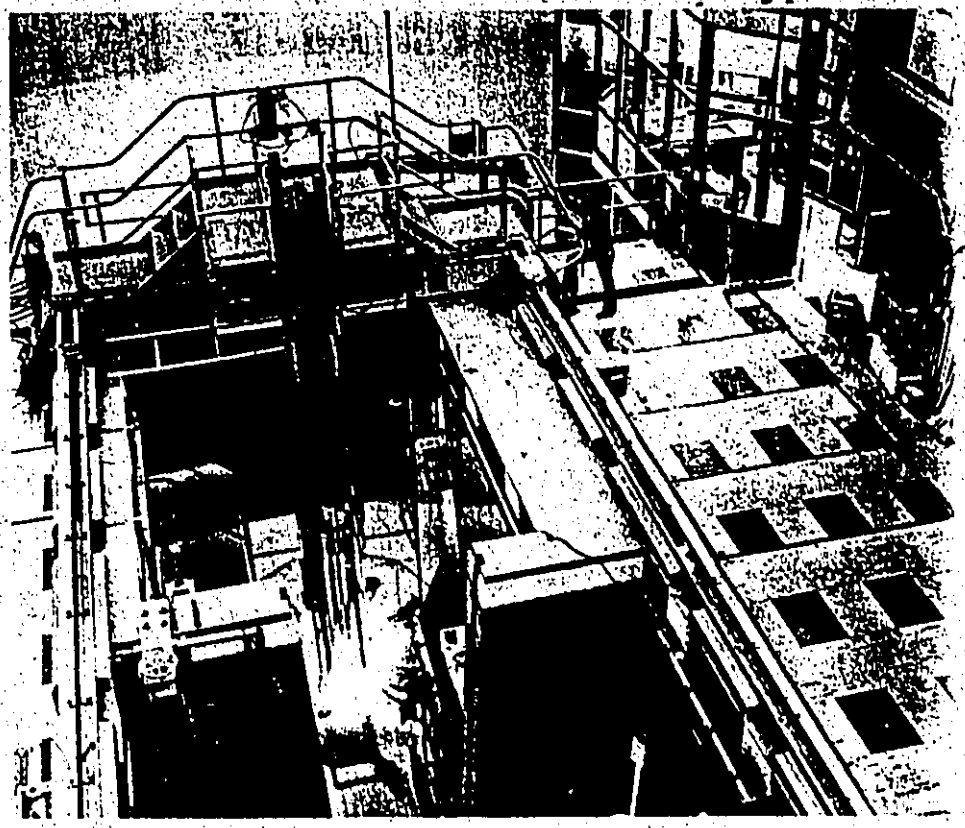

The top picture shows a general view of McMaster's nuclear reactor from the top of the building. The core of the reactor is immersed under ten metres of water which acts as a biological shield and as a coolant. The glow visible in the pool is caused by Čerenkov radiation, a phenomenon produced by electrons leaving the core with a velocity faster than that of light in water. Experimental facilities are located at the core level, on the lower floor of the building. The control room is located on the upper floor and is visible in this photograph. The bottom picture is a view of a triple-axis spectrometer. The target is located in the centre of the instrument; the incident beam tube is visible on the centre left while the analyzer is on the left. In this case, a high temperature neutron scattering study is in progress; the phonon spectrum of copper is being investigated up to the melting point, i.e. 1083°C.

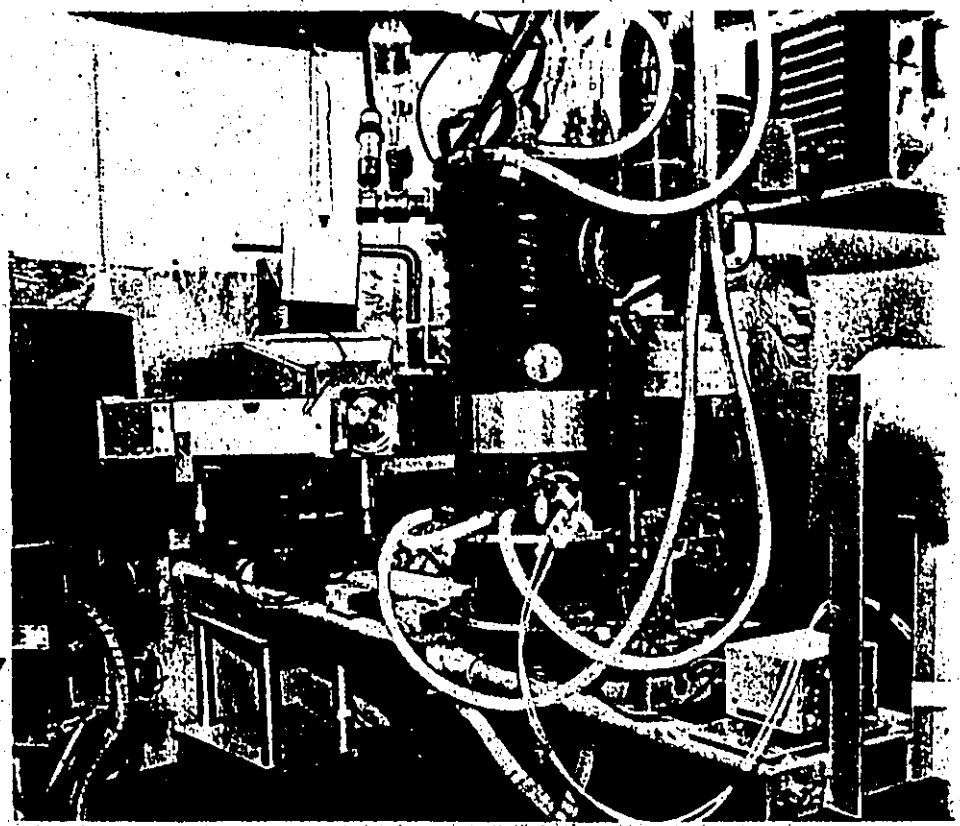

Fig. III-10.
Other views of the set-up at the McMaster University reactor, from "Contact" 4, #41 (1973), and originally published for the benefit of the University community.

CHAPTER IV

COPPER: TEMPERATURE DEPENDENCE OF THE PHONON SPECTRUM BETWEEN 22°C AND THE MELTING POINT (1083°C).

A - INTRODUCTION

We now come to the major chapter of this research, where the results of a detailed study of the temperature dependence of the phonon spectrum of Cu will be discussed. This element belongs to the family of noble metals which also includes Ag and Au. The noble metals are particularly interesting from the point of view of the solid state physicist in the sense that they are monovalent and also have completely filled d-shells; consequently, they are somewhat similar to the alkali metals, which are thought to be theoretically well understood, at least as far as their main features are concerned. As a result of the large spatial extent of these d-shells within the unit cells, the d-electrons are not strictly localized and contribute to the overlap of the ionic cores. This overlap plays an important role in the static and dynamical behaviour of noble metals; unfortunately, it adds to the complexity of any first principles calculations. For this reason, the noble metals are often viewed as a link between the "simple" alkali metals and the transition metals.

In order to illustrate the challenge facing the theoreticians working on the noble metals, it may be useful to the reader to refer to two recent publications [MO72; CO74] where various formalism are used in the calculation of the phonon spectra of these metals;

with a very unsatisfactory degree of success. Now that this work makes available experimental data over an extended temperature range, it is hoped that this will stimulate further theoretical work.

Experimentally, the phonon spectra (at 22°C) of all three noble metals have been determined. Both Ag and Au have relatively unfavorable neutron properties (see table IV-1) and, for this reason, were not studied until recently [KA69; LY73]; as expected however, their spectra turned out to be homologous with that of Cu. The superior neutron properties of Cu have long made it possible to measure its spectrum [CR60]. This initial work was crude by today's standard, however; it was later followed by the more detailed studies of Sinha [SI66], Svensson et al [SV67] and Nicklow et al [NI67]. Their analysis has demonstrated the predominance of the first-neighbour interaction which results mainly from the overlaping of the d-shells on adjacent ions. The longer range interactions were found to extend up to possibly the sixth-nearest neighbours and to satify the conditions for axial symmetry.

Amongst other interesting features of this spectrum, their work showed the fact that the T_1 branch appears to be remarkably dispersionless (i.e. linear in wavevector) up to $\zeta \approx 0.5$. This is in sharp contrast to the corresponding situation observed at the same temperature (i.e. 22°C) in some other FCC metals, as will be seen for example in the next chapter in the case of Pd.

A first attempt to observe manifestations of anharmonicity on the phonon spectrum of Cu was made by Nicklow et al [NI67] who

have performed systematic measurements at 49 K and 298 K. For most phonons, they found a very weak dependence on temperature, the most dramatic effects being of the order of 4% in the case of the lowest frequencies. Thus, already at 298 K ($T/T_m \approx 0.22$), anharmonicity starts to manifest itself! Later, the study of the anharmonic regime was extended further when Miiller et al [MI71] published their results for 293 K, 473 K and 673 K, obtained as part of their determination of the electronic specific heat of Cu. Finally, this was complemented by the work of Nilsson et al [NI73] who obtained data in the off-symmetry directions at 80 K.

In monovalent metals like the alkali and the noble metals, the electron-phonon interaction is weak, contrary to the situation prevailing in multivalent metals, e.g. Pb [BR61; ST67]. The weakness of the electron-phonon interaction is reflected in the fact that none of these monovalent metals are known to become superconductor at the presently attainable temperatures. A corollary to this is the absence of strong manifestations of the Kohn effect in the phonon spectra of these metals (see section II-C). However, it is possible that the magnitude of Kohn effects may also depend on the crystal structure [VO65; NI74] and that the FCC structure may be more favorable for such an effect than the BCC. In the case of Cu, a Kohn effect was unobservable in the data of Svensson et al [SV67] although it was expected in the $[0\zeta\zeta]T_1$ and $[0\zeta\zeta]L$ branches. Following this work, however, Nilsson et al [NI68; NI74] have published the results of very high resolution measurements which have revealed unambiguous manifestations of the Kohn effect both in symmetry and off-symmetry directions.

The purpose of our study is to complement the relatively complete set of phonon data for Cu at room temperature and below, by an equally extensive and systematic study of the high temperature regime. Considering that the most dramatic manifestations of anharmonicity are likely to occur in the immediate vicinity of the melting point, the measurements of the phonon spectrum were performed from room temperature up to within 20°C of the melting point (T_m = 1083°C; [H5]). The apparatus described in chapter III was designed and built for this purpose.

Since the anharmonic frequency shifts and lifetimes are only weakly temperature dependent, particular care was given to minimizing and correcting for instrumental aberrations. The various phonons were measured at each temperature using the same instrumental setting, i.e. same calibration, same region in $(\underset{\sim}{Q},\omega)$ space. Also, the resolution effects on the observed peak positions and linewidths were numerically calculated and compensated for in the determination of the intrinsic values. Finally, the internal consistency was verified by performing the measurements on two different triple-axis spectrometers.

The experimental results can be divided in two distinct categories dealing respectively with phonons of general wavevectors and those of "small" wavevectors, all wavevectors being along directions of major symmetry; the reason for this distinction will be explained later. Suffice it to say now that the first and second categories respectively provided information about the temperature dependence of the AFC's and of the zero-sound elastic constants (see sections II-B, -D and -E).

B - SPECIMEN, APPARATUS AND PROCEDURE

The specimen used in this experiment was a monocrystal* having a near perfect cylindrical geometry with a (001) axis within 5° off its cylindrical axis. Its diameter and height were 19 mm and 78 mm respectively. Its mosaicity was measured by rocking a Cu(200) Bragg peak against a perfect Ge(311) monochromator which was set up to measure neutrons of $\lambda = 2.17$ A; this corresponds to a scattering angle of approximately 75° for both the Cu and Ge reflections. A parallel scattering configuration was used and a value of 0.2° was obtained for the mosaicity of the Cu crystal..

The specimen was mounted in a graphite holder in the manner described in sub-section III-C-1-e. This required the machining of a small conical seat ($\sim$ 1 mm deep) on the centre of each of the two flat faces in order to provide the required support at "low" temperatures when the crystal was not in close contact with the walls of the crystal holder. The quality of the alignment was found to be maintained up to the highest operating temperatures, as long as all measurements were performed in the order of increasing temperatures, for the reasons already outlined in sub-section III-C-1-e.

The crystal holder with its mini-crucibles containing the temperature reference standards was mounted inside the furnace and coarsely aligned (within 1°) relative to the scattering plane, using the internal adjustments and with the furnace axis approximately set in a vertical position. Then, the internal adjustments were tightened and the furnace cover inserted. The system was evacuated and the fine alignment (within 0.1°) was achieved using the external adjustments which were then locked in place. Finally, the electrical

*) Supplier: Research Crystals, Richmond, Virginia, U.S.A.; nominal purity: 99.999%.

and water connections were completed and, from here on, the furnace was left untouched for the duration of the experiment in order not to affect, however minutely, the crystal's alignment and orientation (ψ_o) with respect to the incident beam.

The temperature was measured using four chromel-alumel thermocouples (sensitivity: $\sim$ 40 μV/°C) and mounted as discussed in chapter III. These were sensing respectively the temperature at the lower and upper levels of the hot zone and also at the centre and lower portions of the irradiated volume of the crystal. We were particularly cautious to avoid systematic errors in the thermometry process, as the precautions outlined in sub-section III-C-1-f indicate. Exclusive reliance on thermocouple readings was avoided by verifications "in situ". One such verification involved the determination of the E.M.F. reading corresponding to the melting of a temperature standard (Ag; T_m= 960.8°C [H5]) inserted in one of the minicrucibles.

Also, during the course of an experiment, the mini-crucibles, both above and below the neutron beam, contained other temperature standards, consisting of flattened pellets of Au (T_m=1063°C [H5]) and Cu (T_m = 1083°C [H5]). The purpose of the Au standard was to indicate if the maximum temperature reached is within 20°C of the melting point of the Cu specimen while the Cu standards, being of a much smaller mass than the bulk specimen, would reveal the existence of localized "hot spots". After termination of a series of measurements extending up to near the melting point, the value of the highest temperature reached could be confirmed (within 20°C) by examination of the contents of the mini-crucibles. In all

instances, the Cu standards have maintained their original shapes (i.e. they never exceeded 1083°C) while the Au standards had melted and resolidified into perfectly spherical droplets (i.e. the temperature exceeded 1063°C).

The Cu specimen itself acted as a temperature standard. However, it could not be visually inspected after each series of measurements since this would have affected its alignment. When it was finally removed from its holder at the very end of the experiment, it was discovered that its lower portion ($\sim$ 9 mm) had melted and resolidified into a polycrystalline mass. For most of the measurements, the highest operating temperature was within a few degrees of the gold point; this permitted safe operation for extended periods without being uncomfortably close to the melting point of the specimen. However, as will be discussed later, a short series of measurements were performed within 7°C of the melting point in order to examine the behaviour of the T_1 branch in the immediate vicinity of T_m. It seems that an onset of melting occurred during this period in a localized area of the specimen. This, as well as the behaviour of the Au pellets, confirms that the temperature readings obtained from the thermocouples were well within 1% of the true temperature of the specimen.

C - THE EXPERIMENT

The neutron scattering measurements were performed using the two McMaster University triple-axis spectrometers respectively located at the NRU reactor of the Chalk River Nuclear Laboratories (CRNL) and at the McMaster Nuclear Reactor (MNR); these instruments have been described elsewhere [RO66A; BR68; HA69A]. Under favourable

conditions, all of the measurements could have been performed using the NRU facility since this is an amazingly versatile instrument#, considering its low capital cost. It can be operated indifferently in either a fixed ν_o or a fixed ν' configuration and the range of incident frequencies extends from 3.7 to 15.3 THz using a permanently mounted pair of Cu(220) monochromators [DY70]. Such a range is sufficient to permit suitable calibrations for the measurements of both the overall spectrum and the zero-sound elastic constants. Most important of all, as anyone aware of the serious flux limitations in triple-axis spectrometry will appreciate, this instrument is mounted on possibly the second best thermal neutron beam hole (#E2) in the wall of a first class research reactor.

Unfortunately, the timing of this project did not coincide with the priorities of CRNL and NRU was shut down from 5/VI/72 until 2/VIII/74. Since the construction of the furnace was completed only seven months before this shut-down, top priority was initially given to the completion of systematic measurements of the whole phonon spectrum; indeed, most of these phonons could only be observed using a high flux reactor like NRU.

After the NRU shut-down, the experiment was moved to the MNR*. Since the available flux was some 30 times lower than that of NRU, the MNR facility could only be used to provide data on the low energy phonons and, consequently, the zero-sound elastic constants.

*) In anticipation of the NRU shut-down, the heat exchangers at MNR had been upgraded to permit operation at 5 MW from the previous 1.5 MW.

#) The most recent improvement is described in appendix I.

In addition, certain regions along various branches were investigated using the MNR facility in order to examine in detail the behaviour of phonon energies and lifetimes; these regions included those where a manifestation of the Kohn effect was expected as well as one where a peculiar temperature dependent feature (along the T_1 branch) had been observed for the first time. Some of these measurements were at the practical limit of the MNR spectrometer, often requiring up to 4 days to accumulate acceptable statistics.

The considerations of sub-section II-G were taken into account in the calibration of the spectrometers. For the NRU measurements, where the whole frequency spectrum was being investigated, most of the scans were performed using the method of neutron energy loss with a fixed analysed frequency of 5.2 THz. This has permitted the systematic observation of phonons between room temperature and the melting point. However, at the highest temperature, phonons which underwent extreme line broadening were also measured by neutron energy gain with a definite improvement in the background level; in this instance, a fixed value of 5.5 THz was chosen for the incident neutron frequency.

In the case of the MNR measurements, a high resolution calibration was selected in order to observe phonons at the smallest possible wavevector without interference from the Bragg peak. For lack of sufficient intensities, the scans were limited to, at best, the lower half of the phonon spectrum; this dictated the use of a fixed neutron frequency of 4.2 THz in order to satisfy equations (G10-2) and (G10-3) and to permit measurements at small energy transfers both by the method of neutron energy gain and loss.

Since the monochromator scattering angle cannot be conveniently changed on this instrument, a fixed ν_o procedure had to be adopted for all of the MNR measurements. Whenever possible, each phonon was observed both by the method of neutron energy gain and neutron energy loss, for reasons already outlined in sections II-D and II-G; in other instances, i.e. for energy transfers larger than 1.4 THz, only the energy gain method could be used, because of the low value of the incident frequency purposefully chosen for high resolution.

The calibrations and instrumental parameters relevant to both the NRU and MNR measurements are summarized in table IV-2.

The specimen was mounted in the furnace with its (001) plane in the scattering plane; this meant that its cylindrical axis was nearly vertical. Space limitation did not permit mounting it in any other planes. Consequently, none of the phonons belonging to the $[0\zeta\zeta]T_2$, $[\zeta\zeta\zeta]T$ and $[\zeta\zeta\zeta]L$ branches could be observed. The vertical alignment was always within 0.1° and did not shift significantly with temperature. The angular width of the ψ-rocking scans, both in the case of the Cu(200) and Cu(220) reflections measured with the same instrumental configuration as for the phonon measurements, was always $0.5° \pm 0.03°$, independently of the spectrometer used, and remained so at all temperatures. Similarly, the value of ψ_o, i.e. the specimen orientation relative to the incident beam, was regularly verified and, in particular, at the beginning and the end of a series of measurements at a given temperature; it remained constant throughout.

Phonons were measured at 22°C, 400°C, 700°C and 1063°C (i.e. the Au point; see table IV-1). In the case of the measurements

performed at the MNR, data was also obtained at 920°C in order to gather more information about the trends near the melting point. The 22°C data served both as a standard from which to measure energy shifts and line broadening as well as a means of verifying the published data [SV67] and the validity of the numerical lineshape calculations required to estimate instrumental resolution effects.

In the case of the NRU measurements (see table IV-5), all data were obtained by constant-Q scans, since the experimental conditions were designed to optimize the observation of phonons of "large" energy whose q-gradients were never so large as to prohibit the use of constant-Q. On the other hand, the MNR measurements (see table IV-4) were concerned with the examination of phonons of "small" energy; by their very nature, these usually have large q-gradients. For each branch, a comparative experimental determination was done for selecting the most suitable type of scan; the constant-E method turned out to be definitely superior in the case of the longitudinal branches and marginally superior in the case of the [00ζ]T branch. However, in the case of the T_1 branch, the constant-Q method proved to be superior.

The actual scans were done in a straightforward manner and the overall spectrometer performances were reliable. The temperature was maintained by manual adjustments within ±2°C and a chart recording of the four thermocouple voltages, neutron flux and furnace vacuum helped to locate anomalies. During the NRU measurements, the reactor operated at its maximum power of 120 MW with the usual occurrence of shut-downs expected from a research reactor. The easiest phonon ([0ζζ]T_1, ζ=0.2) required some 45 minutes,

while the most difficult ones, e.g. [00ζ]L,ζ=1.0, required some 15 hours. In the case of the MNR measurements, the reactor operated mostly at its maximum power of 5 MW with some extended periods at 1.5 MW and with very few shut-downs. During operation at 5 MW, the easiest phonon ([0ζζ]T_1, ζ=0.05) required some 2 hours, while the most difficult ones, e.g. [0ζζ]L,ζ=0.30, required over 4 days. Under such difficult situations, the scans were usually repeated two or three times and the counts, added together.

D - ELASTIC SCATTERING RESULTS: TEMPERATURE DEPENDENCE OF THE LATTICE PARAMETER OF Cu

The lattice parameter of Cu at room temperature has been determined, using X-ray methods, by numerous authors and their results, as listed for example by Pearson [H3], are consistent with the value of 3.6147 A (at 20°C) obtained by very careful measurements on a degassed specimen [FR53]. However, there is no profusion of data at high temperatures, and particularly near the melting point. (T_m= 1083°C; [H5]). The highest temperature measurements were performed up to 871°C by Hume-Rothery et al [HU42], up to 530°C by Mitra et al [MI63], up to 1050°C by Simmons et al [SI63]* and up to 910°C by Gehlen [GE69]. Two other determinations are that of Eppelsheimer et al [EP50] who have searched (up to 770°C) for a possible anisotropy in the thermal expansion, and that of Esser et al [ES38] performed up to 1000°C; however, both of these references appear to be unreliable and will not be further considered.

At room temperature, the values found by two of these groups [MI63; GE69] are in mutual agreement but somewhat lower (by ~0.0006 A)

*) It should be noted that this reference has been overlooked by Pearson in the second volume of his comprehensive handbook [H4] which covers this period.

than those of the other two groups [HU42; SI63] who quote values in excellent agreement with what seems to be the best room temperature data available [FR53]; typical accuracies on these measurements are ~0.0001 A. Similarly, at higher temperatures, there are no major discrepancies in the results of these various groups. Between 910°C and 1050°C, the only available data are those of Simmons et al [SI63] who have determined relative, rather than absolute, changes in the lattice parameter.

The lattice parameter of our Cu monocrystal was measured at various temperatures ranging from 23°C to 1063°C in order to complement the X-ray data, particularly near the melting point. The method used was that of elastic scattering described by Ng et al [NG67]; the specimen and experimental configurations were the same as used for the phonon measurements. Consequently, the precision on the measured values of the lattice parameter is not representative of the ultimate capabilities of this technique. Indeed, the quoted uncertainties would have been smaller, had the measurements been performed at the largest possible scattering angle (~140°) using a perfect analyser (typically quartz) and tight collimations (typically ~1/160 FWHM). However, these requirements are incompatible with those for inelastic scattering work where resolution has to be sacrificed in order to obtain practical counting rates.

Measurements of the lattice parameter were obtained both at the NRU and MNR facilities, for temperatures at which phonon measurements were performed, i.e. 22°C, 400°C, 700°C, 920°C (at MNR only) and 1063°C. Generally, the required scans were done

at the beginning of a phonon run at a new temperature and after a minimum stabilization period of some twelve hours. However, toward the end of the phonon measurements (at MNR), a systematic determination of the temperature dependence of the lattice parameter was carried out at 1063°C, 1030°C, 980°C, 930°C, ..., 630°C; the specimen was then allowed to cool to room temperature (during a two week period when the reactor was shut-down) and, upon reactor start-up, similar measurements were performed at 23°C, 134°C, 234°C, 335°C, 434°C, 530°C, 630°C, 680°C, 580°C and 480°C. These scans were usually done after a stabilization period of approximately only one hour; however, below 400°C, the stabilization period was nearly twice as long and the pressure in the furnace was purposefully maintained "high" (~25μm Hg) in order to homogenize the temperature distribution in the hot zone. Since no hysteresis phenomenon was observed in the values measured during cooling and heating and, in particular, since the results obtained at 630°C (and 680°C) were identically the same in both cases, it confirms that the stabilization period was sufficient to allow thermal equilibrium to be reached.

Figure IV-1 illustrates the temperature dependence of the envelopes of families of ψ-rocking scans obtained in this systematic series of measurements; for clarity, only part of the data (~100°C apart) are reproduced. The angular width of these curves is the same at all temperatures, as it should be. The decrease in the peak intensity with temperature reflects the behaviour of the Debye-Waller factor, i.e. of the increased importance of the multi-phonon processes; the through beam is similarly affected, as figure IV-2

illustrates. Because the crystal was mounted in the furnace with a (001) axis vertical, it was not possible, with an incident neutron frequency of 4.2 THz, to use a larger index reflection than Cu(220). A larger index reflection, of course, would have resulted in a larger scattering angle with a corresponding improvement in the resolution, although it would still be limited by the choice of analyser and collimators.

Using the accepted values for the lattice parameter and the thermal expansion coefficient at 20°C [FR53; SI63], the corresponding value for the lattice parameter for the lowest temperature scan was calculated. For example, in the case of the MNR data (see fig. IV-1), this yielded 3.61488 A for the magnitude of the lattice parameter corresponding to the standardization scan at 23.1°C; a slightly different quantity was obtained in the case of the NRU data where the lowest temperature was slightly different. Measurements at high temperatures are relative to these low temperature standards in either cases and the final uncertainties were determined from the RMS of the $1/20^{th}$ of the full (angular) width at half maximum of the envelopes of families of ψ-rocking scans at the standardization and at the high temperatures. This is a very conservative estimate as far as the relative shifts by thermal expansion are concerned, but it is probably a realistic measure of the absolute uncertainties, i.e. $\pm$0.0024 A. During this part of the measurements, temperature stability was within 1.5°C, except at 134°C and 234°C where it was three times worse; following the considerations of section IV-B, the uncertainty on the temperature is estimated at $\pm$5°C and possibly $\pm$2°C.

The resulting values for the lattice parameter are listed in table IV-3 and plotted in figure IV-3 where the results of the other four high temperature measurements (by X-rays) have also been included. The absolute accuracy of these latter measurements is typically one order of magnitude better than that of our results and cannot be represented on this figure. All the experimental values listed in table IV-3 were obtained with the MNR spectrometer and were substantiated by the relatively few similar measurements performed on the NRU spectrometer.

In comparison with the X-ray results, the agreement is excellent below 500°C, except possibly in the case of the data of Hume-Rothery et al [HU42] which tends to be consistently larger than either the neutron or other X-ray results. Above 500°C, on the other hand, the neutron results fall systematically below those of X-rays and also show a more pronounced upward curvature, particularly above 700°C. In all cases, however, the discrepancies are smaller then the uncertainties on the neutron results.

Our results were fitted to a polynomial using a least-squares method; a cubic expansion was found to provide a suitable convergence, with only marginal improvements when including higher order terms. The resulting coefficients are listed in table IV-3. Using this polynomial, the coefficient of thermal expansion and the density (for a Cu monocrystal with a negligible concentration of vacancies; see below) have been calculated and are also listed in this table; at room temperature, both these coefficients agree with previous results within 0.3% [SI63; H1].

How do these values compare with those obtained on a massive crystal? There have been many such determinations at temperatures less than 550°C [NI41; HA70A; PA70; PO73] and they yielded the same thermal expansion coefficient as did the measurements of the lattice parameter. On the other hand, the three separate investigations covering the higher temperature range up to the melting point are in mutually poor agreement, as illustrated by the dilatometric results in figure IV-3. At least two of these curves [RI42; LE63], i.e. those yielding the largest thermal expansion coefficient, can be discarded immediately on the grounds that such a large discrepancy compared with the X-ray or neutron results would imply an unusually large concentration of vacancies, and hence an extremely small (<1 ev) vacancy formation energy; this would contradict the very reliable data obtained by radio-active tracer methods [AS70] as well as by careful expansivity determinations [SI63].

The dilatometric work of Simmons et al [SI63] was done in conjunction with X-ray measurements in order to determine the fractional number of vacancy-type defects; they found this fraction to be $\sim 1.9 \times 10^{-4}$ at 1075°C, a reasonable value for a metal near its melting point, and the vacancy formation energy to be 1.17 ± 0.11 ev. These quantities were obtained from the difference of two other small quantities, i.e. the relative expansion of the length of the massive crystal and of the lattice parameter, both of which being, at best, of the order of 0.02% (near the melting point). Consequently, the dilatometric and the X-ray values differ by less than 0.00025 A at this temperature and this is far to small to be resolved on figure IV-3. However, the very procedure used in this determination

(i.e. high resolution observations of simultaneous relative changes in both the microscopic and macroscopic values with temperature) clearly demonstrates the fact that the macroscopic thermal expansion coefficient never deviates by more than 0.007% from the microscopic coefficient. This will allow us to later calculate the zero-sound elastic constants (section IV-G) without the need to take vacancies into account; this has already been discussed in section II-D (page 33).

E - INELASTIC SCATTERING RESULTS: PHONON ENERGIES IN Cu

The procedure for the phonon measurements was described in section IV-C and the experimentally obtained lineshapes were corrected for resolution effects following the method discussed in section II-H. In principle, this method requires an "a priori" knowledge of the atomic force constants (AFC's) at each temperature of interest in order to calculate the corrections applicable to the experimental values. The AFC's, however, are the very quantities that such an experiment is meant to determine in the first place; thus, the method is really a self-consistent one.

In practice, one can make use of the fact that these corrections are usually small relative to the experimental uncertainties, except possibly near the reciprocal lattice points. Thus, the required AFC's can be determined from the inversion of uncorrected phonon data, obtained in the usual manner, in regions of reciprocal space where the resolution induced distortions are known to be negligible. A major simplification will result if these corrections are assumed to be practically temperature independent. This is a reasonable assumption in the case of Cu since, as will be seen below,

its phonon spectrum undergoes no drastic changes between room temperature and the melting point; consequently, the phonon q-gradients, which are known to affect the degree of focussing, are not greatly modified. The validity of this assumption can be verified by explicit calculation of the resolution corrections, using AFC's appropriate to both temperature extremes. One should note that this is not a general rule; perovskites, like $SrTiO_3$ for example, exhibit a strongly temperature dependent "soft mode" [CO64A].

In all of the resolution calculations for this chapter, the AFC's appropriate to 23°C were used. We had the choice of selecting between the AFC's (and the Debye-Waller factor) determined from this work or from the work of Svensson et al [SV67]. We opted for the latter option since, in this case, the AFC's had been determined from measurements in all of the major symmetry directions, contrary to ours (see p. 104).

The complete results, including the values of the resolution induced shifts and linewidths, are to be found in tables IV-4 and IV-5, respectively for the cases of phonons of "small" and general wavevectors in the accessible directions of major symmetry. One will notice that, in table IV-4, the resolution corrections are always more important at the smallest energy transfers, particularly so, in the case of the longitudinal phonons. This is as expected since the Bragg peak is effectively a singularity in the dispersion surface. However, compared with the experimental uncertainties determined in the usual manner [SV67], the corrections for the transverse phonons are usually of insignificant magnitude, contrary to the case for the longitudinal phonons. The accurate

determination of these corrections for the "small" wavevector phonons will be of fundamental importance when later determining the values of the initial phonon q-gradients and, hence, of the zero-sound elastic constants. The situation is simpler in the case of the phonons of general wavevectors (table IV-5) where the resolution corrections introduce no significant changes on the experimental values. For the sake of rigour, however, the resolution corrections, big or small, were always performed in order to obtain the true intrinsic eigenfrequencies for the analysis which will follow.

Figure IV-4 illustrates the temperature dependence of two representative types of phonons, both measured about half-way to the Brillouin zone boundary. This graph, as well as the following one, was made using the programm PHOPLOT described in appendix II-C. Each of the phonons within these two groups has been normalized to a common monitor value in order to illustrate the temperature dependence of the integrated intensity; the monitor value selected for the normalization is approximately an average of the experimental ones used for these phonons. The longitudinal phonon shown in this figure belongs to what may be rightly called "a difficult branch", especially at high temperatures as will be seen below; however, at this particular wavevector, the phonon remained observable up to near the melting point. On the other hand, the transverse phonon shown in the same figure could be classified as belonging to "an easy branch" because of the fact that this branch has relatively low energies (see equation (II-F6)) and also offers good focussing possibilities (see sub-section II-G-2). In this case, the phonon also remained clearly observable up to near the melting point.

This is not to indicate that the situation was always so favourable. Indeed, figure IV-5 illustrates a situation typical of higher energy phonons. The temperature induced widening and the increased background level are of such a magnitude as to render the signal practically unobservable at the highest temperatures in the case of measurements performed by neutron energy loss. On the other hand, the situation could be greatly improved by measuring the same phonon using the method of neutron energy gain, as this same figure illustrates. Why this should be so can be understood as follows. One will recall that the series of equations (II-G10) provide a rule for selecting an instrumental calibration which minimizes, but does not eliminate, the spurions likely to be encountered at high temperatures and resulting from high-order scattering in the monochromator and/or the analyser; this rule is satisfied here. However, in the method of neutron energy gain and fixed incident energy (see p. 55), high order contamination will arise mainly from the monochromator (because $\nu_o \leq \nu'$); for an incident neutron frequency of 5 THz or greater, there are relatively few neutrons, in the near-maxwellian distribution impinging on the monochromator, which have energies high enough to undergo high order scattering in the monochromator. Hence, the signal remains relatively unspoiled.

Conversely, with the method of neutron energy loss and fixed analysed neutron energy, high order contamination will arise mainly from the analyser (because $\nu' \leq \nu_o$). As the temperature of the specimen is increased, the analyser will be illuminated by an increasing proportion of neutrons which have undergone a process of energy gain in the specimen through multi-phonon scattering.

During measurements at large energy transfers, the incident neutron energy may be so high as to make it impossible to satisfy inequality (II-G12-0). Figure IV-5 illustrates the progressive breakdown of this inequality as a sloping background level in the signal as well as in the background channels.

This brief discussion has demonstrated the superiority of the method of neutron energy gain in the case of measurements performed at high temperatures. However, it cannot be used throughout a series of systematic temperature measurements since the low occupancy of the phonon states prohibits its use at low temperatures.

Figure IV-6 illustrates the temperature dependence of the phonon spectrum of Cu and, for completeness, includes the data at 49 K and 298 K obtained by two other groups [NI67; SV67]. Certain high energy segments, e.g. in the [0ζζ]L and [0ζ1]Π branches, could not be unambiguously observed at the highest temperature. On the other hand, extensive data was accumulated on the behaviour of the low energy phonons; however, these have not been included in the figure since the scale does not permit their representation.

These low energy phonons, which are listed in table IV-4, are represented separately in figure IV-7 for all the four branches that could be observed. Neutron energy gain and energy loss results have been plotted separately, respectively as negative and positive phonon frequencies. At such small wavevectors, if the dispersion relation is linear, i.e. if there is no dispersion of the phonon frequencies, and if there are no systematic errors in the resolution corrected data points, the best fit should be straight lines which go through the origin for all branches and at all temperatures,

as it does here. The corresponding resolution contours, measured by the method of Møller [MO68] (with the specimen at room temperature), are also included. One will observe that most of the low energy phonons selected for this systematic study are separated in wavevector by about one full resolution ellipsoid width. For all these branches, the lowest energy phonons that were measured are those closest to the Bragg peak which could be observed without interference from the elastically scattered neutrons.

Qualitatively speaking, figures IV-6 and IV-7 show that, up to near the melting point, most phonons still have lifetimes long enough to make their observation possible. The apparently larger temperature dependence of the transverse modes compared with the longitudinal ones is confirmed by figure IV-8 which depicts both the absolute and relative frequency shifts with respect to the room temperature values. Indeed, although the absolute shifts are comparable for all branches at a given temperature, reaching a value of approximately -0.5 THz near the melting point, this implies a proportionately greater relative shift of the transverse branches as a result of their low energy relative to the longitudinal ones. Typically, the maximum relative shifts are of the order of -15% for transverse branches and -10% for longitudinal ones. The behaviour at small wavevectors is more dramatic and, contrary to the absolute shifts which must naturally go to zero in the long wavelength limit, the greatest relative shifts are, nonetheless, encountered in this limit, reaching -20% to -30% in the case of the transverse phonons and -15% in the case of the longitudinal ones.

Yet another peculiar qualitative feature of the temperature dependence of the phonon spectrum of Cu concerns the behaviour of the T_1 branch. This is an effect which does not stand out clearly on a reduced scale like that of figure IV-6 and which is better illustrated by figure IV-9; this effect, then, is the emergence, at high temperatures, of a point of inflexion in the dispersion relation. Indeed, this branch which is practically dispersionless at room temperature up to about half way to the Brillouin zone boundary, clearly manifests, at elevated temperatures, an increase in slope at $\zeta \approx 0.2$.. This phenomenon has a temperature dependence which is the opposite of a similar one found in the same branch in Pd [MI71] and in Pt [DU72] and which has been interpreted in terms of the Kohn effect (see section II-C). We will discuss this "anomaly" later on, in the next section.

The published data of Svensson et al [SV67] for room temperature compares favourably with ours. The average frequency ratio of our frequencies to those of Svensson et al is 99.6% ± 0.28%, this value being obtained from 24 individual ratios of phonon frequencies with pairwise identical wavevectors. The largest discrepancies occur at the smallest wavevectors, i.e. where the resolution corrections are most important. This could reflect the fact that our data have been corrected for resolution while those of Svensson et al have not. If a similar calculation is repeated using our uncorrected data, the average ratio now becomes 100.03% ± 0.28%, thus indicating that our data are in excellent agreement with those of Svensson, inasmuch as the crude (i.e. uncorrected for resolution) experimental values are concerned.

The phonon data obtained at 920°C does not contain enough orthogonal information to permit the calculation of the AFC's at this temperature; it can only serve in the determination of the zero-sound elastic constants (see section IV-H). The resolution corrected data for the other temperatures (tables IV-4 and IV-5) were inverted to yield the AFC's appropriate to these temperatures, using a computer programme written by E.C. Svensson [SV67A]. Although the first-sound elastic constants in Cu are known up to 800 K from ultrasonic data [CH66], they were not explicitly used in the fitting procedure, in order to treat similarly both the low and the high temperature data.

The AFC's were calculated under the assumption of a general first-neighbour interaction; the axial-symmetry constraints imposed upon the interaction between the more distant neighbours has permitted the extraction of physically meaningful AFC's up to the fifth neighbours. This range could have been extended had phonons been measured along the $[\zeta\zeta\zeta]$ and the $[0\zeta\zeta]T_2$ branches. However, the restriction of axial symmetry on all but the first neighbour interactions is consistent with what Svensson et al [SV67] found in their extensive analysis of the phonon spectrum at 23°C; there is no "a priori" reason to suspect that the situation should be any different at higher temperatures.

We have already discussed the good agreement between our room temperature data and those of Svensson et al [SV67] in the case where the lowest energy phonons, which are the most affected by resolution effects, are ignored. Having thus verified a selected number of Svensson's data points, our measurements at 22°C were not

carried out as extensively as at higher temperatures; however, they were complemented with those of Svensson's high energy phonons for which we also had measurements at high temperatures. These phonons were along the $[0\zeta\zeta]L$, $[0\zeta 1]\Pi$ and $[0\zeta 1]\Lambda$ branches; none of Svensson's data for the $[0\zeta\zeta]T_2$, $[\zeta\zeta\zeta]T$ and $[\zeta\zeta\zeta]L$ were considered in the determination of the AFC's at 22°C since we had no similar data at the other temperatures. The lowest energy phonons, for which we have extensive and systematic measurements (see section IV-H), were also used in the determination of the AFC's and have resulted in improving the agreement between the observed [OV55] and calculated (from the AFC's) elastic constants; more specifically, this agreement is within 2% in this case whileiit is four times worse if Svensson's AFC's are used, the largest discrepancies then occurring on the elastic constants which depend directly on the initial energy q-gradient of longitudinal phonons, i.e. those most affected by resolution effects. Table IV-6 summarizes the temperature dependence of the fifth-neighbour AFC's thus calculated. It will be noticed that some of the AFC's at 1063°C have rather large relative uncertainties; this reflects the fact that some branches at this temperature could not be as extensively measured as at other temperatures because of extreme line broadening (see pp. 115-116).

F - THE PECULIAR TEMPERATURE DEPENDENCE OF THE T_1 BRANCH

The low segment of the T_1 branch manifests an unusual behaviour at high temperatures, as has already been pointed out, and was the subject of a careful and extensive examination. This is the same branch which also shows remarkable temperature "anomalies" in other FCC metals, e.g. Pd [MI71] and Nb_3Sn [AX73]. In both of

these instances, the dispersion, at low temperatures, is enhanced and becomes positive, i.e. the phonon q-gradient along the branch exceeds its value at $q = 0$; this leads to an apparent softening of the initial segment along this branch. In these two particular cases, however, the mechanisms involved are different. In the first one, the effect has been unambiguously interpreted as a manifestation of the Kohn effect [MI75], while in the second one, it results from the vanishing of a shear wave velocity near a structural transition temperature. Both of these manifestations involve the electron-phonon interaction.

The phenomenon which is observed in Cu has an opposite temperature dependence, as figure IV-9 illustrates. The small wavevector segment ($0 < \zeta < 0.2$) undergoes a softening with temperature as the rest of the spectrum does, but to a much larger extent (see figure IV-8). On the other hand, the segment lying between $0.2 < \zeta < 0.4$ also undergoes a softening but appears to maintain the same slope relative to the 22°C dispersion relation. At all temperatures, these two segments appear to be linear and to intersect at $\zeta \approx 0.2$ *.

There is an indication that a similar effect may be observable in the other noble metals, although none of them have been investigated at temperatures other than 23°C. In the case of Ag [KA69], this branch was not observed at a sufficiently fine mesh of wavevectors to show a definite pattern; nonetheless, there seems to be an indication, from the distribution of the experimental points, that a point of inflexion should also manifest itself in Ag even at temperatures as low as 23°C. On the other hand, there is a much

*) The ratio $|\nu/\zeta|$ is a more sensitive indicator of dispersion and, as figure IV-11 shows, there is no discontinuity in slope at $\zeta = 0.2$.

higher density of experimental points available in the case of Au [LY73], particularly in the low segment of the T_1 branch, and these points clearly show a positive dispersion effect (at 23°C) which is as pronounced as that found in Cu (at 1063°C). It would be interesting to eventually study the temperature dependence of this branch in Ag and Au.

Figure IV-9 also illustrates the temperature dependence of of the lineshapes observed in the vicinity of the point of inflexion, both by the methods of neutron energy gain and neutron energy loss. These lineshapes are representative of the observed ones along this branch and did not undergo, for example, any particularly drastic modification in their linewidth, either as a function of wavevector or temperature, as can be seen from figure IV-10. This excludes the possibility that the positive dispersion is accompanied by any unusual damping mechanism.

In order to look for a possible "catastrophe" in the T_1 branch in the immediate vicinity of the melting point, a limited number of T_1 phonons were observed only 7°C below the melting point. The results did not differ significantly at this temperature (1076°C) from those obtained at the gold point (1063°C).

Moriarty [MO72] has done a first principle calculation of the phonon spectrum of the noble metals. In the case of Cu, he makes no mention of a possible singularity in the T_1 branch at $\zeta \simeq 0.2$, but he speculates that a Kohn effect should easily be observable at $\zeta \simeq 0.45$ of the T_1 branch and at $\zeta \simeq 0.25$ of the $[00\zeta]T$ branch. The position along the T_1 branch is the same as the value arrived at by Svensson et al [SV67] from considerations of the Fermi surface

calculated by Segall [SE62]. At such a wavevector, we do not have enough high resolution data since this was at the practical limits of the MNR spectrometer (see p. 103).

The predicted "anomaly" in the [00ζ]T branch falls in a much more convenient energy range which was carefully investigated both at 22°C and at 920°C (see p. 2 of table IV-4). As figures IV-7, IV-10 and IV-11 indicate, there are not the least indications of unusual dispersion or lifetime effects. Similarly, the [0ζζ]L branch, where Svensson et al [SV67] had unsuccessfully searched for a Kohn effect at $\zeta \approx 0.22$, was observed under conditions of high resolution and no peculiarities whatsoever were observed at 920°C (see p. 5 of table IV-4).

We do not possess, at present, an explanation for this feature of the T_1 branch. The temperature dependence is opposite to that usually observed in the Kohn effect; it is "a priori" difficult to see why, in Cu, a turbulent Fermi sea (i.e. a high temperature) would lead to an enhancement of a Kohn-type effect, while, in other substances, a quiescent Fermi sea (i.e. a low temperature) leads to such an enhancement.

We have qualitatively considered the possibility that the phenomenon reflects a transition between first-sound and zero-sound in the mode of propagation of the phonons (see section II-E). It is not clear why this transition should only be observable in the T_1 branch. More importantly, since phonon lifetimes decrease at high temperatures, as reflected for example by their increasing linewidth, one would expect, from consideration of the $\omega\tau \approx 1$ relation, that this transition should move up along the branch to higher frequencies

at high temperatures. Instead, it moves in the opposite way, as a result of the softening of the lattice and appears to remain centered at a fixed wavevector. Thus, the observed effect does not appear to depend on phonon lifetimes but on the dimension of the Fermi surface which changes but little at high temperatures ($k_BT/E_F < 0.017$; $E_F \simeq 7.0$ ev [KI67]).

G - INELASTIC SCATTERING RESULTS: PHONON LIFETIMES IN Cu

Measurements of intrinsic phonon linewidths by thermal neutron spectroscopy require particular cares for the results to be at all meaningful. The procedure involves three basic steps: obtaining good statistical accuracy on the observed neutron groups, properly estimating the background level (and hence, the experimental linewidth) and finally, deconvoluting the instrumental resolution from the experimental lineshape. These considerations have already been discussed in section II-I.

We will recall that the deconvolution procedure can be carried out without the use of numerical methods if the intrinsic linewidth is much larger than the experimental one [BU69]. It is then a valid assumption to proceed as if both the experimental and intrinsic linewidths were gaussian; the deconvolution procedure is thus trivial.

The MNR high resolution data listed in table IV-4 provides reliable estimates about the behaviour of phonon lifetimes. At the smallest wavevectors, the observed widths are comparable to the resolution widths for all of the constant-E data. In this case, the simplified deconvolution procedure is not justified and the calculated "intrinsic" linewidths, listed in the table, do not have

an absolute meaning; they do illustrate, however, that within errors (which are of the order of 25% of the resolution widths), the phonons of frequency less than ∿ 1.0 THz do not undergo any line broadening up to the melting point, except possibly in the $[0\zeta\zeta]T_1$ branch.

At slightly higher energies, the intrinsic linewidths increase and eventually exceed the value of the resolution widths; then, they yield a meaningful estimate of phonon lifetimes. The values obtained for the $[00\zeta]T$, $[0\zeta\zeta]T_1$ and $[0\zeta\zeta]L$ branches are plotted in figure IV-10. At a given temperature, the linewidth increases, and hence the lifetimes decreases, along a branch; for example, a linewidth of 0.5 THz corresponds to a lifetime of ∿ 0.3 picosecond. However, the fact that the phonon linewidths increase with the phonon frequencies indicate that, in this range of wavevectors, all of the phonons undergo, at 920°C, approximately the same number of oscillations before decaying, i.e. ∿0.7 oscillations in the case of the transverse branches and ∿1.2 oscillations in the case of the $[0\zeta\zeta]L$ branch.

On the other hand, the quality of the NRU data (listed in table IV-5) falls short of those obtained at MNR and does not present much interest from the point of view of accurate linewidth determinations. It provides an idea, however, of the orders of magnitude involved. For example, in an extreme case of line broadening like that of the $[00\zeta]L$ phonon depicted in figure IV-5, the linewidth reaches ∿1.5 THz near the melting point. This indicates phonon lifetimes of the order of 0.1 picosecond; thus, such zone-boundary phonons undergo only ∿0.7 oscillations before decaying.

H - INELASTIC SCATTERING RESULTS: TEMPERATURE DEPENDENCE OF THE ZERO-SOUND ELASTIC CONSTANTS OF Cu

The first-sound elastic constants of Cu have been measured by Overton et al [OV55] over a temperature range of 4.2 K to 300 K using standard ultrasonic techniques (pulse frequency: 10 MHz). Their results, quoted with uncertainties ranging from 0.1% to 1.8%, indicate the expected gradual decrease of the elastic constants as the temperature is increased. Higher temperature measurements (from 300 K to 800 K) were later performed, using a similar technique, by Chang et al [CH66] who found a linear decrease with temperature over this range, within their experimental uncertainties of 0.5% to 0.9%. The overlap at 300 K between these two independent results is better than 0.5% and their temperature derivatives are mutually consistent.

The zero-sound elastic constants of Cu (obtained from this work) were determined using the high-resolution phonon data listed in table IV-4 and following the procedure outlined in section II-D. The first step involves finding the intrinsic value of

$$\lim_{\zeta \to 0} (|\nu/\zeta|)$$

for the long wavelength phonons and we have such data along the $[00\zeta]T\&L$ and $[0\zeta\zeta]T_1\&L$ branches. In figure IV-11, the ratios $|\nu/\zeta|$ have been plotted for the various wavevectors and temperatures. Since the resolution corrections are small in the case of the transverse phonons, these ratios are not drastically altered, whether or not the resolution corrections are considered; but, the inclusion of these corrections does shift them to values somewhat lower by at most 2% for the $[00\zeta]T$ branch and by up to

15% for the low segment of the $[0\zeta\zeta]T_1$ branch. On the other hand, we have already noticed that the longitudinal phonons of small wavevectors are greatly affected by resolution effects and, consequently, so are the values of the ratios $|\nu/\zeta|$. For comparison purposes, figure IV-11 also includes the plots obtained for these longitudinal phonons without the resolution corrections (as well as with these corrections); the qualitative and quantitative differences are striking, particularly with respect to the apparent divergence at $\zeta=0$ for the uncorrected data.

If there are no systematic errors (e.g. crystal misalignment) and if the resolution correction procedure is valid, one expects "a priori" that the $|\nu/\zeta|$ plots should be symmetrical in relation to the origin. A best fit satisfying this requirement can be drawn, yielding a value of the vertical intercepts and, hence, of the zero-sound elastic constants; this is the only practical procedure when the AFC's at a given temperature are not known, as will be the case for the experiment on Pd discussed in the next chapter (section V-G). In the case of interest here, we know the AFC's at four temperatures up to the melting point (see section IV-E), and the ratios $|\nu/\zeta|$ calculated from these AFC's were used to determine the vertical intercepts. This method removes the arbitrariness in joining the points at a given temperature; this allows a better interpolation to $\zeta=0$ since the uncertainties on the ratio points obtained from the experimental values are largest at small wavevectors. If the dispersion curves are not drastically altered with temperature, it should be possible to trace the ratio curves by doing, at all temperatures, a best fit parallel to the curve calculated from AFC's.

Because of the peculiar behaviour of the T_1 branch, the AFC's appropriate to each temperature were used to calculate the ratios $|\nu/\zeta|$ and the results are shown as continuous lines in figure IV-11; since no AFC's could be extracted from the 920°C data (see section IV-E), the ratios for this temperature were fitted visually to a curve which follows the pattern of those for 700°C and 1063°C. This figure shows that the ratios calculated from the AFC's are very nearly wavevector independent, in the range of interest, for both the transverse and longitudinal branches in the $[00\zeta]$ direction. On the other hand, the calculated ratios for the T_1 branch follow a pattern which reflects the peculiarity of its structure while those for the $[0\zeta\zeta]L$ follow an inverse pattern; the first case corresponds to positive dispersion and the second one, to negative dispersion (see p. 121). Generally speaking, the ratios calculated from the experimental values are within errors of those calculated from the AFC's; this indicates that the AFC's predict well the very lowest frequencies observed.

Once the limits at $\zeta \to 0$ of the $|\nu/\zeta|$ ratios are known, the elastic constants can be determined following the procedure already outlined (section II-D). The initial slopes of the $[00\zeta]T\&L$ and $[0\zeta\zeta]T_1\&L$ branches are simply proportional to the c_{44}, c_{11}, $(c_{11}-c_{12})/2$ and $(c_{11}+c_{12}+2c_{44})/2$ elastic constants respectively. A least-squares fit to these four initial slopes with various weighting factors for each of these branches produced significantly the same results. The elastic constant c_{12}, which cannot be determined directly from any one individual slope, was obtained from the least-squares fit; all of these results are listed in

table IV-7 and plotted in figure IV-12. The overall agreement with the ultrasonic data at room temperature [OV55] and above [CH66] is within the uncertainties, thus indicating that the first- and zero-sound elastic constants are not appreciably different, at least between 300 K and 800 K.

The uncertainties assigned to the zero-sound elastic constants are absolute quantities which reflect the uncertainties on the determination of the initial slopes, i.e. the vertical intercepts in figure IV-11. It seems that a realistic estimate of their magnitude would be ±0.1 THz for the transverse branches and ±0.25 THz for the longitudinal ones. However, the use of the AFC's to calculate the $|\nu/\zeta|$ ratios results in smaller uncertainties for the relative values of the vertical intercepts, at the various temperatures; indeed, the AFC's reflect the temperature dependence of a large number of experimentally observed phonons, particularly the lowest energy ones since these are the most heavily weighted [SV67]. It thus seems reasonable, for a given branch, to assign relative uncertainties on the vertical intercepts as 1/4 of the absolute ones. Then, the relative uncertainties on the temperature dependence of the elastic constants are proportionately reduced from the absolute ones shown in table IV-7 and figure IV-12.

The conclusions reached in this section largely depend on the validity of the adopted resolution correction procedure. The same method was used in the next chapter and the reader should refer to figure V-7 for an illustration of calculated and observed lineshapes for two types of phonons (and of scans) in Pd which produced results rather similar to those observed in Cu.

Table IV-1. Some physical parameters of the noble metals.

		Cu	Ag	Au	
Atomic number	Z	29	47	79	[H2]
Atomic mass (in a.m.u.)	A	63.54	107.87	196.967	[H2]
Crystalline structure		FCC 0K↔T_m	FCC 77K↔T_m	FCC 0K↔T_m	[H3]
Lattice parameter	a	3.6147A (20°C) [H3]	4.0862A (25°C) [H4]	4.0781A (18°C) [H3]	
Melting temperature	T_m	1083°C	960.8°C	1063°C	[H5]
Debye temperature at 0 K (from calorimetric data)	θ_D	345.8K	227.3K	162.3K	[MA66;MA68]
Cross-section (in $10^{-24}cm^2$) for thermal neutrons					
-absorption	σ_a	3.77	63	98.8	
-coherent scattering	σ_c	7.4	4.6	7.3	[H7]
-incoherent scattering	σ_i	0.6	1.9	?	

Note: References are given by the code within brackets [].

A: at MNR; energy gain & loss.
B: at NRU; energy loss.
C: at NRU; energy gain.

Table IV-2. Instrumental parameters of the triple-axis instruments used in these measurements:

		Ⓐ	Ⓑ	Ⓒ
Monochromator:	type	Cu200	Cu220	Cu220
	plane spacing [A]	1.807	1.278	1.278
	mosaicity	0.5°	0.35°	0.35°
Analyser:	type	Cu200	Cu200	Cu200
	plane spacing [A]	1.807	1.807	1.807
	mosaicity	0.5°	0.5°	0.5°
Horizontal collimations: (FWHM)				
	pre-monochromator	1/40	1/20	1/20
	post-monochromator	1/80	1/80	1/80
	pre-analyser	1/80	1/80	1/160
	post-analyser	1/6	2/15	2/15
Vertical collimations: (FWHM)				
	pre-monochromator	1/40	1/20	1/20
	post-monochromator	1/40	1/40	1/40
	pre-analyser	1/40	1/20	1/20
	post-analyser	2/5	2/5	2/5
Mode of operation: fixed	ν_o [THz]	4.21		5.50
	λ_o [A]	2.167		1.897
	$2\theta_m$	73.7°		95.8°
fixed	ν' [THz]		5.20	
	λ' [A]		1.95	
	$2\theta_a$		65.3°	

Mosaicity of the Cu specimen (re: chapter IV): 0.2°
Mosaicity of the Pd specimen (re: chapter V): 0.2°

Table IV-3. Temperature dependence of the lattice parameter of Cu. (this work)

T	T/T_m	a_x	a_c	a_x-a_c	α	ρ
23.10	.218	3.61488	3.61437	.000505	.1815E-04	8.935
134.25	.300	3.62111	3.62161	-.000506	.1791E-04	8.882
234.00	.374	3.62779	3.62809	-.000303	.1795E-04	8.834
335.00	.448	3.63432	3.63472	-.000399	.1823E-04	8.786
399.75	.496	3.63868	3.63905	-.000368	.1854E-04	8.755
434.25	.522	3.64142	3.64139	.000028	.1874E-04	8.738
480.25	.556	3.64529	3.64456	.000738	.1906E-04	8.715
530.50	.593	3.64857	3.64808	.000490	.1946E-04	8.690
580.00	.629	3.65197	3.65164	.000330	.1991E-04	8.665
630.00	.666	3.65548	3.65532	.000160	.2043E-04	8.638
680.00	.703	3.65943	3.65911	.000317	.2100E-04	8.612
699.75	.717	3.66027	3.66064	-.000369	.2124E-04	8.601
730.00	.740	3.66287	3.66301	-.000143	.2163E-04	8.584
780.00	.777	3.66726	3.66703	.000231	.2231E-04	8.556
830.00	.813	3.67105	3.67119	-.000141	.2305E-04	8.527
880.50	.851	3.67518	3.67554	-.000368	.2386E-04	8.497
919.85	.880	3.67869	3.67904	-.000357	.2453E-04	8.472
930.00	.887	3.67953	3.67996	-.000432	.2471E-04	8.466
980.00	.924	3.68423	3.68460	-.000364	.2562E-04	8.434
1030.25	.961	3.69025	3.68943	.000819	.2659E-04	8.401
1063.25	.985	3.69284	3.69271	.000133	.2725E-04	8.379

N.B.: value of a_x at 23.1°C is the standard relative to which, other values of a_x (at higher temperatures) have been determined.

$$a_0 = .361285520E+01$$
$$a_1 = .658838824E-04$$
$$a_2 = -.667142097E-08$$
$$a_3 = .144304066E-10$$

$$(a_x-a_c)_{rms} = .403548096E-03$$

Symbols, units and descriptions.

T: [°C]: temperature; T_m=1083°C: melting temperature.
T/T_m: reduced temperature, i.e. T[K]/T_m[K].
a_x: [A]: experimental value of the lattice parameter (±.0024A).
a_c: [A]: calculated value of the lattice parameter, using a cubic polynomial expansion...

$$a_c = a_0 + a_1T + a_2T^2 + a_3T^3 \ ; \ (T \text{ in units of } °C).$$

α: [$°C^{-1}$]: thermal expansion coefficient calculated from the polynomial expansion; $\alpha = \frac{1}{a_c}\frac{da_c}{dT}$

ρ: [$\frac{gr}{cm^3}$]: density calculated from the polynomial expansion; $\rho = (4 \times 63.54 \times 1.66)/a_c^3$

Table IV-4. Phonon Frequencies [ν:THz] and Reduced Wavevectors [ζ] for Copper at Various Temperatures; Low Energy Data. Page 1 of 6. [00ζ]T branch measured at aQ/2π = (2,ζ,0).

$\hat{\nu}$	ζ_x	$2\Gamma_{\zeta x}$	$\Delta\zeta$	C_ζ	ζ	$C_{2\Gamma\zeta}$	$2\Gamma_\zeta$	Constant-E
.975	.1222	.025	.003	.000631	.1228	.024	.007	
.838	.1030	.024	.003	.000980	.1040	.024	0.000	
.703	.0880	.027	.003	.001069	.0891	.024	.012	
.557	.0720	.025	.003	.001010	.0730	.026	0.000	
.417	.0530		.003	.000860	.0539	.027		
-.417	-.0500		.004	-.000260	-.0503	.029		22°C
-.559	-.0710	.028	.003	.000080	-.0709	.028	0.000	
-.709	-.0900	.026	.003	.000176	-.0898	.026	0.000	
-.840	-.1070	.028	.003	.000120	-.1069	.026	.010	
-.978	-.1240	.026	.003	-.000113	-.1241	.026	0.000	
.975	.1270	.027	.003	.000631	.1276	.024	.012	
.838	.1120	.032	.004	.000980	.1130	.024	.021	
.703	.0930	.029	.003	.001069	.0941	.024	.016	
.557	.0750	.032	.004	.001010	.0760	.026	.019	
.417	.0550	.028	.003	.000860	.0559	.027	.007	
-.417	-.0530	.028	.003	-.000260	-.0533	.029	0.000	400°C
-.559	-.0740	.028	.003	.000080	-.0739	.028	0.000	
-.709	-.0950	.030	.003	.000176	-.0948	.026	.015	
-.840	-.1120	.030	.003	.000120	-.1119	.026	.015	
-.978	-.1320	.032	.004	-.000113	-.1321	.026	.019	
.975	.1410	.030	.003	.000631	.1416	.024	.018	
.838	.1200	.030	.003	.000980	.1210	.024	.018	
.703	.1013	.026	.003	.001069	.1024	.024	.010	
.557	.0800	.027	.003	.001010	.0810	.026	.007	
.417	.0585	.026	.003	.000860	.0594	.027	0.000	
-.417	-.0575	.030	.003	-.000260	-.0578	.029	.008	700°C
-.559	-.0775	.030	.003	.000080	-.0774	.028	.011	
-.709	-.1003	.028	.003	.000176	-.1001	.026	.010	
-.840	-.1180	.030	.003	.000120	-.1179	.026	.015	
-.978	-.1370	.031	.004	-.000113	-.1371	.026	.017	
.975	.1460	.032	.004	.000631	.1466	.024	.021	
.838	.1260	.032	.004	.000980	.1270	.024	.021	
.703	.1040	.026	.003	.001069	.1051	.024	.010	
.557	.0845	.027	.003	.001010	.0855	.026	.007	
.417	.0615	.024	.003	.000860	.0624	.027	0.000	
-.417	-.0620	.031	.004	-.000260	-.0623	.029	.011	920°C
-.559	-.0835	.026	.003	.000080	-.0834	.028	0.000	
-.709	-.1075	.026	.003	.000176	-.1073	.026	0.000	
-.840	-.1255	.033	.004	.000120	-.1254	.026	.020	
-.978	-.1470	.032	.004	-.000113	-.1471	.026	.019	
.975	.1510	.042	.005	.000631	.1516	.024	.034	
.838	.1310	.031	.004	.000980	.1320	.024	.020	
.703	.1120	.023	.003	.001069	.1131	.024	0.000	
.557	.0905	.028	.003	.001010	.0915	.026	.010	
.417	.0655	.025	.003	.000860	.0664	.027	0.000	
-.417	-.0645	.030	.003	-.000260	-.0648	.029	.008	1063°C
-.559	-.0870	.029	.003	.000080	-.0869	.028	.008	
-.709	-.1105	.025	.003	.000176	-.1103	.026	0.000	
-.840	-.1300	.030	.003	.000120	-.1299	.026	.015	
-.978	-.1515	.034	.004	-.000113	-.1516	.026	.022	

N.B.: Experimental details in table IV-2, under column Ⓐ.
Definition of symbols in table I-1.

[00ζ]T branch measured at aQ/2π = (2,ζ,0); continued.

ζ	ν_x	$2\Gamma_{\nu x}$	Δν	C_ν	ν	$C_{2\Gamma\nu}$	$2\Gamma_\nu$	Constant-Q
.150	1.1800		.020	.009000	1.1890	.180		
-.100	-.7540	.250	.030	-.017500	-.7715	.210	.136	
-.125	-.9700	.240	.030	-.013000	-.9830	.200	.133	
-.150	-1.1630	.220	.030	-.009000	-1.1720	.190	.111	
-.175	-1.3600	.220	.030	-.006300	-1.3663	.180	.126	22°C
-.200	-1.5630	.250	.030	-.004200	-1.5672	.170	.183	
-.225	-1.7500		.020	-.001700	-1.7517	.160		
-.250	-1.9420	.265	.030	0.000000	-1.9420	.150	.218	
-.275	-2.1250		.030	.001700	-2.1233	.140		
-.300	-2.3150		.030	.003000	-2.3120	.130		
.150	1.1000	.260	.030	.009000	1.1090	.180	.188	400°C
-.150	-1.1000	.260	.030	-.009000	-1.1090	.190	.177	
.150	1.0230	.220	.030	.009000	1.0320	.180	.126	700°C
-.150	-1.0500	.220	.030	-.009000	-1.0590	.190	.111	
.150	.9630	.240	.030	.009000	.9720	.180	.159	
-.100	-.6400	.205	.030	-.017500	-.6575	.210	0.000	
-.125	-.8260	.200	.020	-.013000	-.8390	.200	0.000	
-.150	-.9910	.225	.030	-.009000	-1.0000	.190	.121	
-.175	-1.1660	.230	.030	-.006300	-1.1723	.180	.143	920°C
-.200	-1.3420	.285	.030	-.004200	-1.3462	.170	.229	
-.225	-1.5080	.320	.040	-.001700	-1.5097	.160	.277	
-.250	-1.6820	.340	.040	0.000000	-1.6820	.150	.305	
-.275	-1.8200	.380	.040	.001700	-1.8183	.140	.353	
-.300	-2.0170	.480	.050	.003000	-2.0140	.130	.462	
.150	.9300	.240	.030	.009000	.9390	.180	.159	1063°C
-.150	-.9600	.240	.030	-.009000	-.9690	.190	.147	

[00ζ]L branch measured at aQ/2π = (2+ζ,0,0).

ζ	ν_x	$2\Gamma_{\nu x}$	Δν	C_ν	ν	$C_{2\Gamma\nu}$	$2\Gamma_\nu$	Constant-Q
.150	-1.8000	.240	.030	.064300	-1.7357	.240	0.000	400°C
.150	-1.7300	.270	.030	.064300	-1.6657	.240	.124	700°C
.150	-1.6750	.270	.030	.064300	-1.6107	.240	.124	920°C
.150	-1.6250		.030	.064300	-1.5607	.240		1063°C

[00ζ]L branch measured at aQ/2π = (2+ζ,0,0); continued.

ν̂	ζ_x	$2\Gamma_{\zeta x}$	Δζ	C_ζ	ζ	$C_{2\Gamma\zeta}$	$2\Gamma_\zeta$	Constant-E
1.318	-.1060	.021	.003	-.004600	-.1106	.020	.006	
1.102	-.0860	.024	.003	-.005448	-.0914	.022	.010	
.876	-.0640		.002	-.006599	-.0706	.019		
.660	-.0460		.002	-.007520	-.0535	.022		22°C
-.658	.0450		.002	.009654	.0547	.029		
-.867	.0620		.003	.009549	.0715	.022		
-1.093	.0840	.025	.003	.008097	.0921	.023	.010	
-1.335	.1050	.022	.003	.007100	.1121	.022	0.000	
1.539	-.1270		.003	-.004055	-.1311	.019		
1.318	-.1080	.023	.003	-.004600	-.1126	.020	.011	
1.102	-.0890	.022	.003	-.005448	-.0944	.022	0.000	
.876	-.0690	.022	.003	-.006599	-.0756	.019	.011	
.660	-.0470	.024	.003	-.007520	-.0545	.022	.010	400°C
-.658	.0470		.003	.009654	.0567	.029		
-.867	.0670	.027	.003	.009549	.0765	.022	.016	
-1.093	.0870	.022	.003	.008097	.0951	.023	0.000	
-1.335	.1100	.024	.003	.007100	.1171	.022	.010	
-1.530	.1290		.002	.006498	.1355	.022		
1.539	-.1330		.002	-.004055	-.1371	.019		
1.318	-.1110	.020	.002	-.004600	-.1156	.020	0.000	
1.102	-.0920	.020	.002	-.005448	-.0974	.022	0.000	
.876	-.0700	.020	.002	-.006599	-.0766	.019	.006	
.660	-.0500	.028	.003	-.007520	-.0575	.022	.017	700°C
-.658	.0500	.027	.003	.009654	.0597	.029	0.000	
-.867	.0720	.026	.003	.009549	.0815	.022	.014	
-1.093	.0910	.025	.003	.008097	.0991	.023	.010	
-1.335	.1140	.030	.003	.007100	.1211	.022	.020	
-1.530	.1330	.025	.003	.006498	.1395	.022	.012	
1.539	-.1345		.003	-.004055	-.1386	.019		
1.318	-.1165	.023	.003	-.004600	-.1211	.020	.011	
1.102	-.0925	.023	.003	-.005448	-.0979	.022	.007	
.876	-.0730	.024	.003	-.006599	-.0796	.019	.015	
.660	-.0510	.023	.003	-.007520	-.0585	.022	.007	920°C
-.658	.0545	.023	.003	.009654	.0642	.029	0.000	
-.867	.0710	.028	.003	.009549	.0805	.022	.017	
-1.093	.0945	.029	.003	.008097	.1026	.023	.018	
-1.335	.1165	.023	.003	.007100	.1236	.022	.007	
-1.530	.1375	.024	.003	.006498	.1440	.022	.010	
1.539	-.1365		.005	-.004055	-.1406	.019		
1.318	-.1175	.023	.003	-.004600	-.1221	.020	.011	
1.102	-.0990	.029	.003	-.005448	-.1044	.022	.019	
.876	-.0755	.024	.003	-.006599	-.0821	.019	.015	
.660	-.0540	.021	.003	-.007520	-.0615	.022	0.000	1063°C
-.658	.0530	.024	.003	.009654	.0627	.029	0.000	
-.867	.0750	.024	.003	.009549	.0845	.022	.010	
-1.093	.0965	.026	.003	.008097	.1046	.023	.012	
-1.335	.1205	.023	.003	.007100	.1276	.022	.007	
-1.530	.1390	.030	.003	.006498	.1455	.022	.020	

$[0\zeta\zeta]T_1$ branch measured at $aQ/2\pi = (2+\zeta, 2-\zeta, 0)$.

ζ	ν_x	$2\Gamma_{\nu x}$	$\Delta\nu$	C_ν	ν	$C_{2\Gamma\nu}$	$2\Gamma_\nu$	Constant-Q
-.200	1.3300		.010	-.010400	1.3196	.085		
-.150	.9950	.120	.020	-.013500	.9815	.087	.083	
-.100	.6700	.095	.010	-.018680	.6513	.095	0.000	
-.050	.3600	.130	.020	-.028530	.3315	.110	.069	
.050	-.3400	.130	.020	.032530	-.3075	.123	.042	
.100	-.6700	.130	.020	.024680	-.6453	.105	.077	
.150	-.9880	.160	.020	.018500	-.9695	.104	.122	22°C
.200	-1.3350		.020	.014400	-1.3206	.105		
.250	-1.6700	.180	.020	.012400	-1.6576	.105	.146	
.300	-2.0200	.190	.020	.011200	-2.0088	.115	.151	
.350	-2.3650	.170	.020	.010700	-2.3543	.125	.115	
.400	-2.7100	.210	.030	.010600	-2.6994	.144	.153	
.450	-3.0400	.280	.030	.010800	-3.0292	.165	.226	
.500	-3.3600		.040	.011000	-3.3490	.190		
-.200	1.2400	.170	.020	-.010400	1.2296	.085	.147	
-.150	.9200	.160	.020	-.013500	.9065	.087	.134	
-.100	.6200	.140	.020	-.018680	.6013	.095	.103	
-.050	.3150	.160	.020	-.028530	.2865	.110	.116	
.050	-.3250	.130	.020	.032530	-.2925	.123	.042	
.100	-.6300	.150	.020	.024680	-.6053	.105	.107	
.150	-.9200	.150	.020	.018500	-.9015	.104	.108	400°C
.200	-1.2450	.210	.030	.014400	-1.2306	.105	.182	
.250	-1.5800	.290	.030	.012400	-1.5676	.105	.270	
.300	-1.9100	.360	.040	.011200	-1.8988	.115	.341	
.350	-2.2500		.030	.010700	-2.2393	.125		
.400	-2.5800	.390	.040	.010600	-2.5694	.144	.362	
.450	-2.8900	.280	.030	.010800	-2.8792	.165	.226	
.500	-3.1900	.380	.040	.011000	-3.1790	.190	.329	
-.200	1.1400		.020	-.010400	1.1296	.085		
-.150	.8500		.020	-.013500	.8365	.087		
-.100	.5600	.140	.020	-.018680	.5413	.095	.103	
-.050	.3000	.150	.020	-.028530	.2715	.110	.102	
.050	-.2900	.170	.020	.032530	-.2575	.123	.117	
.100	-.5800	.180	.020	.024680	-.5553	.105	.146	
.150	-.8780	.210	.030	.018500	-.8595	.104	.182	
.175	-1.0300	.220	.030	.016300	-1.0137	.104	.194	700°C
.200	-1.1750	.245	.030	.014400	-1.1606	.105	.221	
.225	-1.3300	.240	.030	.013300	-1.3167	.105	.216	
.250	-1.4750	.310	.040	.012400	-1.4626	.105	.292	
.300	-1.7500	.420	.050	.011200	-1.7388	.115	.404	
.350	-2.0950	.360	.040	.010700	-2.0843	.125	.338	
.400	-2.4100		.040	.010600	-2.3994	.144		
.450	-2.7100	.440	.050	.010800	-2.6992	.165	.408	
.500	-3.0300	.540	.060	.011000	-3.0190	.190	.505	

$[0\zeta\zeta]T_1$ branch measured at $aQ/2\pi = (2+\zeta, 2-\zeta, 0)$; continued.

ζ	ν_x	$2\Gamma_{\nu x}$	$\Delta\nu$	C_ν	ν	$C_2\Gamma_\nu$	$2\Gamma_\nu$	Constant-Q
-.200	1.0400		.020	-.010400	1.0296	.085		
-.150	.7900	.200	.020	-.013500	.7765	.087	.180	
-.100	.5250	.150	.020	-.018680	.5063	.095	.116	
-.050	.2750	.150	.020	-.028530	.2465	.110	.102	
.050	-.2800	.150	.020	.032530	-.2475	.123	.086	
.075	-.4100	.160	.020	.028800	-.3812	.112	.114	
.100	-.5500	.165	.020	.024680	-.5253	.105	.127	
.125	-.6850	.190	.020	.021300	-.6637	.104	.159	
.150	-.8300	.240	.030	.018500	-.8115	.104	.216	
.175	-.9550	.265	.030	.016300	-.9387	.104	.244	920°c
.200	-1.1010	.285	.030	.014400	-1.0866	.105	.265	
.225	-1.2480	.295	.030	.013300	-1.2347	.105	.276	
.250	-1.3820	.320	.040	.012400	-1.3696	.105	.302	
.275	-1.5350	.380	.040	.011700	-1.5233	.110	.364	
.300	-1.6850	.410	.050	.011200	-1.6738	.115	.394	
.350	-2.0200	.440	.050	.010700	-2.0093	.125	.422	
.400	-2.2900		.050	.010600	-2.2794	.144		
.450	-2.6100	.480	.050	.010800	-2.5992	.165	.451	
.500	-2.8700		.050	.011000	-2.8590	.190		
-.200	.9600		.040	-.010400	.9496	.085		
-.150	.7250	.210	.030	-.013500	.7115	.087	.191	
-.100	.4850	.150	.020	-.018680	.4663	.095	.116	
-.050	.2650	.130	.020	-.028530	.2365	.110	.069	
.050	-.2520	.150	.020	.032530	-.2195	.123	.086	
.100	-.4900	.210	.030	.024680	-.4653	.105	.182	
.150	-.7450	.210	.030	.019500	-.7265	.104	.182	1063°C
.200	-1.0300		.040	.014400	-1.0156	.105		
.250	-1.2750	.330	.040	.012400	-1.2626	.105	.313	
.300	-1.5900	.360	.040	.011200	-1.5788	.115	.341	
.350	-1.9250	.560	.060	.010700	-1.9143	.125	.546	
.400	-2.2300	.630	.070	.010600	-2.2194	.144	.613	

$[0\zeta\zeta]L$ branch measured at $aQ/2\pi = (2+\zeta, 2+\zeta, 0)$.

ζ	ν_x	$2\Gamma_{\nu x}$	$\Delta\nu$	C_ν	ν	$C_2\Gamma_\nu$	$2\Gamma_\nu$	Constant-Q
.100	-1.7100	.300	.030	.031500	-1.6785	.295	.055	
.125	-2.1310	.340	.040	.029700	-2.1013	.277	.197	
.150	-2.5500	.380	.040	.029300	-2.5217	.261	.276	
.175	-2.9460	.440	.050	.027400	-2.9186	.250	.362	
.200	-3.3000	.400	.040	.027000	-3.2730	.245	.316	
.225	-3.6900	.480	.050	.027400	-3.6626	.239	.416	920°C
.250	-4.0020	.600	.060	.028100	-3.9739	.237	.551	
.275	-4.3220	.600	.060	.029100	-4.2929	.237	.551	
.300	-4.7350	.700	.070	.030500	-4.7045	.240	.658	
.325	-5.0300	.750	.080	.031800	-4.9982	.245	.709	

[0ζζ]L branch measured at aQ/2π = (2+ζ,2+ζ,0); continued.

$\hat{v}$	ζ_x	$2\Gamma_{\zeta x}$	$\Delta\zeta$	C_ζ	ζ	$C_{2\Gamma\zeta}$	$2\Gamma_\zeta$	Constant-E
1.753	-.0890		.002	-.002250	-.0913	.019		
1.402	-.0700		.001	-.002658	-.0727	.019		
1.045	-.0520		.002	-.003082	-.0551	.018		
.703	-.0330	.019	.002	-.003281	-.0363	.017	.008	
-.709	.0360		.003	.002791	.0388	.018		22°C
-1.063	.0530	.019	.002	.003822	.0568	.016	.010	
-1.399	.0690	.018	.002	.002899	.0719	.017	.006	
-1.737	.0890	.015	.002	.002500	.0915	.017	0.000	
-2.109	.1097	.020	.002	.002427	.1121	.017	.011	
2.099	-.1150		.004	-.001879	-.1169	.019		
1.753	-.0920		.003	-.002250	-.0943	.019		
1.402	-.0730		.002	-.002658	-.0757	.019		
1.045	-.0540	.016	.002	-.003082	-.0571	.018	0.000	
.703	-.0330	.020	.002	-.003281	-.0363	.017	.011	400°C
-.709	.0360	.022	.003	.002791	.0388	.018	.013	
-1.063	.0560	.022	.003	.003822	.0598	.016	.015	
-1.399	.0740	.018	.002	.002899	.0769	.017	.006	
-1.737	.0950	.022	.003	.002500	.0975	.017	.014	
-2.109	.1150	.016	.002	.002427	.1174	.017	0.000	
2.099	-.1150		.002	-.001879	-.1169	.019		
1.753	-.0940		.002	-.002250	-.0963	.019		
1.402	-.0770		.002	-.002658	-.0797	.019		
1.045	-.0560	.017	.002	-.003082	-.0591	.018	0.000	
.703	-.0350	.018	.002	-.003281	-.0383	.017	.006	700°C
-.709	.0370	.018	.002	.002791	.0398	.018	0.000	
-1.063	.0590	.022	.003	.003822	.0628	.016	.015	
-1.399	.0770	.020	.002	.002899	.0799	.017	.011	
-1.737	.0970	.016	.002	.002500	.0995	.017	0.000	
-2.109	.1190	.020	.002	.002427	.1214	.017	.011	
2.099	-.1175		.004	-.001879	-.1194	.019		
1.753	-.1035		.003	-.002250	-.1058	.019		
1.402	-.0765		.003	-.002658	-.0792	.019		
1.045	-.0570	.021	.003	-.003082	-.0601	.018	.011	
.703	-.0365	.020	.002	-.003281	-.0398	.017	.011	920°C
-.709	.0400	.020	.002	.002791	.0428	.018	.009	
-1.063	.0575	.019	.002	.003822	.0613	.016	.010	
-1.399	.0805	.018	.002	.002899	.0834	.017	.006	
-1.737	.0995	.022	.003	.002500	.1020	.017	.014	
-2.109	.1235	.020	.002	.002427	.1259	.017	.011	
1.753	-.1015		.001	-.002250	-.1038	.019		
1.402	-.0815	.022	.003	-.002658	-.0842	.019	.011	
1.045	-.0615		.002	-.003082	-.0646	.018		
.703	-.0380	.016	.002	-.003281	-.0413	.017	0.000	
-.709	.0405	.020	.002	.002791	.0433	.018	.009	1063°C
-1.063	.0605	.022	.003	.003822	.0643	.016	.015	
-1.399	.0810	.015	.002	.002899	.0839	.017	0.000	
-1.737	.1035	.026	.003	.002500	.1060	.017	.020	
-2.109	.1275	.022	.003	.002427	.1299	.017	.014	

Table IV-5. Phonon Frequencies [ν:THz] and Reduced Wavevectors [ζ] for Copper at Various Temperatures; High Energy Data. Page 1 of 3.

[00ζ]T branch measured at $aQ/2\pi = (2,\zeta,0)$.

$\hat{\zeta}$	ν_x	$2\Gamma_{\nu x}$	$\Delta\nu$	C_ν	ν	$C_{2\Gamma\nu}$	$2\Gamma_\nu$	Constant-Q
.200	1.6200	.240	.030	-.006300	1.6137	.185	.153	
.400	3.0400	.270	.030	-.007500	3.0325	.110	.247	
.600	4.1600	.180	.020	-.010900	4.1491	.110	.142	22°C
.800	4.8300	.220	.030	-.017500	4.8125	.275	0.000	
1.000	5.0400	.380	.040	-.004200	5.0358	.490	0.000	← Note ①
.200	1.5200	.280	.030	-.006300	1.5137	.185	.210	
.400	2.9000	.360	.040	-.007500	2.8925	.110	.343	
.600	4.0300	.320	.040	-.010900	4.0191	.110	.300	400°C
.800	4.7100	.350	.040	-.017500	4.6925	.275	.217	
1.000	4.9200	.550	.060	-.004200	4.9158	.490	.250	← Note ①
.200	1.4300	.300	.030	-.006300	1.4237	.185	.236	
.400	2.7900	.530	.060	-.007500	2.7825	.110	.518	
.600	3.8700	.500	.050	-.010900	3.8591	.110	.488	
.800	4.4900		.030	-.017500	4.4725	.275		700°C
1.000	4.7500	.520	.060	-.004200	4.7558	.490	.174	← Note ①
.100	.6700	.240	.030	-.006000	.6640	.240	0.000	
.200	1.3200	.280	.030	-.006300	1.3137	.185	.210	
.300	1.9500	.460	.050	-.006800	1.9432	.140	.438	
.400	2.5600	.480	.050	-.007500	2.5525	.110	.467	
.600	3.6500	1.040	.110	-.010900	3.6391	.110	1.034	1063°C
.800	4.2000		.070	-.017500	4.1825	.275		
1.000	4.5000		.100	-.004200	4.4958	.490		← Note ①

[00ζ]L branch measured at $aQ/2\pi = (2+\zeta,0,0)$.

$\hat{\zeta}$	ν_x	$2\Gamma_{\nu x}$	$\Delta\nu$	C_ν	ν	$C_{2\Gamma\nu}$	$2\Gamma_\nu$	Constant-Q
.200	2.4400	.400	.040	-.065400	2.3746	.340	.211	
.400	4.4400	.330	.040	-.037500	4.4025	.360	0.000	
.600	6.0200	.400	.040	-.020100	5.9999	.410	0.000	22°C
.800	6.9700	.420	.050	-.013300	6.9567	.495	0.000	
1.000	7.2500	.700	.070	-.013300	7.2367	.630	.305	
.200	2.3500	.420	.050	-.065400	2.2846	.340	.247	
.400	4.3700	.360	.040	-.037500	4.3325	.360	0.000	
.600	5.8800		.050	-.020100	5.8599	.410		
.800	6.6800	.620	.070	-.013300	6.6667	.495	.373	400°C
1.000	6.9600	.740	.080	-.013300	6.9467	.630	.388	
.200	2.2300	.360	.040	-.065400	2.1646	.340	.118	
.400	4.1700	.400	.040	-.037500	4.1325	.360	.174	
.600	5.7200		.060	-.020100	5.6999	.410		
.800	6.6000		.100	-.013300	6.5867	.495		700°C
1.000	6.8100		.110	-.013300	6.7967	.630		
.100	1.1000		.030	-.080500	1.0195	.335		
.150	1.6000	.440	.050	-.073500	1.5265	.337	.283	
.200	2.1500	.560	.060	-.065400	2.0846	.340	.445	
.300	3.1300	.460	.050	-.051000	3.0790	.347	.302	
.400	4.0300	.690	.070	-.037500	3.9925	.360	.589	1063°C
.600	5.4500		.100	-.020100	5.4299	.410		
.800	-6.6700	1.640	.170	.113000	-6.5570	.730	1.469	
1.000	-6.7200	1.760	.180	.078300	-6.6417	.910	1.506	

N.B.: Experimental details in table IV-2, under columns Ⓑ & Ⓒ.
Definition of symbols in table I-1.

$[0\zeta\zeta]T_1$ branch measured at $aQ/2\pi = (2+\zeta, 2-\zeta, 0)$.

$\hat{\zeta}$	ν_x	$2\Gamma_{\nu x}$	$\Delta\nu$	C_ν	ν	$C_{2\Gamma\nu}$	$2\Gamma_\nu$	Constant-Q
.200	1.3300	.160	.020	-.020400	1.3096	.108	.118	
.400	2.7000	.180	.020	-.009800	2.6902	.106	.145	
.600	3.8500	.220	.030	-.002300	3.8477	.188	.114	22°C
.750	4.5400	.280	.030	-.001900	4.5381	.276	.047	
1.000	5.0400	.380	.040	-.004200	5.0358	.490	0.000	
.200	1.2700	.180	.020	-.020400	1.2496	.108	.144	
.400	2.5700	.300	.030	-.009800	2.5602	.106	.281	
.600	3.7100	.380	.040	-.002300	3.7077	.188	.330	
.750	4.3900	.380	.040	-.001900	4.3881	.276	.261	400°C
.875	4.7900	.460	.050	-.001900	4.7881	.370	.273	
1.000	4.9200	.550	.060	-.004200	4.9158	.490	.250	
.200	1.1700	.260	.030	-.020400	1.1496	.108	.237	
.400	2.4100	.400	.040	-.009800	2.4002	.106	.386	
.600	3.5700	.360	.040	-.002300	3.5677	.188	.307	
.750	4.2400	.400	.040	-.001900	4.2381	.276	.290	700°C
.875	4.6300	.480	.050	-.001900	4.6281	.370	.306	
1.000	4.7600	.520	.060	-.004200	4.7558	.490	.174	
.100	.5000	.220	.030	-.026000	.4740	.130	.177	
.150	.7700	.240	.030	-.023000	.7470	.115	.211	
.200	1.0200	.250	.030	-.020400	.9996	.108	.225	
.250	1.2800	.380	.040	-.017000	1.2630	.108	.364	
.300	1.5800	.450	.050	-.014200	1.5658	.106	.437	
.350	1.8600	.420	.050	-.011800	1.8482	.106	.406	
.400	2.1700	.740	.080	-.009800	2.1602	.106	.732	1063°C
.450	2.5000	.840	.090	-.007500	2.4925	.115	.832	
.500	2.7200	.840	.090	-.005800	2.7142	.135	.829	
.600	3.3100	.840	.090	-.002300	3.3077	.188	.819	
.750	4.0100	.680	.070	-.001900	4.0081	.276	.621	
.875	4.4000	1.000	.100	-.001900	4.3981	.370	.929	
1.000	4.5000		.100	-.004200	4.4958	.490		

$[0\zeta 1]\pi$ branch measured at $aQ/2\pi = (3, -\zeta, 0)$.

ζ	ν_x	$2\Gamma_{\nu x}$	$\Delta\nu$	C_ν	ν	$C_{2\Gamma\nu}$	$2\Gamma_\nu$	Constant-Q
0.000	6.9600	.740	.080	-.013300	6.9467	.630	.388	← Note ②
.200	6.8600	1.000	.100	-.007000	6.8530	.470	.883	
.350	6.3000		.050	-.002000	6.2980	.405		
.500	5.8800	.320	.040	.000200	5.8802	.325	0.000	400°C
.650	5.4200	.380	.040	-.001000	5.4190	.350	.148	
.800	5.0700	.430	.050	-.003100	5.0669	.420	.092	
1.000	4.9200	.550	.060	-.004200	4.9158	.490	.250	← Note ①
0.000	6.8100		.110	-.013300	6.7967	.630		← Note ②
.200	6.6200	1.400	.140	-.007000	6.6130	.470	1.319	
.350	6.2000	1.160	.120	-.002000	6.1980	.405	1.087	
.500	5.6400	.640	.070	.000200	5.6402	.325	.551	700°C
.650	5.2000	.530	.060	-.001000	5.1990	.350	.398	
.800	4.8500	.480	.050	-.003100	4.8469	.420	.232	
1.000	4.7600	.520	.060	-.004200	4.7558	.490	.174	← Note ①

[0ζζ]L branch measured at $aQ/2\pi = (2+\zeta, 2+\zeta, 0)$.

ζ	ν_x	$2\Gamma_{\nu x}$	$\Delta\nu$	C_ν	ν	$C_{2\Gamma\nu}$	$2\Gamma_\nu$	Constant-Q
.200	3.6500	.500	.050	-.044000	3.6060	.450	.218	
1.000	5.0400	.380	.040	-.004200	5.0358	.490	0.000	22°C ← Note ①
.200	3.5200	.460	.050	-.044000	3.4760	.450	.095	
.400	5.7800	.600	.060	-.040300	5.7397	.465	.379	
.600	6.2600	.570	.060	-.061900	6.1981	.650	0.000	
.750	5.4900	.500	.050	.003400	5.4934	.650	0.000	400°C
.850	5.0800	.600	.060	0.000000	5.0800	.610	0.000	
1.000	4.9200	.550	.060	-.004200	4.9158	.490	.250	← Note ①
.200	3.4200	.480	.050	-.044000	3.3760	.450	.167	
.400	5.6900	.680	.070	-.040300	5.6497	.465	.496	
.600	6.2500	1.000	.100	-.061900	6.1881	.650	.760	
.750	5.4100	.800	.080	.003400	5.4134	.650	.466	700°C
.850	4.9800	.520	.060	0.000000	4.9800	.610	0.000	
1.000	4.7600	.520	.060	-.004200	4.7558	.490	.174	← Note ①
.050	.8800		.040	-.055800	.8242	.470		
.100	1.6300	.500	.050	-.052000	1.5780	.465	.184	
.150	2.4300	.650	.070	-.047500	2.3825	.460	.459	
.200	3.2200	.700	.070	-.044000	3.1760	.450	.536	1063°C
.250	3.9200	.720	.080	-.040500	3.8795	.450	.562	
.400	5.5000	1.200	.120	-.040300	5.4597	.465	1.106	
1.000	4.5000		.100	-.004200	4.4958	.490		← Note ①

[0ζ1]Λ branch measured at $aQ/2\pi = (3+\zeta, 1, 0)$.

ζ	ν_x	$2\Gamma_{\nu x}$	$\Delta\nu$	C_ν	ν	$C_{2\Gamma\nu}$	$2\Gamma_\nu$	Constant-Q
.500	4.6300	.480	.050	-.008800	4.6212	.485	0.000	
.650	4.7000	.400	.040	-.010000	4.6900	.490	0.000	
.800	4.8100	.480	.050	-.014400	4.7956	.510	0.000	400°C
1.000	4.9200	.550	.060	-.004200	4.9158	.490	.250	← Note ①
.500	4.4200	.680	.070	-.008800	4.4112	.485	.477	
.650	4.4900	.480	.050	-.010000	4.4800	.490	0.000	
.800	4.6400	.600	.060	-.014400	4.6256	.510	.316	700°C
1.000	4.7600	.520	.060	-.004200	4.7558	.490	.174	← Note ①
.500	4.2200	1.280	.130	-.008800	4.2112	.485	1.185	
.650	4.3400	1.320	.140	-.010000	4.3300	.490	1.226	
.800	4.4200	.920	.100	-.014400	4.4056	.510	.766	1063°C
1.000	4.5000		.100	-.004200	4.4958	.490		← Note ①

Notes: ① Phonon measured as $[0\zeta\zeta]T_1$ ⇒ ζ = 1.0

② Phonon measured as [0Qζ]L, ζ = 1.0

Table IV-6. Temperature dependence of the atomic force constants of Cu. (units: dynes/cm)

AFC	Ⓧ	Ⓐ	Ⓑ	Ⓒ	Ⓓ
1XX	13102(120)	13282(128)	12275(112)	11682(180)	11718(535)
1ZZ	-1417(186)	-1253(163)	-1321(153)	-1424(199)	-1787(382)
1XY	14820(240)	15090(484)	14062(361)	14384(423)	13653(833)
2XX	361(246)	289(537)	698(405)	1554(499)	238(599)
2YY	-238(147)	52(328)	-355(288)	74(328)	-279(540)
3XX	642(103)	560(74)	744(60)	656(74)	325(202)
3YY	315(68)	176(38)	246(40)	193(47)	95(101)
3YZ	190(133)	128(22)	165(20)	155(22)	76(51)
3XZ	385(52)	256(43)	331(40)	310(45)	153(101)
4XX	104(80)	-51(156)	-174(124)	-490(143)	-246(234)
4ZZ	-284(132)	-87(90)	-24(113)	-24(123)	93(168)
4XY	396(206)	36(160)	-150(128)	-466(142)	-339(234)
5XX	-137(58)	-76(51)	-190(50)	-122(57)	-74(112)
5YY	9(74)	-62(21)	-80(32)	-63(35)	-92(46)
5ZZ	-16(79)	-60(24)	-67(35)	-55(39)	-95(52)
5XY	-55(32)	-5(20)	-41(20)	-22(23)	7(44)
6XX	-138(63)				
6YZ	-232(87)				

Quantities in parenthesis are uncertainties.

Notes: Ⓧ : 22°C; from Svensson et al, model M3 [SV67].
Ⓐ : 22°C; this work, general first-neighbour AFC's.
Ⓑ : 400°C; " " " " " "
Ⓒ : 700°C; " " " " " "
Ⓓ : 1063°C; " " " " " "

Table IV-7. Temperature dependence of the zero-sound elastic constants of Cu. (units: 10^{12} dynes/cm^2)

		22°C	400°C	700°C	920°C	1063°C
$(c_{11}-c_{12})/2$	(±0.006)	0.2361	0.2004	0.1686	0.1393	0.1198
c_{44}	(±0.016)	0.732	0.649	0.578	0.507	0.464
c_{11}	(±0.064)	1.678	1.528	1.430	1.352	1.267
$(c_{11}+c_{12}+2c_{44})/2$	(±0.050)	2.183	1.984	1.838	1.716	1.608
c_{12}	(±0.075)	1.21	1.13	1.09	1.07	1.03

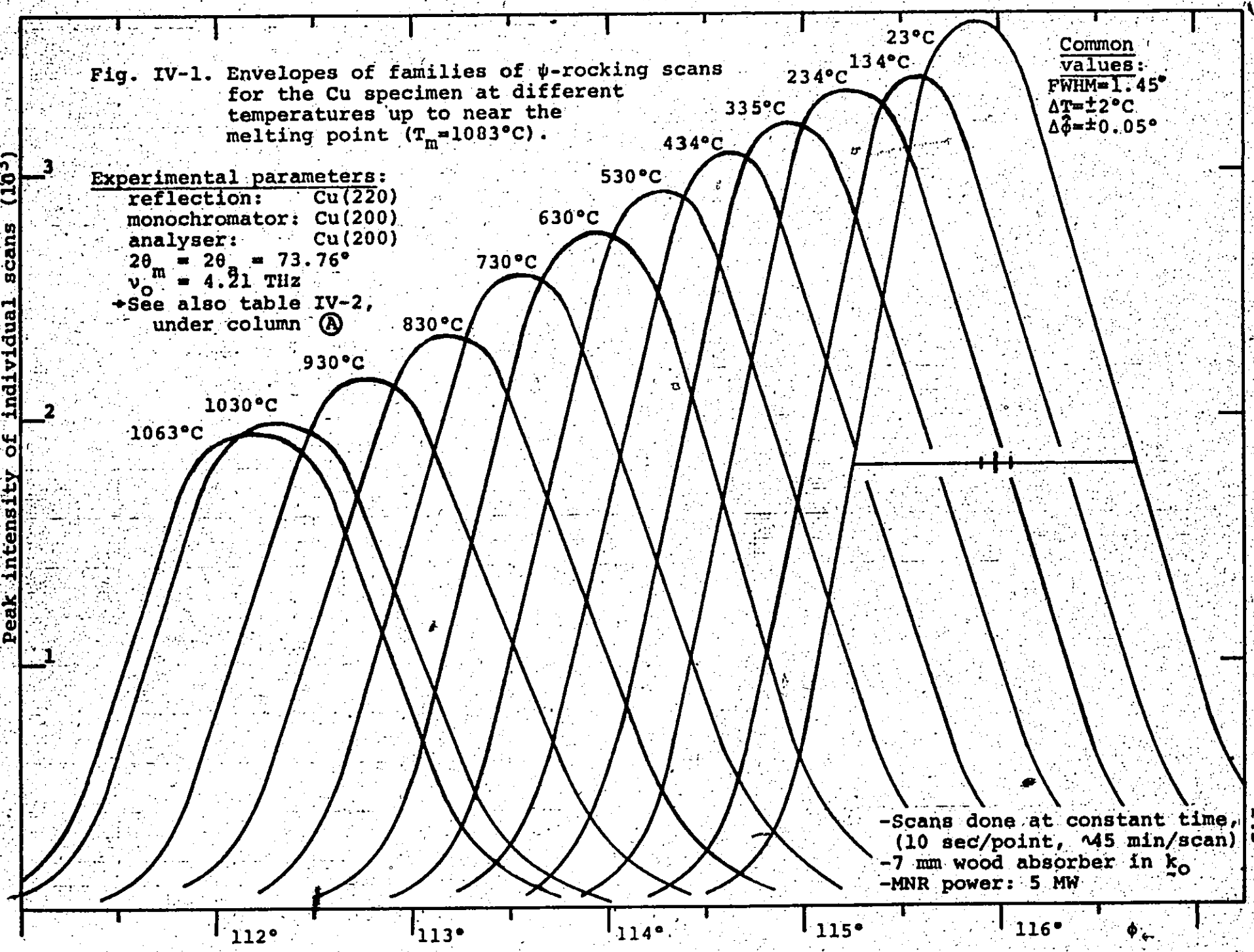
Fig. IV-1. Envelopes of families of ψ-rocking scans for the Cu specimen at different temperatures up to near the melting point (T_m=1083°C).
Experimental parameters:
reflection: Cu(220)
monochromator: Cu(200)
analyser: Cu(200)
$2\theta_m = 2\theta_a = 73.76°$
$\nu_o = 4.21$ THz
→See also table IV-2, under column Ⓐ
Common values:
FWHM=1.45°
ΔT=±2°C
Δφ̂=±0.05°
23°C
134°C
234°C
335°C
434°C
530°C
630°C
730°C
830°C
930°C
1030°C
1063°C
-Scans done at constant time, (10 sec/point, ~45 min/scan)
-7 mm wood absorber in k_o
-MNR power: 5 MW
Peak intensity of individual scans (10^3)
1
2
3
112°
113°
114°
115°
116°
φ
142

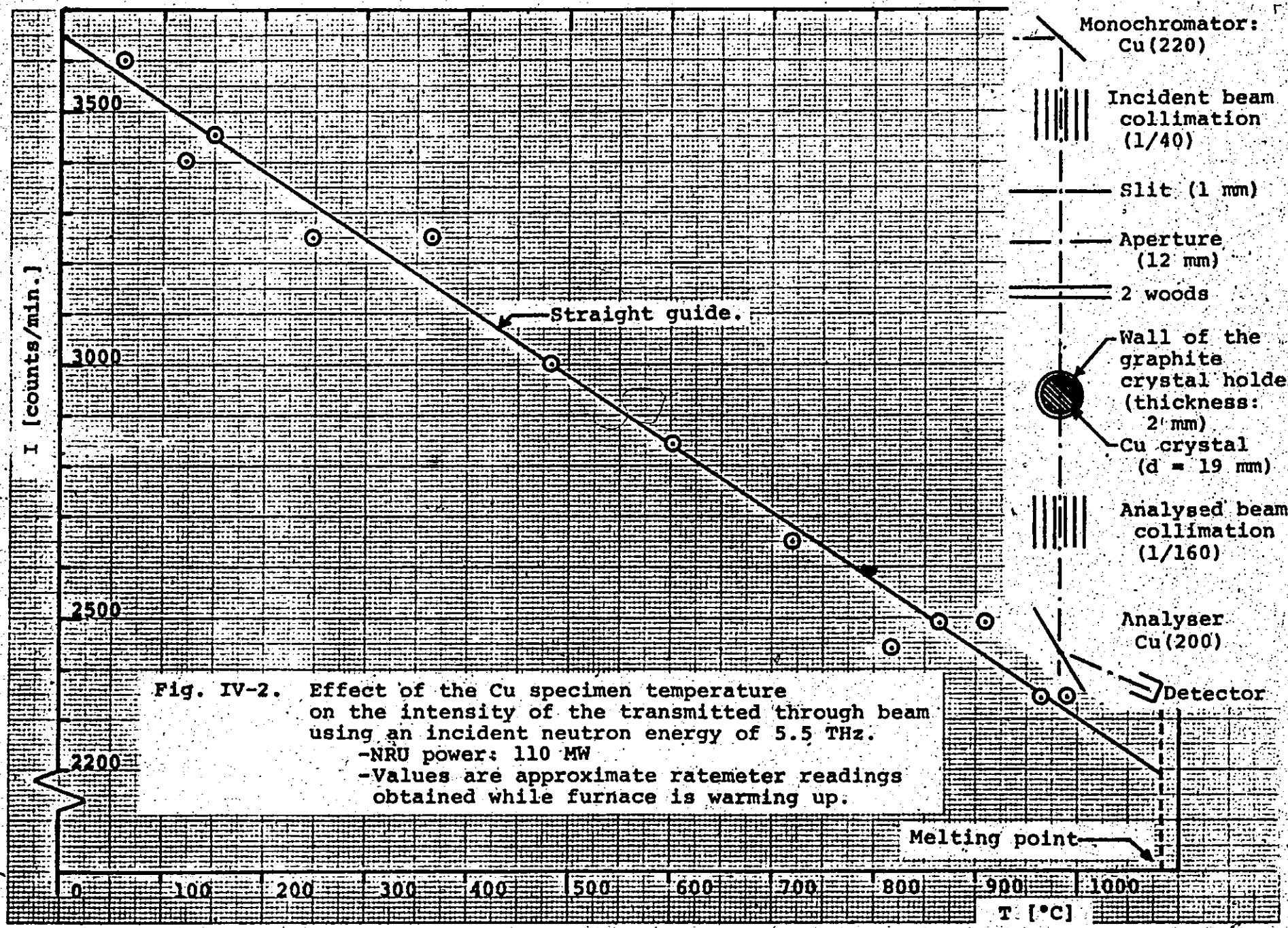

Fig. IV-2. Effect of the Cu specimen temperature on the intensity of the transmitted through beam using an incident neutron energy of 5.5 THz.
-NRU power: 110 MW
-Values are approximate ratemeter readings obtained while furnace is warming up.

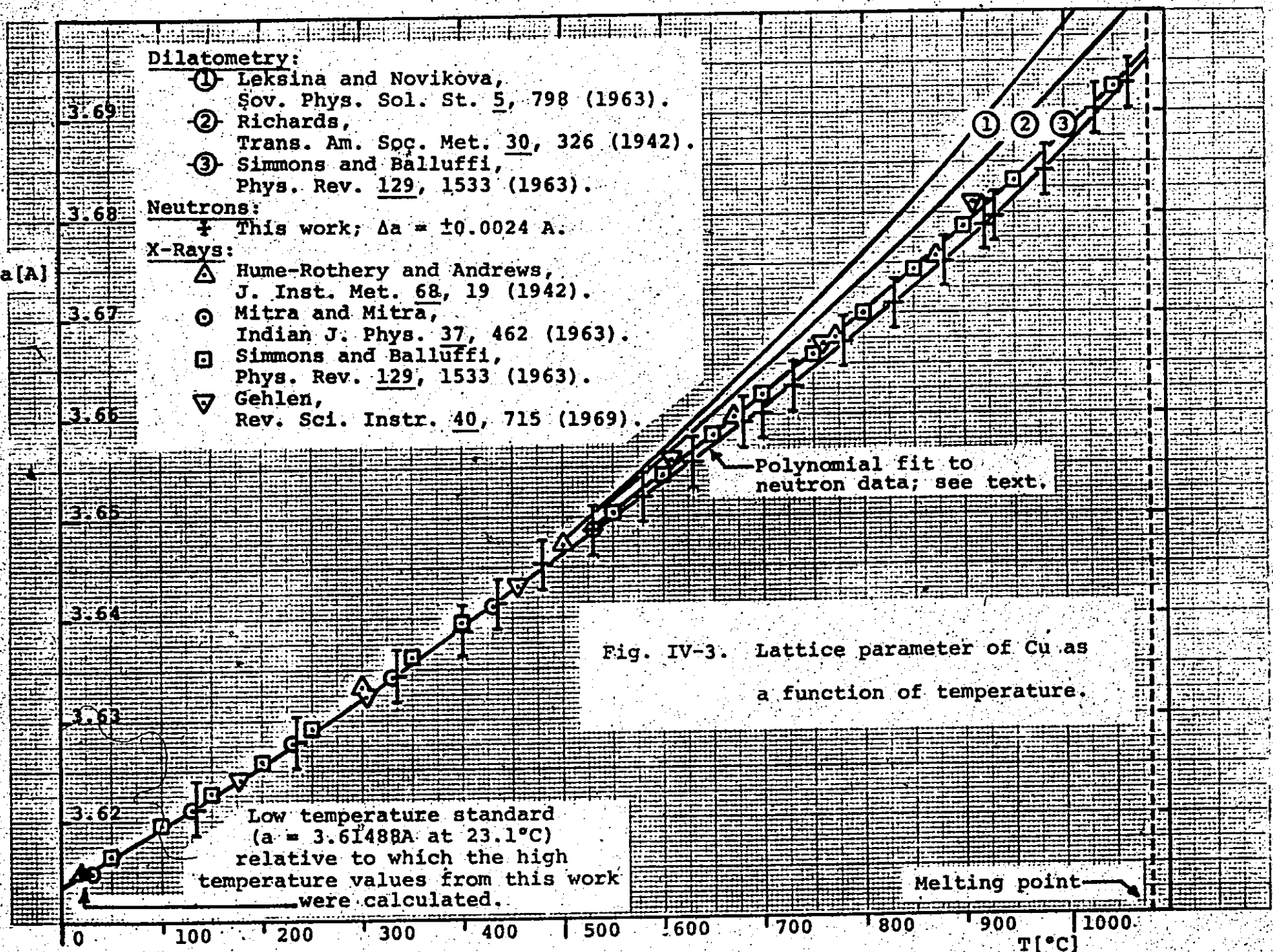

Fig. IV-3. Lattice parameter of Cu as a function of temperature.

Figure IV-4. Temperature dependence of the single-phonon lineshape in Cu.

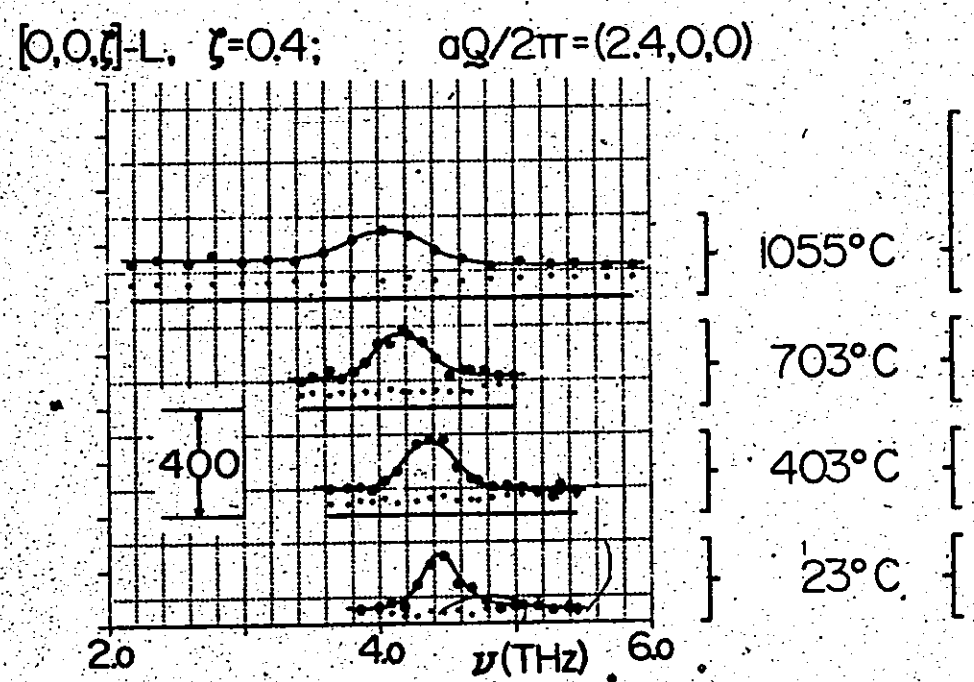

Fixed ν' = 5.2 THz
Normalized monitor: 25E4
Experimental details in table IV-2, under column Ⓑ

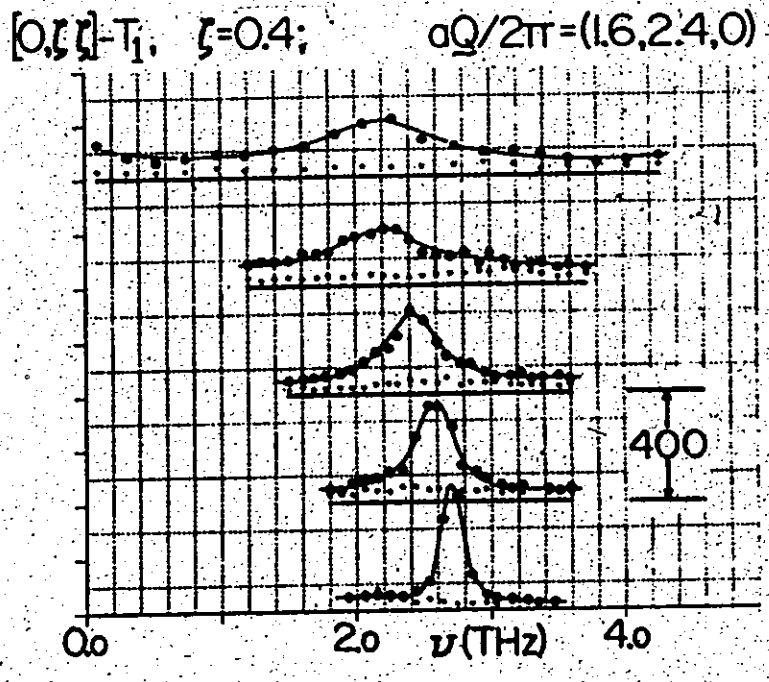

Fixed ν' = 5.2 THz
Normalized monitor: 10E4
Experimental details in table IV-2, under column Ⓑ

N.B.: -The curves joining the points are guides only.
-The baselines are represented by straight lines under their respective neutron groups.

Figure IV-5. Temperature dependence of the [00ζ]L zone boundary phonon in Cu.

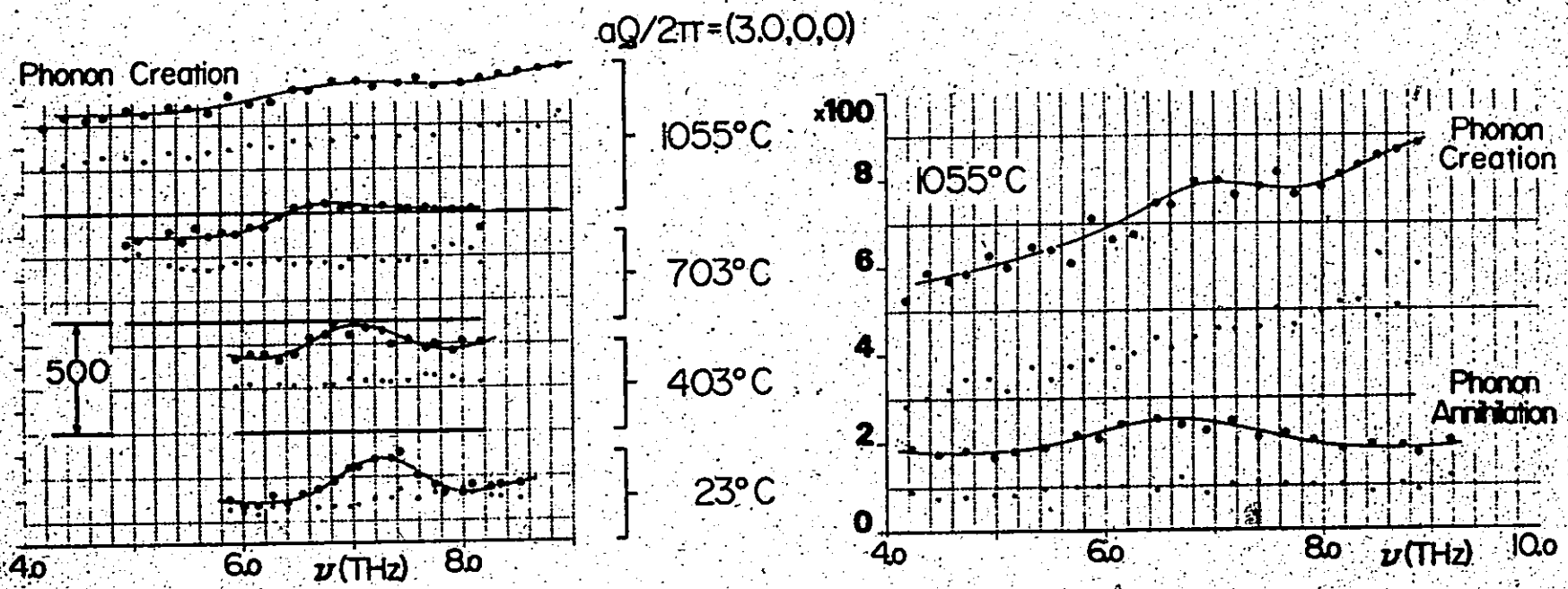

Fixed ν' = 5.2 THz
Normalized monitor: 75E4
Experimental details in table IV-2, under column Ⓑ
N.B.: The baselines are represented by straight lines under their respective neutron groups.

Fixed { ν' = 5.2 THz (upper curve); ν_o = 5.5 THz (lower curve)
Normalized monitor: 100E4
Experimental details in table IV-2, under column Ⓑ (upper curve) under column Ⓒ (lower curve)
N.B.: Baseline is common to both phonons.

N.B.: -The curves joining the points are guides only.
-The upper phonon is the same in both cases, except for scale and normalized monitor.

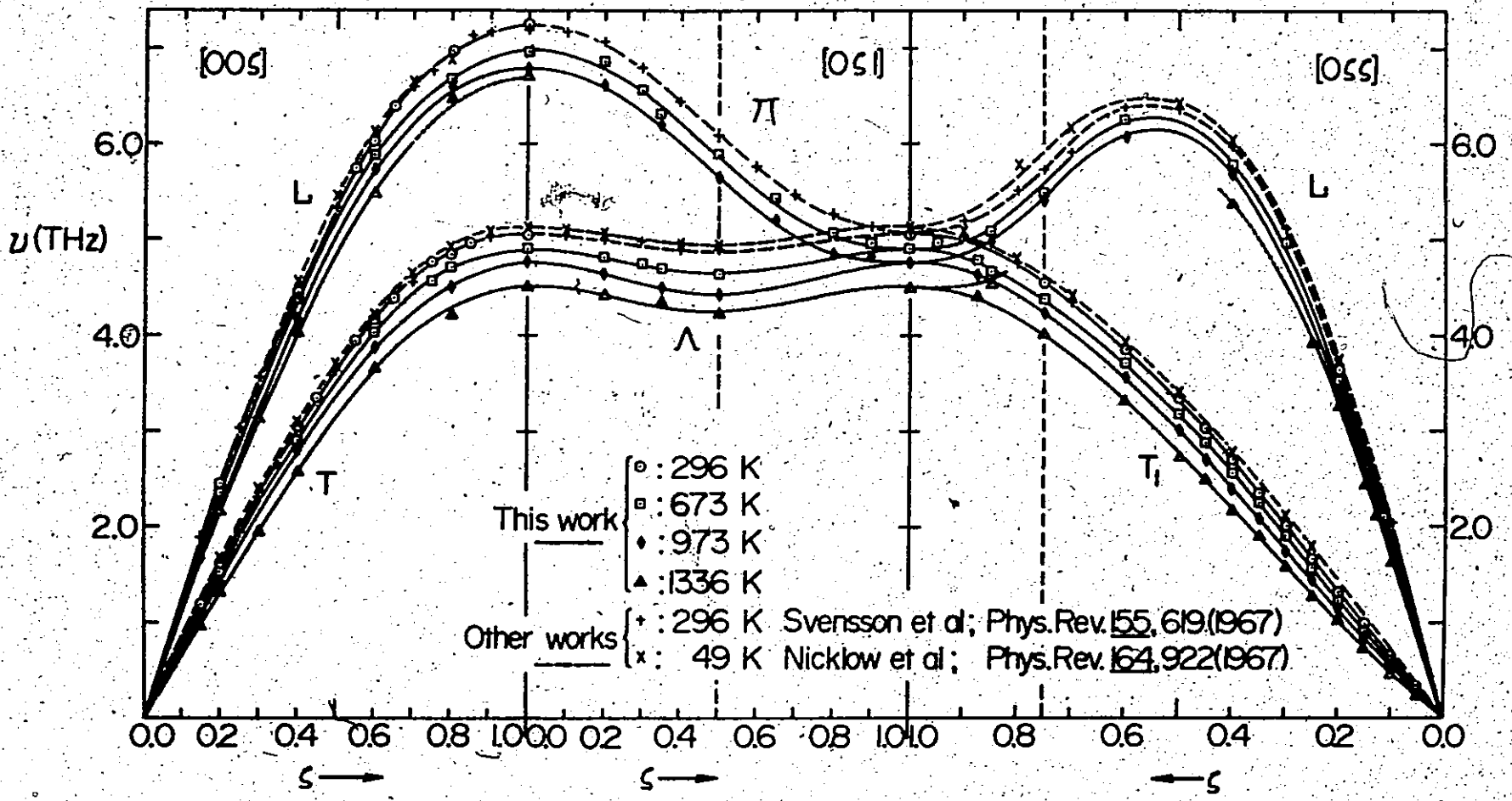

Figure IV-6. Phonon spectrum of Cu at various temperatures.

N.B.: The curves joining the points are guides only.

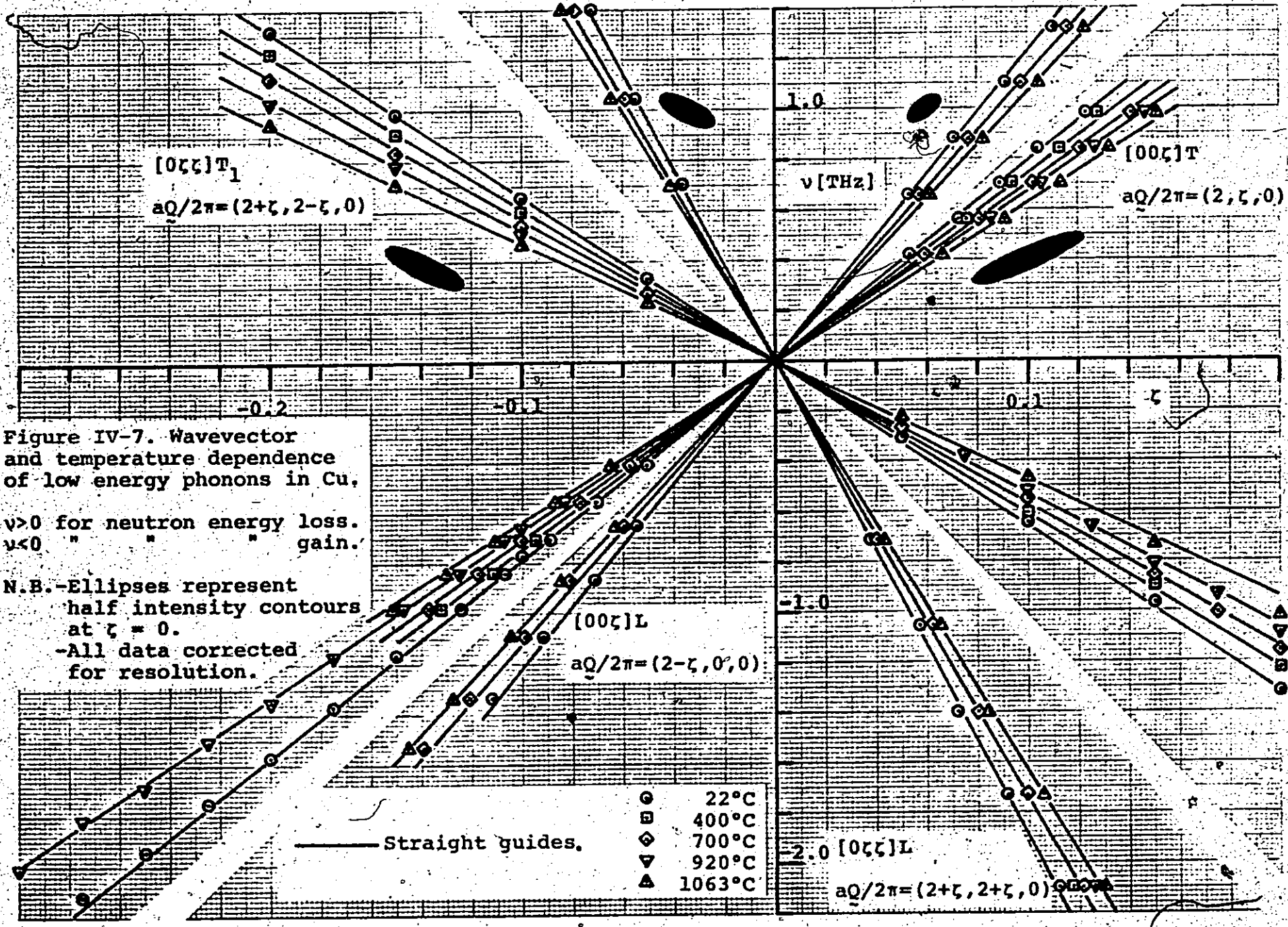

Figure IV-7. Wavevector and temperature dependence of low energy phonons in Cu.

ν>0 for neutron energy loss.
ν<0 " " " gain.

N.B.-Ellipses represent half intensity contours at ζ = 0.
-All data corrected for resolution.

Figure IV-8. Phonon frequency shifts in Cu at various temperatures.

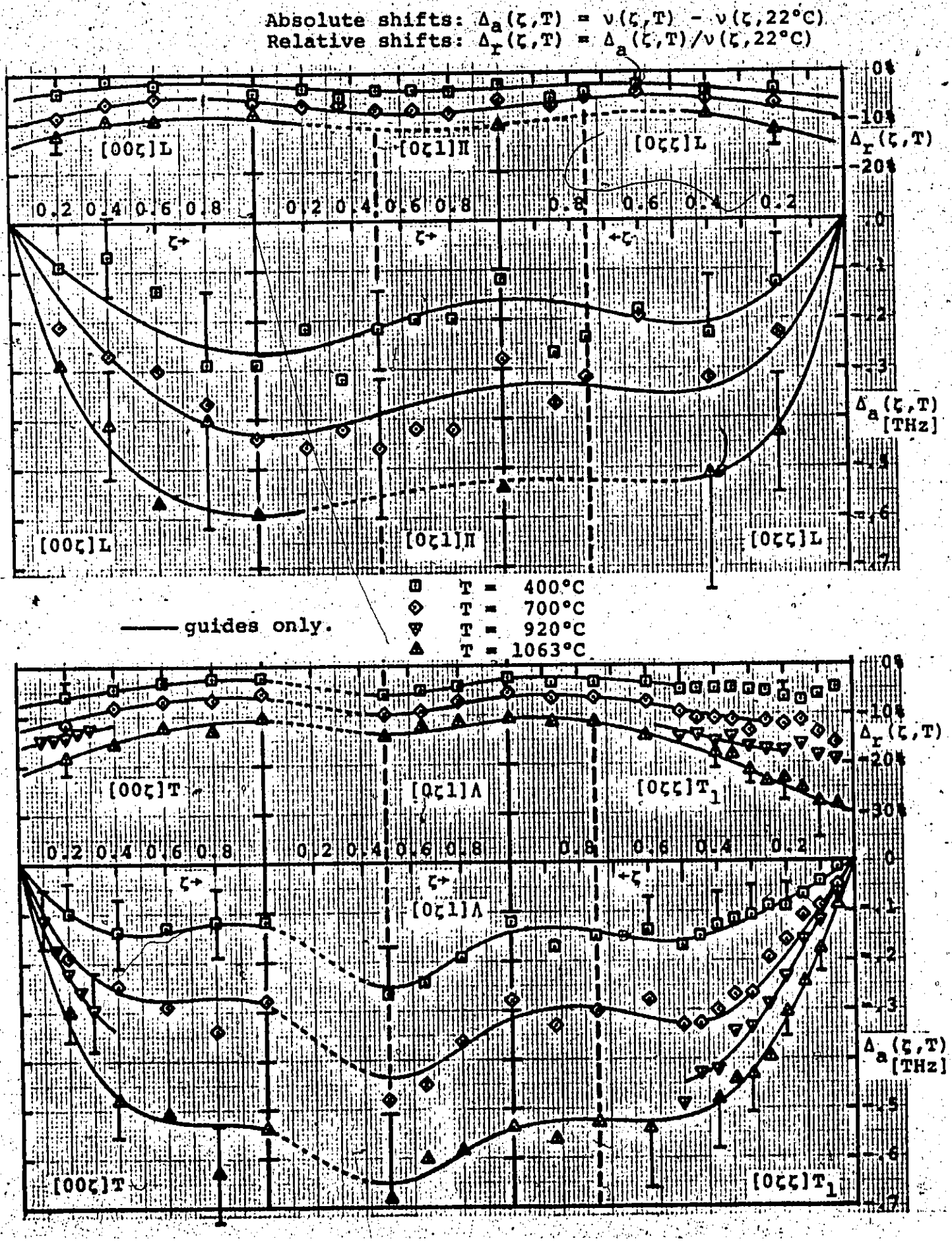

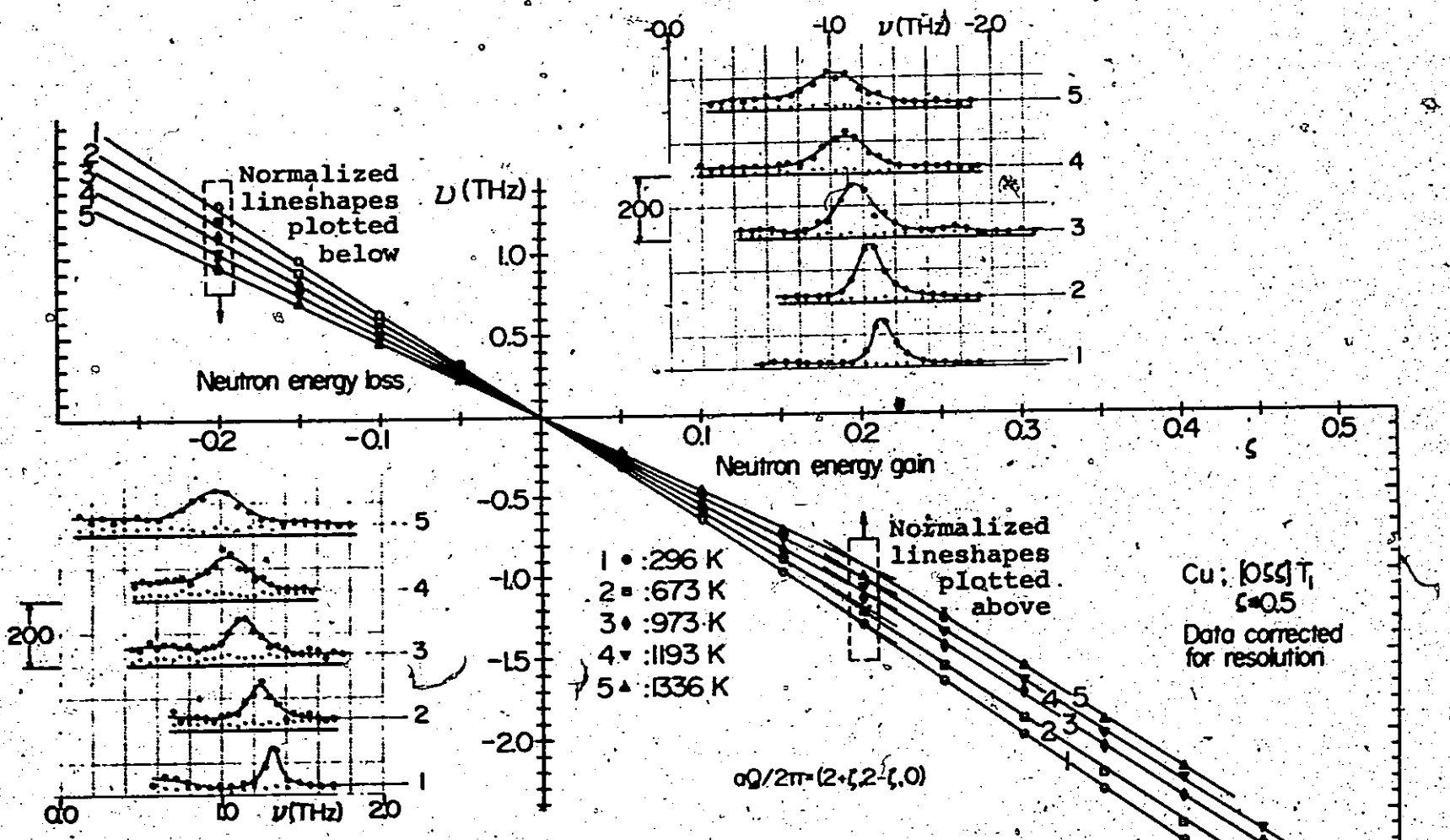

Figure IV-9. Behaviour of the low energy $[0\zeta\zeta]T_1$ phonons in Cu at various temperatures.
(For experimental details on the normalized lineshapes shown, refer to column Ⓐ, in table IV-2.

Figure IV-10. Wavevector and temperature dependence of the intrinsic linewidth of some selected low energy phonons in Cu.

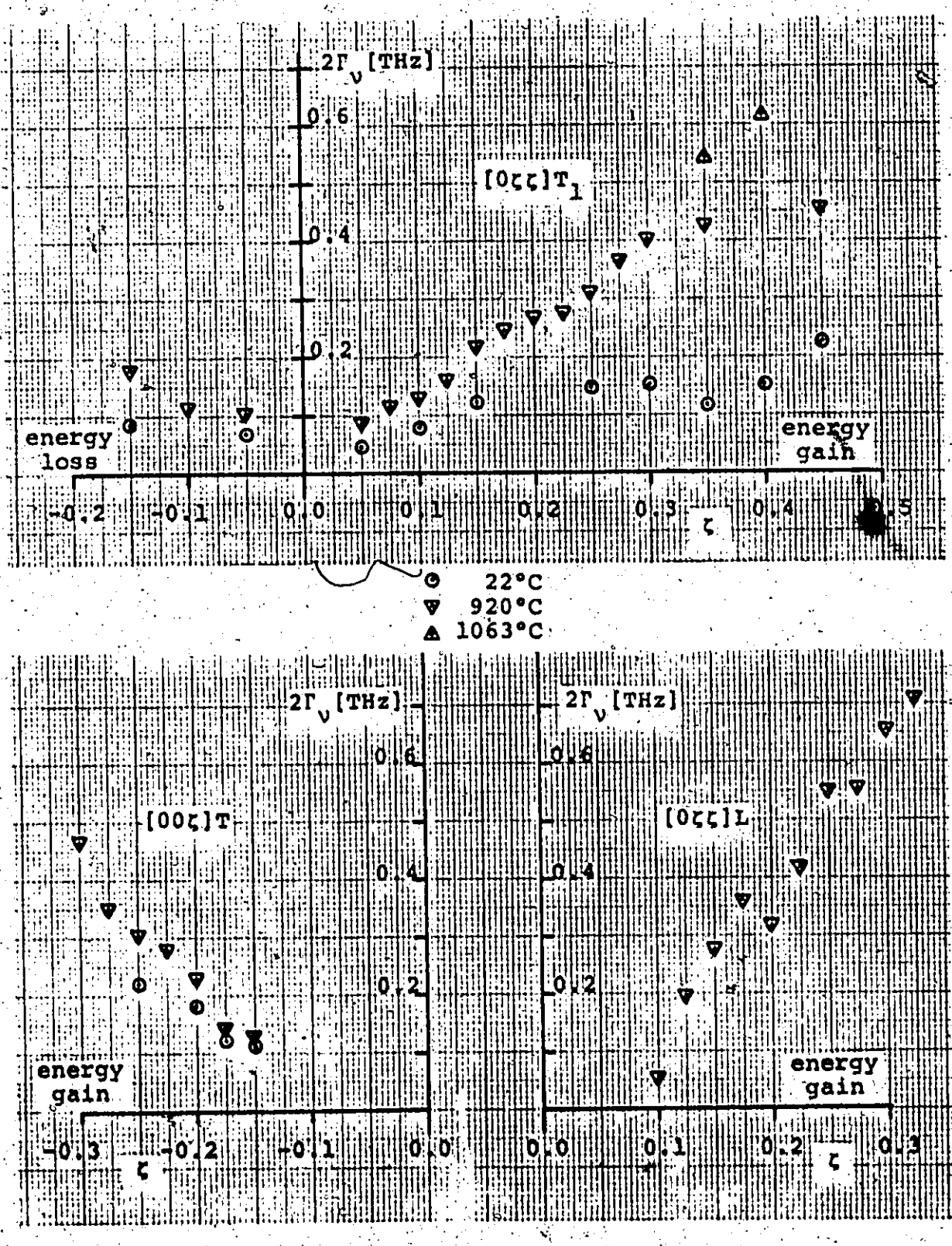

Figure IV-11. Wavevector and temperature dependence of the ratio $|\nu/\zeta|$ for low energy phonons in Cu using resolution corrected data except where indicated.

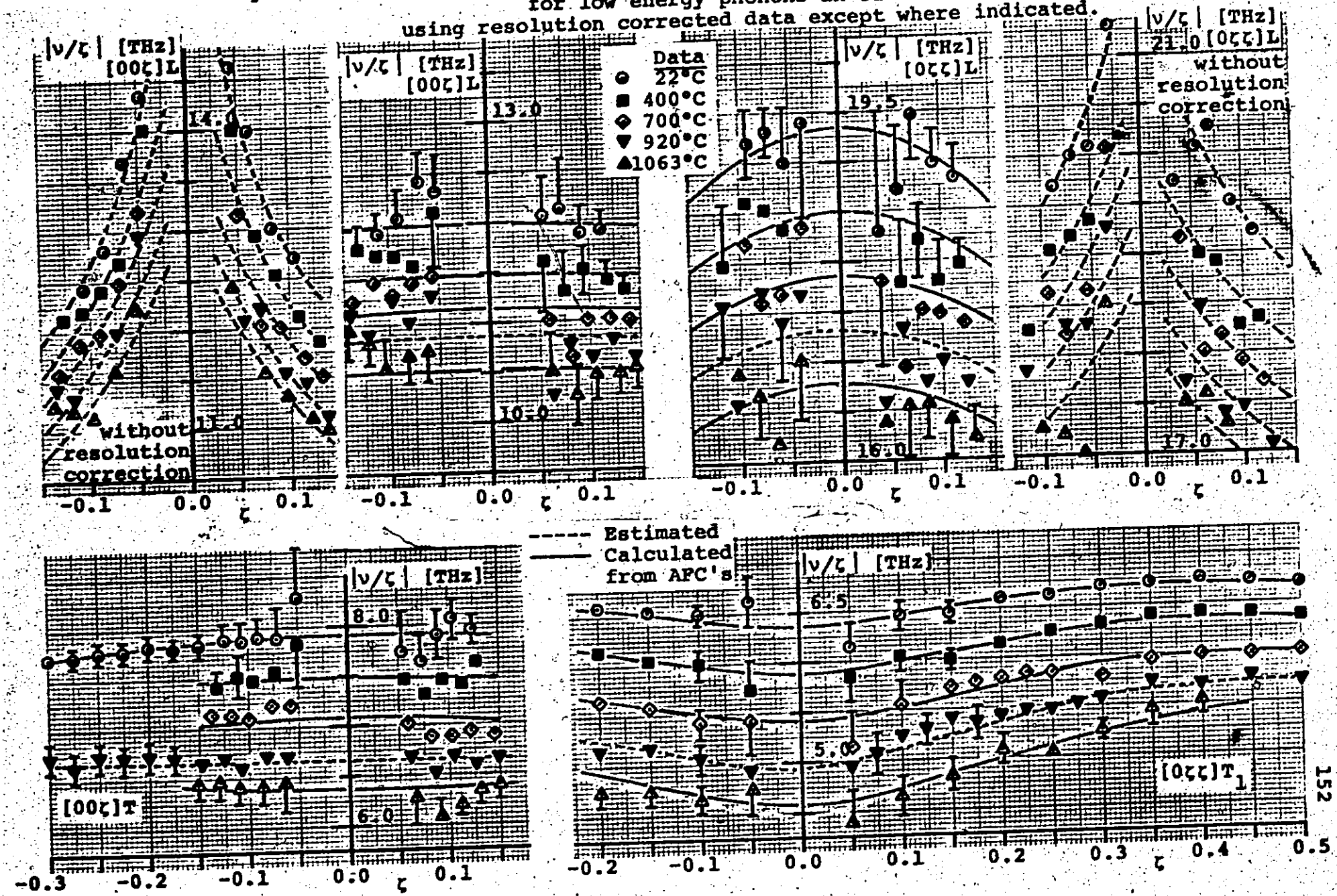

Figure IV-12.

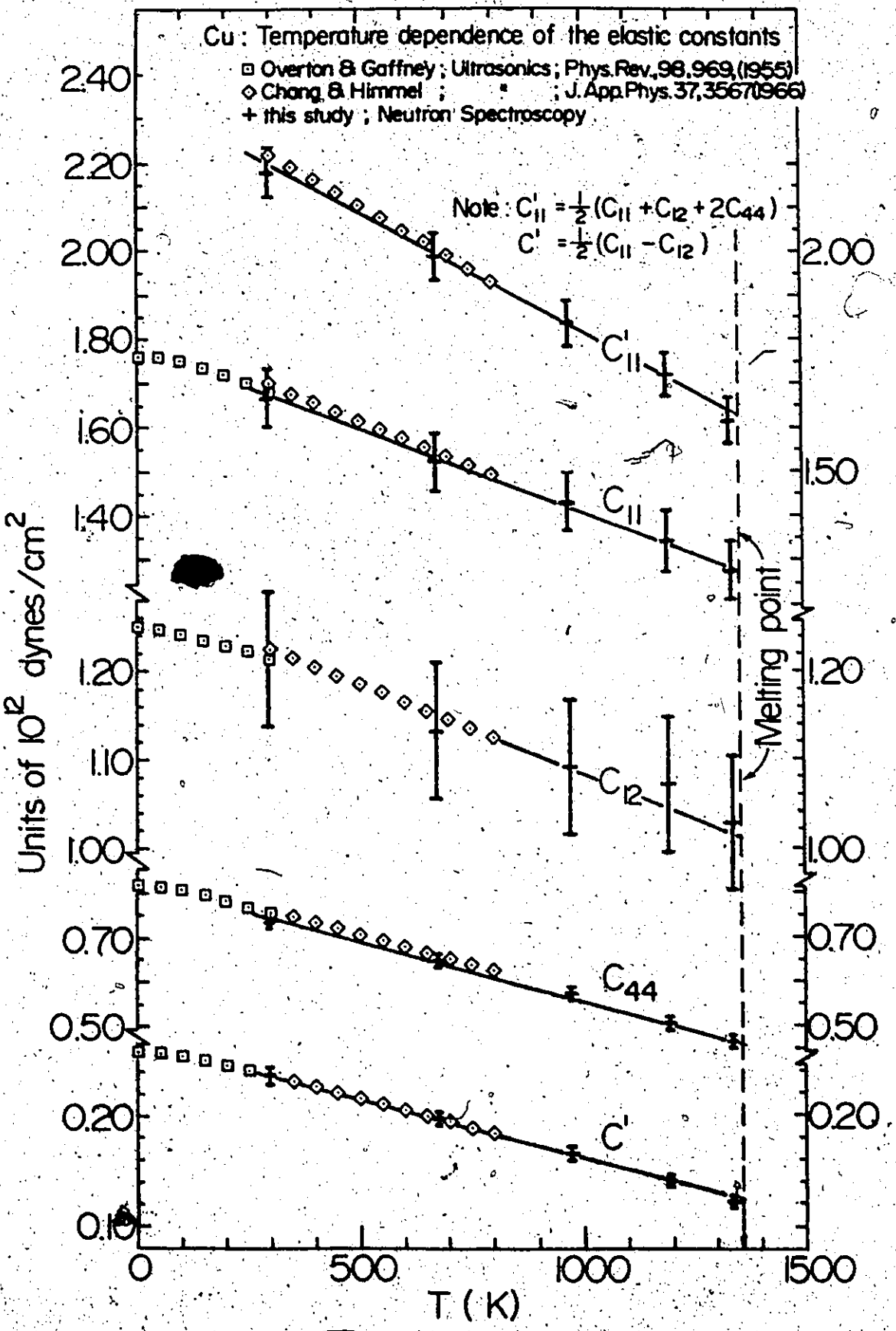
Cu : Temperature dependence of the elastic constants
Overton & Gaffney ; Ultrasonics ; Phys.Rev.,98,969,(1955)
Chang & Himmel ; " ; J.App.Phys.37,3567(1966)
+ this study ; Neutron Spectroscopy
Note : C'11 = 1/2 (C11 + C12 + 2C44)
C' = 1/2 (C11 - C12)
C'11
C11
C12
C44
C'
Melting point
Units of 10^12 dynes/cm^2
T (K)
2.40
2.20
2.00
1.80
1.60
1.40
1.20
1.10
1.00
0.70
0.50
0.20
0.10
0
500
1000
1500

CHAPTER V

PALLADIUM: TEMPERATURE DEPENDENCE OF THE LOW ENERGY PHONONS BETWEEN 22°C AND 1050°C

A - INTRODUCTION

Palladium, like copper, discussed in the previous chapter, is a transition metal which crystallizes in the FCC structure; it belongs to the same group of elements as nickel and platinum. Its phonon spectrum has previously been observed at 120 K, 296 K 673 K and 853 K by Miiller and Brockhouse [MI71] who have done systematic measurements of frequency shifts as function of temperature. This allowed them to calculate the total lattice heat capacity and, hence, to extract the electronic heat capacity over a temperature range extending up to 853 K. The work provided a confirmation that the electronic specific heat of Pd, which has an unusually large value at low temperatures compared with other metals, tends to saturate at high temperatures where it can no more be expressed as a relationship of the form $C_e = \gamma T$ as in the case of simple metals, unless γ is now considered as temperature dependent.

For technical reasons, their measurements were limited to temperatures inferior to 853 K (580°C); this is far below the melting point for palladium, i.e. 1825 K (1552°C) [H2]. Hopefully, some interesting information might be obtainable by going to higher temperatures. There are at least three questions that such an experiment would help to clarify. The first concerns

the temperature dependence of the zero-sound elastic constants; this has been discussed at length in the previous chapters. The second point of interest deals with the linewidth of the [00ζ]T branch following such a study attempted by Miiller [MI75] at 120 K. His instrumental resolution was not sufficient to allow him to observe any intrinsic linewidth along this branch, except near the zone boundary. This pointed out to the possibility of phonon lifetimes significantly longer than in the T_1 branch. We proceeded to investigate this branch with good enough resolution and statistics so as to perform a valid study of the linewidth.

The third and final point of interest deals with the behaviour of the [0ζζ]T_1 branch as a function of temperature. Miiller had found that this branch shows a pronounced variation in slope near $\zeta = 0.35$ (at 22°C) and that the magnitude of the effect decreases at higher temperatures [MI68]. This temperature dependence is of the type expected from a Kohn-type anomaly and this was later confirmed from analysis of the Fermi surface [MI75]. It is remarkable that this anomaly occurs in the same branch as the anomaly observed in copper and discussed at length in the previous chapter. The temperature dependence of the two effects is opposite, however. Whereas, in copper, the T_1 branch is nearly linear up to $\zeta = 0.5$ at room temperature ($T/T_m = .22$; T_m being the melting temperature) and has an upward change of curvature which increases as $T/T_m \to 1$, palladium, on the other hand, shows a strong upward curvature at room temperature or

below ($T/T_m < 0.17$) which all but disappears at the highest temperature at which Miiller operated (853 K; $T/T_m = .47$). Thus, the third point that a high temperature experiment on Pd may help to clarify concerns the behaviour of this branch over an extended temperature range.

Since we had a furnace capable of reliable operation at the gold point (1336 K or 1063°C), we proceeded to investigate palladium further. It was "a priori" out of the question to measure high energy phonons ($\nu > 4$THz) and, hence, the whole spectrum of this metal, the low flux available on the McMaster University nuclear reactor (MNR) being the limiting factor (NRU reactor was shut down from the 5/VI/72 to the 2/VIII/74). Because of the similarity between the phonon spectra of Cu (chapter IV) and Pd [MI68], the same spectrometer calibration and resolution were used as had been chosen for the measurement of the zero-sound elastic constants of copper (also done on the MNR). This also provided a satisfactory resolution to investigate the behaviour of the phonon lifetimes along the [00ζ]T branch as well.

B - SPECIMEN, APPARATUS AND PROCEDURE

The palladium specimen was the same one as used by Miiller [MI68; MI71]. Basically it is a boule some 66 mm long and of irregular diameter averaging about 20 mm. As in the case of the copper crystal, it had a (001) crystallographic axis within 5° of its axis of growth and a mosaic spread of 12', as measured by Miiller [MI71]. Miiller had cut small samples of material off the ends and the centre of the boule which he had

analyzed spectrographically; the purity of the specimen was thus found to be 99.9% with aluminum and iron being the largest impurities (at 225 ppm and 140 ppm respectively) followed by copper, platinum and rhodium (all three at 100 ppm).

The specimen was mounted in a graphite holder, as described in detail in chapter III. This only required the machining of a small conical seat on the centre of the bottom face of the crystal. This, as well as a conically machined graphite piston designed to grip the upper end of the crystal, provided a satisfactory method of maintaining the alignment of the crystal at elevated temperatures, as long as the measurements were performed in the order of increasing temperature (see sub-section III-C-1-e.

The holder with the minicrucibles containing the temperature standards was mounted inside the furnace and aligned in the scattering plane within 1°, using the internal adjustments, relative to the furnace chamber which had previously been set in a nearly vertical position using the external adjustments. After this, the internal adjustments were tightened and the furnace cover inserted; the furnace was then evacuated. Final alignment was then done using the external adjustments which were locked in place when the desired alignment had been reached (typically within 0.1°). The electrical and water connections were then completed and then the ψ-rocking scans were done, i.e. after completion of all steps likely to modify the alignment of the crystal.

The temperature was measured with four chromel-alumel thermocouples arranged as discussed in chapter III. These were sensing respectively the temperature at the lower and upper levels of the hot zone and also at the centre and lower portions of the crystal relative to the neutron beam. As previously said, the accuracy of the thermocouples was verified by using mini-crucibles containing convenient temperature standards. In this case, since the maximum operating temperature was of the order of the gold point (the furnace was originally designed to study copper whose melting point is 20°C higher than that of gold), the temperature standards were the same as had been used for the copper experiment, i.e. copper and gold wires inserted in different crucibles both at the top and the base of the hot zones. After the termination of the measurements on Pd, we have verified that the Cu wires did not melt while the Au ones melted and solidified in a perfectly rounded shape. This indicates that the maximum temperature reached was between 1063°C and 1083°C, probably during one of a few deviations away from the nominal value of 1050°C at which most of the high temperature experiment was done. Visual examination of the specimen revealed that it had not distorted at high temperature, as expected and contrary to what happened to the copper crystal. It is interesting to note, however, that its external surface, which was previously greyish, had turned to a highly reflecting silver-like finish, probably as a result of thermal etching.

C - THE EXPERIMENT

Similarly as, and following, the measurements of the zero-sound elastic constants of copper, the measurements on palladium were made on the triple-axis spectrometer [RO66A] located in the MNR. The same calibration was used in both experiments; details may be found in table IV-2. As for the specimen itself, it could only be mounted with a (001) plane in the scattering plane because of the fact that it had a (001) axis nearly parallel to its axis of growth and of the severe space limitations in the furnace. Consequently, the only "small" wave-vector phonons which could be measured were those belonging to the $(00\zeta)T$, $(00\zeta)L$, $(0\zeta\zeta)T_1$ and $(0\zeta\zeta)L$ branches.

The vertical alignment of the specimen was within 0.1° and was maintained as such at all temperatures, as was verified regularly. The ψ-rocking scans were 0.4° wide using the same instrumental configuration as for the phonon measurements, and remained so at all temperatures. The value of ψ_o, i.e. the specimen orientation with respect to the incident beam, was verified regularly during the course of the measurements as well as at the beginning and the end of a series of measurements at a given temperature; the observed values were never significantly different, even at various temperatures.

Phonon measurements were performed at 22°C in order to obtain basic data from which to measure energy shifts as a function of temperature; this also provided a verification of Miiller's

data. Then, the same phonons were measured at 1193 K (920°C) and 1323 K (1050°C); (recall that Miiller's data was obtained at 120 K, 296 K, 673 K and 853 K). As in the case of the copper experiment, best results were obtained with constant-$\underline{Q}$ scans for the $[0\zeta\zeta]T_1$ measurements (ζ = .075, .100, .15, .20, .25, .30, .40) and constant-E scans for the $[00\zeta]T$ ($\nu \leq 1.000$), $[00\zeta]L$ ($\nu \leq 1.145$) and $(0\zeta\zeta)L$ ($\nu \leq 1.626$) measurements. Also, constant-$\underline{Q}$ scans were used in the study of the intrinsic linewidth along the $[00\zeta]T$ branch of which the phonons at ζ = 0.2, 0.3 and 0.4 were observed.

Whenever this was possible, each phonon was measured both by the method of neutron energy gain and neutron energy loss for reasons already discussed at length previously in sections II-D and G. Only the high part of the $(0\zeta\zeta)T_1$ branch and of the $(00\zeta)T$ branch ($|\nu| > 1.4$ THz) were measured solely by neutron energy gain because of limitations (in the analyser) resulting from the low value of the incident neutron energy, purposefully chosen for high resolution measurements.

Measurements at the highest temperature (1050°C) had to be terminated without completing the neutron energy loss measurements and the measurement of the $[00\zeta]T$ and $[0\zeta\zeta]T_1$ branches (ζ = 0.25, 0.30, 0.40) because of the failure of one of the two heaters; this was the first such failure since the shutdown of the NRU reactor. It was decided that sufficient information had already been obtained at 1050°C to reach some conclusion

about the values of the elastic constants up to this temperature. Because of this problem, however, measurements of phonons along the $[00\zeta]T$ and $[0\zeta\zeta]T_1$ branches ($\zeta \geq 0.20$) were not made since fabrication of a new heater element would have required more time than the measurement of the remaining phonons would warrant.

The actual scans were done in a straightforward manner. Angles were routinely checked and the overall spectrometer performance was reliable. The temperature was maintained by manual adjustments within ±2°C and a recording of the voltages of the four thermocouples, neutron flux and furnace vacuum helped to spot anomalies. On the average, for a given statistical accuracy, neutron energy gain scans were some twice as fast as corresponding scans done by neutron energy loss because of the higher luminosity of the analyser at small scattering angles, i.e. poorer resolution. Compared with the previous results on Cu, the Bragg peaks were some two times stronger in the case of Pd while, inversely, phonons of the same energy were some three times weaker in Pd than in Cu. To understand why such is the case, it helps to remember that the reflectivity in elastic scattering is a function of extinction while in inelastic scattering, the integrated intensity is an inverse function of the atomic mass of the target nuclei (see section II-F), all other things being nearly equal in these two cases.

During the whole of the measurements, the reactor operated at full power, i.e. 5 MW. The easiest phonon ($[0\zeta\zeta]T_1$, $\zeta = 0.075$) required 2 hours while the most difficult , e.g $[00\zeta]T$, $\zeta=0.40$, required some 86 hours. In the latter instances, the scans were

usually repeated two or three times and the counts, added together.

D - ELASTIC SCATTERING RESULTS: TEMPERATURE DEPENDENCE OF THE LATTICE PARAMETER OF Pd

The value of the lattice parameter of Pd at room temperature has been determined, using X-ray methods, by numerous authors; these are listed, for example, in Pearson's comprehensive handbook [H3]. In this handbook, Pearson quotes the work of Coles [CO56] as providing the most reliable data, "for in this examination only, are the conditions of measurement fully specified". However, Coles' value, i.e. 3.8908 A at 22°C, falls significantly higher than those of the other groups, whose values lie in the range 3.888 A to 3.8908 A. Since these references were published, there were other determinations. Dutta et al [DU63] and, more recently, Schröder et al [SC72] have published their results for a wide temperature range. At room temperature, the values listed by these authors are in good agreement with each other, but somewhat lower than that of Coles [CO56]; see table V-1. Miiller [MI71] mentions the value of 3.8904 A obtained by his colleague D.H. Dutton who measured the room temperature lattice parameter of his Pd specimen; this is also the same crystal as used for the present experiment. Dutton's measurements were performed relative to a perfect germanium crystal which served as the standard; his results are in excellent agreement with the other recent determination, all performed by X-ray scattering.

The only high temperature data available for the lattice parameter are those of Dutta and Dayal [DU63] and Schröder et al [SC72]. The first reference quotes experimental values at seven discrete temperatures ranging from 25°C to 878°C. The second one covers the range between -182°C and 1536°C, i.e. up to within 20°C of the melting point. It does not give actual experimental values but, instead, the coefficients of a third degree polynomial which fits the experimental data over this temperature range. There is however a serious discrepancy between the high temperature data obtained by these two groups. Since there is mutual agreement at room temperature, it is likely that the discrepancy results from an inaccurate determination of the temperature; this will be discussed below.

In order to lift this ambiguity, the lattice parameter of the Pd crystal was measured at the temperatures at which phonon measurements were performed (i.e. 22°C, 920°C and 1050°C) using the elastic neutron scattering method of Ng et al [NG67]. The specimen and experimental configuration were the same as used for the phonon measurements. Consequently, the precision on the various values of the lattice parameter so obtained is not representative of what this technique can provide. Indeed, high precision measurements of this nature are better performed at large scattering angles with a perfect analyser (typically quartz) and tight collimations. None of the configurations, however, is suitable for inelastic scattering work where resolution has to be sacrificed in order to obtain practical counting rates. The

problem of intensity in the phonon measurements was particularly acute here because of the low flux of the McMaster University reactor where all the data on Pd were obtained. In this case, the determinations of the lattice parameter were performed at the beginning of a phonon run at a new temperature and after a minimum stabilization period of some twelve hours.

Figure V-1 shows the envelopes of the family of ψ rocking scans obtained in the determination of the lattice parameter for Pd. The width of these curves is the same at all temperatures as it should be. Since the crystal was mounted in the furnace with a (001) axis vertical, it was not possible, with an incident energy of 4.2 THz, to use a larger index reflection and, hence, a larger scattering angle than for Pd (220). Had it been possible to do so, the precision would have been improved even though it would still have been limited by the choice of the analyzer and collimators.

A value of 3.8903 A was chosen as the value of the lattice parameter of Pd at 22°C from comparison of the available X-ray data (see table V-1). All our measurements are relative to this 22°C value and are listed also in the same table. The uncertainties were determined from the RMS of the 1/20th of the full widths at half maximum of the room temperature and high temperature curves in fig. V-1; a close examination will reveal that this is a very conservative estimate of the uncertainties. During this part of the measurements, temperature stability was of the order of ±0.5°C; following the consideration of the previous section

V-B , we estimate the temperature uncertainty to be of the order of ±5°C and very possibly ±2°C.

The resulting values of the lattice parameter are plotted in fig. V-2 along with the results of the other two high temperature (X-ray) measurements. One observes that our data falls between these other measurements. The precision on the value determined by X-ray is likely to be about 10 times better than the uncertainty on our results; unfortunately, it is not specified in any of these two X-ray references. In fact, Schröder et al [SC72] quote the work of Dutta and Dayal [DU63] but they do not even attempt to put forward an explanation for the discrepancy. These first authors even show a figure with "calibration points" obtained using a Debye-Scherrer camera. These points are above the curve representing the experimental points obtained using a diffractometer and are shifted about the right amount and in the right direction so as to agree with our measurements.

Schröder et al [SC72] used a furnace supposedly capable of reaching 1709°C(1982K). This, of course, is much above the melting point of Pd but, unfortunately, they apparently terminated their measurements 20 K below the melting point of Pd. Had they tried to melt "in situ" their specimen after completion of their measurements, they could have verified the accuracy of their thermometry measurements. Indeed, if the diffraction pattern disappears within a few degrees of the melting point, all is well. But, if as seems likely, their temperatures are overestimated by possibly as much as 100 K near the melting point (see fig. V-2), then the diffraction pattern would persist high

above the apparent melting temperature. This argument is reinforced by the fact that although these authors claim to have operated up to 20 K below the melting point of Pd, yet their plotted high temperature data do not show any of the non-linear behaviour as do our data on copper (see chapter IV), also plotted on the same graph. Since both metals are transition metals in adjacent columns of the periodic table; it is not unreasonable to expect that they both should show similar qualitative behaviour as a function of reduced temperature (T/T_m).* However, the values of the lattice parameter that they have obtained being very nearly linear at high temperature may be an indication that their actual specimen temperature never even came close to the melting point.

The data of Dutta and Dayal [DU63], on the other hand, show the emergence of an upward curvature at $T/T_m \gtrsim 0.5$ (fig. V-2) and this in contrast with the results of Schröder [SC72] which, as we already said, show no significant such upward curvature and the result of this work on copper which only shows such a behaviour at $T/T_m \gtrsim 0.8$. This seems to indicate that these workers have underestimated their specimen temperature, possibly by mounting their thermocouple in a "cold spot" of their furnace; at ~ 800°C, such an occurrence would not be uncommon and could easily cause a 50°C error resulting from internal temperature gradients and/or heat loss along the thermocouple wires.

*) This apparently intuitive statement can be justified. Indeed, the melting temperature depends on the binding forces; it is known to be correlated with the fractional amplitude of thermal vibrations (see p.19) and, hence, with the degree of anharmonicity. The non-linear behaviour of the lattice parameter at high temperatures is an anharmonic effect and, consequently, should start to manifest itself at a definite value of the reduced temperature.

E - INELASTIC SCATTERING RESULTS: PHONON ENERGIES IN Pd

The procedure for the phonon measurements was described in section V-C and the experimentally obtained lineshapes were corrected for resolution effects following the method discussed in section II-H. Since this method requires a knowledge of atomic force constants (AFC's) at each temperature of interest in order to calculate the corrections applicable to the experimental values, it is really a self-consistent approach in the sense that a knowledge of the corrections requires a knowledge of the AFC's which themselves require a knowledge of the intrinsic eigenfrequencies which themselves require a knowledge of the corrections. Because of the fact that the limited number of phonons that we have been able to measure did not provide us with enough orthogonal information (throughout the Brillouin zone) to determine the AFC's at 920°C and 1050°C, (they are known at 23°C, 400°C and 580°C from the work of Müller [MI71]), we have used the same set of correction functions for our three temperatures and these were calculated using Müller's AFC's for 8th neighbours at 580°C. This is approximately at the mid-position of our temperature range and allows us to calculate the corrections (and the Debye-Waller factor needed to compute the theoretical lineshape) which are equally valid for both the room temperature and high temperature data, in the first order. This is particularly important since an inadequate value of the slope along transverse branches may have a pronounced effect on focussing and, hence, on the calculated corrections.

The complete results are to be found in table V-2 for the three temperatures (22°C, 920°C and 1050°C) at which measurements were performed. One sees that, like in the case of the previous experiment on copper, the resolution corrections are more important than the experimental uncertainties in the case of longitudinal phonons and usually much less important in the case of transverse ones; these uncertainties were determined in the conventional manner [SV67]. The size of these corrections decreases as the absolute magnitude of the neutron energy transfer increasss. This indicates that the effect of resolution is, as expected, more pronounced in the vicinity of the Bragg peak as a result of the strong curvature of the dispersion surface in this region; the Bragg peak is effectively a singularity in the dispersion surface. Unfortunately, this is where the initial phonon energy-gradient needs to be accurately determined to obtain the elastic constants, as will be seen below.

The resulting "small" wavevector dispersion relations are shown in fig. V-3 for all four branches measured. Neutron energy gain and energy loss results have been plotted separately, respectively below and above the horizontal axis. If the small wavevector dispersion relation is linear and if there are no systematic errors, the best fit through all corrected data points should be straight lines through the origin for all branches and at all temperatures, as it does here. The corresponding resolution contours, measured by the method of Møller [MO68] (with the specimen at room temperature) are also included. One will ob-

serve that the phonons chosen for a systematic study of their temperature dependence are separated in wavevector by about one resolution ellipsoid width, except for some low energy transverse ones for which measurements were performed on a finer mesh of wavevector points, as a result of the relative ease of their measurements. For all branches, the lowest energy phonons that were measured are those closest to the Bragg peak that could be observed without interference from the elastically scattered neutrons.

The T_1 anomaly, first observed by Müller [MI68], is readily noticable in the room temperature plot of fig. V-3 as a change in slope beginning at about $\zeta \approx 0.2$. On the other hand, the 920°C data shows that this effect has all but disappeared at this temperature. This leads to a cross-over of the 22°C and 920°C branches at around $\zeta \approx 0.225$; hence the $\zeta = 0.225$ T_1 phonon appears to be temperature independent. The temperature dependence of the anomaly is best shown in the lower right hand portion of fig. V-5 where the T_1 branch ratio $|\nu/\zeta|$, which is a measure of the phonon phase velocity, is plotted (to allow us to later determine the elastic constants). Qualitatively, one sees that this ratio, which should be constant if the T_1 phonons were dispersionless (at "small" wavevectors), shows a structure which reflects the slope variation along this branch. At 22°C there is a relative minimum at about $\zeta \approx 0.275$ and the minimum has shifted to $\zeta \approx 0$ at 920°C. The fact that the ratio is monotonically increasing at these two temperatures for $\zeta > 0.3$ suggests that the anomaly may still be observable although weakly at 920°C

but we lack enough experimental information in the region $\zeta \geq 0.3$ to allow a meaningful quantitative conclusion. It seems that the structure of the T_1 branch continuously weakens with temperature as a result of the softening of the low energy phonons ($\zeta < 0.2$) and of the increased width of the anomaly, which probably reflects the less sharply delineated Fermi surface at high temperature.

Fig. V-4 shows the dispersion relation and the phonon linewidths in the case of the two transverse branches as obtained from the energy gain measurements in the range $0.0 \leq \zeta \leq 0.4$. We mentioned before (section V-C) that the $\zeta = 0.4$ phonons were at the practical limits of the spectrometer used, indeed requiring some three days of counting to accumulate about 100 events, in the peak, above the background. Although the linewidth of such difficult phonons can only be measured poorly (see below), their phonon frequencies were determined with reasonable accuracy. Fig. V-4 illustrates the nearly perfect linear behaviour of the $[00\zeta]T$ branch in the range $0 \leq \zeta \leq 0.4$ both at 22°C and 920°C. In the case of the T_1 branch, the high temperature dispersion relation, in the same wavevector range as above, is more linear than at 22°C although there is an indication of an upward curvature at $\zeta \approx 0.4$ possibly hinting that the anomaly is still observable at 920°C.

F - INELASTIC SCATTERING RESULTS: PHONON LINEWIDTHS IN Pd

Measurements of linewidths in neutron scattering require particular care for the results to be meaningful. In this series of measurements, we have applied the procedure outlined

in section II-I on the neutron groups of the two transverse branches in order to determine their true experimental and intrinsic linewidths. The intrinsic linewidth was obtained from a deconvolution of the experimental and theoretical linewidths (i.e. resolution) assuming gaussian lineshapes throughout. This procedure is only valid in the case where the intrinsic linewidth is larger than the resolution width [BU69]. Table V-2 shows that this is only satisfied for transverse phonons with $\zeta \geq 0.2$.

Let us consider in turn the $[00\zeta]T$ and $[0\zeta\zeta]T_1$ branches for which constant-$\underset{\sim}{Q}$ data are available at three wavevectors (ζ = 0.2, 0.3, 0.4) and two temperatures. Fig. V-4 shows the wavevector dependence of the linewidth for these branches at the two temperatures. Miiller's measurements [MI75] along the $[00\zeta]T$ direction indicated that, within an experimental resolution which was rather worse than ours, this branch does not undergo any broadening at 120K except near the zone boundary. In our case, the intrinsic linewidth is definitely non-zero at 22°C even at ζ = 0.2 and increases with wavevector and temperature.

The T_1 branch shows a similar pattern. Miiller's data [MI75] allowed him to extract the linewidth of this branch at 8, 296 and 853K. His data for the intrinsic (i.e. resolution corrected) linewidth fall in the range 0.12 to 0.18 THz and are in rather good agreement with ours. Like in the case of the other transverse branch, the linewidth of the T_1 branch becomes quite strongly wavevector dependent at 920°C.

In the case of the small wavevector phonons ($\zeta < 0.2$) in the transverse as well as longitudinal branches, the resolution widths are comparable to the observed widths and, consequently, the simplified deconvolution procedure used above does not apply [BU69]. For these phonons, the numbers listed in table V-2, especially in the case of the longitudinal phonons, have a rather dubious significance. However, they were left as such in order to give a zeroth order approximation of the linewidth in this region. When the calculated linewidths are much smaller than the resolution linewidths, as in the case of the longitudinal branches, the numbers listed should really be understood as zero within the experimental uncertainty.

G - INELASTIC SCATTERING RESULTS: TEMPERATURE DEPENDENCE OF THE ZERO-SOUND ELASTIC CONSTANTS OF Pd

The first-sound elastic constants of Pd were measured by Rayne [RA60] over a temperature range of 4.2 K to 300 K using standard ultrasonic techniques (pulse frequency: 10 MHz; duration: 1 μsec; risetime: 0.1 μsec). His results show that while $(c_{11}-c_{12})/2$ decreases non-linearly as a function of temperature, c_{44} and $(c_{11}+c_{12}+2c_{44})/2$ actually go through minima respectively centered near 100 K and 200 K. Rayne assigns the effect to "the change with temperature of the contribution to the shear constants, resulting from the holes in the 4d band" [RA60].

More recently, there were two other determinations. Walker et al [WA70] have measured the elastic constants of monocrystalline alloys of Pd-Rh and Pd-Ag between 4.2 K and 300 K. Their results for pure Pd did not show any indication of the minimum

in $(c_{11}+c_{12}+2c_{44})/2$ reported by Rayne [RA60] although two different Pd crystals were used with identical results. No possible explanations are provided for this difference.

Finally, Weinmann et al [WE74] recently published the result of their ultrasonic (at 10 MHz) and bulk modulus measurements on Pd. Temperature was varied between 295 K to 850 K while pressure could be increased up to 7000 kg/cm^2 in order to separate the electronic and lattice contributions to the elastic constants. The experimentally measured quantities were $(c_{11}-c_{12})/2$, c_{44} and the compressibility $(c_{11}+2c_{12})/3$ with a quoted overall (relative) accuracy of 0.5% (0.01%). The first two of the above measured quantities join well with the data of Rayne [RA60]. However, the quantity $(c_{11}+c_{12}+2c_{44})/2$, calculated from the experimental data does not match with the same quantity measured by Rayne [RA60]; both the magnitude and the temperature derivative are discontinuous (see fig. V-6). On the other hand, the data of Walker et al [WA70] and Weinmann et al [WE74] seem to be mutually consistent; quantitative conclusions cannot be drawn, however, since no table of experimental values is provided in either reference.

Since this last reference was only published recently, i.e. after completion of our Pd experiment, we were unable to elucidate this discrepancy. To do so would have required measurements at intermediate temperatures, possibly at 400°C and 700°C, like in the experiment on Cu, in addition to the data that we now have.

The zero-sound elastic constants of Pd (obtained from this work) were determined using the phonon data from table V-2 and following the same procedure as for Cu (see sections II-D and IV-H). The first step involves finding the intrinsic value of

$$\lim_{\zeta \to 0} (|\nu/\zeta|)$$

for all the branches studied ([00ζ]T&L and [0ζζ]T_1&L). Hence, in figure V-5, the ratios $|\nu/\zeta|$ have been plotted for the various wavevectors and temperatures. Since the resolution corrections are small in the case of the transverse phonons, these ratios are not qualitatively different, whether or not the resolution corrections are considered. They are quantitatively different, however; the inclusion of these corrections introduce shifts to values lower by by at most 1.6% for the [00ζ]T branch and 7.2% for the [0ζζ]T_1 branch. As far as the longitudinal phonons are concerned, the two cases are both qualitatively and quantitatively different; for this reason, they were both represented in figure V-5, particularly in order to illustrate the apparent divergence at $\zeta \to 0$ for the uncorrected data.

The $|\nu/\zeta|$ plots for the transverse branches were drawn in a symmetrical manner on each side of the vertical axis. This is as expected "a priori" if there are no systematic errors (e.g. crystal misalignment) and if the resolution correction procedure is valid. Both at 22°C and at 920°C, the plotted ratios show a well-behaved distribution. The 1050°C data, being rather sketchy as a result of the technical difficulties encountered (see section V-C), were sufficient, just the same, to determine the vertical intercepts

by extrapolating parallel to the best fit for the 920°C ratios. It should be noted that, in the case of the T_1 branch, the vertical intercepts at 920°C and 1050°C cannot be resolved and were assumed to be equal in the calculation for the elastic constants.

In the case of the two longitudinal branches, the resolution corrected ratios are not wavevector independent and indicate the existence of negative dispersion, even at such small wavevectors (see p. 121). The distribution of these ratio points does not make it possible to draw a family of nearly parallel curves (for all three temperatures) which intercept the vertical axis with a zero slope. This lack of mirror symmetry around the vertical axis could be the result of the uncertainty on the value of the lattice parameter (at all temperatures) or of a remnant of resolution distortion in the corrected data.

Using Miiller's AFC's [MI71] for either 296 K or 853 K, the expected behaviour of the ratio $|\nu/\zeta|$ at small wavevectors can be calculated; in particular, the calculated ratios for both longitudinal branches show the observed negative dispersion and the best fits (in figure V-5) were drawn with the same curvature as for the calculated ratios. The vertical intercepts thus determined are not significantly different from the values obtained if the corrected ratios are fitted to straight lines (horizontal or inclined).

Once the limits at $\zeta \to 0$ of the $|\nu/\zeta|$ ratios are known, the elastic constants can be determined following the procedure already outlined (section II-D). The initial slopes of the $[00\zeta]T\&L$ and $[0\zeta\zeta]T_1\&L$ branches are simply proportional to the c_{44}, c_{11}, $(c_{11}-c_{12})/2$ and $(c_{11}+c_{12}+2c_{44})/2$ elastic constants respectively.

A least-squares fit to these four initial slopes with various weighting factors for each of these branches produced significantly the same results. The elastic constant c_{12}, which cannot be determined directly from any one individual slope, was obtained from the least-squares fit; all of these results are listed in table V-1-e and plotted in figure V-6.

At room temperature, we obtain excellent agreement with the ultrasonic data, thus indicating that the first- and zero-sound elastic constants are equal, within experimental uncertainties. Overall agreement with the ultrasonic data of Rayne [RA60] is remarkable but our absolute uncertainties do not exclude agreement with the work of Weinmann et al [WE74]. This point could be clarified by further measurements at intermediate temperatures.

The uncertainties assigned to the zero-sound elastic constants are absolute quantities which reflect the uncertainties on the determination of the initial slopes, i.e. the vertical intercepts in figure V-5. These absolute uncertainties are a function of the error bars on the individual $|\nu/\zeta|$ ratio points and were assigned values of ±0.1 THz and ±0.25 THz for the transverse and longitudinal branches respectively.

However, once a rule has been set (e.g. from the behaviour of the $|\nu/\zeta|$ ratio calculated from the AFC's) to join the ratio points, the relative shifts of a few selected points as a function of temperature can be used to estimate the relative shifts of the vertical intercepts. This was done in the case of the 1050°C data which is far from complete, having been obtained mostly by neutron energy gain. It seems reasonable to assign to these relative

estimates an uncertainty which is 1/4 of the absolute ones. Thus, the relative uncertainties on the temperature dependence of the elastic constants are proportionately reduced from the absolute ones shown in table V-1-e and figure V-6.

The conclusions reached in this chapter largely depend on the validity of the resolution correction procedure which was adopted. Representative neutron groups from two different branches measured at 22°C and 920°C as well as the lineshapes calculated using the 580°C AFC's obtained by Miiller et al [MI71] are shown in figure V-7. No lineshapes for 1050°C ($T/T_m \simeq 0.725$) are included since they are not significantly different from those observed at 920°C ($T/T_m \simeq 0.654$). It should be noted that these two branches were best measured by constant-$\underline{Q}$ scans in the case of the $[0\zeta\zeta]T_1$ branch and by constant-E scans in the case of the $[00\zeta]L$ branch. The former is an example of "easy" phonons in terms of scattered intensities, while the latter is an example of "difficult" measurements.

Table V-1. Some physical parameters of Pd.

a) General constants.

Atomic number	Z	46	[H2]
Atomic mass (a.m.u.)	A	106.4	[H2]
Crystalline structure		F.C.C.	[H3]
Melting temperature	T_m	1552°C	[H5]
Debye temperature at 0 K (from calorimetric data)	θ_D	274±3K	[HO57]

Cross-section (in 10^{-24} cm^2) for thermal neutrons

-absorption	σ_a	8.0±1.5	[H7]
-coherent scattering	σ_c	5.0±0.3	[H7]
-incoherent scattering	σ_i	< 0.4	[H7]

b) Lattice parameter (room temperature values).

X-Rays	18°C	3.8902 A ±.0003 A	[H1,H2]
	22°C	3.8908 A	[CO56]
	23°C	3.8902 A	[SC72]
	25°C	3.8899 A	[DU63]
(by D.H. Dutton) neutrons	23°C	3.8904 A	[MI71]

c) Temperature dependence of the lattice parameter (this work).

Standard reference value:	22°C	3.8903 A	
	920°C	3.9384 A	± 0.0023 A
	1050°C	3.9465 A	± 0.0023 A

d) Elastic constants (27°C data from ultrasonic measurements [RA60]).

(units: 10^{12} dynes/cm^2)

$(c_{11}-c_{12})/2$	0.2553	± 0.0005
c_{44}	0.7173	± 0.0030
$(c_{11}+c_{12}+2c_{44})/2$	2.733	± 0.023

e) Temperature dependence of the elastic constants (this work).

(units: 10^{12} dynes/cm^2)		22°C	920°C	1050°C
$(c_{11}-c_{12})/2$	(±0.009)	0.2565	0.2136	0.2132
c_{44}	(±0.022)	0.706	0.640	0.614
c_{11}	(±0.100)	2.278	1.959	1.862
$(c_{11}+c_{12}+2c_{44})/2$	(±0.079)	2.727	2.392	2.286
c_{12}	(±0.115)	1.76	1.53	1.45

Table V-2. Palladium data [page 1 of 2].

[00ζ]T branch measured at $aQ/2\pi = (2,\zeta,0)$

ϑ	ζ_x	$2\Gamma_{\zeta x}$	$\Delta\zeta$	C_ζ	ζ	$C_{2\Gamma\zeta}$	$2\Gamma_\zeta$	Constant-E
.6530	.1025	.028	.003	.000688	.1032	.022	.017	
.5340	.0865	.025	.003	.000720	.0872	.023	.010	
.4070	.0641	.026	.003	.001065	.0652	.025	.007	
-.4100	-.0703	.030	.003	-.000651	-.0710	.026	.015	22°C
-.5280	-.0848	.029	.003	-.000249	-.0850	.024	.016	
-.6520	-.1036	.025	.003	-.000325	-.1039	.022	.012	
-1.0000	-.1582	.028	.003	-.000341	-.1585	.021	.019	
.6530	.1078	.029	.003	.000688	.1085	.022	.019	
.5340	.0875	.026	.003	.000720	.0882	.023	.012	
.4070	.0658	.027	.003	.001065	.0669	.025	.010	
-.4100	-.0690	.027	.003	-.000651	-.0697	.026	.007	920°C
-.5280	-.0885	.026	.003	-.000249	-.0887	.024	.010	
-.6520	-.1098	.025	.003	-.000325	-.1101	.022	.012	
-1.0000	-.1678	.029	.003	-.000341	-.1681	.021	.020	
-.4100	-.0703	.030	.003	-.000651	-.0710	.026	.015	
-.5280	-.0902	.032	.004	-.000249	-.0904	.024	.021	
-.6520	-.1120	.026	.003	-.000325	-.1123	.022	.014	1050°C
-1.0000	-.1728	.030	.003	-.000341	-.1731	.021	.021	
ξ	ν_x	$2\Gamma_{\nu x}$	$\Delta\nu$	C_ν	ν	$C_{2\Gamma\nu}$	$2\Gamma_\nu$	Constant-Q
-.2000	-1.2380	.180	.020	-.002000	-1.2400	.128	.127	
-.3000	-1.9050	.200	.020	.001000	-1.9040	.106	.170	22°C
-.4000	-2.5600		.030	.001000	-2.5590			
-.2000	-1.1700	.170	.020	-.002000	-1.1720	.128	.112	
-.3000	-1.7580	.260	.030	.001000	-1.7570	.106	.237	920°C
-.4000	-2.3250	.400	.040	.001000	-2.3240	.084	.391	

[00ζ]L branch measured at $aQ/2\pi = (2+\zeta,0,0)$

ϑ	ζ_x	$2\Gamma_{\zeta x}$	$\Delta\zeta$	C_ζ	ζ	$C_{2\Gamma\zeta}$	$2\Gamma_\zeta$	Constant-E
.7100	-.0542	.028	.003	-.006318	-.0605	.024	.014	
.4720	-.0350	.018	.002	-.006482	-.0415	.021	0.000	
-.4800	.0360	.025	.003	.008140	.0441	.021	.014	22°C
-.7030	.0570	.021	.003	.008151	.0652	.025	0.000	
.9460	-.0832	.029	.003	-.005394	-.0886	.023	.018	
.7100	-.0602	.020	.002	-.006318	-.0665	.024	0.000	
.4720	-.0355	.020	.002	-.006482	-.0420	.021	0.000	
-.4800	.0395	.024	.003	.008140	.0476	.021	.012	920°C
-.7030	.0610	.028	.003	.008151	.0692	.025	.013	
-.9440	.0850	.025	.003	.007202	.0922	.023	.010	
-1.1450	.1041	.022	.003	.006860	.1110	.023	0.000	
-.4800	.0405	.019	.002	.008140	.0486	.021	0.000	
-.7030	.0625	.025	.003	.008151	.0707	.025	0.000	
-.9440	.0845	.028	.003	.007202	.0917	.023	.016	1050°C
-1.1450	.1072	.025	.003	.006860	.1141	.023	.010	

N.B.: Experimental details in table IV-2, under column Ⓐ.
Definition of symbols in table I-1.

[0ζζ]T_1 branch measured at aQ/2 = (2+ζ,2−ζ,0)

ζ	ν_x	$2\Gamma_{\nu x}$	Δν	C_ν	ν	$C_{2\Gamma\nu}$	$2\Gamma_\nu$	Constant-Q
−.2000	1.0120		.020	−.009000	1.0030	.064		
−.1500	.7900		.020	−.011400	.7786	.072		
−.1000	.5360	.110	.020	−.016300	.5217	.080	.075	
−.0750	.4075	.090	.010	−.020900	.3866	.084	.032	
.0750	−.4260		.020	.026100	−.3999	.104		
.1000	−.5540	.110	.020	.022300	−.5317	.100	.046	22°C
.1500	−.8180	.170	.020	.018250	−.7998	.102	.136	
.2000	−1.0400	.180	.020	.015000	−1.0250	.104	.147	
.2500	−1.2550	.155	.020	.012250	−1.2428	.109	.110	
.3000	−1.4970	.200	.020	.010000	−1.4870	.114	.164	
.4000	−2.1400		.050	.006000	−2.1340	.114		
−.2000	.9680	.190	.020	−.009000	.9590	.064	.179	
−.1500	.7350	.140	.020	−.011400	.7236	.072	.120	
−.1000	.5050	.110	.020	−.016300	.4887	.080	.075	
−.0750	.3810	.110	.020	−.020900	.3601	.084	.071	
.0750	−.4000		.020	.026100	−.3739	.104		
.1000	−.5180	.140	.020	.022300	−.4957	.100	.098	920°C
.1500	−.7650	.140	.020	.018250	−.7468	.102	.096	
.2000	−1.0180	.220	.030	.015000	−1.0030	.104	.194	
.2500	−1.2660	.210	.030	.012250	−1.2538	.109	.179	
.3000	−1.5210	.310	.040	.010000	−1.5110	.114	.288	
.4000	−2.1120	.340	.040	.006000	−2.1060	.114	.320	
.0750	−.3900		.020	.026100	−.3639	.104		
.1000	−.5200	.160	.020	.022300	−.4977	.100	.125	1050°C
.1500	−.7700	.180	.020	.018250	−.7518	.102	.148	
.2000	−1.0180	.220	.030	.015000	−1.0030	.104	.194	

[0ζζ]L branch measured at aQ/2 = (2+ζ,2+ζ,0)

ζ	ζ_x	$2\Gamma_{\zeta x}$	Δζ	C_ζ	ζ	$C_{2\Gamma\zeta}$	$2\Gamma_\zeta$	Constant-E
.9820	−.0530	.015	.002	−.002996	−.0560	.017	0.000	
.6530	−.0335	.016	.002	−.003408	−.0369	.017	0.000	
−.6520	.0380	.020	.002	.003347	.0413	.018	.009	22°C
−.9720	.0545	.019	.002	.003584	.0581	.016	.010	
−1.2980	.0752	.015	.002	.003150	.0784	.016	0.000	
1.3060	−.0790	.017	.002	−.002445	−.0814	.017	0.000	
.9820	−.0565	.018	.002	−.002996	−.0595	.017	.006	
.6530	−.0352	.019	.002	−.003408	−.0386	.017	.008	
−.6520	.0388	.019	.002	.003347	.0421	.018	.006	920°C
−.9720	.0586	.013	.002	.003584	.0622	.016	0.000	
−1.2980	.0795	.015	.002	.003150	.0827	.016	0.000	
−1.6260	.1014	.012	.002	.002765	.1042	.015	0.000	
1.3060	−.0800	.020	.002	−.002445	−.0824	.017	.011	
−.6520	.0390	.019	.002	.003347	.0423	.018	.006	
−.9720	.0590	.018	.002	.003584	.0626	.016	.008	1050°C
−1.2980	.0810	.018	.002	.003150	.0842	.016	.008	
−1.6260	.1030	.015	.002	.002765	.1058	.015	0.000	

Fig. V-1. Envelopes of families of ψ-rocking scans for the Pd specimen at three temperatures.

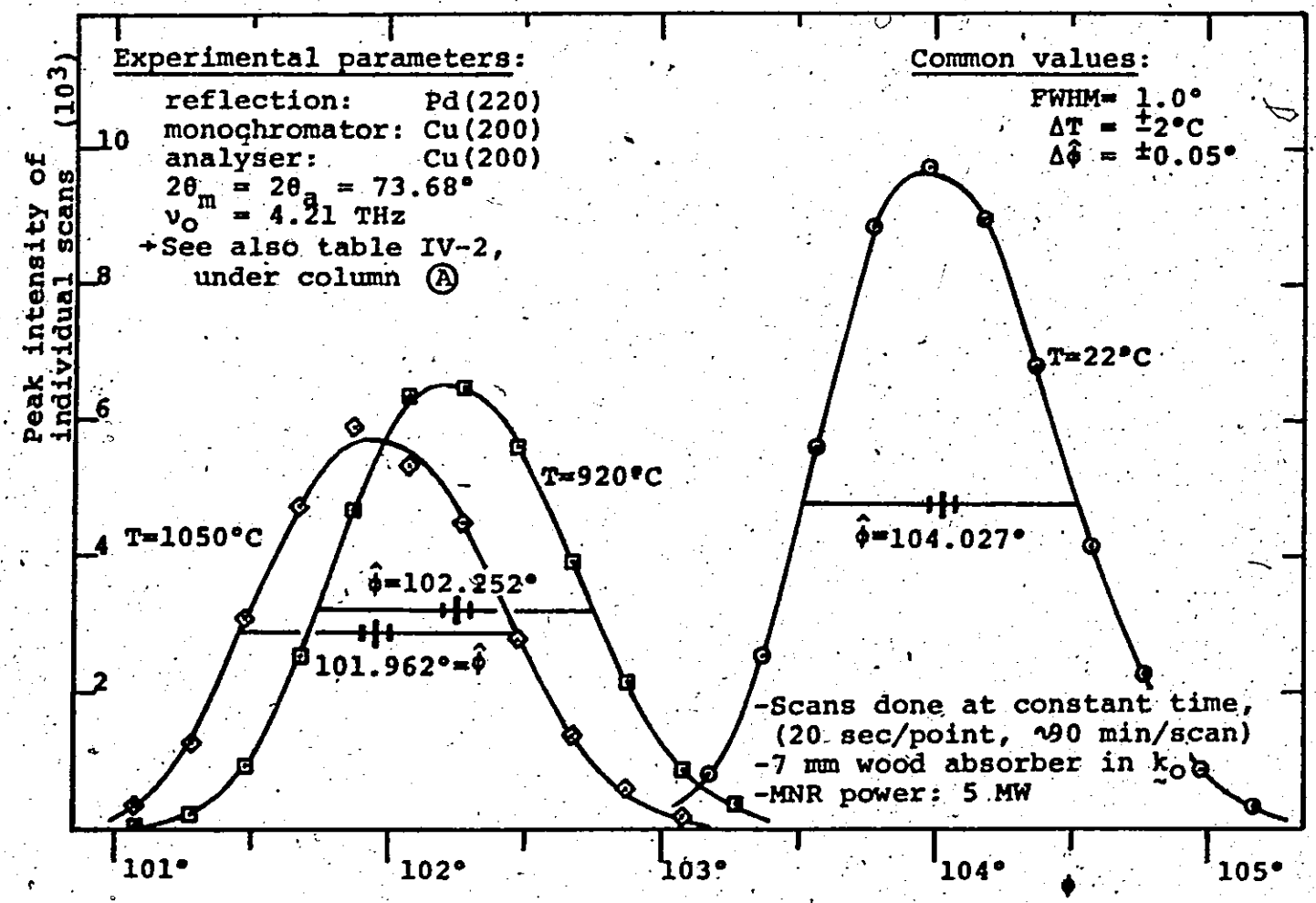

Figure V-2.

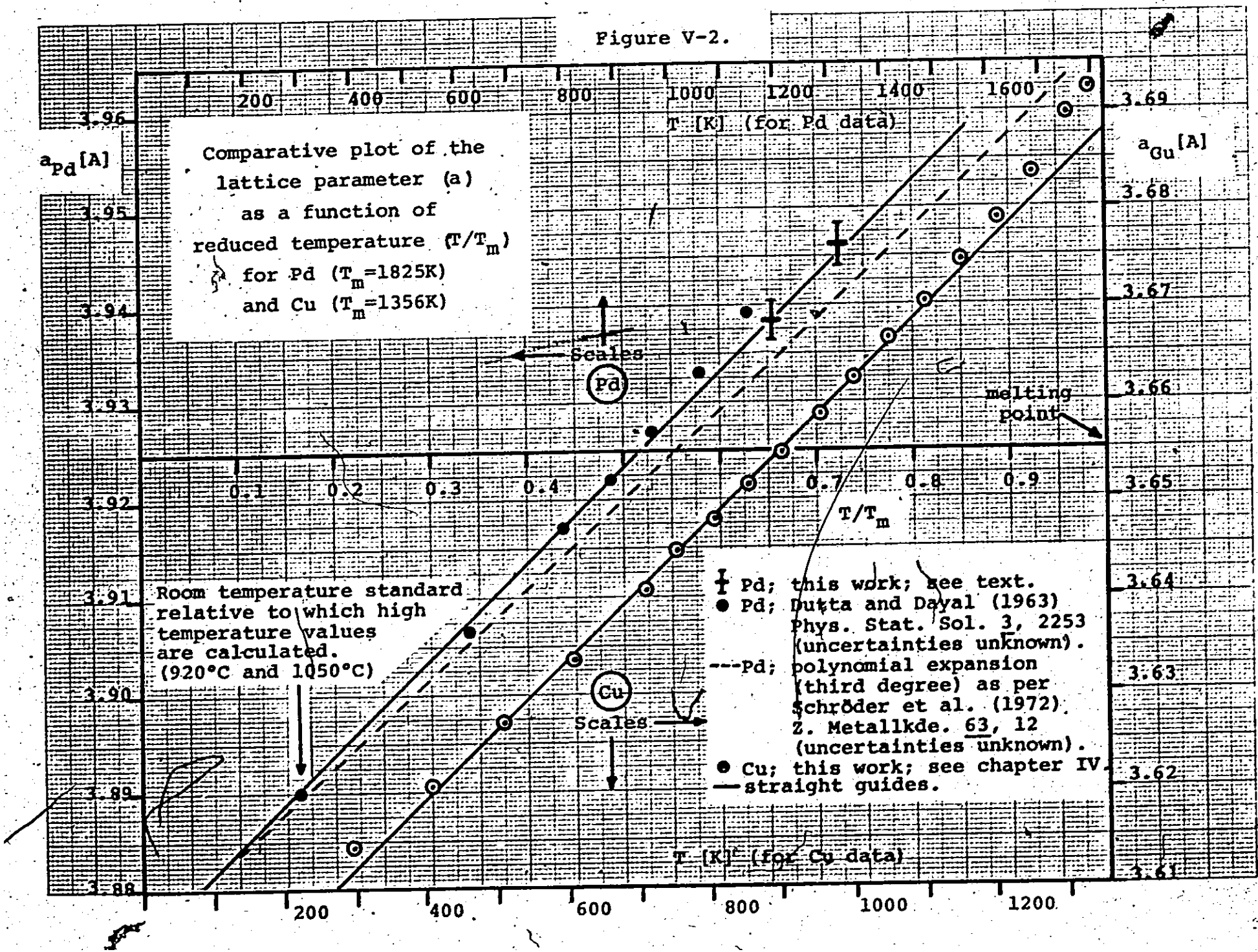
Comparative plot of the lattice parameter (a) as a function of reduced temperature (T/T_m) for Pd (T_m=1825K) and Cu (T_m=1356K)
a_{Pd}[A]
a_{Cu}[A]
T [K] (for Pd data)
T [K] (for Cu data)
T/T_m
melting point
Scales
Pd
Cu
Scales
Room temperature standard relative to which high temperature values are calculated. (920°C and 1050°C)
Pd; this work; see text.
Pd; Dutta and Dayal (1963) Phys. Stat. Sol. 3, 2253 (uncertainties unknown).
Pd; polynomial expansion (third degree) as per Schröder et al. (1972) Z. Metallkde. 63, 12 (uncertainties unknown).
Cu; this work; see chapter IV.
straight guides.

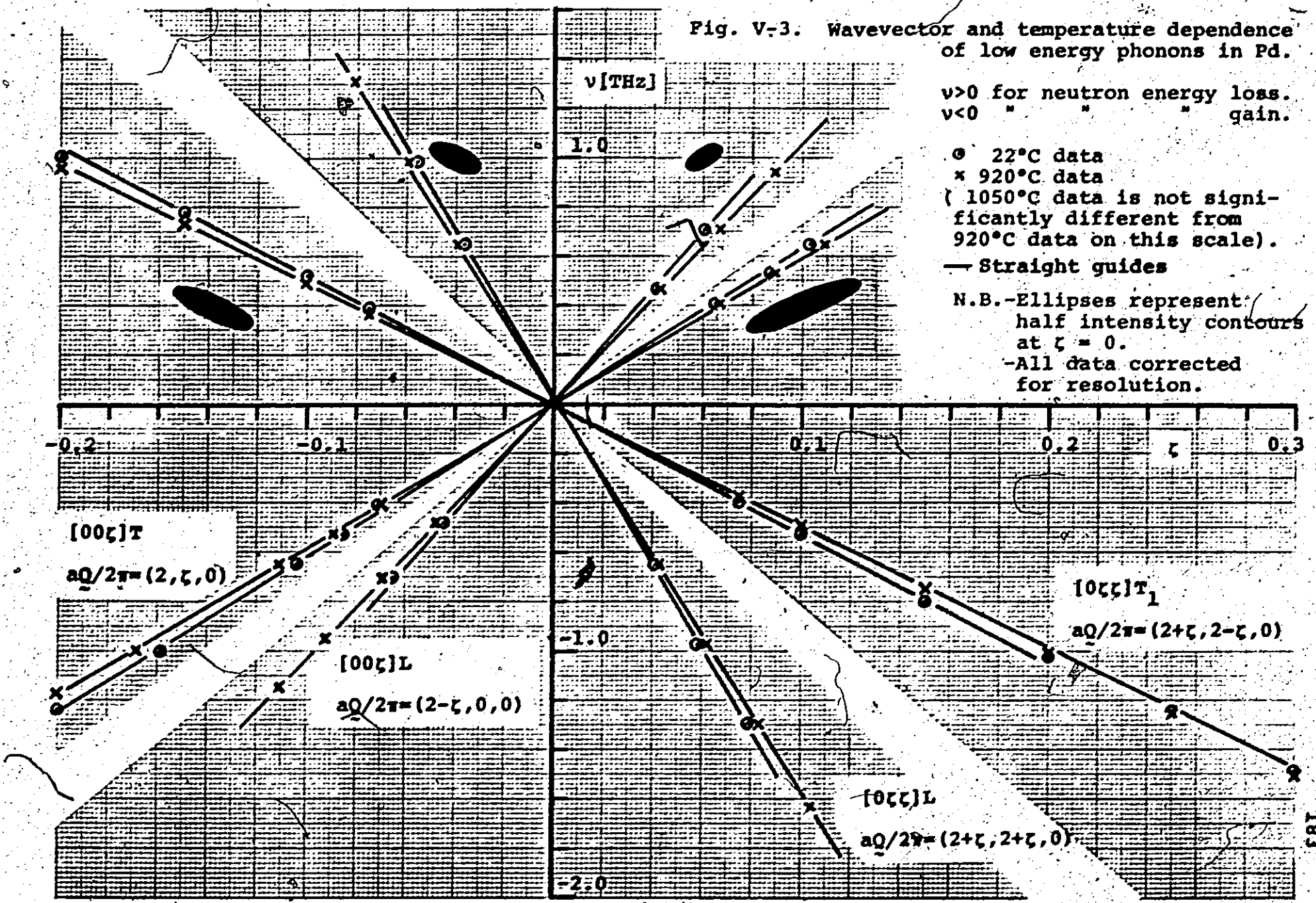

Fig. V-3. Wavevector and temperature dependence of low energy phonons in Pd.

ν>0 for neutron energy loss.
ν<0 " " " gain.

● 22°C data
× 920°C data
(1050°C data is not significantly different from 920°C data on this scale).
— Straight guides

N.B.-Ellipses represent half intensity contours at ζ = 0.
-All data corrected for resolution.

Fig. V-4. Transverse phonons in Pd: intrinsic eigenvalues (ν [THz]) and linewidths ($2\Gamma_\nu$ [THz]) at 22°C and 920°C.

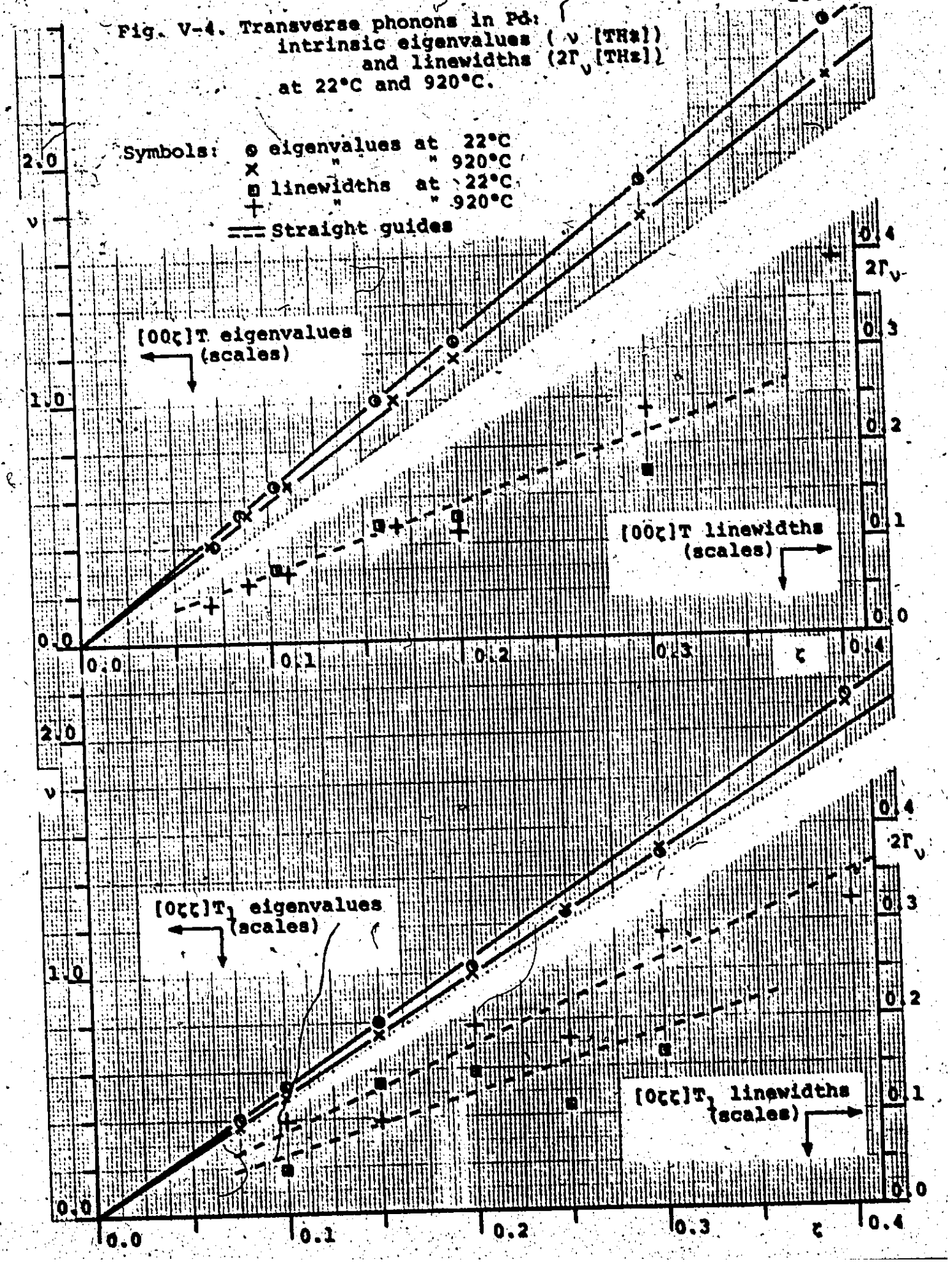

Fig. V-5. Wavevector and temperature dependence of the ratio $|\nu/\zeta|$ for low energy phonons in Pd using resolution corrected data except where indicated.

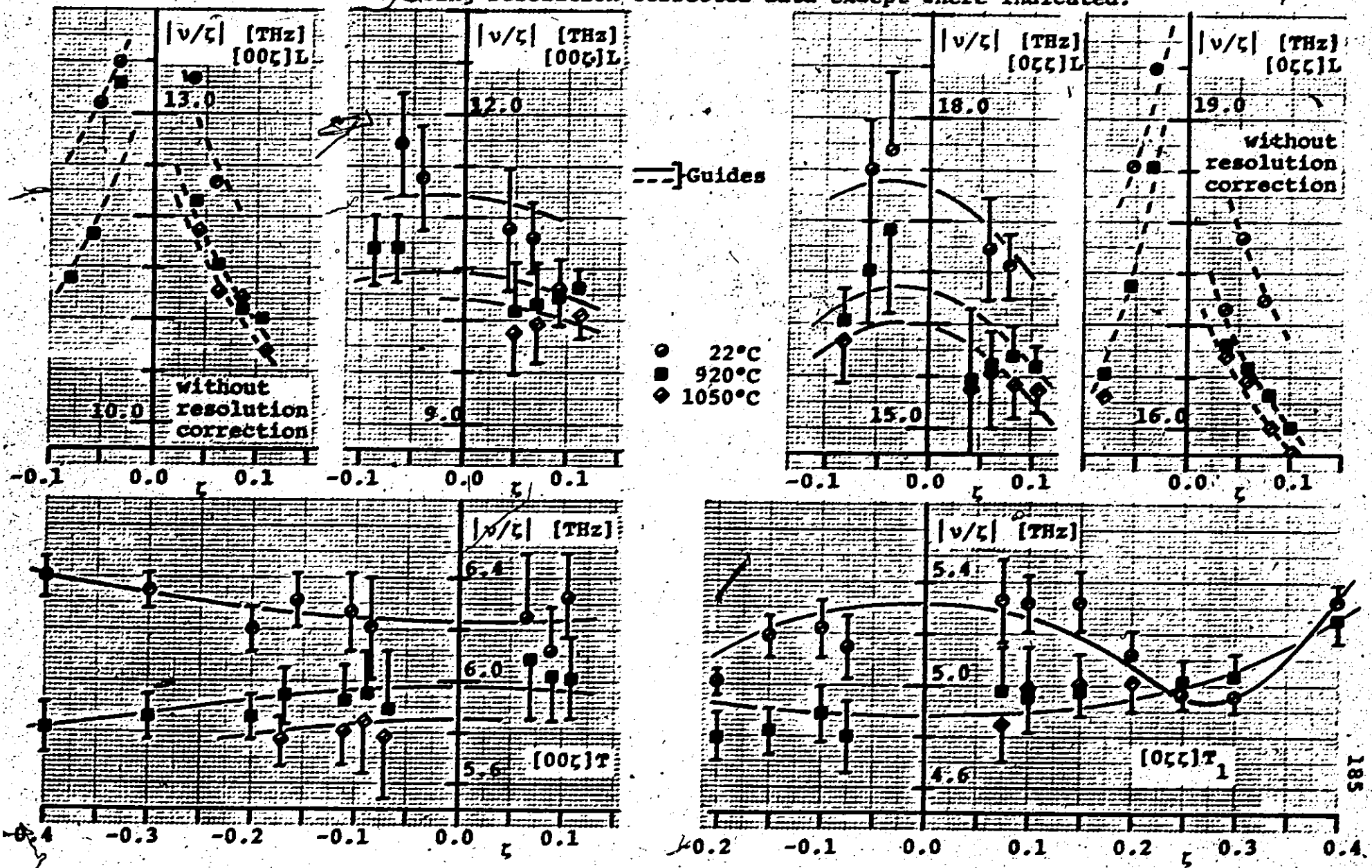

Fig. V-6. Temperature dependence of the elastic constants of Pd in units of 10^{12} dynes/cm^2. (page 1 of 2)

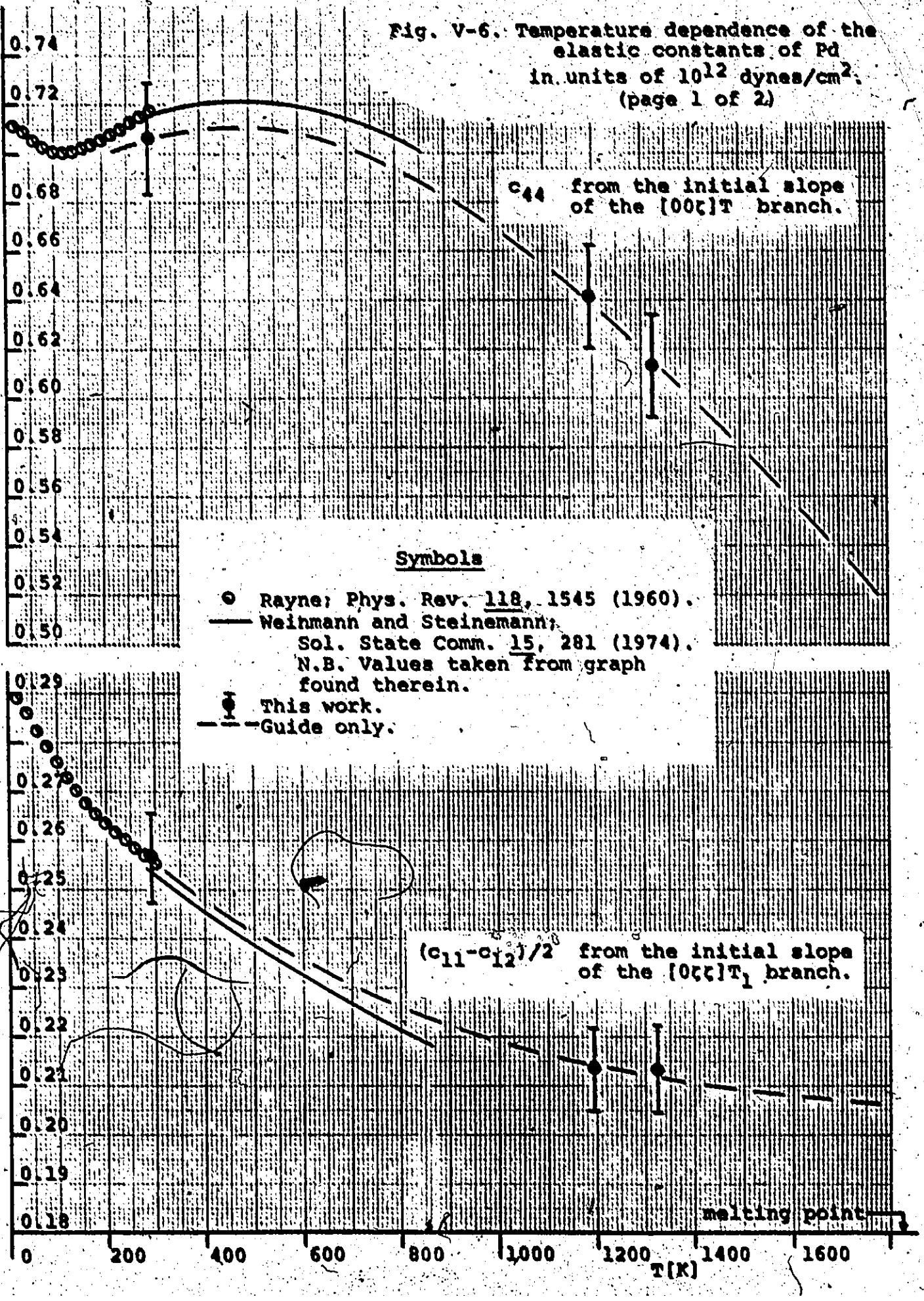

Temperature dependence of the elastic constants of Pd in units of 10^{12} dynes/cm^2. (page 2 of 2)

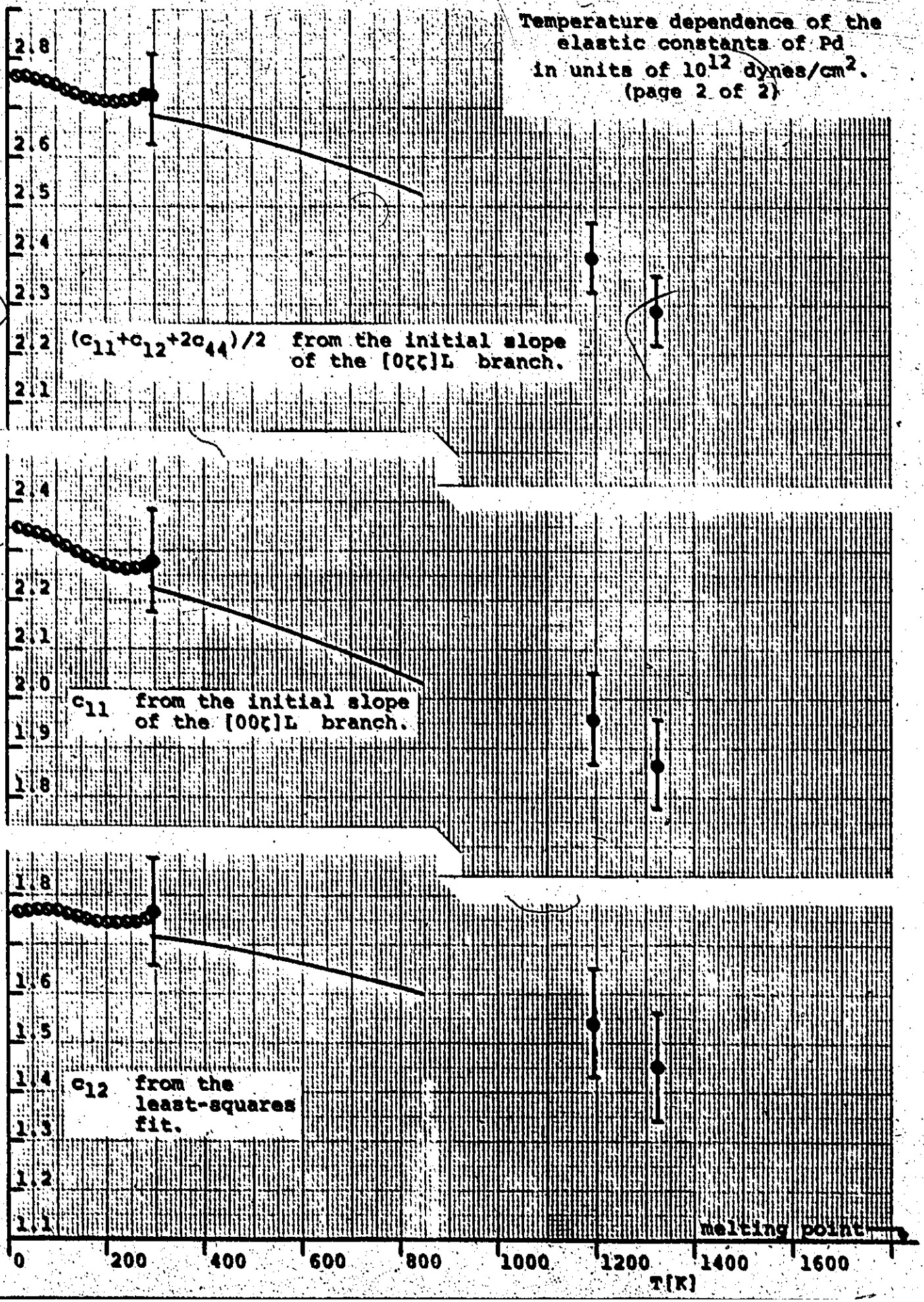

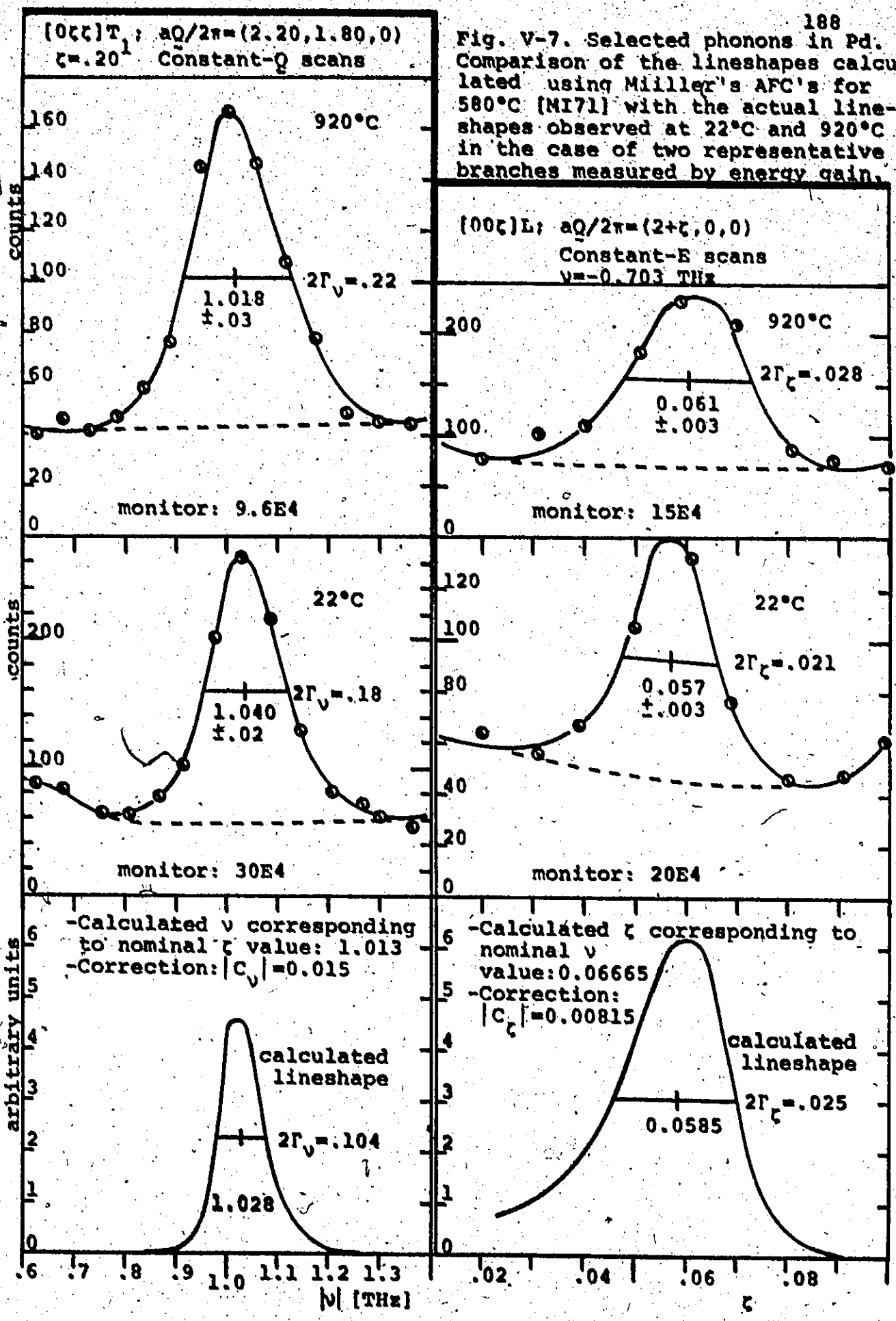

Fig. V-7. Selected phonons in Pd. Comparison of the lineshapes calculated using Miiller's AFC's for 580°C [MI71] with the actual lineshapes observed at 22°C and 920°C in the case of two representative branches measured by energy gain.

CHAPTER VI

TUNGSTEN: PHONON SPECTRUM AT 22°C

A - INTRODUCTION

Tungsten is a transition metal of the 5d series and of the same group VI ($5d^4 6s^2$) of elements as chromium and molybdenum. These three elements crystallize in a BCC structure with one atom per unit cell; their Fermi surfaces are believed to be similar [LO62; LO64; LO65]. The phonon spectra for the three metals have been previously studied [MO64 and SH71; WO64 and PO68; CH64 and CH64A] and, not surprisingly, display common features. Recently however, there was a suggestion that a Kohn effect might be observable in tungsten near the H-point [RI70]. This prediction could not be confirmed using the then available data partly because of the relatively coarse spacing of the experimental points in the region of interest [CH64A]. The experiment whose results are reported herein was attempted in order to investigate this prediction; we have also used this opportunity to improve on the density of experimentally determined phonon frequencies and to verify the published data.

The measurements were made by neutron scattering using triple-axis spectrometry and the specimen was the same one as used by Chen [CH64;CH64A] except for a minor modification discussed below.

Although the expected effect sits in a frequency range conveniently accessible by neutron spectroscopy, the experiment was complicated by the unfavourable neutron properties of tungsten itself (table VI-1). For this reason, as well as because of the limitations resulting from the neutron flux available, we have not been able to resolve unambiguously the predicted structure in the phonon spectrum.

B - THEORY

Before proceeding to the experimental results, it may be appropriate to review some known facts about tungsten. From ultrasonic data [FE63], this metal is known to be remarkably isotropic (within 1%); this behaviour is not confined to the long wavelength phonon domain as shown, for example, by the near-degeneracy of the T_1 and T_2 branches all the way to the zone boundary; see fig. 2. Chen and Brockhouse [CH64] found that a third-neighbour central force model provided a satisfactory representation of the general features of their experimentally determined dispersion curves. Upon consideration of more distant neighbours, the goodness of fit improved only marginally except, perhaps, in going from the 6th to 7th neighbour models. Even then, however, they were unable to fit the structure of the T_2 branch near the zone boundary; this, in itself, reflects the importance of long range forces (extending possibly up to and beyond the 12th neighbours) in tungsten.

Although the basic mechanism responsible for a Kohn "anomaly" is well known [KO59; WO62; TA63; RO66], it is not a

trivial problem to calculate "a priori" its magnitude; however, its position in reciprocal space can be estimated in a straightforward manner once the Fermi surface is well known. In the case of tungsten, the work of Girvan, Gold and Phillips [GI68] has provided high-quality de Haas-van Alphen data from which a parameterized model of the Fermi surface was obtained; this was used by Rice and Halperin [RI70] in their calculation of possible Kohn effects. Their results indicate the existence of a closely spaced group of ordinary and cusp-type "anomalies" near the H point along the ΓH direction of the Brillouin zone. Several approximations were made, however, in their calculations and the dependence of the phonon frequencies on electronic polarizability was written as a function of two adjustable parameters. These parameters were fitted to the then available data of Chen and Brockhouse [CH64] in the reciprocal space region of interest, using three experimental phonon frequencies of the [00ζ]L branch at $\zeta = 0.8$, 0.9 and 1.0.

With these parameters, Rice and Halperin [RI70] were able to predict a Kohn type structure in the [00ζ]L branch near the H-point; more precisely, the interesting feature turned out to be at $\zeta \approx 0.92$ and could not be experimentally substantiated by the three experimental values then available.

The predicted structure is indeed a very small effect, even at low temperatures. The depression in the dispersion curve is $\approx$ 0.2 THz over a region $\approx 0.02\ (\frac{2\pi}{a})$ wide along the ΓH direction.

In order to resolve it unambiguously, a resolution in energy and wavevector equal to at least one half the expected magnitude of the effect is required. This is a stringent requirement by usual standards in neutron spectroscopy and here the difficulties were compounded by the unfavorable neutron properties of tungsten.

C - SPECIMEN AND APPARATUS

As can be seen from table VI-1, the thermal neutron properties of tungsten are far from ideal. The main difficulty arises mainly as a result of the high value for the absorption cross-section relative to the coherent scattering cross-section. For this reason, a compromise in the specimen geometry is required, i.e. one wants a geometry offering a small penetration depth in the scattering plane and a sufficient volume to provide as strong a (scattered) signal as possible. In this particular case, the specimen consisted of three cylinders each approximately 6 mm in diameter and 6 cm long. They initially came from a single long crystal which was cut in three parts of nearly equal lengths and they were mounted in-line, parallel to each other, and with a centre-to-centre spacing of approximately 15 mm. The cylindrical axis was within 5° of a (011) crystallographic axis, resulting in the cylinders being very nearly vertical for the configuration in which the (011) reciprocal lattice plane is parallel to the scattering plane.

The crystal holder arrangement used for the measurements was basically the same as the one used by Chen [CH64; CH64A],

except that he also had a fourth crystal mounted in-line with the others. However, this fourth crystal came from a different melt and also had a slightly double orientation resulting in a 10% secondary peak relative to the main reflections of the composite crystal. The removal of this component obviously worsened the signal-to-noise ratio, but this was done in order to have as perfect a crystal as possible for high resolution measurements.

The individual crystals were aligned to well within 0.1° on the double-axis spectrometer located at the McMaster University reactor [CH64A; BR68]. Horizontal and vertical alignments were performed in an iterative way, masking all but one crystal at a time, and using two reflections perpendicular to each other. After the desired relative alignment of the individual crystals had been achieved, the whole arrangement was epoxied together and installed on a crystal base which allowed easy adjustment of the composite crystal taken as a whole.

The full width at half height of the composite crystal was found to be of the order of 20', using Bragg-scattered neutrons of various incident energies and the same collimation arrangement as for the phonon measurements. The fact that the width was dependent on the degree of collimation used indicates that the observed width contains a large contribution from instrumental resolution. We believe that the mosaic spread of the specimen is less than 15'. It must be added, however, that the composite crystal also had a weak parasitic reflection, 1.1°

off the main ones. We have not attempted to isolate the origin of this reflection in the volume of the crystal on the grounds that its 3% contribution in intensity to the elastic peak would not appreciably affect the measurements of the phonons.

The phonon measurements proper were performed using the McMaster University spectrometer at the NRU reactor, Chalk River [BR68]. Before proceeding to the experimental results, we will briefly mention a major improvement made to the monochromator assembly by R. R. Dymond [DY70].

A new set of monochromator crystals was installed in the pile during the month of April 1971. The purpose of this change was the elimination of a contaminant reflection which had been adversely affecting the instrument since it was first put into use. The new monochromator, like the old one, uses a (220) reflection of two single crystals of copper mounted parallel to each other. Unfortunately, because of lowered reflectivity of the new monochromating crystals and because of tighter in-pile collimation, inserted in the hope of reducing the fast neutron and diffuse backgrounds, the incident intensity was decreased by a factor of about two in series II measurements (with the new monochromator/collimation arrangement) compared with those of series I (with the old arrangement). In measurements of the first series, the presence of the contaminant had restricted the range of accessible values of the energy transfer; unnecessarily large values of the fixed incident energy had to

be used resulting in less than optimum energy resolution. In series II measurements, the absence of the contaminant has allowed choosing instrumental variables from considerations of intensity and resolution rather than for avoidance of the contaminant.

All measurements were made at room temperature. Since the melting point of tungsten is so high (table VI-1), there is really not much to be gained by going to lower temperatures from the point of view of operating in the harmonic regime. However, the calculations of Rice [RI70] show a slightly more pronounced Kohn effect on the dispersion curve at 0 K as compared with room temperature, but this small improvement could not justify the added complexity of measurements at low temperatures.

The monochromator and analyser crystals were Cu(220) and Cu(200) respectively. The monochromator is permanently installed in the reactor shielding and cannot be changed easily; the particular choice of the analyser was made because it had the highest reflectivity of all our crystals and from considerations of resolution. The collimation values were variable (21' to 86'), with the incident beam horizontal collimation (α_1) and the analysed beam horizontal collimation (α_2) equal most of the time. However, in some few cases, resolution in momentum transfer was sacrificed in order to match the energy spread of the incident and analysed beam and consequently, gain in intensity. In this case, we had $\alpha_2 = 2\alpha_1$.

D - RESULTS

Measurements were made on phonons propagating in all symmetry directions including the $(\frac{1}{2},\frac{1}{2},\zeta)$ and $(\zeta,\zeta,1)$ directions. The specimen was maintained with the (011) plane in the scattering plane throughout and, for this reason, phonons of the $[0,\zeta,\zeta]T_1$ or $[\zeta,\zeta,1]\pi_1$ types were not measured. The scans were done in a standard way with a fixed E_o configuration in series I measurements while a fixed E' configuration was used for most of those in series II [BR60], both with neutron energy loss. The methods of constant-$\underline{Q}$ and constant-E were selected depending on the value of the energy $\underline{q}$-gradient of the phonon being measured [BR60]. Because of the experimental difficulties already mentioned, most of the scans were kept as narrow as possible, the data of Chen [CH64A] being used in order to minimize the counting time in the tail region of the lineshape.

The existence of focussing configurations in triple-axis spectrometry is well known [CO67; PE67; ST68]. In general, focussing is important in the measurement of phonons of transverse polarization because of the correlation between the resolution contour of the spectrometer in $(\underline{Q},\omega)$ space and the dispersion surface of such phonons at the positions in reciprocal space appropriate for their measurements. Such is not the case in the measurement of longitudinal phonons, usually performed radially away from reciprocal lattice points. However, it is possible to find an intermediate position whereby resolution effects improve the linewidth of longitudinal phonons while the integra-

ted intensity is relatively unaffected. As for transverse phonons, the idea is to achieve some correlation between the dispersion surface and the resolution of the spectrometer while maintaining the ratio $|\underline{Q}\cdot\underline{e}(\lambda)|/|\underline{Q}|$ as close to unity as possible ($\underline{e}(\lambda)$ is the polarization vector of the phonon under consideration; see eq.F6-1). This can be achieved by measuring longitudinal phonons in an intermediate position between a truly radial and a truly tangential position of the phonon wavevector relative to the nearest reciprocal lattice point. This method is applicable however, only if the transverse and longitudinal branches are well separated and if the phonon energy gradient is large; hence, it is not applicable to measurements near a reciprocal lattice point or near the zone boundary.

Fig.VI-1 shows the result of the measurements performed on a [00ζ]L phonon at various positions in reciprocal space. A radial position would correspond to the cases illustrated in "a", "e" and "g" for example. One sees that there is a significant improvement in the linewidth when this phonon is measured as in "b" or "c". Correspondingly, the same phonon is found to be defocussed when observed at position "f", while a measurement at the mirror image point "d" would have yielded a more focussed lineshape. In this figure, all phonons were observed under identical conditions except for the position in reciprocal space. For this reason, the statistics of the small momentum transfer phonons are poor, reflecting a smaller value of the cross-section as a result of its dependence on $|\underline{Q}|^2$ in equation (F6-1).

The same figure can also be used to illustrate the quality of the data. For example, phonons like in "a", "b" and "c" are considered to be well defined while a situation as depicted in "e" and "f" is judged to be of insufficient quality to be included in the table below (table VI-2). Phonons like "d" and "g" are considered to be of marginal quality; in the final analysis, they are given a very small weight and are used mostly as a check with other measurements of the same phonon. Table VI-2 and figure VI-2 both show our results along with those of Chen [CH64A]. Actually, the total number of phonons observed was considerably larger than those listed in table VI-2. Some were measured at several positions in reciprocal space; others were measured under various spectrometer calibrations. The values quoted are a weighted average of what were considered good data; scans of poor quality were not included.

Fig.VI-3 shows experimental lineshapes for phonons along the [00ζ]L branch in the region of the predicted Kohn effect. These measurements were performed with a fixed incident neutron energy of 11 THz using constant-Q scans. A lower value of energy with a corresponding improvement in resolution could not be used for this particular range of energy transfer because of the restrictions resulting from the contaminant in the incident beam; measurements of these same phonons were not attempted in series II because the loss in intensity resulting from the insertion of tighter in-pile collimation introduced when the new monochromator was installed made them impractical.

Using an old convention [SV67], the uncertainty on the peak positions is taken to be one tenth of the full width at half maximum. The resulting ν versus ζ relation in the reciprocal space region of interest, along with the position of the expected anomaly, is also shown. The resolution in momentum is of the order of $\Delta\zeta = \pm 0.007$ as determined by the Bragg peak scanning method of Møller [MO68;NI69] while the resolution in energy is about $\Delta\nu = \pm 0.08$ THz, as given by the magnitude of the error bars. Most of these phonons have been measured both at $aQ/2\pi = (0,0,2+\zeta)$ and $(0,0,4-\zeta)$; the peak positions are in very good agreement.

E - DISCUSSION

In comparing the smallness of the calculated effect with the experimental uncertainties on the phonon energies (see fig. VI-3), one can see that, at best, conditions are marginal for an unambiguous manifestation of a Kohn effect of such small magnitude. Indeed, while the experimental uncertainty in ζ is slightly less than the wavevector width of the calculated anomaly, the experimental uncertainty in ν, on the other hand, is comparable to the magnitude of the expected dip in frequency. However, the neutron groups near $\zeta = 0.92$ are reasonably well defined and there is not the least indication of a narrow local minimum in ν at such a wavevector with such an instrumental resolution.

Whereas the previously available data [CH64A] indicated a monotonically decreasing frequency along ΓH near H $(0.8 \leq \zeta \leq 1.0)$,

our data tends to show that the frequency is somewhat wave-vector independent in the range $0.9 \leq \zeta \leq 1.0$. The uncertainty in energy does not allow us to conclude unambiguously on the existence of a wide and shallow local minimum in this range, as the smooth curve joining the experimental points tends to indicate. In either case, i.e. whether the frequency has a local minimum or is flat in the range $0.9 \leq \zeta \leq 1.0$, this can be interpreted as a probable manifestation of the expected Kohn effect. Similar features on the same branch and also near H were found in Mo [WO64] and antiferromagnetic Cr [SH71]. If the "smeared-out" effect that we observe is really a Kohn effect, then the weakness of the perturbation on the dispersion curve illustrates the weak electron-phonon interaction which is known to exist in W whose superconductivity temperature is only 0.011 K [GI64]. Possibly, a more rigorous calculation than the one performed by Rice and Halperin [RI70] would have predicted the weak effect that was observed.

Instrumental resolution is expected to introduce a common correction on all the [00ζ]L phonons in this range of interest since all these scans were performed in the same general region of (Q,ω) space and were all centered on the same energy. Also, resolution corrections are expected to be small because of the fact that these phonons have a relatively large energy and a very small, if not zero, q-gradient. A quick resolution calculation using the formalism of Werner and Pynn [WE71] has verified this assertion; see section II-H.

It should be mentioned that the lineshape of the phonon measured at $\zeta = 0.98$ is not reliable, as fig. VI-3 shows. Both times, when measured at $aQ/2\pi = (0,0,2+\zeta)$ and $(0,0,4-\zeta)$, it showed an ill-defined neutron group which could be interpreted as somewhat double peaked. The zone boundary phonon itself has even a more pronounced double peaked structure when measured at $aQ/2\pi = (0,0,3)$. This cannot be caused by the spurious detection of the transverse branch, since both the transverse and longitudinal phonons are degenerate at the zone boundary. The possibility remains that it may be caused by a strong dependence of the phonon eigenvectors on the wavevector component out of the scattering plane [CO71]. However, at the zone boundary, the eigenvectors have a second order dependence on wavevectors out of the scattering plane and the calculated phonon lineshape, using the previously mentioned formalism [WE71], did not reproduce this effect. The present hypothesis is that the double peak is caused by a spurious reflection from the somewhat imperfect specimen (see section VI-C).

This interpretation is given some credibility by the fact that this same zone boundary phonon, when measured at various other positions in reciprocal space, showed no such double-peaked nature; in these cases, the peak values were in very good mutual agreement. For this reason, the phonon frequency of the zone boundary phonon shown in figure VI-3 was taken from a weighted average of the less ambiguous measurements of the same phonon performed elsewhere in reciprocal space.

The published values of the atomic force constants of tungsten [CH64] were verified using the data listed in table VI-2. The data of Chen [CH64A] and of this work were fitted, both separately and together; the resulting values are not significantly different from the published ones. The inclusion of the elastic constants [FE63] in the fit modified somewhat the values of the largest AFC's and this produced a minor improvement of the fit to the low energy data. Table VI-3 lists the resulting values for the AFC's.

Table VI-1. Some physical parameters of the Cr-group metals.

		Cr	Mo	W	
Atomic number	Z	24	42	74	[H2]
Atomic mass (in a.m.u.)	A	51.996	95.94	183.85	[H2]
Crystalline structure (at 20°C)		BCC	BCC	BCC	[H3]
Lattice parameter	a	2.8839A (25°C)	3.147A (21.5°C)	3.1652A (25°C)	[H4]
Melting temperature	T_m	1890°C	2610°C	3380°C	[H5]
Debye temperature at 0 K (from calorimetric data)	Θ_D	580K [CL62]	454K [CL59]	380K [CL59]	
Superconducting transition temp.	T_c	none see 2	0.92K [GE62]	0.011K [GI64]	
Cross-section (in $10^{-24}cm^2$) for thermal neutrons					
-absorption	σ_a	3.1	2.7	19.2	
-coherent scattering	σ_c	1.56	5.6	2.74	[H7]
-incoherent scattering	σ_i	2.54	0.5	2.96	
Elastic constants at 299±2 K (in 10^{12}dynes/cm^2)	c_{11}	3.500	4.4077	5.2327	
	c_{12}	0.678	1.7243	2.0453	
	c_{44}	1.008 [BO63]	1.2165 [FE63]	1.6072 [FE63]	
Isotropy ratio $2c_{44}/(c_{11}-c_{12})$		.7144	.9067	1.008	

Notes: 1- References are given by the code within brackets [].
2- Cr is not a superconductor since it is antiferromagnetic (its Néel temperature is 311 K).

Table VI-2. List of phonon frequencies [ν:THz] as a function of reduced wavevector [ζ] for tungsten at 22°C.

S.H.Chen; Ph.D. Thesis McMaster University				This Work				
ζ	Δζ	ν	Δν	ζ	Δζ	ν	Δν	[00ζ]T
.1100	.005	1.0000		.0460	.004	.4990		
.2000		1.8300	.030	.1040	.005	1.0040		
.2700	.005	2.5000		.1490	.003	1.3850		
.4000		3.5300	.030	.1945	.003	1.8340		
.6000		4.6000	.050	.2350	.003	2.1830		
.8000		5.2000	.100	.2780	.003	2.5750		
1.0000		5.5000	.100	.3440	.003	3.1120		
				.4020	.003	3.5440		
				.4220	.003	3.6970		
				.5000		4.1600	.040	
				.5500		4.4100	.050	
				.6000		4.5100	.050	
				.6500		4.7600	.030	
				.7000		4.9000	.060	
				.7500		5.0800	.060	
				.8000		5.1200	.050	
				.8500		5.2700	.080	
				.9000		5.0700	.100	
				.9500		5.3800	.050	
				1.0000		5.4700	.100	← Note (1)
ζ	Δζ	ν	Δν	ζ	Δζ	ν	Δν	[00ζ]L
.1250	.003	2.0000		.0255	.004	.4990		
.1900	.005	3.0000		.0615	.004	1.0040		
.2600	.010	4.0000		.0890	.003	1.5010		
.4200	.010	5.5000		.1200	.003	1.9980		
.5000		5.9500	.050	.1480	.003	2.4010		
.6000		6.2000	.020	.1805	.003	2.9970		
.7000		6.3000	.070	.2600	.004	3.9870		
.8000		5.9500	.100	.2620	.004	4.0120		
.9000		5.6500	.100	.2940	.002	4.3670		
1.0000		5.5000	.100	.3335	.004	4.8340		
				.3380	.003	4.8660		
				.3870	.005	5.2900		
				.4350	.006	5.6070		
				.5000		6.0500	.070	
				.6000		6.1500	.100	
				.8400		5.6700	.070	
				.8600		5.5800	.090	
				.8800		5.5100	.080	
				.9000		5.4800	.070	
				.9200		5.4300	.090	
				.9400		5.3900	.070	
				.9600		5.4100	.060	
				.9800		5.3100	.060	
				1.0000		5.4700	.100	

(1) Measured at [00ζ]L, ζ = 1.0

S.H.Chen; Ph.D. Thesis McMaster University				This Work				
								$[0\zeta\zeta]T_1$
ζ		ν	$\Delta\nu$					
.2000		2.3600	.020					
.3000		3.3500	.030					
.4000		4.1200	.030					
.4500		4.3500	.030					
.5000		4.4000	.050					
ζ	$\Delta\zeta$	ν	$\Delta\nu$	ζ	$\Delta\zeta$	ν	$\Delta\nu$	$[0\zeta\zeta]T_2$
.1530	.004	2.0000		.0480	.001	.7010		
.2000		2.5700	.020	.1010	.002	1.3960		
.3000		3.6500	.020	.1530	.002	2.0040		
.3600		4.1000	.050	.1745	.002	2.3060		
.4000		4.3000	.050	.1995	.002	2.5780		
.4500		4.2500	.100	.2220	.002	2.8410		
.5000		4.1500	.050	.2455	.001	3.1090		
				.3240	.001	3.8580		
				.3500		4.0700	.020	
				.5000		4.2000	.070	← Note ②
ζ	$\Delta\zeta$	ν	$\Delta\nu$	ζ	$\Delta\zeta$	ν		$[0\zeta\zeta]L$
.0300	.005	1.0000		.0260	.002	.6050		
.0800	.005	2.0000		.0490	.002	1.1470		
.1000		2.3000	.050	.0760	.002	1.6970		
.1300	.005	3.0000		.0990	.002	2.3060		
.1890	.004	4.0000		.1260	.002	2.7940		
.2000		4.3500	.150	.1500	.002	3.3000		
.2050	.010	4.3000		.1700	.005	3.7950		
.2600	.010	5.0000						
.3000		5.5000	.050					
.4000		6.4000	.200					
.4500		6.6000	.100					
.5000		6.7500	.100					
ζ		ν	$\Delta\nu$	ζ		ν	$\Delta\nu$	$[\frac{1}{2}\frac{1}{2}\zeta]\pi$
0.0000		6.7500	.100	.4000		5.8700	.060	
.5000		5.5000	.050	.5000		5.4200	.080	← Note ④
1.0000		4.4000	.050	.6000		5.1400	.060	
				.7000		4.8200	.060	
				.8000		4.7000	.100	
				.9000		4.4400	.060	
				1.0000		4.3800	.100	← Note ③
ζ		ν	$\Delta\nu$	ζ		ν	$\Delta\nu$	$[\frac{1}{2}\frac{1}{2}\zeta]\Lambda$
0.0000		4.1500	.050	0.0000		4.2000	.070	← Note ②
.2000		4.9000	.100	.1000		4.5700	.080	
.5000		5.5000	.050	.3000		5.3800	.080	
.8000		4.9000	.100	.4000		5.4000	.080	
1.0000		4.1500	.050	.5000		5.4200	.080	

② Measured at $[\zeta\zeta 1]\pi_2$, $\zeta = 0.5$
③ Measured at $[\zeta\zeta 1]\Lambda$, $\zeta = 0.5$
④ Measured at $[\frac{1}{4}\frac{1}{4}\zeta]\Lambda$, $\zeta = 0.5$

List of phonon frequencies in tungsten [page 3 of 3]

[ζζζ]T

S.H.Chen; Ph.D. Thesis McMaster University				This Work				
ζ	Δζ	ν	Δν	ζ	Δζ	ν	Δν	
.0640	.005	1.0000		.0690	.002	1.1470		
.1250	.005	2.0000		.1880	.003	2.9970		
.1900	.005	3.0000		.2380	.005	3.4920		
.2700	.005	4.0000		.2670	.002	3.9870		
.3300	.005	4.6000		.2700		3.9700	.070	
.4000		5.0500	.050	.2700	.002	3.9870		
.5000		5.5000	.050	.3170	.003	4.5130		
.6000		5.9000	.150	.5000		5.4100	.070	
.7000		6.0000	.100	1.0000		5.4700	.100	← Note (1)
.8000		5.9500	.100					
1.0000		5.5000	.100					

[ζζζ]L

ζ	Δζ	ν	Δν	ζ	Δζ	ν	Δν	
.1450	.005	4.0000		.0900	.004	2.8760		
.1550	.010	4.2000		.1150	.004	3.4270		
.2400	.010	5.4000		.1420	.005	3.9260		
.3000		5.9000	.050	.1600	.002	4.2140		
.4000		6.0500	.050	.1660	.005	4.3800		
.5000		5.5000	.050	.1900		4.6500	.030	
.6000		4.8500	.050	.1935	.004	4.7900		
.7000		4.7800	.050	.1970	.004	4.8920		
.8000		5.1000	.100	.2100		4.9800	.030	
.8500		5.2500	.050	.2250		5.1900	.070	
.9000		5.4500	.150	.2750		5.6700	.050	
1.0000		5.5000	.100	.3250		5.9800	.060	
				.3750		6.0600	.060	
				.5000		5.4100	.070	← Note (5)
				1.0000		5.4700	.100	← Note (1)

[ζζ1]π_2

ζ		ν	Δν	ζ		ν	Δν	
0.0000		5.5000	.100	0.0000		5.4700	.100	
.2500		4.7300	.030	.1000		5.3500	.060	
.5000		4.1500	.050	.2000		4.8600	.080	Note (1)
				.3000		4.5900	.070	
				.4000		4.3400	.080	
				.5000		4.2000	.070	

[ζζ1] Λ

ζ		ν	Δν	ζ		ν	Δν	
0.0000		5.5000	.100	0.0000		5.4700	.100	
.2500		5.2500	.100	.1000		5.4700	.100	
.5000		4.4000	.050	.2000		5.4700	.100	Note (1)
				.3000		5.2200	.100	
				.4000		4.5800	.100	
				.5000		4.3800	.100	

[ζζ1]π_1

ζ		ν	Δν
0.0000		5.5000	.100
.2500		6.3500	.200
.5000		6.7500	.100

(5) Measured at [ζζζ]T, ζ = 0.5

Table VI-3. Atomic force constants (in units of 10^4 dynes/cm) for tungsten at 22°C.

AFC	"A" Chen's work [CH64]	"B" This work ⓐ	"B" This work ⓑ	"C" Using data from this work and Chen's[CH64A] ⓐ	"C" Using data from this work and Chen's[CH64A] ⓑ
1xx	2.30±.02	2.16±.02	2.20±.02	2.19±.02	2.21±.02
1xy	1.92 .03	1.83 .06	1.61 .06	1.96 .03	1.89 .03
2xx	4.73 .05	4.61 .05	4.43 .05	4.60 .04	4.57 .04
2yy	-0.08 .03	0.01 .04	0.15 .03	0.04 .02	0.07 .02
3xx	0.32 .01	0.46 .02	0.41 .02	0.38 .01	0.37 .01
3zz	0.14 .02	-0.08 .02	-0.22 .02	-0.05 .02	-0.13 .02
3xy	0.49 .02	0.35 .05	0.65 .04	0.45 .03	0.52 .02

Note: The results of the fit in "B" were obtained using the data of this work (table VI-2) and thus, lack the inclusion of phonons belonging to the $[0\zeta\zeta]T_1$ and $[\zeta\zeta 1]\pi_1$ branches.

Notes: ⓐ - fit excluding elastic constants.
ⓑ - fit including elastic constants [FE63].

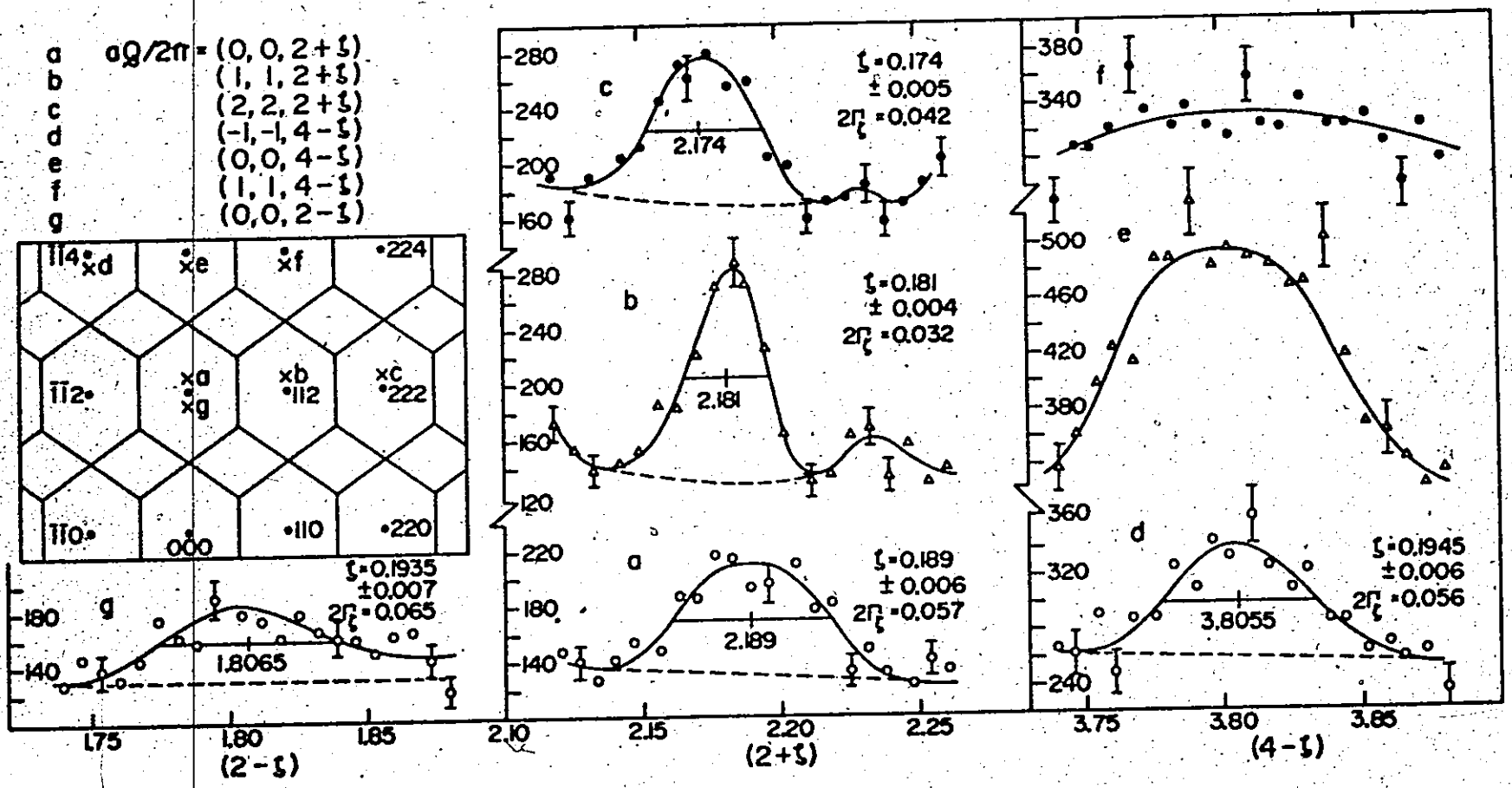

Fig. VI-1. - Effect of focussing on the lineshape of a phonon of longitudinal polarization in tungsten. This particular phonon belongs to the [00ζ]L branch and has an energy of 2.997 THz.

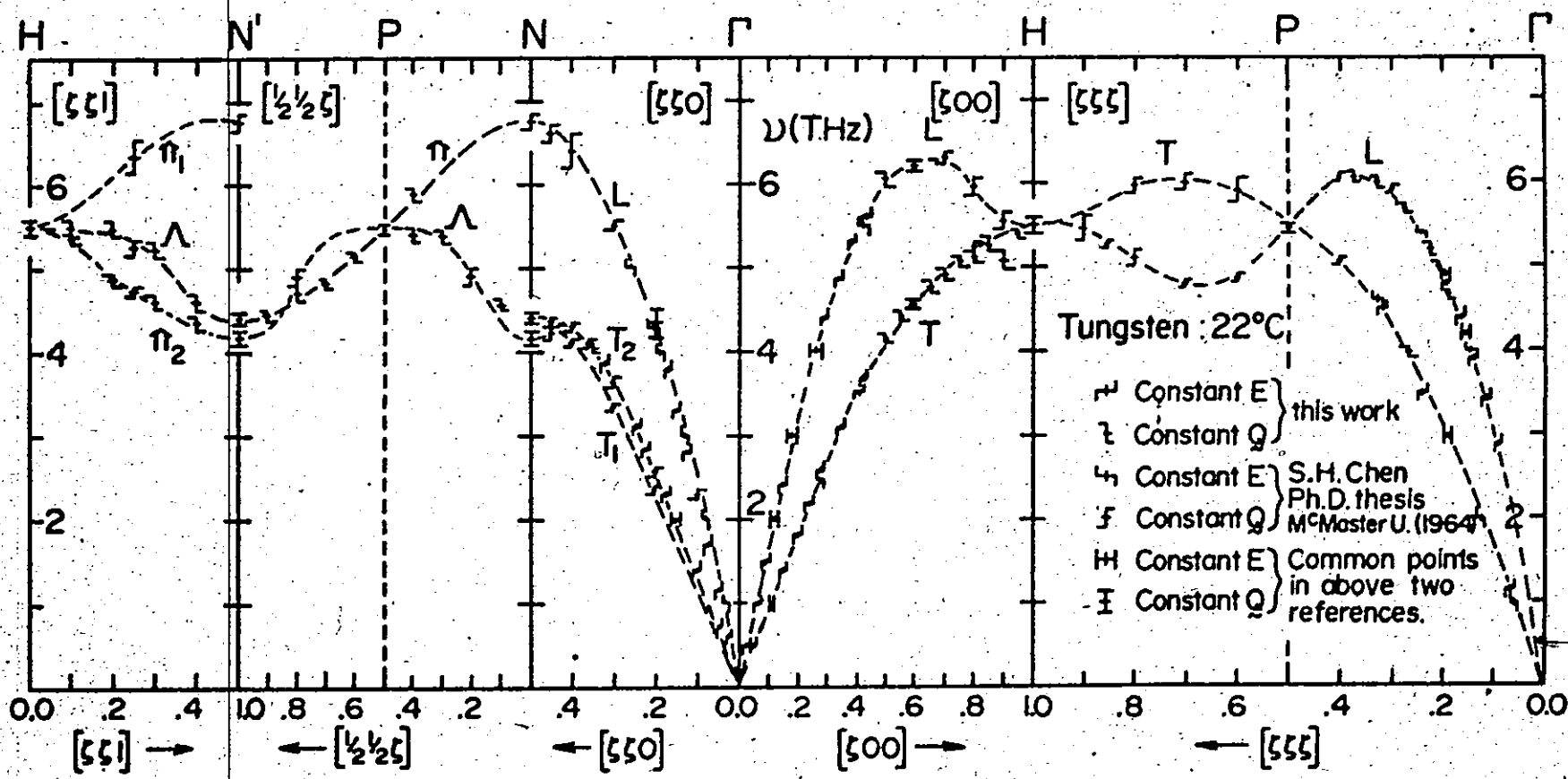

Fig. VI-2. - Dispersion curves for tungsten in the major symmetry directions. The lines through the points are only guides. Note the T_1 and T_2 cross-over near the point N.

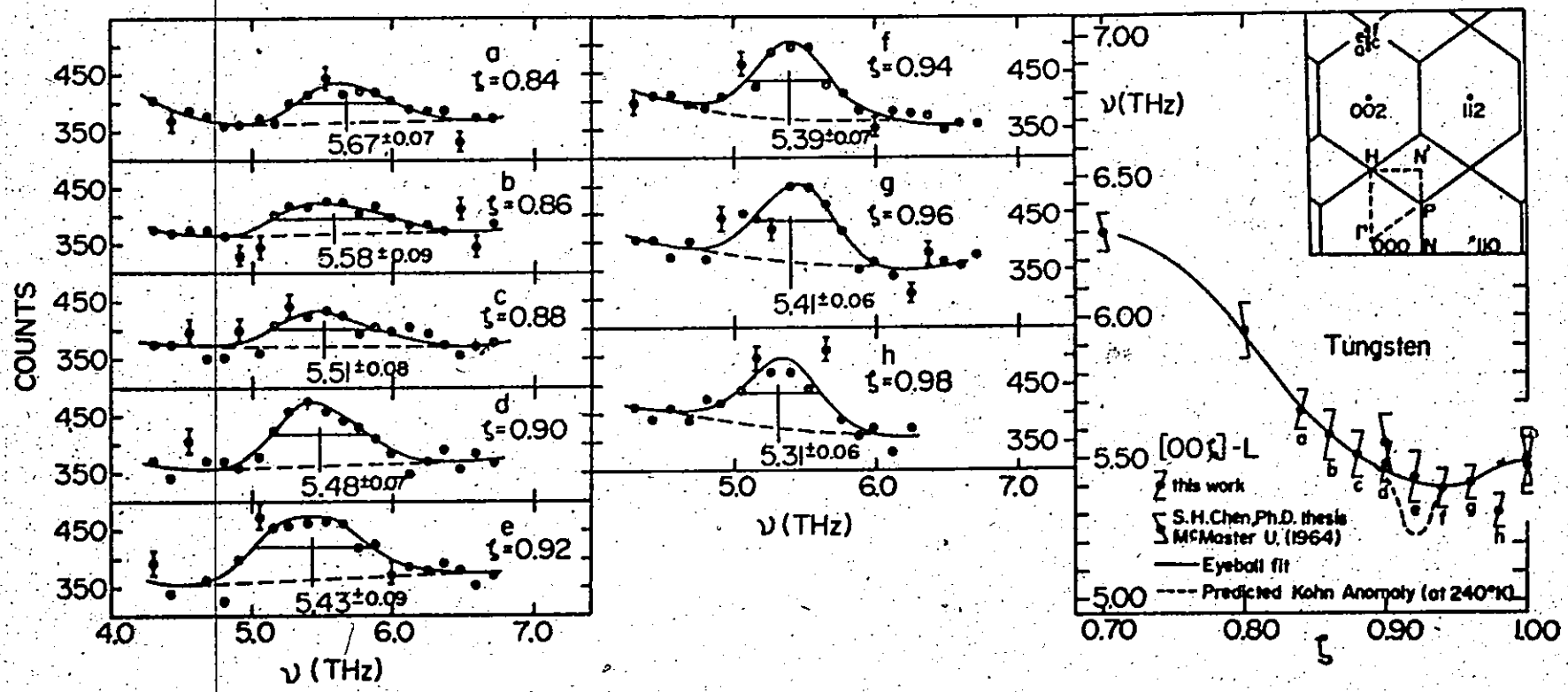

Fig. VI-3. - Lineshape and dispersion of the observed phonons in the region of the predicted Kohn "anomaly". The neutron groups were all obtained with a constant monitor and each required some 9 hours. The neutron group at $\zeta=0.98$ is not reliable; see text. In the case of the points corresponding to this work, the uncertainties in ζ and ν are given by the magnitude of the horizontal (x 2) and vertical segments.

We must all learn from [Norman Bethune]
this perfect spirit of selflessness.
Thus, anyone can become very useful to society.
Whether one is more or less gifted,
one only needs to possess this spirit
to be a man of nobility and integrity,
a man of high morality, above vulgar interests,
a man of value to society.

Mao Tse-Tung (1939)

I believe that the rendering of useful service
is the common duty of mankind
and that only in the purifying fire of sacrifice
is the dross of selfishness consumed
and the greatness of the human soul set free.

John D. Rockefeller, Jr.

Slaves, obey your earthly masters,
with fear and trembling, ...

Ephesians 6:5.

APPENDIX I

TRIPLE-AXIS SPECTROMETER CONTROL BY PAPER TAPE

This topic was already discussed in a previous thesis [LA70, p. 142]. Paper tape control was put in service in mid-1971 and has more than paid for itself by removing the need for the leased IBM-026 card punch/reader previously used; economic advantages are not the only ones, however. In this appendix, we will review briefly the system; further details may be obtained in the above reference. An updated circuit diagram and encoding table are given below.

A - The System

The advantage in using paper tape is that a single standard teletype (model 33), needed to print the scalers data, can be modified to control the spectrometer as well. This is possible because a teletype comes equipped with a paper tape reader (and punch) capable of reading 8-bits, even-parity ASCII* code. The modification to the teletype consists of connecting a decoder to the tape reader; the output of this decoder is fed to the teletype and the spectrometer control unit. Thus the information on the tape being read can now be used to write on the printer (alpha mode) or to control the spectrometer (control mode). In the latter case, the coded information read from the tape goes through the decoding circuit where it is translated into the appropriate combination of spectrometer commands.

* ASCII: American Standard Code for Information Interchange

B - Coding

The choice of the actual coding was based on the following considerations.

- All 3 independent motors of a triple-axis spectrometer ($\psi, \phi, (\theta_a$ or $\theta_m)$) had to be movable independently of each other. The total number of such possibilities is 26.
- The spectrometer commands should be generated directly from the keyboard as well as from the TRIPLX3 programme; see appendix II.
- The chosen code should allow motor move symbols to be printed, in order to help in the diagnosing of possible troubles and also to verify manually punched codes.

The simplest ASCII code satisfying these requirements was that corresponding to the letters of the alphabet and a few other special symbols.

C - Alpha Mode and Control Mode

In the "alpha" mode, all ASCII characters can be read and printed at the rate of 10 characters/second, except ASCII code 074_8 (i.e. "Bra" <) which is used for switching over from "alpha" to "control" mode. In the "control" mode, only the limited number of characters corresponding to spectrometer commands may be read; the speed of the reader is then approximately 1 character/second, except for the count signal which stops the reader until a preset number of accumulated counts has been reached in the monitor scaler.

Within the "control" mode , there are two sub-modes. The "θ_a" mode corresponds to the situation where ψ, ϕ, $\theta_a (2\theta_a)$ may

be simultaneously moved (K-23 de-energized, cf. fig. A1-3). Similarly, in the "θ_m" mode, ψ, ϕ, θ_m may be simultaneously moved (K-23 energized).

D - Manual Operation

A spectrometer scan can be manually programmed using truth table A1-1. The procedure is as follows,

a) Set the instrument in the "alpha" mode by pressing the appropriate switch.

b) Turn the paper tape punch "on"
Press ">"
Press "Break" for ∿ 3 seconds
Press ">"

c) Punch the header section, if any. This consists of carriage return, line feed, possibly a short title and/or a reminder as to change certain switches (e.g. "change from signal to 60 Hz generator"). When the tape will be read, this will print on the teletype.

d) Immediately and only immediately preceding the first spectrometer command, ASCII character 074_8 (i.e. "bra" <) is punched.

e) Spectrometer commands are punched according to the truth table A1-1.

f) When it is desired to terminate the "control" mode, the ASCII code 276_8 (i.e. "ket" >) is punched. Upon reading the tape and encountering this code, the instrument will return to the "alpha" mode.

g) Write the terminator section, if any, as in "c".

h) Press "break" for ∿ 3 seconds.
Turn the punch off.
Tear the tape off.

The resulting tape is now ready to be fed in the tape reader and automatic operation takes over. In the case of a repetitive operation (e.g. family of ψ-rocking curves) the tape may be formed into a closed loop; in which case,

however, care must be given that no angular limits are exceeded during the repetitive cycle.

E - Computer Programmed Operation

As will be seen in the next appendix, the spectrometer may be controlled automatically to perform an arbitrary scan in (Q,ω) space by programme TRIPLX3 which does the necessary calculations to move any of the four angular variables in the appropriate way. On the tape punched by this programme, each scan contains an alphanumeric title section, the spectrometer control section proper and a runback or terminator section depending on whether or not a runback to a following phonon is calculated. Each scan is separated from the adjacent ones by a blank strip region 10 cm long. [Being an ardent nationalist, not of the common flag-waving variety however, I could not resist the temptation to encode the beginning of a scan with the first four notes of "O Canada", to be played by the bell of the teletype.]

Table A1-2 shows how each of the 64 CDC display codes is translated into ASCII. Each code is accompanied by a symbol indicating whether it is meant to be used in the "alpha" and/or "control" mode. The explicit function of "control" mode characters is defined in table A1-1.

The punch can be used to produce a tape containing the result of each scan. This tape contains the accumulated counts in the scalers punched in between the spectrometer commands duplicated from the control tape. Thus, it contains the complete experimental information ready for computer processing.

MOTOR MOVES SYMBOLS			ψ	ϕ	θ_A | θ_M
A	101	01000.001	0	0	+
B	102	01000.010	0	0	−
D	104	01000.100	0	+	0
H	110	01001.000	0	−	0
P	120	01010.000	+	0	0
C	303	11000.011	−	0	0
E	305	11000.101	0	+	+
I	311	11001.001	0	−	+
F	306	11000.110	0	+	−
J	312	11001.010	0	−	−
T	321	11010.001	+	0	+
S	123	01010.011	−	0	+
B	322	11010.010	+	0	−
W	327	11010.111	−	0	−
R	322	11010.100	+	+	0
G	107	01000.111	−	+	0
X	330	11011.000	+	−	0
K	113	01001.011	−	−	0
U	125	01010.101	+	+	+
L	314	11001.100	−	+	+
Y	131	01011.001	+	−	+
V	126	01010.110	+	+	−
M	115	01001.101	−	−	+
N	116	01001.110	−	+	−
Z	132	01011.010	+	−	−
O	317	11001.111	−	−	−

OTHER SYMBOLS			
1	261	10110.001	PUNCH BEFORE INITIATING THETA-A MOVE.
2	262	10110.010	PUNCH BEFORE INITIATING THETA-M MOVE.
$	044	00100.100	COUNT.
.	056	00101.110	RELEASE LINE COUNTER: CODE NOW UNUSED.
BRA <	074	00111.100	CHANGE FROM ≠ALPHA≠ TO ≠CONTROL≠ MODE.
KET >	276	10111.110	CHANGE FROM ≠CONTROL≠ TO ≠ALPHA≠ MODE.
RUB-OUT	377	11111.111	ERROR CORRECTION (≠ALPHA≠ OR ≠CONTROL≠ MODE); DELAY WHEN REVERSING MOTORS (≠CONTROL≠ MODE).
BLANK TAPE	000	00000.000	NO EFFECT IN ≠ALPHA≠ MODE; STOPS SPECTROMETER IN ≠CONTROL≠ MODE.
BELL	207	10000.111	(IN ≠ALPHA≠ MODE ONLY).
LINE FEED	012	00001.010	(IN ≠ALPHA≠ MODE ONLY).
CARRIAGE RETURN	215	10001.101	(IN ≠ALPHA≠ MODE ONLY).

Table A1-1.

Truth table for spectrometer control by paper tape.

Notes: The first column represents the various possible symbols and function possible in the "control" mode.
The second and third are the corresponding octal and binary representations in ASCII (the points represent the sprocket holes positions on the paper tape).
The fourth column describes the resulting command.

SEE NOTES	(1)	(2)	(3)	(4)	(5)		(1)	(2)	(3)	(4)	(5)	
	001	A	101	01000.001	AC		041	6	066	00110.110	A	
	002	B	102	01000.010	AC		042	7	267	10110.111	A	
	003	C	303	11000.011	AC		043	8	270	10111.000	A	
	004	D	104	01000.100	AC		044	9	071	00111.001	A	
	005	E	305	11000.101	AC		045	+	053	00101.011	A	
	006	F	306	11000.110	AC		046	-	055	00101.101	A	
	007	G	107	01000.111	AC		047	*	252	10101.010	A	
	010	H	110	01001.000	AC		050	/	257	10101.111	A	
	011	I	311	11001.001	AC		051	(	050	00101.000	A	
	012	J	312	11001.010	AC		052	)	251	10101.001	A	
	013	K	113	01001.011	AC		053	$	044	00100.100	AC	
	014	L	314	11001.100	AC		054	=	275	10111.101	A	
	015	M	115	01001.101	AC		055		240	10100.000	A	
	016	N	116	01001.110	AC		056	,	254	10101.100	A	
	017	O	317	11001.111	AC		057	.	056	00101.110	AC	
	020	P	120	01010.000	AC		060	≡	000	00000.000		UNUSED
	021	Q	321	11010.001	AC		061	[	333	11011.011	A	
	022	R	322	11010.010	AC		062	]	335	11011.101	A	
	023	S	123	01010.011	AC		063	%	245	10100.101	A	
	024	T	324	11010.100	AC		064	≠	000	00000.000		UNUSED
	025	U	125	01010.101	AC		065	↑	215	10001.101	A	CARRIAGE RETURN
	026	V	126	01010.110	AC		066	∨	377	11111.111	AC	SEE NOTE(6)
	027	W	327	11010.111	AC		067	∧	207	10000.111	A	BELL
	030	X	330	11011.000	AC		070	↑	012	00001.010	A	LINE FEED
	031	Y	131	01011.001	AC		071	↓	000	00000.000		UNUSED
	032	Z	132	01011.010	AC		072	<	074	00111.100	AC	SEE NOTE(7)
	033	0	060	00110.000	A		073	>	276	10111.110	AC	SEE NOTE(8)
	034	1	261	10110.001	AC		074	≤	000	00000.000		UNUSED
	035	2	262	10110.010	AC		075	≥	000	00000.000		UNUSED
	036	3	063	00110.011	A		076	¬	000	00000.000	AC	SEE NOTE(9)
	037	4	264	10110.100	A		077	:	273	10111.011	A	
	040	5	065	00110.101	A		000	;	072	00111.010	A	

NOTE(1): CDC DISPLAY CODE (OCTAL) OF SYMBOLS UNDER NOTE(2).
NOTE(2): THE 64 CDC SYMBOLS.
NOTE(3): EVEN-PARITY, A.S.C.I.I. CODE (OCTAL) OF SYMBOLS UNDER NOTE(2).
NOTE(4): BINARY EQUIVALENT OF ABOVE; POINTS ARE SPROCKET HOLES ON TAPE.
NOTE(5): ≠A≠ IF CODE IS ALLOWED IN ≠ALPHA≠ MODE; ≠C≠ IF IT IS IN ≠CONTROL≠ MODE.
NOTE(6): PUNCHED BY PROGRAMME ≠TRIPLX3≠ WHEN MOTORS ARE REVERSED.
NOTE(7): ≠BRA≠ INDICATES CHANGE-OVER FROM ≠ALPHA≠ TO ≠CONTROL≠ MODE.
NOTE(8): ≠KET≠ INDICATES CHANGE-OVER FROM ≠CONTROL≠ TO ≠ALPHA≠ MODE.
NOTE(9): BLANK TAPE.

Table A1-2. Conversion table between the CDC display code and the ASCII code.

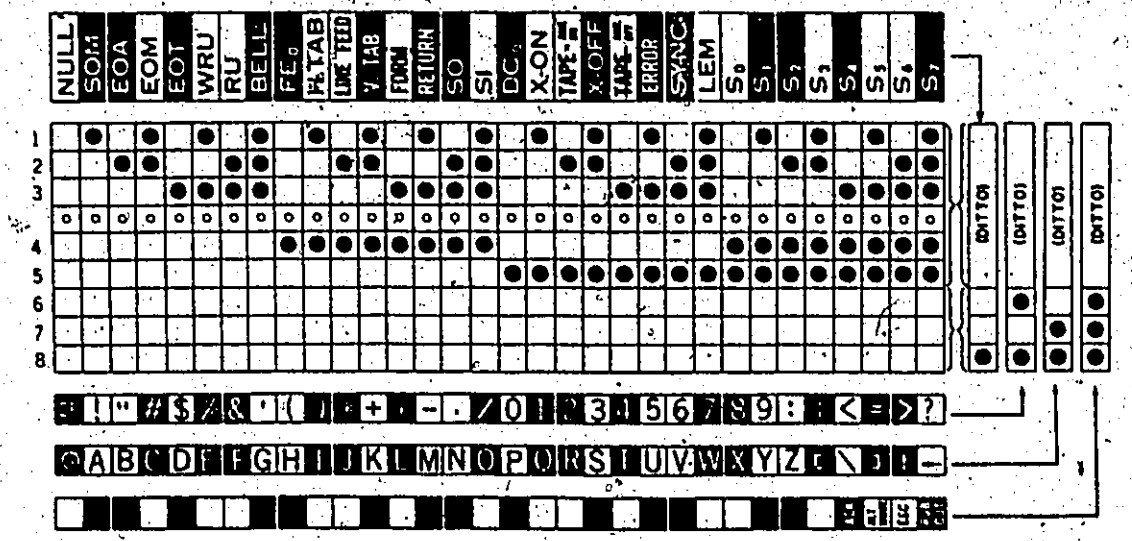

Fig. A1-1. CHARACTER ARRANGEMENT (ASCII CODE)

* * * * * * * * * * * * *

Fig. A1-2.

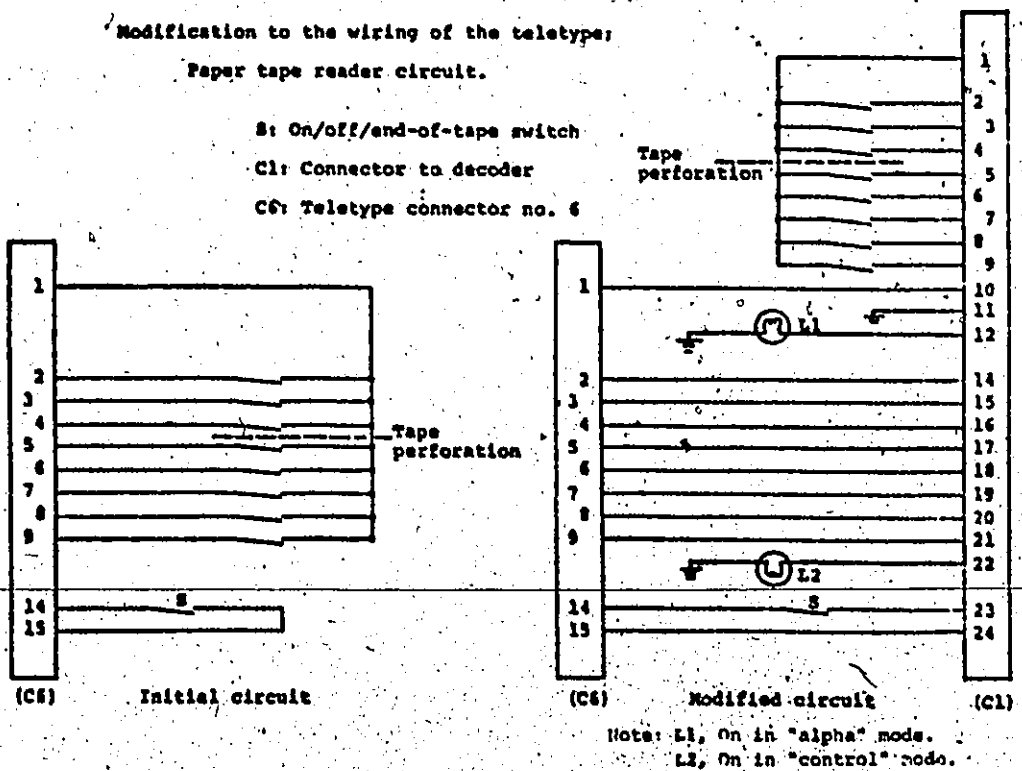

Pins of connector C1

1: +24 V. to reader contacts (8)
2-9: From reader contacts (8)
10: Teletype write-inhibit
12+22: To incandescent lamps (2)
14-21: Teletype write signal
23-24: Teletype advance

Pins of connector C2

1-2: Analyser motors
3-4: Phi-motor
5-6: Psi-motor
7-8: Monochromator motor
9: skip) 9&10: Release
10: Count)
14: Advance pulse

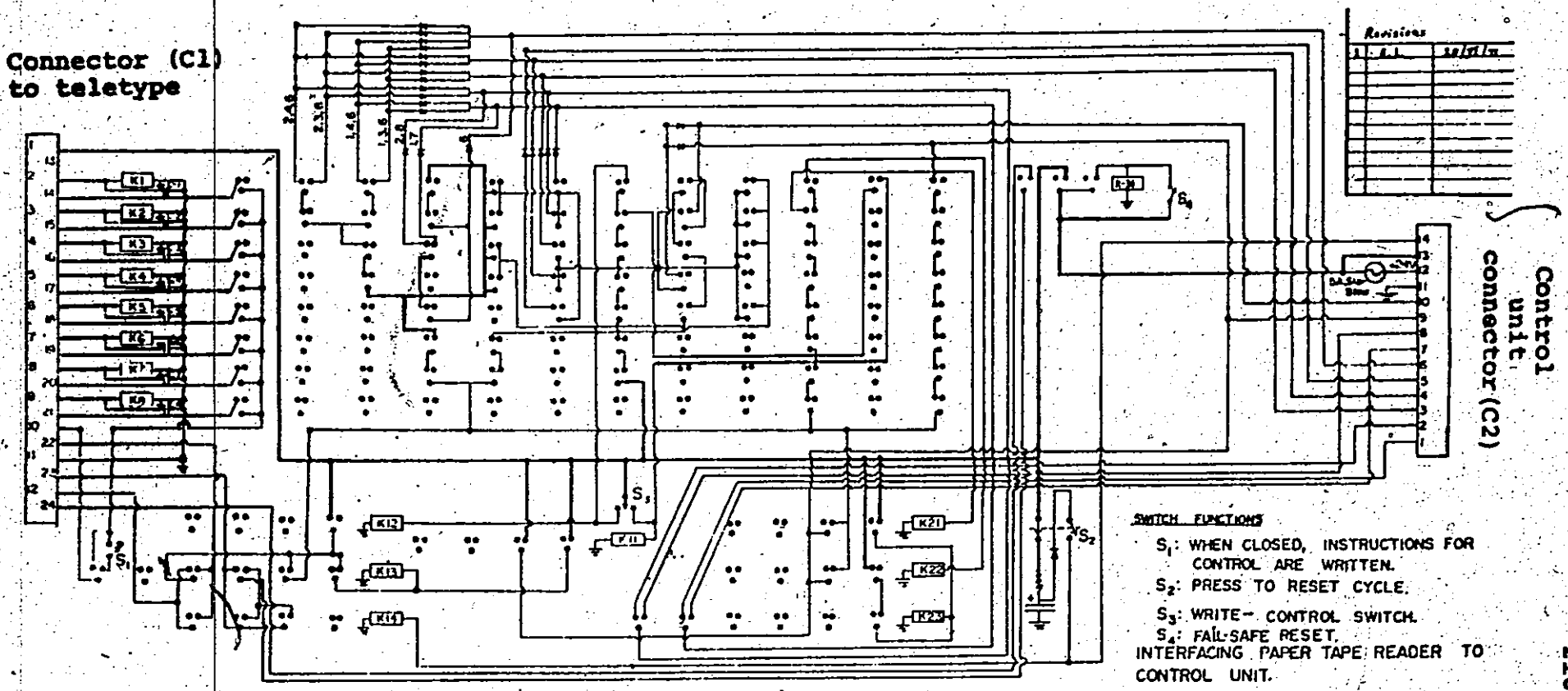

Fig. A1-3. Circuit diagram of the decoder.

Fig. A1-4. Control unit of the McMaster triple-axis spectrometer at the NRU reactor, Chalk River. The paper tape decoder, discussed in this appendix, is located in the base of the teletype. The card reader, shown in the foreground, is no longer required.

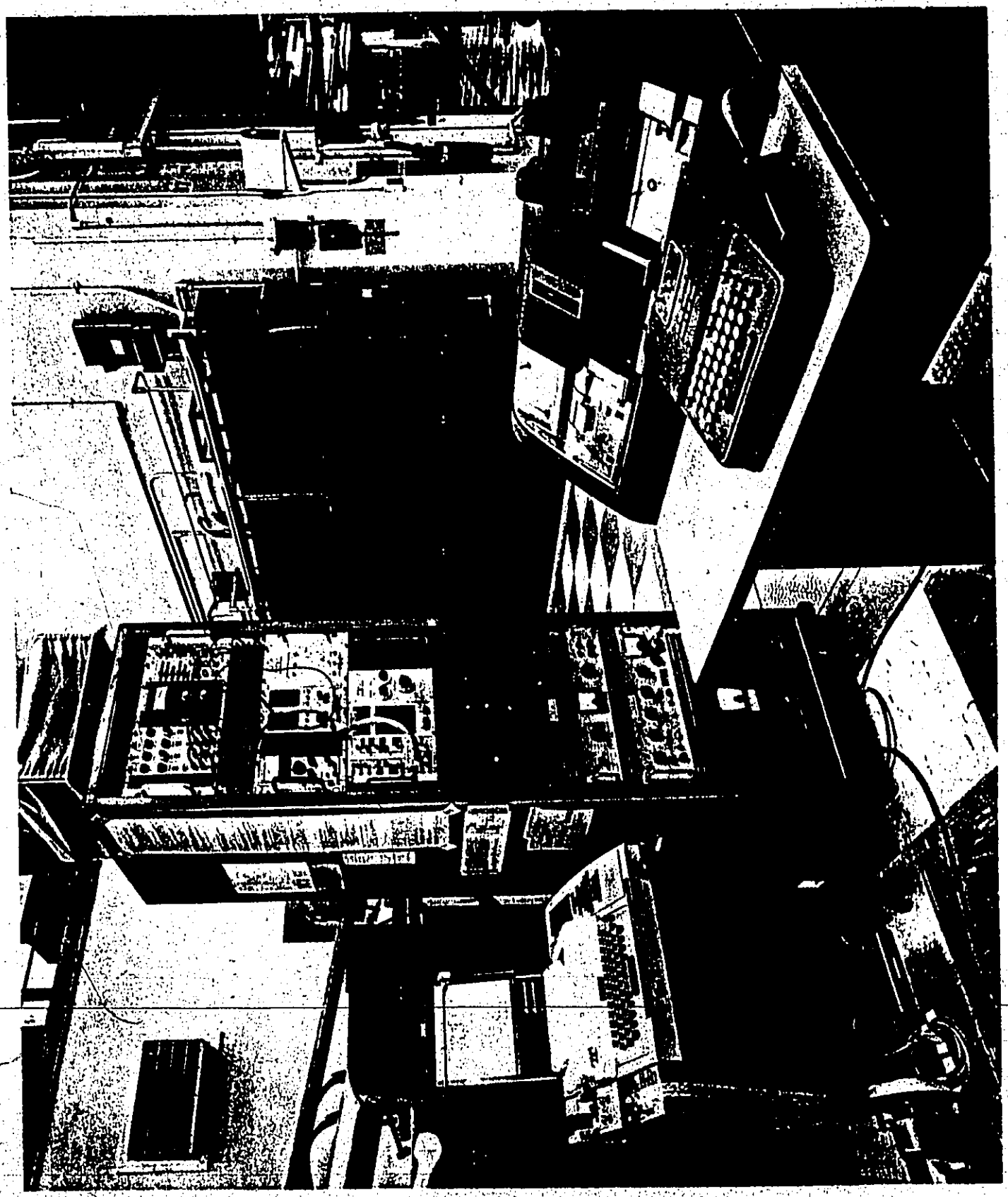

APPENDIX II

ON VARIOUS COMPUTER PROGRAMMES WHICH WERE WRITTEN

In this appendix, we will briefly consider various computer programmes written during this research project; we will not, however, be concerned with any of the numerous programmes related to the published bibliographies [LA73 ; LA74] since this will be discussed in the following appendix. This part will necessarily be brief.

A - PROGRAMME TRIPLX3

This programme is used to control the triple-axis instruments along the various types of scans required in neutron spectrometry; the original version was written by E. C. Svensson and improved by J.R.D. Copley. Interfacing between computer and spectrometer is done through punched cards or, since 1970, by paper tape (cf: appendix I).

The following modifications are among the major ones made to this programme:

- Arbitrary scans, not only constant-$\underset{\sim}{Q}$ scans, are programmable. (This was done in cooperation with J.R.D. Copley). A general scan whereby $\underset{\sim}{Q}$ and ν are varied is required when it is desired to intersect the dispersion surface at normal incidence, in order to have the narrowest possible linewidth [LA70, p. 65]. However, this modification was made mainly to allow the operation in constant-E as well as constant-$\underset{\sim}{Q}$ modes [BR60; BR64]. Other types of scans

are convenient only if a very fine angular incrementing (0.01° or better) of the spectrometer is possible so that the scan is "linear" in the 4-dimensional ($\underset{\sim}{Q},\omega$) space. All McMaster spectrometers presently operate with 0.1° increments [BR68; HA69A, p.119].

- Scans with variable incident neutron energy are now possible, making full use of the potentialities of the McMaster spectrometer at NRU reactor (beam #E2) [KA72, pp.141-144].
- All angles are rounded to the nearest tenth of degree of the actual scale values. This requires the insertion of the zero-values of the angles (i.e. θ_{m_o}, ψ_o, ϕ_o, θ_{a_o} and $2\theta_{a_o}$) as input data. The resulting scale values are printed so as to facilitate the running of the scans and the ($\underset{\sim}{Q},\omega$) values corresponding to these rounded-off scale angles are computed.
- Angular limits are also fed in; if these are ever exceeded, the scan is truncated. This is obviously a protective measure against serious mechanical damage should the angular limits be inadvertently exceeded. This is always a possibility, as the experience of our group has shown.
- Backlash compension is taken into account for all angles. Backlash values are fed as input data because they vary from one instrument to another.
- In order to minimize the down time of the spectrometer during initial calibration, a subroutine was added whereby the results of the vanadium and copper powder procedures [HA69A,

p117] are used to calculate the instrumental parameters (i.e. the fixed incident or analysed energy and the zero-angles) immediately before calculating the required scans.

- A subroutine was added to calculate the expected linewidth of the scans being generated. This calculation is based on the formalism of Cooper and Nathans [CO67] using the approximation of a planar dispersion surface.
- Finally, now that a paper tape punch has been hooked up to the CDC 6600 at Chalk River, the programme has been modified so as to get the tape punched directly at execution time rather than by a separate programme (PAPYRUS; cf LA70, p.150)meant to be run consecutively on the Bendix G20 computer (now removed from service).

The paper tape subroutine not only punches the spectrometer commands (e.g. motor moves, count commands, etc...) but also writes the scan's alphanumeric identifiers as well as the scan terminator when no runback to the next phonon is desired. As with the card control, backlash is compensated for and a delay is introduced when the motors are reversed so as to allow the motor to stop before beingre-energized. The previous appendix contains the details on spectrometer control by paper tape.

B - PROGRAMME INTRPLN

Phonons with wavevectors in direction of high symmetry have their eigenvectors determined also by symmetry. Consequently, experiment need only determine their eigenvalues. Along such

directions, in a crystal with one atom per primitive unit cell, the eigenvalues can be written as a Fourier sum of the form [FO57]

$$M\,\omega^2(q) = \phi_o + \sum_{p\geq 1} \phi_p \left(1-\cos \frac{p\pi q}{q_{max}}\right) \qquad (1)$$

The coefficient ϕ_o is identically zero only when $\underset{\sim}{q}$ is of the form $\frac{a\underset{\sim}{q}}{2\pi} \equiv (00\zeta)$, $(0\zeta\zeta)$ or $(\zeta\zeta\zeta)$. In equation (1), the ϕ_p are called interplanar coefficients since each ϕ_p is a linear combination of interatomic force constants between the atom at the origin and other atoms all belonging to the same plane [ref. BR67]. Obviously the range of the ϕ_p cannot be greater than that of the AFCs.

Taking the limit of equation (1) as $q \to 0$, we obtain, both in the cases where $\phi_o = 0$ and $\phi_o \neq 0$:

$$\lim_{q\to 0} \left(\frac{\partial\omega(q)}{\partial q/q_{max}}\right)^2 = \frac{\pi^2}{2M} \sum_{p\geq 0} p^2\phi_p \qquad (2)$$

This expression is related to the energy gradient of the dispersion relation at small wavevectors and physically, two cases are of interest.

- if $\phi_o = 0$, the long wavelength energy q-gradient depends on the elastic constants,
- if $\phi_o \neq 0$, this energy gradient is in general naught because of symmetry requirements.

In either case, however, the appropriate value of the gradient may be fitted with an arbitrary weight. Similarly, for the eigenvalues, various weighting schemes are possible,

with preference being given to weights of the form $w_i \alpha \frac{1}{(\nu_i \delta\nu_i)^2}$ where $\delta\nu_i$ is the uncertainty corresponding to the eigen-frequency ν_i. This programme was written because a previous version [SV67A , p.176] used by the group in the past was found to contain an error in the way the $\delta\phi_p$ are calculated; this error would show up whenever the weighting scheme was not of the form $1/(\nu\delta\nu)^2$. Rather than to check an unfamiliar programme, it was decided to write a new version. The two programmes were checked against each other and no other discrepancies were found.

C - PROGRAMME PHØPLØT

The purpose of this programme is to plot experimental constant-Q lineshapes by computer either as they were obtained or after normalization and/or background substraction. Some of the plots in chapter IV showing the temperature dependence of various phonons are produced by this programme. The scale factors in the x-direction (i.e. THz/cm) and in the y-direction (i.e. counts/cm) are adjustable; so is the vertical translation factor when it is desired to displace vertically the various groups being compared so as to improve clarity.

Presently, the data from a phonon scan has to be manually punched on cards before execution of the programme; this is obviously a time consuming process. In the case when the spectrometer is controlled by paper tape, it would be possible, in principle, to use directly the tape punched by the teletype . Such a tape would contain the (Q,ω) values (i.e. the x-axis)

duplicated from the tape generated by TRIPLX3 for controlling the spectrometer along the various points of the scan, as well as the counts in the signal and background scalers (i.e. the y-axis) punched during the actual running of the experiment; see appendix I.

D - SUBROUTINE ALASØRT

A CDC computer of the 6400-6600 family has a word length 60 bits long. It may sometimes be necessary to sort composite words having a larger number of bits. For cases where less than 120 bits are required, double precision operation will give the desired result if used in conjunction with the ordinary sorting routines. In other cases, a different approach has to be used; subroutine ALASORT is one such approach. The need for such a routine was realized when the subroutine generating the author index for the bibliography (cf. appendix III) was being written. After discussion with Messrs. Masterson and Bhargava of the "Academic Systems" group of the Computer Centre of this university, it was learned that such a subroutine was not available but could possibly be useful if it were. The version listed at the end of this appendix is the best one of two such subroutines written for that purpose. The listed version will sort an array of up to 900 words, each being composed of 12×60 bits; sorting is based on 9×60 bits of each word.

E - PROGRAMME NUMERØ

This programme is a housekeeping programme; it is used when it is desired to copy a programme card deck, each card

to be numbered in columns 73 to 80. Each programme and/or subroutine is labelled with a letter, a number and a code. This code is the letter "R" for a read statement and "W" for a write statement; it allows these I/O statements to stand out, especially on large listings.

F - PROGRAMME CØMPARE

Duplicated decks were always compared with the corresponding originals using this programme. Our experience shows that this this has not been an unnecessary precaution; mispunched cards are not uncommon.

```
      SUBROUTINE ALASORT(IRANG)
      DIMENSION IALASTO(12,900), IALARAN(900), IALADU1(900),IALADU2(900)
      COMMON /X1/ IALASTO
      COMMON /X4/ IALARAN
      IF (IRANG .LE. 0) GO TO 99999
      DO 1 J=1, IRANG
      IALARAN(J)=0
    1 CONTINUE
      IF (IRANG .GT. 1) GO TO 10
      IALARAN(1)=1
      GO TO 99999

   10 M=-1
      DO 2 J=1, IRANG
      IALADU1(J)=IALASTO(1,J)
    2 CONTINUE
      CALL TGSORT(IALADU1,IALARAN,IRANG,M)
      IALAPRE=0 $ IALORDR=0
      DO 3 J=1, IRANG
      JDUMMY=IALARAN(J)
      IF (IALADU1(JDUMMY) .EQ. IALAPRE) GO TO 4
      IALAPRE=IALADU1(JDUMMY)
      IALORDR=IALORDR +1
    4 IALADU1(JDUMMY)=IALORDR
    3 CONTINUE
      IF (IALORDR .EQ. IRANG) GO TO 99999

      DO 11 I=2, 9
      DO 12 J=1, IRANG
      IALADU2(J)=IALASTO(I,J)
   12 CONTINUE
      CALL TGSORT(IALADU2,IALARAN,IRANG,M)
      IALAPRE=0 $ IALORDR=0
      DO 13 J=1, IRANG
      JDUMMY=IALARAN(J)
      IF (IALADU2(JDUMMY) .EQ. IALAPRE) GO TO 14
      IALAPRE=IALADU2(JDUMMY)
      IALORDR= IALORDR +1
   14 IALADU2(JDUMMY)=IALORDR
   13 CONTINUE

      DO 15 J=1, IRANG
      IALADU1(J)=900*IALADU1(J) +IALADU2(J) -1
   15 CONTINUE
      CALL TGSORT(IALADU1,IALARAN,IRANG,M)
      IALAPRE=0 $ IALORDR=0
      DO 23 J=1, IRANG
      JDUMMY=IALARAN(J)
      IF (IALADU1(JDUMMY) .EQ. IALAPRE) GO TO 24
      IALAPRE=IALADU1(JDUMMY)
      IALORDR=IALORDR +1
   24 IALADU1(JDUMMY)=IALORDR
   23 CONTINUE
      IF (IALORDR .EQ. IRANG) GO TO 99999
   11 CONTINUE
99999 RETURN
      END
```

APPENDIX III

THE MAKING OF A BIBLIOGRAPHY OF PAPERS RELEVANT TO THE SCATTERING OF THERMAL NEUTRONS (OR, HOW TO ADD SOME 18 MONTHS TO THE DURATION OF A PH.D. PROGRAMME)

A - INTRODUCTION

The purpose of this appendix is to describe the various steps that have finally resulted in the two published editions of a bibliography of papers relevant to the scattering of thermal neutrons, henceforth referred to as BTN [LA73, LA74]. A lot could be written on the various procedural aspects; however, we will content ourselves with a very schematic exposé.

B - EVOLUTION OF THE PROJECT

The preliminary phase ran from mid-1968 to mid-1970 and is briefly described in a previous thesis [LA70]. Basically, it consisted of a literature search with the cooperation of Mr. R. R. Dymond; this resulted in a file containing 2477 entries. Various modes of handling this information were attempted but they all were quite inefficient until the present approach, which is computer oriented, was adopted. At that time, the format used for individual records was made compatible with that required by a programme (KWIC: Key Word In Context) which was then to be implemented by the Computer Centre. This however resulted in a less than optimum storage of information and did not provide satisfactory versatility. A programme (SISYPHE) was

written to remedy this situation; its first version was quite primitive but, over the years, it grew in complexity and versatility up to the present version (#9) which will be described below. At the end of this preliminary phase, the BTN consisted of a file (2477 entries) and the then most up to date version (#3) of SISYPHE. The file was subdivided into 4 sections: elastic scattering, inelastic scattering, theoretical and technical studies. The format for the records is described elsewhere [LA70]. Suffice it to say that entries grouped under the first two sections did not include the title of the reference and that no author index had been generated.

It was obvious then that if the invested effort was not to lie forgotten on some bookshelves and reach a level of perfection suitable for publication, major improvements were necessary; once again, however, the required amount of labour was drastically underestimated! Basically the second phase, mid-1970 to mid-1972, was carried along the following lines;

i) Keeping up with the literature production and adding a few journals to the survey.

ii) Subdividing the file into a larger number of subsections to facilitate information retrieval.

iii) Translating the record format of the existing file into a new format which would allow the generation of an author index and the elimination of limitations from the previous format that had gradually manifested themselves. This was a major task because of the nearly free format of the old file.

iv) Collecting titles for the references already on file and their insertion in the records.

v) Further improving SISYPHE and making of an author index file generating subroutine.

vi) Creation of the author index corresponding to the existing file.

vii) Creation of an updated file and correction of countless inconsistencies and errors.

The third phase, mid-1972 to mid-1973, begins when the co-editor, Mr. Jake Vanderwal, joined the project. This was the time when the eventual completion of the BTN seemed more uncertain than ever since the labour involved was incompatible with the pursuit of a Ph.D. programme. The coming of Mr. Vanderwal turned out to be a blessing since he was conscientious, efficient and also a physicist. He worked exclusively on the BTN for some six months during which time the updating was continued and the status of the files was finalized for publication.

In March, 1973 a total of 300 copies of the BTN were produced by the McMaster University Printing Department using a photo-reduction (35% reduction) of the computer generated print-out.* As of mid-1974, we had distributed more than 220 copies. A publicity leaflet, describing the first edition, which contained 5163 entries and an author index of 3978 names, is included at the end of this appendix (fig. A3-1).

The fourth and final phase (mid-1973 to mid-1974) was devoted to:

* One page of the published version consists of 120 lines on the computer generated version, i.e. nearly two computer pages.

i) Improving the BTN programmes where inefficient programming can be costly when one is working with large files (≈ one full 400 metres magnetic tape at 556 density, or 7×10^5 words).

ii) Correcting the inconsistencies from the BTN file; most of them dealing with the authors' names and initials.

iii) Updating and backdating the BTN file.

iv) Subdividing the BTN into a larger number of sections (47) in order to facilitate information retrieval.

The definite version for the second edition contains 8543 entries. It covers the period ranging from 1932, the year when the existence of the neutron was confirmed, up to mid 1974. By a strange coincidence, the literature search ended within a few days of the death, on 24/VII/74, of Chadwick, the discoverer of the neutron. The publication of this work, in a hard bound format*, was done by Plenum Publishing Corporation of New York, U.S.A., after an unsuccessful attempt to interest the University of Toronto Press in this venture.

C - PROCEDURE FOR UPDATING THE BTN FILE

The purpose of this section is to communicate what we found to be the most effective procedure for the data collection.

i) The journals of interest are scanned systematically and the following information is recorded in three separate files: the issues being searched, the missing issues if any, the reference of any paper judged to be relevant. Note that the search is simplified if the updating is done at short intervals, thus one can use the journals in their original formats. After a few months it is customary for libraries to have the journals bound, after which they are

* As for the first edition, the second one was published after a 35% photo-reduction of the computer generated copy (at 128 lines/page).

more awkward to scan because of the larger size and, often, the loss of the back cover index. (The search was often complicated by the disorderly state of the Science Library of this University.)

ii) Using the list of relevant papers, xerox copies were made of the first page of the article and the resulting copies were put in order. These copies were made to minimize the possibility of transcription errors and also to have readily available a copy of the abstracts of the collected papers.

iii) Before keypunching, we found it preferable to write the information for the first of the five cards making up each record (see below) on a standard coding form. This is so because this card contains a rather high density of information which can easily cause keypunching problems if the fields are not explicitly defined. Another reason is that very often, in the case where the update data comes from the same volume of a given journal, a large fraction of keypunching can be done by straight duplication of the fields common with those on the previous card. This accelerates the process and minimizes keypunching errors.

iv) When the first cards of a stack have been punched, the keypunch operator then proceeds to do, directly from the xeroxed pages, the corresponding cards #s 2,3,4,5 which contain the title and the authors list, according to a well-defined format (see below).

In order to facilitate the task of keypunching, the relevant information on the xerox sheets is underlined and a key (see below) is handwritten in the margin.

v) Each punched record contains an alphanumeric key in the first 8 columns of each of the 5 cards making one record. For a given stack this is used to merge each of the first cards with the appropriate cards #s 2,3, 4 and 5. This is done automatically by using an IBM83 card sorter. This key is made up of the card number (1 to 5), the section (5 to 47) and the page of the reference.

vi) Each stack is then checked for illegal format or improper merging by a small programme called "BIFØCHK".

vii) It is then a matter of checking visually between the original (i.e. xerox) and the keypunched information. This is a very time consuming procedure since it has to be done extra carefully in order to be completed with confidence before insertion of the new entries in the master file.

viii) When this has been done for all the stacks, the IBM card sorter is again used to order the records according to sections (i.e. 5 to 47).

ix) The resulting stack is again checked by BIFØCHK. After this, it is ready for the update. N.B.: In the case where the search is done through an abstracts journal there is no advantage to be gained by punching the first card of each record separately because there is usually no common field-

that can be duplicated in consecutive entries. It is then better to write the full record on the coding form. (after checking that it is not already in the bibliography). The checking procedure is the same, however.

x) The updating usually takes place when the update file contains some 1000 entries. The procedure involves checking first the integrity of the master file stored on magnetic tape and then copying it to Permanent File (PF). The update file is usually broken up in sub-groups of some 200 entries corresponding to a central processor time for the update of approximately one second per entry. During the course of updating, it is desirable to keep in the system the grand-parent, the parent and the daughter files for obvious safety reasons. When this is completed, the update file is copied to a minimum of four magnetic tapes with at least two at low density. These tapes are to be stored at different locations, again for obvious safety reasons. It may then be decided to obtain a printed copy of the BTN (~ 90 minutes of printer time). After a final check, the PF's are then purged.

This procedure normally requires two days if one does not buy block time on the computer. For this reason, updates are done on weekends when the computer is not too busy. This also allows us to benefit freely of the PF devices since there are no user charges during this period. Otherwise, the very large size of the files (~11000 PRUS/each) would result in a daily charge of

~ $200.00 at other times. Similarly, for magnetic tapes, as for the PF, we keep copies of the grandparents, parents and created files.

D - COMPUTER PROGRAMMES RELATED TO THE BIBLIOGRAPHY

i) Programme SISYPHE (version #9)

This is the programme that is used to update and/or obtain a listing of the BTN. Its Fortran version consists of ~ 2400 cards and its binary version is 166 PRUS (1 physical record units = 64 words).

Basically, this programme handles the updating procedure as follows. The update file is checked for gross errors upon reading. Each update record is then handled by a subroutine (appropriately called "FUSSYAL") which does left and right justification, puts the full stops at the appropriate places, etc. The update records are then given an ascending order tag based on the chemical formula (for sections 5 and 6) or the name and year of the journal (for sections 7 to 47.). They are then ordered, one by one, at which time the field of the author's name is scanned and each author's name is stored on a file with other information (i.e. the address of the insertion of the record, etc.). Scanning stops after encountering a full stop symbol; this allows to write "editor's notes" or "et al" in the authors field without these words appearing in the author index! After the bibliography file is updated, the author index is in turn updated using the parent file and the

author file just generated from the update. Various internal consistency checks are then performed and the programme terminates after giving, if requested, a copy of the updated file.

ii) Programme KØRECT5

This is a programme whose purpose it is to correct or delete records from the BTN file. Various modes of operation are possible depending on the type of correction requested.

iii) Format of References Entries for Above Two Programmes (5 cards per record)

Card 1	Col 1	: 1
	Col 2-3	: Section number } key #1
	Col 4-8	: Page
	Col 9-14	: Type of study key #2
	Col 15-16	: Year of publication (last 2 digits)
	Col 17-18	: Journal and volume
	Col 49-80	: Formula of compound studied, if applicable
Card 2	Col 1	: 2
	Col 2-8	: Same as for card 1
	Col 9-80	: Title of paper
Card 3	Col 1	: 3
	Col 2-8	: Same as for card 1
	Col 9-80	: Title continuation, if necessary
Card 4	Col 1	: 4
	Col 2-8	: Same as for card 1
	Col 9-80	: Author's list
Card 5	Col 1	: 5
	Col 2-8	: Same as for card 1
	Col 9-80	: Author's list continuation, if necessary.

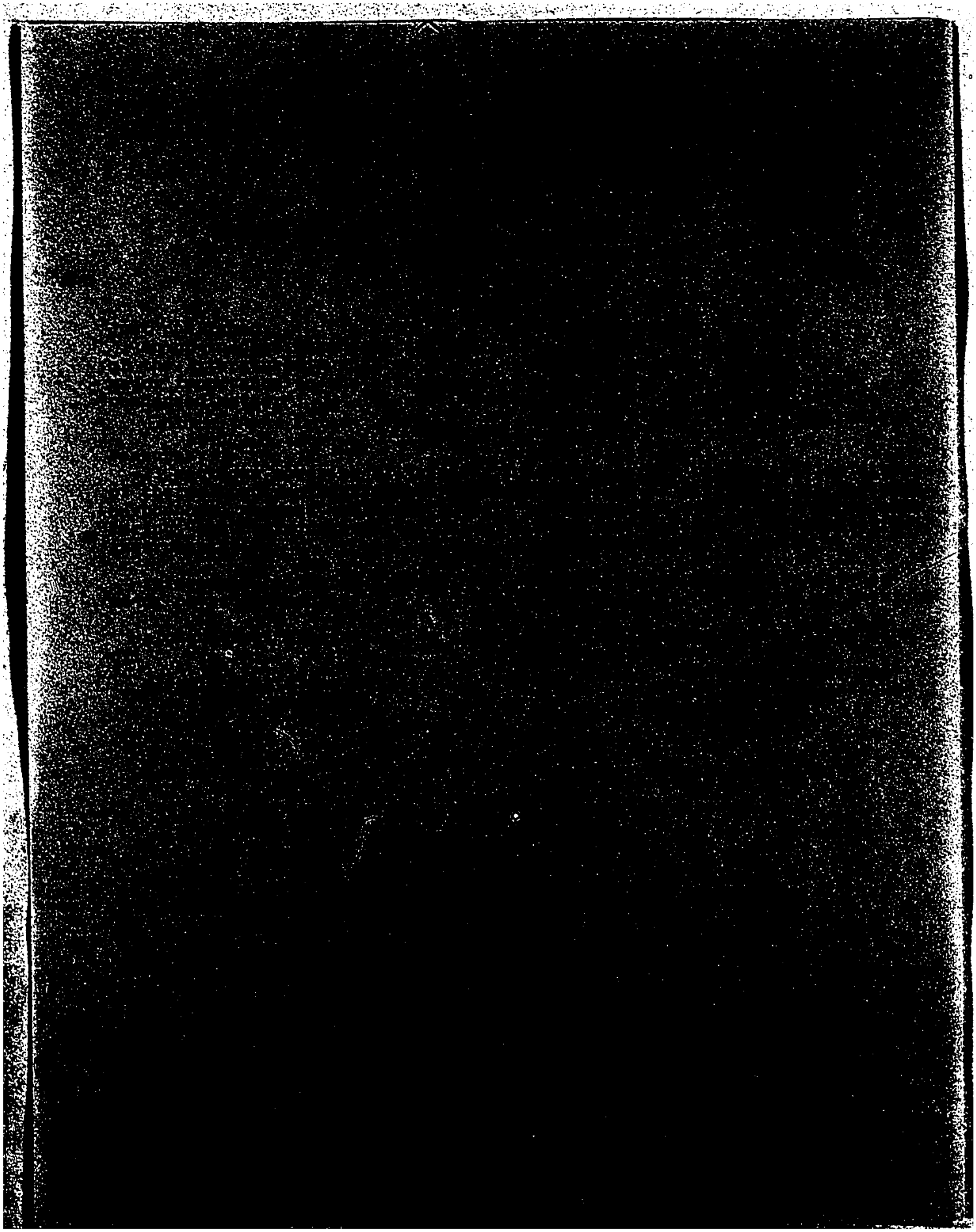

SECTION 5 -STRUCTURE AND CROSS-SECTION DETERMINATIONS . . . . . .

1005 FE*F2, ... A2 . . . PHYS. REV. VOL.30, ... 779, (1957).
*NEUTRON DIFFRACTION STUDIES OF ANTIFERROMAGNETISM IN MANGANOUS FLUORIDE AND SOME ISOMORPHOUS COMPOUNDS.
*ERICKSON(A.A.).

1006 FE*F3, ... A4 . . . J. PHYS. C VOL.7, ... 783, (1974).
*A NEUTRON DIFFRACTION DETERMINATION OF COVALENCY PARAMETERS FOR FE(3+) AND CR(3+) IN FE*F3 AND CR*F3.
*JACOBSON(A.J.), MCBRIDE(E.), FENDER(B.E.F.).

1007 FE*F3, ... A2 . . . PHYS. REV. VOL.112, ... 1132, (1958).
*ANTIFERROMAGNETIC PROPERTIES OF THE IRON-GROUP TRIFLUORIDES.
*HOLLAN(E.O.), CHILD(H.R.), KOEHLER(W.C.), WILKINSON(M.K.).

1008 FE-GA, ... A2 . . . . . REF. SECTION 3, 67/HOLDEN, ...

1009 FE-GA-O, ... A1,A2 . . . PHYS. STAT. SOL. 29, ... 323, (1968).
*A NEUTRON DIFFRACTION STUDY ON GALLIUM-SUBSTITUTED MAGNETITE.
*GAMARI-SEALE(H.), PAPAMANTELLOS(P.).

1010 (FE-GA)*O4, ... A2 . . . . . COMP. REND. 260, ... 6075, (1965).
*ETUDE D'UNE SPINELLE FER GALLIUM PAR DIFFRACTION DE NEUTRONS.
*OLES(A.).

1011 (FE-GA)*O3, ... A2 . . . . . J. PHYSIQUE TOME 27, ... 433, (1966).
*STUDY OF FE(1.15)-GA(0.85)*O3 BY MOSSBAUER EFFECT, X-RAYS, NEUTRON DIFFRACTION AND MAGNETIC MEASUREMENTS.
*BERTAUT(E.F.), MASS(G.) ET AL. (IN FRENCH).

1012 (FE-GA)*O4, ... A2 . . . . . ACTA PHYS. POLON. VOL.38, ... 125, (1966).
*NEUTRON DIFFRACTION STUDY OF THE GA2*O3*FE*O-FE2*O3*FE*O SYSTEM.
*OLES(A.). (IN FRENCH).

1013 (FE-GA)*O3, ... A1 . . . . . J. PHYS. CHEM. SOL. 28, ... 1451, (1967).
*ETUDE CRISTALLOGRAPHIQUE DU COMPOSE FE(X)*CA(2-X)*O3.
*OFLAPALME(A.).

1014 (FE-GA)*O3, ... A2,A4 . . . . REF. SECTION 3, 66/BERTAUT, ...

1015 FE-GARNETS (RARE-EARTH), ... A4 . . . . . J. PHYSIQUE TOME 32 COL.1 VOL.1, ... 212, (1971).
*NEUTRON DIFFRACTION STUDY OF SOME RARE EARTH IRON GARNETS RIG (R=ER,DY, YB, IM).
*TCHEOU(F.), BERTAUT(E.F.), FUESS(H.).

1016 FE-GE, ... A1,2 . . . . . PROC. INT. CONF. (NOTTINGHAM), ... 524, (1964).
*THE CRYSTALLOGRAPHIC AND MAGNETIC STRUCTURE OF FE(1.67)-GE.
*FORSYTH(J.B.), BROWN(P.J.).

1017 FE*GE2, ... A2 . . . . . SOL. STATE COMM. 3, ... 117, (1965).
*COMMENTS ON THE MAGNETIC STRUCTURES OF DELTA-FE*GE2.
*BERTAUT(E.F.), CHENAVAS(J.).

1018 FE-GE, ... A2 . . . . . SOL. STATE COMM. 3, ... 113, (1965).
*MAGNETIC STRUCTURES IN THE IRON-GERMANIUM SYSTEM.
*MURTHY(N.S.S.), BEGUM(R.J.), SOMANATHAN(C.S.), MURTHY(N.R.L.).

1019 FE*GE2, ... A2 . . . . . SOL. STATE COMM. 4, ... 255, (1966).
*ON THE MAGNETIC STRUCTURE OF FE&GE2.
*SOLYOM(J.), KRENIE(.).

1020 FE*GE2, ... A2 . . . . . PHYS. LETT. 11, ... 215, (1964).
*ANTIFERROMAGNETIC STRUCTURE OF FE*GE2.
*KREN(E.), SZABO(P.).

1021 FE-GE, ... A2 . . . . . J. PHYS. CHEM. SOL. 26, ... 1795, (1965).
*MAGNETIC STRUCTURES OF IRON GERMANIDES.
*ADELSON(E.), AUSTIN(A.E.).

1022 FE-GE, ... A2 . . . . . REV. ELECT. COMMUN. LAB. VOL.12, 424, (1964).
*NEUTRON DIFFRACTION STUDY OF FE(1.76)-GE SINGLE CRYSTAL.
*KATSURAKI(H.), SUZUKI(K.).

1023 FE*GE, ... A2 . . . . . J. PHYS. SOC. JAPAN VOL.21, . . . 1932, (1966).
*ON THE NEUTRON DIFFRACTION STUDY OF FE*GE.
*HATANABE(H.), KUNITOMI(N.).

1024 FE-GE, ... A2 . . . . . J. PHYS. SOC. JAPAN VOL.19, . . . 863, (1964).
*NEUTRON DIFFRACTION STUDY OF FE(1.76)-GE SINGLE CRYSTALS.
*KATSURAKI(H.).

1025 FE*GE2, ... A2 . . . . . PHIL. MAG. VOL.10, ... 713, (1964).
*THE MAGNETIC STRUCTURE AND HYPERFINE FIELD OF FE*GE2.
*FORSYTH(J.B.), JOHNSON(C.E.), BROWN(P.J.).

1026 FE-GE, ... A2 . . . . . REF. SECTION 3, 67/HOLDEN, ...

1027 FE2*GE*S4, ... A2 . . . . . J. PHYS. CHEM. SOLIDS VOL.34, . . . 151, (1973).
*ETUDE CRISTALLOGRAPHIQUE ET MAGNETIQUE DE FE2*GE*S4 STRUCTURES MAGNETIQUES A 85 ET 4.2 DEGRES.
*VINCENT(H.), BERTAUT(E.F.).

1028 FE*(H*C*O2)2*2(H2*O), ... A2 . . . . . SOL. STATE COMM. VOL. 9, . . . 1633, (1971).
*ETUDE PAR DIFFRACTION NEUTRONIQUE DU FORMIATE DE FER DIHYDRATE.
*BURLET(MME.P.), BURLET(P.), BERTAUT(E.F.).

1029 FE*I2, ... A2 . . . . . SOL. STATE COMM. VOL.14 NO.2, . . . 187, (1974).
*MAGNETIC STRUCTURE OF FE*I2 BY NEUTRON DIFFRACTION EXPERIMENTS.
*GELARD(J.), FERT(A.R.), MERIEL(P.), ALLAIN(Y.).

1030 FE-(IR), ... A4 . . . . . REF. SECTION 3, 65/COLLINS, ...

1031 FE*LA*O3, ... A4 . . . . . PROC. INT. CONF. (NOTTINGHAM), . 327, (1964).
*NEUTRON DIFFRACTION DATA AND COVALENCY EFFECTS.
*NATHANS(R.), WILL(G.), COX(D.E.).

1032 (FE-LI)*(LI-FE-CR)2*O4, ... A2 . . . . . ACTA PHYS. POLON. VOL.A44, . . . 587, (1973).
*THE INFLUENCE OF THERMAL TREATMENT ON THE MAGNETIC STRUCTURE OF THE FERRITE FE(X)-LI(1-X)-(LI-FE-CR)2*O4.
*DARGEL(L.), KUBEL(W.), MIGON(K.).

1033 FES*LI*O8, ... A2 . . . . . COLL. INTER. N.126 (GRENOBLE), . . . 79, (1963).
*SUBLATTICE MAGNETIZATION IN LITHIUM FERRITE AS A FUNCTION OF TEMPERATURE
*PRINCE(E.).

Fig. A3-2. Typical page from a section where the entries deal with particular substances; here, the ordering is based on chemical formulae. This is reproduced from the second edition of the bibliography [LA74].

SECTION 9A-DIFFRACTION: REVIEW PAPERS . . . . . .

1 ADV. INORG. CHEM. RADIOCHEM. 8, 225, (1966). APPLICATIONS IN INORGANIC CHEMISTRY (REVIEW)
NEUTRON DIFFRACTION AND ITS
BACON(G.E.).

2 ADV. STRUC. RES. DIFFR. METHOD 1, 1, (1966). APPLICATION
THE DETERMINATION OF CRYSTAL STRUCTURES BY NEUTRON-DIFFRACTION
MEASUREMENTS (REVIEW).
BACON(G.E.).

3 ADV. STRUC. RES. DIFFR. METHOD 2, 1, (1966). BY NEUTRON DIFFRACTION (REVIEW)
THE INVESTIGATION OF MAGNETIC STRUCTURES
BACON(G.E.).

4 ADV. STRUC. RES. DIFFR. METHOD 2, 1, (1966). BY NEUTRON DIFFRACTION (REVIEW)
THE INVESTIGATION OF MAGNETIC STRUCTURES
BACON(G.E.).

5 AMER. J. PHYS. VOL.22, ... 263, (1954). . . . . .
TECHNIQUES AND APPLICATIONS OF NEUTRON DIFFRACTION (REVIEW).
WILKINSON(H.K.).

6 ANN. DE PHYSIQUE TOME 7 NO.4, . 203, (1972). . . . . .
MAGNETIC STRUCTURES (REVIEW PAPER).
BERTAUT(E.F.). (PRESENTED AT AUTRANS SUMMER SCHOOL 1972).

7 ANN. REV. BIOPHYS. BIOENGNG. 1, . 529, (1972). . . . . .
NEUTRON SCATTERING (REVIEW).
SCHOENBORN(B.P.), NUNES(A.C.).

8 AT. ENERGY AUST. VOL.12, ... 2, (1969). . . . . .
NEUTRON DIFFRACTION IN STRUCTURAL AND QUANTUM CHEMISTRY (REVIEW PAPER).
MASLEN(E.N.).

9 CAHIERS DE PHYS. VOL.113, ... 29, (1960). . . . . .
THE APPLICATION OF NEUTRON DIFFRACTION TO THE STUDY OF MAGNETIC
SUBSTANCES (REVIEW PAPER).
MERIEL(P.). (IN FRENCH).

10 CHEM. APPL. THERMAL NEUTRON SCAT 278, (1973). . . .T,E. . . . . .
NEUTRON DIFFRACTION AND COVALENCY (REVIEW).
JACOBSON(A.J.). (IN BOOK: CHEMICAL APPLICATIONS OF THERMAL NEUTRON
SCATTERING. ED. BY B.T.M. WILLIS; OXFORD UNIV. PRESS: LONDON).

11 CHEM. APPL. THERMAL NEUTRON SCAT 278, (1973). . . .T,E. . . . . .
NEUTRON DIFFRACTION AND COVALENCY (REVIEW).
JACOBSON(A.J.). (IN BOOK: CHEMICAL APPLICATIONS OF THERMAL NEUTRON
SCATTERING. ED. BY B.T.M. WILLIS; OXFORD UNIV. PRESS: LONDON).

12 ENDEAVOUR VOL.25, ... 129, (1966). . . . . .
THE APPLICATIONS OF NEUTRON DIFFRACTION (REVIEW PAPER).
BACON(G.E.).

13 IAEA SYMP. GRENOBLE, ... 529, (1972). . . . . .
MAGNETISM IN ONE AND TWO DIMENSIONS (REVIEW PAPER).
BLUME(M.).

14 INSTRUM. EXP. TECH. NO.2, . . . 183, (1960). . . .T. . . . . .
THEORY OF NEUTRON CRYSTAL MONOCHROMATORS (REVIEW).
ARKOV(YU.G.).

15 J. PHYS. SOC. JAPAN VOL.17 B-II, 324, (1962). . . .E. . . . . .
RECENT PROGRESS IN NEUTRON DIFFRACTION.
BACON(G.E.).

16 NAT. BUR. STAND. PUBL. NO.301, . 57, (1969). . . . . .
NEUTRON AND X-RAY DIFFRACTION TECHNIQUES (REVIEW).
BACON(G.E.). (U.S. NBS SPEC. PUBL. 1967; PUBL. 1969).

17 NATURE VOL.164, ... 205, (1949). . . . . .
NEUTRON DIFFRACTION BY CRYSTALS (REVIEW).
LONSDALE(K.).

18 NUCLEONICS VOL.3 NO.2, . . . 17, (1948). . . . . .
NEUTRON DIFFRACTION AND ASSOCIATED STUDIES-II. (REVIEW).
HOLLAN(E.O.), SHULL(C.G.).

19 NUCLEONICS VOL.3 NO.1, . . . 8, (1948). . . . . .
NEUTRON DIFFRACTION AND ASSOCIATED STUDIES-I. (REVIEW).
HOLLAN(E.O.), SHULL(C.G.).

20 NUCLEONICS VOL.7 NO.6, . . . 31, (1950). . . .E. . . . . .
RECENT APPLICATIONS OF NEUTRON DIFFRACTION.
WEBER(A.H.).

21 PROC. ROY. SOC. A VOL.196, . . . 50, (1949). . . .T. . . . . .
NEUTRON DIFFRACTION.
BACON(G.E.), THEWLIS(J.).

22 PURE APPL. CHEM. VOL.18, . . . 217, (1969). . . . . .
NEUTRON DIFFRACTION STUDIES OF ORGANIC MOLECULES (REVIEW PAPER).
BACON(G.E.).

23 REP. PROGR. PHYS. VOL.16, . . . 1, (1953). . . .E. . . . . .
NEUTRON DIFFRACTION (REVIEW).
BACON(G.E.), LONSDALE(K.).

24 SCIENCE VOL.108, . . . 69, (1948). . . . . .
X-RAY, ELECTRON, AND NEUTRON DIFFRACTION (REVIEW).
SHULL(C.G.), HOLLAN(E.O.).

25 SOL. STATE PHYS. VOL.2, . . . 137, (1956). . . . . .
APPLICATIONS OF NEUTRON DIFFRACTION TO SOLID STATE PROBLEMS (REVIEW).
SHULL(C.G.), HOLLAN(E.O.). (REFER TO SECTION 4).

26 SOV. PHYS. USPEKHI VOL.7, . . . 855, (1965). . . . . .
STRUCTURE OF ANTIFERROMAGNETS (REVIEW PAPER).
FARZTDINOV(M.M.).

27 USPEKHI FIZ. NAUK VOL.45, . . . 481, (1951). . . .T,E. . . . . .
STRUCTURAL NEUTRONOGRAPHY (REVIEW PAPER).
OZEROV(R.P.). (IN RUSSIAN).

Fig. A3-3. Typical page from a section where the entries deal with a general topic; here, the ordering is based on the name of the journals and their year of publication. This is also reproduced from the second edition of the bibliography [LA74].

Fig. A3-4. Typical page from the author index, also reproduced from the second edition of the bibliography [LA74]. The composite number in brackets refer to the section and rank (within this section) where the entry is explicitely listed.

INDEX

Fig. A3-5. Reproduction of the index from the last printed page of the second edition of the bibliography [LA74], i.e. page 527. This should help to illustrate the size of the project as well as the diversity of the topics covered.

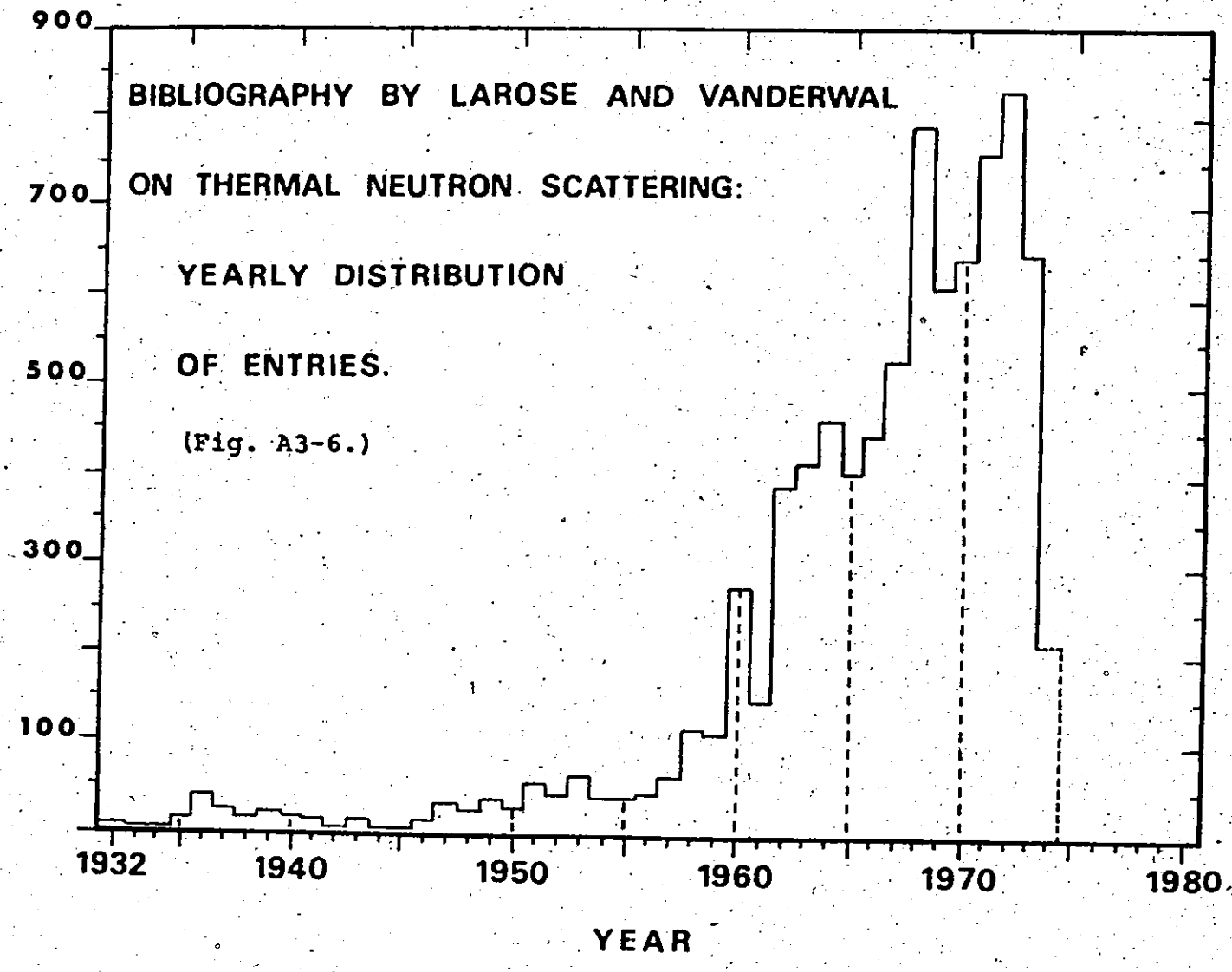
BIBLIOGRAPHY BY LAROSE AND VANDERWAL
ON THERMAL NEUTRON SCATTERING:
YEARLY DISTRIBUTION
OF ENTRIES.
(Fig. A3-6.)
900
700
500
300
100
1932
1940
1950
1960
1970
1980
YEAR

BIBLIOGRAPHY

A-TECHNICAL REFERENCES AND SUPPLIERS

T 1: SYLVANIA-EMISSIVE/PORTSMOUTH-AV/EXETER,N.H.03833,USA.
TUNGSTEN MATERIAL

T 2: THERMON-CANADA/45,NANTUCKET-BLVD/SCARBOROUGH,ONTARIO.
HEAT-TRANSFER NO.185

T 3: WILLIAMS+WILSON/71,FRONT-ST-EAST/TORONTO,ONTARIO.
FIBERFRAX REFRACTORY

T 4: FERRO-ENAMELS-CANADA/354,DAVIS-RD/OAKVILLE,ONTARIO.
KANTHAL A1 STRIP

T 5: THERMO-ELECTRIC-CANADA/12,RUTHERFORD-RD/BRAMPTON,ONT.
THERMOCOUPLE:5K1110A

T 6: WESTRONIC/3605,MCCART/FORT-WORTH,TEXAS,USA.
CHART RECORDER M11A

T 7: HEWLETT-PACKARD-CANADA/50,GALAXY-BLVD/REXDALE,ONTARIO.
DIFF.VOLTMETER 3420A

T 8: DAVIS-CONTROLS/4097,MCINTOSH-PLACE/BURLINGTON,ONTARIO.
MERCOID-DA31-3-3A

T 9: GEORGE-KELK-LTD/TORONTO,ONTARIO.
STEDIVOLT; NO. SL15T

T10: ALCATEL/8650,LE-CREUSOT/ST-LEONARD/MONTREAL,QUEBEC.
PRIMARY PUMP NO.2012

T11: EDWARDS-VACUUM/430,SOUTH-SERVICE-RD-WEST/OAKVILLE,ONT.
OIL DIFF. PUMP E02

T12: DOW-CORNING SILICONES/1,TIPPET-RD/DOWNSVIEW,ONTARIO.
DIFF. PUMP OIL 704

T13: NRC-EQUIPMENT-CORP/NEWTON-HIGHLANDS,61/MASS.,USA.
IONIZATION MANOMETER

T14: KEITHLEY:TECHNO-PRODUCTS/STITTSVILLE,ONTARIO.
MULTIMETER NO.160

B-HANDBOOKS

H 1: A.I.P. HANDBOOK;MCGRAW-HILL;NY,USA(1957).
ED:GRAY/DE.

H 2: A.I.P. HANDBOOK;2ND EDITION;MCGRAW-HILL;NY,USA(1963)
ED:GRAY/DE.

H 3: HANDBOOK/SPACINGS/METALS/ALLOYS;PERGAMON,NY,USA(1958)V1
PEARSON/WB.

H 4: HANDBOOK/SPACINGS/METALS/ALLOYS;PERGAMON,NY,USA(1967)V2
PEARSON/WB.

H 5: HANDBOOK/CHEM./PHYS.;49TH ED;CHEM. RUBBER CO;CLEVELAND
ED:HEAST/RC.

H 6: HANDBOOK OF PHYSICS;MCGRAW-HILL;NY,USA(1958)
ED:CONDON/EU,ET-AL.

H 7: NEUTRON CROSS-SECTIONS;2ND ED;BNL;UPTON,NY,USA(1958)
ED:HUGHES/DJ,ET-AL.

C-GENERAL REFERENCES

G 1: /..NEUTRONS:A BIBLIOGRAPHY(1932-74);PLENUM;NY,USA(1974)
LAROSE/A,VANDERHAL/J

G 2: BIBLIOGRAPHY/THERMAL NEUTRONS(1963-72);MCMASTER U(1973)
LAROSE/A,VANDERHAL/J

G 3: INELASTIC SCATT./SOLIDS/LIQUIDS-1960;PROCEEDINGS, 1 V.
PUB:IAEA,VIENNA-1961

G 4: INELASTIC SCATT./SOLIDS/LIQUIDS-1962;PROCEEDINGS, 2 V.
PUB:IAEA,VIENNA-1963

G 5: INELASTIC SCATTERING OF NEUTRONS-1964;PROCEEDINGS,2 V.
PUB:IAEA,VIENNA-1965

G 6: NEUTRON INELASTIC SCATTERING-1968;PROCEEDINGS,2 V.
PUB:IAEA,VIENNA-1968

G 7: NEUTRON INELASTIC SCATTERING-1972;PROCEEDINGS,2 V.
PUB:IAEA,VIENNA-1972

G 8: INSTRUMENTATION/NEUTRON/SCATT.RES.-1969;PROCEEDINGS
PUB:IAEA,VIENNA-1970

G 9: NEUTRON DIFFRACTION;2ND ED;OXFORD(1962)
BACON/GE.

G10: INTERACTION/RADIATION/SOLIDS;N-HOLLAND;AMSTERDAM(1964)
ED:STRUMANE/R, ET AL

G11: THERMAL NEUTRON SCATTERING;ACADEMIC PRESS;NY,USA(1965)
ED:EGELSTAFF/PA.

G12: METALL.SOCIETY CONF(1967);GORDON+BREACH;NY,USA(1968)
ED:ROWLAND/TJ, ET AL

G13: THEORY OF THERMAL NEUTRON SCATTERING;OXFORD(1971)
MARSHALL/W,LOVESEY/S

G14: DYNAMICAL THEORY OF CRYSTAL LATTICES;OXFORD(1954,68)
BORN/M,HUANG/K.

G15: QUANTUM THEORY OF SOLIDS;OXFORD(1955,65)
PEIERLS/RE.

G16: THEORY/PROPERTIES/METALS/ALLOYS;DOVER;NY,USA(1958)
MOTT/NF,JONES/H.

G17: ELECTRONS AND PHONONS;OXFORD(1960,62)
ZIMAN/JM.

G18: PHONONS AND PHONON INTERACTIONS;BENJAMIN;NY,USA(1964)
ED:BAK/TA.

G19: LATTICE DYNAMICS;PERGAMON;LONDON,ENGLAND(1965)
ED:WALLIS/RF.

G20: PRINCIPLES/THEORY/SOLIDS;CAMBRIDGE UNIV. PRESS(1965)
ZIMAN/JM.

G21: PHONONS/PERFECT LATTICES../;OLIVER+BOYD;EDIMBURGH(1966)
ED:STEVENSON/RWH.

G22: INTROD.SOL.STATE PHYSICS;3RD ED;WILEY;NY, USA (1967)
KITTEL/C.

G23: SOLID STATE THEORY;MCGRAW-HILL;NY,USA(1970)
HARRISSON/WA.

G24: SOLID STATE PHYSICS: ADVANCES...;ACADEMIC PRESS;NY,USA.
ED:SEITZ/F, ET AL

G25: SOLID STATE PHYSICS: SUPPLEMENTS;ACADEMIC PRESS;NY,USA.
ED:SEITZ/F, ET AL

G26: SUPERCONDUCTIVITY;GORDON+BREACH;NY,USA
ED:WALLACE/PR.

D-SPECIFIC REFERENCES

N.B. : WORDS IN BRACKETS [] ARE KEY WORDS FROM TITLE AND/OR EXPLICIT REFERENCE NUMBERS IN ≠LA74≠.

* * * * * * * * * * * *

1- AS70 : TRACER DIFFUSION DATA...;PLENUM;NY,USA. .....(1970).
ASKILL/J.

2- AX73 : PHYS.REV.B . . . . . 8, 1965,(1973).
AXE/JD,SHIRANE/G. [NEUTRON/PHONONS/NB3*SN]
[IN ≠LA74≠ : (6 ,1691)]

3- BA37 : PHYS.REV.. . . . . 52, 688,(1937).
BARDEN/J. [/MONOVALENT METALS.]

4- BA53 : REP.PROG.PHYS. . . . . 16, 1,(1953).
BACON/GE,LONSDALE/K. [NEUTRON DIFFRACTION]
[IN ≠LA74≠ : (9A, 23)]

5- BA62 : IN GENERAL REFERENCE NUMBER G 9. . . . .,.....,(1962).
BACON/GE.

6- BL28 : Z.PHYSIK . . . . . 52, 555,(1928).
BLOCH/F. [/ELEKTRONEN/KRISTALL.]

7- BO12 : PHYS.ZEIT. . . . . 13, 297,(1912).
BORN/M,VON-KARMAN/T. [UBER SCHWINGUNGEN/]

8- BO27 : ANN.PHYSIK . . . . . 84, 457,(1927).
BORN/M,OPPENHEIMER/R. [QUANTENTHEORIE/MOLEK.]

9- BO51 : PHYS.REV.. . . . . 84, 836,(1951).
BOHM/D,STAVER/T. [/COLLECTIVE/VIBRATIONS]

10- BO54 : IN GENERAL REFERENCE NUMBER G14. . . . .,.....,(1954).
BORN/M,HUANG/K.

11- BO63 : PHYS.REV.. . . . . 129, 1063,(1963).
BOLEF/DI,DE-KLERK/J. [ELASTIC CONSTANTS/CR]

12- BO73 : PH.D.THESIS,MCMASTER,UNPUBLISHED.. . . . .,(1973).
BORONKAY/S. [CRITICAL/NEUTRONS/FE]

13- BR36 : PHYS.REV.. . . . . 49, 519,(1936).
BREIT/G,WIGNER/E. [CAPTURE/SLOW NEUTRONS]
[IN ≠LA74≠ : (7A, 59)]

14- BR53 : CANAD.J.PHYS. . . . . 31, 432,(1953).
BROCKHOUSE/BN. [RESONANT SCATTERING/]
[IN ≠LA74≠ : (7A, 22)]

15- BR59 : REV.SCIENT.INST. . . . . 30, 136,(1959).
BROCKHOUSE/BN. [FILTER/PURE BEAM]
[IN ≠LA74≠ : (20D, 30)]

16- BR60 : IN GENERAL REFERENCE NUMBER G 3. . . . . 113,(1960).
BROCKHOUSE/BN. [METHODS/SPECTROMETRY.]
[IN ≠LA74≠ : (18A, 13)]

17- BR60A: IN GENERAL REFERENCE NUMBER G 3. . . . . 531,(1960).
BROCKHOUSE/BN,ARASE/T,CAGLIOTI/ [CRYSTAL DYNAMICS OF PB]
[IN ≠LA74≠ : (6 ,1801)]

18- BR61 : PHYS.REV.LETT. . . . . 7, 93,(1961).
BROCKHOUSE/BN,RAO/KR,WOODS/ADB. [IMAGE/FERMI/LATTICE/PB]
[IN ≠LA74≠ : (0 ,1816)]

19- BR64 : IN GENERAL REFERENCE NUMBER G10. . . . . 580,(1964).
BROCKHOUSE/BN,HAUTECLER/S,ETAL. [INELASTIC SCATTERING/]
[IN ≠LA74≠ : (17A, 46)]

20- BR65 : IN GENERAL REFERENCE NUMBER G21. . . . . 110,(1965).
BROCKHOUSE/BN. [NEUTRON/PHONONS]
[IN ≠LA74≠ : (10A, 17)]

21- BR67 : IN GENERAL REFERENCE NUMBER G12. . . . . 43, 161,(1967).
BROCKHOUSE/BN,HALLMAN/ED,NG/SC. [ATOMIC VIBRATIONS/]
[IN ≠LA74≠ : (10C, 52)]

22- BR68 : IN GENERAL REFERENCE NUMBER G 6. . . . . 2, 259,(1958).
BROCKHOUSE/BN,DEWIT/GA,ETAL... [MCMASTER/SPECTROMETERS]
[IN ≠LA74≠ : (23 , 33)]

23- BR72 : BULL.AMER.PHYS.SOC. . . . . 17, 123,(1972).
BROCKHOUSE/BN;SHIRANE/G. [T-DEPENDENCE/GRAPHITE]
[IN ≠LA74≠ : (6 , 201)]

24- BU69 : PHYS.REV. . . . . 180, 755,(1969).
BUYERS/WJL,COWLEY/RA. [/DYNAMICS/K/ANHARMONIC]
[IN ≠LA74≠ : (6 ,1244)]

25- CA69 : IN GENERAL REFERENCE NUMBER G26. . . . . 1, 491,(1959).
CARBOTTE/JP. [CALCULATION/TC/PHONON/]

26- CH64 : SOL.STATE COMM. . . . . 2, 73,(1964).
CHEN/SH,BROCKHOUSE/BN. [LATTICE VIBRATIONS/W]
[IN ≠LA74≠ : (6 ,2276)]

27- CH64A: PH.D.THESIS,MCMASTER,UNPUBLISHED. . . . . ,(1964).
CHEN/SH. [NEUTRON/LATTICE/METALS]
[IN ≠LA74≠ : (6 ,2271)]

28- CH66 : J.APPL.PHYS. . . . . 37, 3567,(1966).
CHANG/YA,HIMMEL/L. [T-DEP./CIJ/CU/AG/AU]

29- CL59 : Z.NATURFORSCH. . . . . A14, 99,(1959).
CLUSIUS/K,FRANZONISI/P. [/CP/CV/MO/W.]

30- CL62 : Z.NATURFORSCH. . . . . A17, 522,(1962).
CLUSIUS/K,FRANZOSINI/P. [/CP/CV/GR.]

31- CO56 : J.INST.METALS. . . . . 84, 346,(1956).
COLES/BR. [LATTICE SPACINGS/PD-AG]

32- CO63 : ADV.PHYS.(PHIL.MAG.SUPPL.) . . . . . 12, 421,(1963).
COWLEY/RA. [/DYNAMICS/ANHARMONIC/]
[IN ≠LA74≠ : (10D, 2)]

33- C064 : IN GENERAL REFERENCE NUMBER G 5. . . . . 1, 3,(1964).
COCHRAN/W. [/DISPERSION/METALS.]
[IN ≠LA74≠ : (10B, 35)]

34- C064A: PHYS.REV.. . . . . 134, A981,(1964).
COWLEY/RA. [/TRANSITIONS/SR*TI*03/]
[IN ≠LA74≠ : (6 ,2092)]

35- C067 : ACTA CRYST.. . . . . 23, 357,(1967).
COOPER/MJ,NATHANS/R. [RESOLUTION/PHONON]
[IN ≠LA74≠ : (17D, 1)]

36- C067A: PROC.PHYS.SOC.LONDON . . . . . 90, 1127,(1967).
COWLEY/RA. [/SOUND OF SOLIDS.]
[IN ≠LA74≠ : (10D, 52)]

37- C068 : REP.PROG.PHYS. . . . . 31, 123,(1968).
COWLEY/RA. [ANHARMONIC CRYSTALS]

38- C068A: IN GENERAL REFERENCE NUMBER G 6. . . . . 1, 281,(1968).
COWLEY/RA,BUYERS/WJL,SVENSSON/ [NEUTRON/ELASTIC CONST.]
[IN ≠LA74≠ : (10G, 37)]

39- C070 : IN GENERAL REFERENCE NUMBER G24. . . . . 24, 37,(1970).
COHEN/ML,HEINE/V. [FITTING/PSEUDO...]

40- C070A: PH.D.THESIS,MCMASTER,UNPUBLISHED.. . . . . ,(1970).
COPLEY/JRD. [/VIBRATIONS/RB METAL]
[IN ≠LA74≠ : (6 ,1955)]

41- C071 : SOL.STATE COMM.. . . . . 9, 531,(1971).
COPLEY/JRD. [...≠FORBIDDEN MODES≠..]
[IN ≠LA74≠ : (17A, 93)]

42- C074 : PHYS.REV.B . . . . . 9, 1261,(1974).
COWLEY/ER,SHUKLA/RC. [THEORIES/ANHARMONICITY]

43- CR60 : IN GENERAL REFERENCE NUMBER G 3. . . . . , 549,(1960).
CRIBIER/D,JACROT/B,SAINT-JAMES/ [DIFFUSION/NEUTRONS/]
[IN ≠LA74≠ : (6 , 582)]

44- DE56 : IN GENERAL REFERENCE NUMBER G24. . . . . 2, 219,(1956).
DE-LAUNAY/J. [/THEORY/VIBRATIONS.]

45- DE67 : PHYS.REV.. . . . . 164, 993,(1967).
DEEGAN/RA,THOSE/WD. [MODIFICATIONS/UPH/NB.]

46- DU63 : PHYS.STAT.SOL. . . . . 3, 2253,(1963).
DUTTA/BN,DAYAL/B. [LATT.CONST./PD/H/*878C]

47- DU72 : CANAD.J.PHYS.. . . . . 50, 2915,(1972).
DUTTON/DH,BROCKHOUSE/BN,ETAL. [/DYNAMICS/PT/NEUTRON/]
[IN ≠LA74≠ : (6 ,1944)]

48- DY70 : IN GENERAL REFERENCE NUMBER G 8. . . . . 105,(1970).
DYMOND/RR,BROCKHOUSE/BN. [REFLECTIVITY/NEUTRONS]
[IN ≠LA74≠ : (17A, 37)]

49- EI07 : ANN.PHYSIK . . . . . 22, 180,(1907).
EINSTEIN/A. [PLANCKSCHE THEORIE/CV]

50- EP50 : PHYSICA. . . . . 16, 792,(1950).
EPPELSHEIMER/DS,PENMAN/RR. [THERMAL DILATATION/CU]

51- ES38 : ARCH.EISENHUTTENW. . . . . 12, 157,(1938).
ESSER/H,EILENDER/W,BUNGARDT/K. [ROENTGEN/METALS]

52- FE36 : RICERCA SCI. . . . . 7/II, 13,(1936).
FERMI/E. [/NEUTRONS/HYDROGENOUS/]
[IN ≠LA74≠ : (7B, 110)]

53- FE63 : PHYS.REV. . . . . 130, 1324,(1963).
FEATHERSTON/FH,NEIGHBOURS/JR. [ELASTIC CONST./TA/W/MO]

54- FO57 : PROC.PHYS.SOC.LONDON . . . . . 870, 1143,(1957).
FOREMAN/AJE,LOMER/WM. [HARMONIC FORCES]
[IN ≠LA74≠ : (10B, 202)]

55- FR53 : ACTA CRYST. . . . . 6, 19,(1953).
FROHNMEYER/G,GLOCKER/R. [GITTERKONSTANTEN---]

56- GE62 : PHYS.REV.LETT. . . . . 8, 313,(1962).
GEBALLE/TH,MATTHIAS/BT,ETAL... [SUPERCONDUCTIVITY/MO.]

57- GE69 : REV.SCIENT.INST. . . . . 40, 715,(1969).
GEHLEN/PC. [77-1300K/X-RAY/]

58- GI64 : PHYS.REV.LETT. . . . . 12, 668,(1964).
GIBSON/JW,HEIN/RA. [SUPERCONDUCTIVITY/W.]

59- GI68 : J.PHYS.CHEM.SOLIDS . . . . . 29, 1485,(1968).
GIRVAN/RF,GOLD/AV,PHILLIPS/RA. [DH-VA EFFECT/FERMI/W.]

60- GO51 : CLASSICAL MECHANICS;ADDISON-WESLEY;MASS.,USA. .....(1951).
GOLDSTEIN/H.

61- GO73 : UKR.FIZ.ZH.(USSR) . . . . . 18, 1628,(1973).
GORBACHEV/BI,IVANITSKII/PG,+AL. [FE/24C TO 874C]
[IN ≠LA74≠ : (6 , 784)]

62- HA69 : PHYS.REV. . . . . 161, 1036,(1969).
HARRISSON/WA. [TRANSITION-METAL...]

63- HA69A: PH.D.THESIS,MCMASTER,UNPUBLISHED. . . . . .(1969).
HALLMAN/ED. [DYNAMICS/IRON GROUP]
[IN ≠LA74≠ : (6 ,1765)]

64- HA70 : IN GENERAL REFERENCE NUMBER G23. . . . .,.....,(1970).
HARRISSON/WA.

65- HA70A: J.APPL.PHYS. . . . . 41, 5090,(1970).
HAHN/TA. [/EXPANSION/CU/20-800K/]

66- HE70 : IN GENERAL REFERENCE NUMBER G24. . . . . 24, 1,(1970).
HEINE/V. [THE PSEUDOPOTENTIAL...]

67- HO57 : PROC.ROY.SOC. . . . . A240, 42,(1957).
HOARE/FE,YATES/B. [LOW T(2-4.2K)CV/PD-AG/]

68- HU42 : J.INST.METALS. . . . . 68, 19,(1942).
HUME-ROTHERY/W,ANDREWS/KW. [/LATTICE/EXPANSION/CU]

69- HU58 : IN GENERAL REFERENCE NUMBER G24. . . . . 7, 213,(1956).
HUNTINGTON/HB. [/ELASTIC CONSTANTS/]

70- KA69 : PHYSICS LETTERS. . . . . 29A, 639,(1969).
KAMITAKAHARA/WA,BROCKHOUSE/BN. [CRYSTAL DYNAMICS/AG]
[IN ≠LA74≠ : (6 , 15)]

71- KA72 : PH.D.THESIS,MCMASTER,UNPUBLISHED. . . . . .(1972).
KAMITAKAHARA/WA. [DYNAMICS/IMPERFECT]
[IN ≠LA74≠ : (6 , 633)]

72- KI67 : IN GENERAL REFERENCE NUMBER G22. . . . .,.....,(1967).
KITTEL/C.

73- KO57 : IN GENERAL REFERENCE NUMBER G24. . . . . 5, 173,(1957).
KOSTER/GF. [SPACE GROUPS AND...]

74- KO59 : PHYS.REV.LETT. . . . . 2, 393,(1959).
KOHN/W. [IMAGE/FERMI/VIBRATION]

75- LA60 : ARK.FYS. . . . . 17, 369,(1960).
LARSSON/KE,DAHLBORG/U,HOLMRYD/S [TEMPERATURE/PHONONS/AL]
[IN ≠LA74≠ : (6 , 42)]

76- LA70 : M.SC.THESIS,MCMASTER,UNPUBLISHED. . . . . ,(1970).
LAROSE/A. [/PHONON/CU-NI-ZN/]
[IN ≠LA74≠ : (6 , 634)]

77- LA73 : IN GENERAL REFERENCE NUMBER G 2. . . . . ,(1973).
LAROSE/A,VANDERHAL/J.

78- LA74 : IN GENERAL REFERENCE NUMBER G 1. . . . . ,(1974).
LAROSE/A,VANDERHAL/J.

79- LE61 : IN GENERAL REFERENCE NUMBER G24. . . . . 12, 275,(1961).
LEIBFRIED/G,LUDWIG/W. [/ANHARMONIC EFFECTS/]

80- LE63 : SOV.PHYS.SOL.STATE . . . . . 5, 798,(1963).
LEKSINA/IE,NOVIKOVA/SI. [THERMAL EXPANSION/CU/]

81- LI10 : Z.PHYSIK . . . . . 11, 609,(1910).
LINDEMAN/FA. [/EIGENFREQUENZEN]

82- LO54 : PROC.ROY.SOC. . . . . A221, 206,(1954).
LOWDE/RD. [/DIFFUSE REFLECTION/]
[IN ≠LA74≠ : (6 , 771)]

83- LO62 : PROC.PHYS.SOC.LONDON . . . . . 80, 489,(1962).
LOMER/WM. [ELECTRONIC STRUCTURE..]

84- LO64 : PROC.PHYS.SOC.LONDON . . . . . 84, 327,(1964).
LOMER/WM. [FERMI SURFACE IN MO]

85- LO65 : PHYS.REV. . . . . 139,A1181,(1965).
LOUCKS/TL. [FERMI/CR/MO/W/APW]

86- LY73 : PHYS.REV.B . . . . . 8, 3493,(1973).
LYNN/JW,SMITH/HG,NICKLOW/RM. [LATTICE DYNAMICS/AU]
[IN ≠LA74≠ : (6 , 111)]

87- MA62 : PHYS.REV. . . . . 128, 2589,(1962).
MARADUDIN/AA,FEIN/AE. [SCATTERING/ANHARMONIC/]
[IN ≠LA74≠ : (10E, 24)]

88- MA63 : IN GENERAL REFERENCE NUMBER G25. . . . . 3, ... ,(1963).
MARADUDIN/AA,MONTROLL/EW,WEISS/ [/LATTICE DYNAMICS/]

89- MA66 : PHYS.REV. . . . . 141, 576,(1966).
MARTIN/DL. [CP OF CU,AG,AU/T<30K]

90- MA68 : PHYS.REV. . . . . 170, 650,(1968).
MARTIN/DL. [CP OF CU,AG,AU/T<3K]

91- MA71 : IN GENERAL REFERENCE NUMBER G25. . . . . 3, ... ,(1971).
MARADUDIN/AA,MONTROLL/EW,WEISS/ [/LATTICE DYNAMICS/]

92- MI58 : SOV.PHYS.-J.E.T.P. . . . . 34/7, 996,(1958).
MIGDAL/AB. [/ELECTRONS/LATTICE/]

93- MI63 : INDIAN J.PHYSICS . . . . . 37, 462,(1963).
MITRA/GB,MITRA/SK. [X-RAY/CU/HIGH TEMP.]

94- MI68 : PHYS.REV.LETT. . . . . 20, 798,(1968).
MILLER/AP,BROCKHOUSE/BN. [ANOMALOUS BEHAVIOR/PD]
[IN ≠LA74≠ : (6 ,1852)]

95- MI71 : CANAD.J.PHYS. . . . . 49, 704,(1971).
MIILLER/AP,BROCKHOUSE/BN. [DYNAMICS/PD/CU]
[IN ≠LA74≠ : (6 ,1850)]

96- MI75 : CANAD.J.PHYS. . . . . IN ,PRESS,(1975).
MIILLER/AP. [REAL/VIRTUAL/KOHN/PD]

97- MO58 : IN GENERAL REFERENCE NUMBER G16. . . . . ,.....,(1956).
MOTT/NF,JONES/H.

98- MO64 : IN GENERAL REFERENCE NUMBER G 5. . . . . 1, 95,(1964).
MOLLER/HB,MACKINTOSH/AR. [INELASTIC/NEUTRONS/CR]
[IN ≠LA74≠ : (6 , 516)]

99- MO68 : J.APPL.PHYS. . . . . 39, 807,(1968).
MOLLER/HB,HOUMANN/JG,ETAL... [MAGNETIC/TB/TB-HO/]
[IN ≠LA74≠ : (6 ,2135)]

100- MO72 : PHYS.REV.B . . . . . 6, 1239,(1972).
MORIARTY/JA. [TOTAL ENERGY/CU;AG,AU]

101- MO73 : SOL.STATE COMM.. . . . . 13, 1465,(1973).
MOSS/SC,KEATING/DT,AXE/JD. [T-DEPENDENCE/HCP-ZR]
[IN ≠LA74≠ : (6 ,2339)]

102- NE74 : PHYS.REV.B . . . . . 10, 612,(1974).
NELIN/G,NILSSON/G. [ANHARMONICITY/GE/880K]
[IN ≠LA74≠ : (6 , 938)]

103- NG67 : MATERIALS RESEARCH BULLETIN. . . . . 2, 69,(1967).
NG/SC,BROCKHOUSE/BN,HALLMAN/ED. [CHARACTERIZATION...]
[IN ≠LA74≠ : (5 , 693)]

104- NI41 : PHYS.REV. . . . . 60, 597,(1941).
NIX/FC,MACNAIR/D. [THERMAL EXPANSION/CU/]

105- NI67 : PHYS.REV. . . . . 164, 922,(1967).
NICKLOW/RM,GILAT/G,SMITH/HG,... [PHONON/CU/ 49K/298K.]
[IN ≠LA74≠ : (6 , 600)]

106- NI68 : IN GENERAL REFERENCE NUMBER G 6. . . . . 1, 187,(1966).
NILSSON/G. [/KOHN EFFECT IN CU]
[IN ≠LA74≠ : (6 , 579)]

107- NI69 : ACTA CRYST. . . . . A25, 547,(1969).
NIELSEN/M,MOLLER/HB. [RESOLUTION/TRIPLE-AXIS]
[IN ≠LA74≠ : (17D, 5)]

108- NI73 : PHYS.REV.B . . . . . 7, 2393,(1973).
NILSSON/G,ROLANDSON/S. [LATTICE DYN./CU/80K]
[IN ≠LA74≠ : (6 , 594)]

109- NI74 : PHYS.REV.B . . . . . 9, 3278,(1974).
NILSSON/G,ROLANDSON/S. [KOHN/FERMI/CU/NEUTRON]
[IN ≠LA74≠ : (6 , 610)]

110- OV55 : PHYS.REV. . . . . 98, 969,(1955).
OVERTON-JR/WC,GAFFNEY/J. [T-DEPENDENCE/CIJ/CU]

111- PA67 : UKAEA AERE REPORT. . . . . 5574,.....,(1967).
PAGE/DI. [S(Q,W)/GRAPHITE/1800K]
[IN ≠LA74≠ : (6 , 211)]

112- PA68 : IN GENERAL REFERENCE NUMBER G 6. . . . . 1, 325,(1966).
PAGE/DI. [/GRAPHITE/HIGH TEMP./]
[IN ≠LA74≠ : (6 , 197)]

113- PA70 : REV.INT.HAUTES TEMPER. ET REFRACT. . . . . 7, 252,(1970).
PAVESE/F,RIGHINI/F,RUFFINO/G. [/THERMAL EXPANSION/CU]

114- PE55 : IN GENERAL REFERENCE NUMBER G15. . . . . ,(1955).
PEIERLS/RE.

115- PE67 : BRIT.J.APPL.PHYS. . . . . 18, 473,(1967).
PECKHAM/GE,SAUNDERSON/DH,SHARP/ [FOCUSING/TRIPLE-AXIS/]
[IN ≠LA74≠ : (18A, 10)]

116- PO68 : PHYS.REV. . . . . 171, 727,(1968).
POWELL/BM,MARTEL/P,WOODS/ADB. [LATTICE DYNAMICS/NB-MO]
[IN ≠LA74≠ : (6 ,1686)]

117- PO72 : IN GENERAL REFERENCE NUMBER G 7. . . . . 43,(1972).
POWELL/BM,WOODS/ADB,MARTEL/P. [T-DEPENDENCE/NB]
[IN ≠LA74≠ : (6 ,1672)]

118- PO73 : J.PHYS.E . . . . . 6, 63,(1973).
POJUR/AF,YATES/B. [/300-800K/EXPANSION/CU]

119- RA60 : PHYS.REV. . . . . 118, 1545,(1960).
RAYNE/JA. [ELASTIC CONST/PD/<300K]

120- RI42 : TRANS.AM.SOC.MET. . . . . 30, 326,(1942).
RICHARDS/JW. [LINEAR EXPANSION/<TM]

121- RI70 : PHYS.REV.B . . . . . 1, 509,(1970).
RICE/TM,HALPERIN/BI. [KOHN/TUNGSTEN/CR-GROUP]
[IN ≠LA74≠ : (6 ,2269)]

122- RO66 : PHYS.REV. . . . . 149, 519,(1966).
ROTH/LM,ZEIGER/HJ,KAPLAN/TA. [RKKY/NONSPHERIC.FERMI]

123- RO66A: PH.D.THESIS,MCMASTER,UNPUBLISHED. . . . . ,(1966).
ROWE/JM. [NEUTRON SPECTROSCOPY:/]
[IN ≠LA74≠ : (6 ,2064)]

124- RO73 : J.PHYS.C . . . . . 6, 3525,(1973).
ROSS/DK. [GRAPHITE/TO 1920C]
[IN ≠LA74≠ : (6 , 212)]

125- SC72 : Z.METALLKDE. . . . . 63, 12,(1972).
SCHRODER/RH,SCHMITZ-PRANGHE/N.. [GITTERPARAMETER/<1709C]

126- SE62 : PHYS.REV. . . . . 125, 109,(1962).
SEGALL/B. [FERMI SURFACE/BANDS/CU]

127- SH63 : IN GENERAL REFERENCE NUMBER G24. . . . . 15, 221,(1963).
SHAM/LJ,ZIMAN/JM. [/ELECTRON-PHONON/]

128- SH65 : PROC.ROY.SOC. . . . . .A283, 33,(1965).
SHAM/LJ. [CALCULATION/PHONON/NA.]
[IN ≠LA74≠ : (6 ,1623)]

129- SH67 : TRANS.AMER.CRYSTALLOGRAPHIC ASSOCIATION. 3, 1,(1967).
SHULL/CG. [/INTERACTIONS/ATOMS]
[IN ≠LA74≠ : (7A, 15)]

130- SH70 : PHYS.REV.B . . . . . 1, 3982,(1970).
SHAPIRO/JN. [LINDEMANN LAW/]

131- SH71 : PHYS.REV.B . . . . . 4, 969,(1971).
SHAW/WM,MUHLESTEIN/LD. [PHONON/CR/NEUTRON...]
[IN ≠LA74≠ : (6 , 515)]

132- SI63 : PHYS.REV. . . . . 129, 1533,(1963).
SIMMONS/RO,BALLUFFI/RW. [/VACANCIES IN CU]

133- SI66 : PHYS.REV. . . . . 143, 422,(1966).
SINHA/SK. [LATTICE DYNAMICS OF CU]
[IN ≠LA74≠ : (6 , 603)]

134- SL51 : QUANTUM THEORY OF MATTER;MCGRAW-HILL;NY,USA. .....(1951).
SLATER/JC.

135- ST67 : PHYS.REV.. . . . . 163, 567,(1967).
STEDMAN/R,ALMQVIST/L,ETAL... [FERMI/PB/KOHN]
[IN ≠LA74≠ : (6 ,1822)]

136- ST68 : REV.SCIENT.INST. . . . . 39, 878,(1968).
STEDMAN/R. [/FOCUSING/SCATTERING/]
[IN ≠LA74≠ : (18A, 26)]

137- SV67 : PHYS.REV.. . . . . 155, 619,(1967).
SVENSSON/EC,BROCKHOUSE/BN,ROWE/ [CRYSTAL DYNAMICS OF CU]
[IN ≠LA74≠ : (6 , 606)]

138- SV67A: PH.D.THESIS,MCMASTER,UNPUBLISHED.. . . . . ,(1967).
SVENSSON/EC. [DYNAMICS/CU/CU-AU]
[IN ≠LA74≠ : (6 , 587)]

139- TA63 : PHYS.REV.. . . . . 131, 1995,(1963).
TAYLOR/PL. [THEORY/KOHN ANOMALIES/]
[IN ≠LA74≠ : (10B, 121)]

140- TU68 : IN GENERAL REFERENCE NUMBER G 6. . . . . 1, 431,(1968).
TUNKELO/E,KUOPPAMAKI/R,PALMGREN [PHONONS/LIQUID BISMUTH]
[IN ≠LA74≠ : (6 , 168)]

141- VA54 : PHYS.REV.. . . . . 95, 249,(1954).
VAN-HOVE/L. [CORRELATIONS/SCATT.]
[IN ≠LA74≠ : (14A, 42)]

142- VO65 : CANAD.J.PHYS.. . . . . 43, 1187,(1965).
VOSKO/SH,TAYLOR/R,KEECH/GH. [/ELECTRON-ION/PHONON/]

143- WA70 : PHYSICS LETTERS. . . . . 31A, 240,(1970).
WALKER/E,ORTELLI/J,PETER/M. [LIJ/PD-RH/PD-AG/≠300K]

144- WE71 : J.APPL.PHYS. . . . . 42, 4736,(1971).
WERNER/SA,PYNN/R. [RESOLUTION EFFECTS/]
[IN ≠LA74≠ : (17D, 10)]

145- WE74 : SOL.STATE COMM.. . . . . 15, 281,(1974).
WEINMANN/C,STEINEMANN/S. [..ELASTIC CONSTANTS/PD]

146- WI54 : PHYS.REV.. . . . . 94, 1228,(1954).
WICK/GC. [/NEUTRONS/LIGHT NUCL.]
[IN ≠LA74≠ : (7B, 67)]

147- WO62 : PHYS.REV.. . . . . 126, 1693,(1962).
WOLL-JR/EJ,KOHN/W. [IMAGES/FERMI/PHONON]

148- WO64 : SOL.STATE COMM.. . . . . 2, 233,(1964).
WOODS/AOB,CHEN/SH. [LATTICE DYNAMICS/MO]
[IN ≠LA74≠ : (6 ,1519)]

149- WO69 : IN GENERAL REFERENCE NUMBER G 6. . . . . 1,(1969).
WOODS/AOB,DOLLING/G,COWLEY/RA. [/COMPARISON/TECHNIQUES]
[IN ≠LA74≠ : (17A, 40)]

150- ZI60 : IN GENERAL REFERENCE NUMBER G17. . . . .,.....,(1960).
ZIMAN/JM.

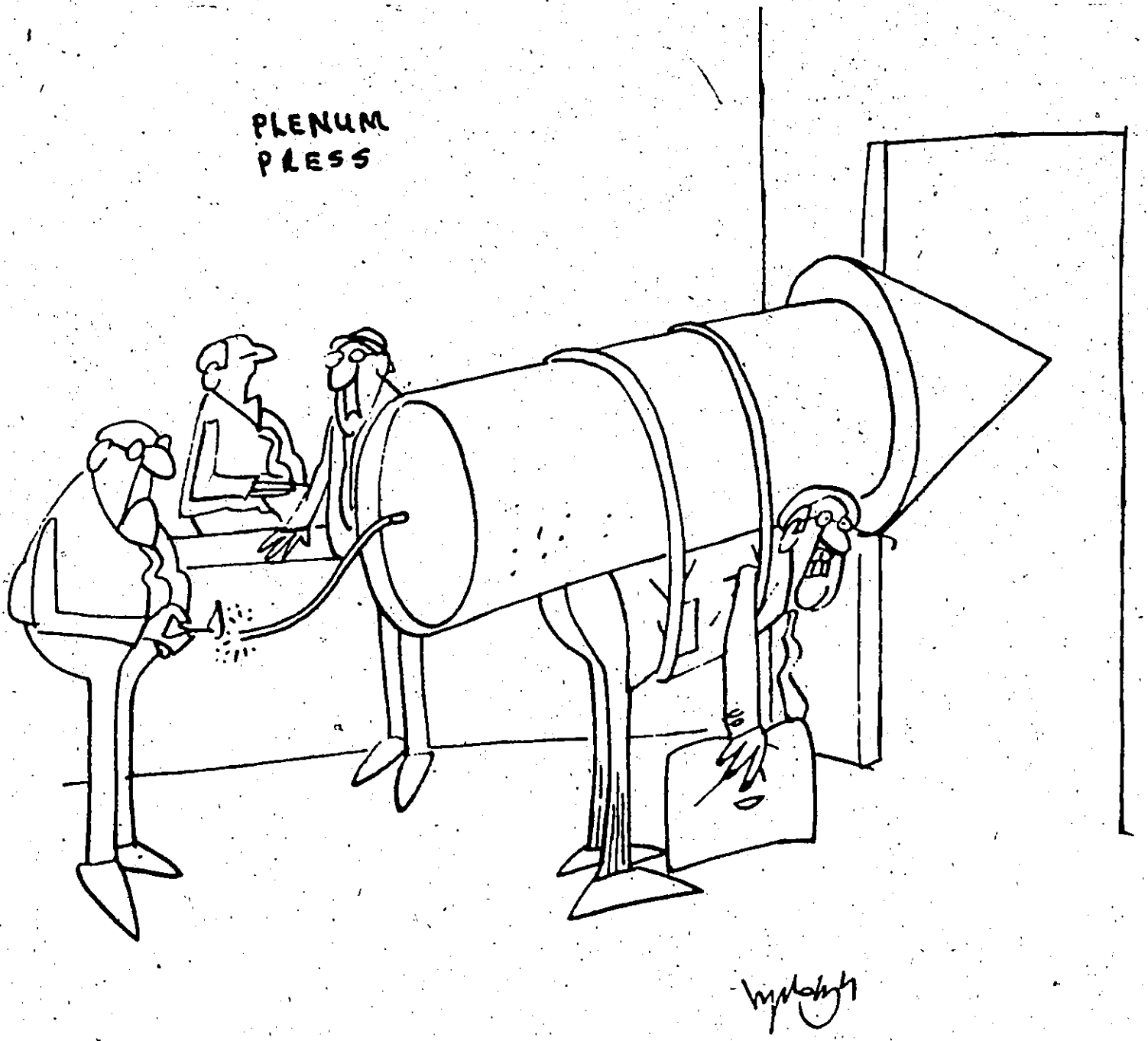

". . . He came in with a 500-page bibliography and wanted it by five."

Warning: Compiling bibliographies may be hazardous to your health.
(Original drawing is a courtesy of the editors of "The Silhouette")